UNIVERSITY OF THESSALY
SCHOOL OF ENGINEERING
DEPARTMENT OF MECHANICAL ENGINEERING

Master Thesis

MODAL IDENTIFICATION AND FINITE ELEMENT MODEL UPDATING OF METSOVO BRIDGE USING VIBRATION MEASUREMENTS

by

DIMITRA – CHRISTINA PAPADIOTI
Diploma in Civil Engineering, University of Thessaly, 2009

A Thesis
Submitted in Partial Fulfilment of the
Requirements for the Degree of
Master of Science
(in Mechanical Engineering)
2011

ΠΑΝΕΠΙΣΤΗΜΙΟ ΘΕΣΣΑΛΙΑΣ
ΠΟΛΥΤΕΧΝΙΚΗ ΣΧΟΛΗ
ΤΜΗΜΑ ΜΗΧΑΝΟΛΟΓΩΝ ΜΗΧΑΝΙΚΩΝ

Μεταπτυχιακή Εργασία

ΑΝΑΓΝΩΡΙΣΗ ΔΥΝΑΜΙΚΩΝ ΜΟΝΤΕΛΩΝ ΤΗΣ ΓΕΦΥΡΑΣ ΤΟΥ ΜΕΤΣΟΒΟΥ ΒΑΣΕΙ ΜΕΤΡΗΣΕΩΝ ΤΑΛΑΝΤΩΣΗΣ

υπό

ΠΑΠΑΔΙΩΤΗ ΔΗΜΗΤΡΑΣ - ΧΡΙΣΤΙΝΑΣ

Διπλωματούχου Πολιτικού Μηχανικού, Π.Θ., 2009

Υπεβλήθη για την εκπλήρωση μέρους των
απαιτήσεων για την απόκτηση του
Μεταπτυχιακού Διπλώματος Ειδίκευσης
2011

Εγκρίθηκε από τα Μέλη της Τριμελούς Εξεταστικής Επιτροπής:

Πρώτος Εξεταστής (Επιβλέπων)	Δρ. Παπαδημητρίου Κωνσταντίνος Καθηγητής, Τμήμα Μηχανολόγων Μηχανικών, Πανεπιστήμιο Θεσσαλίας
Δεύτερος Εξεταστής	Δρ. Σοφιανόπουλος Δημήτριος Επίκουρος Καθηγητής, Τμήμα Πολιτικών Μηχανικών, Πανεπιστήμιο Θεσσαλίας
Τρίτος Εξεταστής	Δρ. Τσόπελας Παναγιώτης Αναπληρωτής Καθηγητής, Τμήμα Πολιτικών Μηχανικών, Πανεπιστήμιο Θεσσαλίας

Ευχαριστίες

Πρώτα απ’ όλα, θέλω να ευχαριστήσω τον επιβλέποντα της μεταπτυχιακής εργασίας μου, Καθηγητή κ. Παπαδημητρίου Κωνσταντίνο, για την πολύτιμη βοήθεια και καθοδήγησή του κατά τη διάρκεια της μεταπτυχιακής εργασίας μου. Επίσης, θα ήθελα να ευχαριστήσω τα υπόλοιπα μέλη της εξεταστικής επιτροπής της μεταπτυχιακής εργασίας μου, Καθηγητές κ. Τσόπελα Παναγιώτη και κ. Σοφιανόπουλο Δημήτριο για τις πολύτιμες υποδείξεις τους. Επίσης θέλω να ευχαριστήσω τον Καθηγητή Siu Kui Au και τον Μεταδιδακτορικό φοιτητή Lequia He από το Καθολικό Πανεπιστήμιο του Leuven για την συνεργασία που είχαμε σε επιμέρους θέματα που αφορούν στην παρούσα εργασία. Ευχαριστίες ακόμη οφείλω στους φοιτητές του Εργαστηρίου Δυναμικής Συστημάτων, Ντότσιο Βαγγέλη, Καραΐσκο Γρηγόρη, και Πέρρο Κυριάκο για την πολύτιμη βοήθειά τους σε θέματα προγραμματισμού σε περιβάλλον Matlab.

Δήμητρα - Χριστίνα Παπαδιώτη

MODAL IDENTIFICATION AND FINITE ELEMENT MODEL UPDATING OF METSOVO BRIDGE USING VIBRATION MEASUREMENTS

Abstract

In the last decades, there has been developing interest and research devotion to the area of Structural Health Monitoring (SHM) of civil infrastructure worldwide. Nowadays, SHM systems have been installed on a significant number of important modern as well as historical structures. Monitoring structures include long suspension and cable-stayed bridges, metallic and R/C highway and railroad bridges, footbridges, museums, monuments and historical churches, buildings and towers. In particular, in Greece there is a relative significant number of bridges that have been densely instrumented with a relative large number of acceleration and strain sensors for SHM purposes. Permanent SHM systems that have been installed in Greek structures include the Chalkida-Evripos and Rio-Antirrio cable-stayed bridges, as well as the G2-Kavala, G9-Polymylo and Metsovo bridges which are part of the Egnatia Odos motorway, while installation of more SHM systems are being planned.

This thesis is concerned with the finite element modeling, modal identification and finite element model updating of the Metsovo bridge, the highest R/C bridge of the Egnatia Odos Motorway in Greece. High fidelity dynamic finite element models for the bridge-foundation-soil system are devoloped using the design drawings of the bridge. Operational modal analysis software is used to obtain the modal characteristics of the bridge for the various sets of available vibration measurements during different construction phases of both the left and right bridge branches. The identified modal characteristics and the modal characteristics predicted by the finite element models are compared to check the adequacy of the finite element models. The identified modal characteristics are then used to calibrate detailed finite element models of the bridge. A multi-objective structural identification method is used for estimating the parameters of the finite element structural models based on minimising the modal residuals. The information for the identified modal models and the updated finite element models is very useful for validating design assumptions, for identifying soil-structure interaction effects and for improving modelling of the Metsovo bridge.

Contents

CHAPTER 1

Introduction

1.1 Structural Health Monitoring

Civil infrastructure systems such as highway and railroad bridges, footbridges, historical structures (e.g. monuments, churches), buildings, offshore platforms, gas distribution networks, nuclear power plants, towers (e.g. high voltage transmission towers), as well as industrial facilities with its components, can suffer structural damage when subjected to potentially damaging extreme events such as sudden moderate to strong earthquakes, tornadoes, hurricanes, as well as long-term environmental effects such as corrosion and fatigue. If such damage is sufficiently severe, it needs to be rapidly detected and corrected, otherwise it may progress to the stage of catastrophic structural failure. For this purpose continual monitoring of the integrity of a structure by rapidly detecting the occurrence of significant damage, and identifying its location and severity, is necessary for assessing the safety of structural systems. The safety assessment can be achieved by estimating the reliability against various structural failure modes using the monitoring information about the degradation condition of structural components for predicting their residual useful life, accounting for future uncertain environmental, operational and earthquake loads. This is the ultimate objective of "Structural Health Monitoring (SHM)".

The term "Structural Health Monitoring (SHM)" refers to continuous observations of the dynamic behaviour of a structure in order to track changes in its structural characteristics and detect damage. The observations typically involve installing permanent sensors in the structure (e.g., acceleration, velocity, and GPS-Global Positioning System sensors) and recording continuously the vibration of the structure. These vibration measurements are usually the acceleration of the structure obtained by accelerometers optimal placed on the structure [Papadimitriou et al. (2000); Papadimitriou (2005); Ntotsios et al. (2006)]

Nowadays, there has been developing interest and research devotion to the area of SHM of bridges worldwide. SHM systems have been installed on a significant number of important modern as well as historical long suspension and cable-stayed bridges ,metallic and R/C highway and railroad bridges, and footbridges. In particular, in Greece there is a relative significant number of bridges that have been densely instrumented with a relative large number of acceleration and strain sensors for SHM purposes. Permanent SHM systems have been initially installed in Chalkida-Evripos and Rio-Antirrio cable-stayed bridges. Nowadays, approximately eight bridges along the Egnatia Odos motorway have been instrumented with permanent acceleration and strain sensors. Data have been collected and analysed for the following bridges: G2-Kavala, G9-Polymylos and Metsovo bridges [Ntotsios et al. (2009); Panetsos et al. (2009)].

1.2 Monitoring of Egnatia Odos Bridges

Egnatia Odos motorway is the largest and most challenging Greek project of design, supervision, construction, operation, maintenance and exploitation linking Europe with Turkish borders, that has been constructed in Northern Greece. Because the 680 km long motorway crosses particularly difficult geological terrain and obstacles such as large rivers and deep ravines it has led to the construction of major structures, including split deck bridges up to 1.0 km long, with large spans, high piers and curved decks, in areas of high seismicity and sometimes in the vicinity of active seismic faults. Since Egnatia Odos motorway is put into service, several hundred bridges are subjected to everyday traffic loading and are expected to be subjected to small or even moderate seismic loadings during their lifetime. Although these newly established bridges have high durability, over their design life of 120 years, their periodical inspection and evaluation is required to ensure appropriate and prompt maintenance and repair of any damage or deterioration.

EGNATIA ODOS S.A., the company responsible for the design, construction, maintenance and exploitation of Egnatia Motorway developed an integrated Bridge Management System [Panetsos P. and Lambropoulos (2005)] for optimizing the maintenance and repair policies for bridges of the motorway. This system consists of the following features:

- A Manual and Guidelines of visual monitoring and inspecting the motorway's bridges and evaluating their structural and functional condition.
- An extensive ORACLE^{TM} based database for recording the as built and as inspected technical and condition data of the bridges, gathered from periodical inspection. This has been connected to a GIS system.
- A user-friendly bridge management software tool. The Egnatia Odos Bridge Management (EOBMS) deterioration prediction and maintenance/repair cost and effectiveness models reflect both Greek and international experience. Seismic risk and bridge vulnerability are also considered in ranking, prioritization and deterioration pattern of the bridges.
- A Manual, Specifications, Hardware (sensors) and specific user friendly software tools of on line periodical instrument monitoring of representative motorway's bridges, for identifying their dynamic characteristics (frequencies, mode shapes, damping), updating their dynamic models and detecting the location and significance of damage.

For evaluating the structural and functional condition of 1750 bridges of Egnatia Odos some of which are longer than 200m, having piers higher than 20m, built over steep ravines in the mountain of Northern Greece, visual inspection seems to be rather difficult to apply (time and personnel consuming, needing for special access equipment) and of limited accuracy. In addition some of Egnatia Odos bridges are Greek records either for the method of their construction (e.g. launching of box girders) or for their span length/ total length (exceeding 235m/1000m respectively), and therefore need advanced and robust inspection and assessment techniques.

So in the last years, some of the major bridges of the motorway like G2-Kavala, G9-Polymylo and Metsovo bridges have been selected to be instrumented to give initial structural and functional condition data. These three bridges are structurally representative of the majority of Egnatia Bridges and are presented here.

The 2nd Kavala Bypass Ravine Bridge (Figure 1.1), has a total length of 170m, 4 identical spans of 42,5m, with a pre-stressed concrete superstructure, each span

constituted of 4 precast post-tensioned beams of 2,80m height supporting a 20-cm-thick deck, without internal expansion joints, continuous over the pier bents. The bridge superstructure is supported through laminated elastomeric bearings on three square hollow piers having heights of 30m (M1, M3) and 50m (M2).

(a) **(b)**

Figure 1.1: (a) Transverse Section of G2 Kavala Bridge , (a) Longitudinal Section of G2 Kavala Bridge.

Twenty four uniaxial forced balanced accelerometers were installed on both edges of the bridge deck (external sidewalk and internal new jersey barrier) cabled to two 12-channels K2 accelerographs (one for each deck side). For common start & common trigger an interconnection cable is connecting the two K2 accelerographs to obtain synchronous data acquisition. Of the 24 sensors, 18 were installed on the deck and 6 on the top of the three pier bents (6 sensors) .

The G9 Ravine Bridge (Veria-Polymylos section) (Figure 1.2), curved in plan, has a total length of 170m, 2 identical spans of 85m, with a box beam pre-stressed concrete superstructure, constructed by in situ balanced cantilever method (its depth varying from 4,00m in abutments to 9,00m in its pier support). The bridge superstructure is supported monolithically to one center pier M1, of 35m height, having massive rectangular section on the basement and two transverse flanges all over its height.

(a) **(b)**

Figure 1.2: (a) Longitudinal Section of G9 Polymylos Bridge , (b) Transverse Section of G9 Polymylos Bridge .

A network of 24 uniaxial forced balanced accelerometers were installed on both edges of the bridge deck sidewalks cabled to two 12-channel K2 accelerographs (one for each deck side). For common start & common trigger an interconnection cable between the two K2 accelerographs was installed to obtain synchronous data acquisition. Of the 24 sensors, 15 were installed on the deck, 3 on the basement of the center pier M1 and 6 on the abutments (laminated elastomeric bearings' level).

Finally, one of the major ravine bridges of the west sector of the Egnatia Motorway, that this thesis is concerned with, is Metsovo Bridge (Figure 1.3). Metsovo Bridge, located in section 3.2 (Anthohori tunnel-Anilio tunnel) of Egnatia Motorway, crosses the deep ravine of Metsovitikos river, 150 m over the river bed.

Figure 1.3: General view of Metsovo ravine bridge.

1.3 Objective of this Thesis

The objective of this thesis is develop a detailed finite element model of the Metsovo bridge and calibrate the model based on vibration measurements collected during the operation of the bridge. Based on the design drawings and the material properties, detailed finite element models of the left branch of the bridge were constructed for two construction phases. A mobile monitoring system for the Metsovo bridge was used to collect ambient vibration measurements. The measured response data offers a unique opportunity to study quantitatively and qualitatively the dynamic behaviour of the bridge within the resulting vibration levels. These vibration measurements are processed for the estimation of the modal characteristics, as well for the calibration of the corresponding finite element models used to simulate the bridge behaviour. Modal identification software was applied to identify the modal characteristics of the bridge. The identified modal characteristics and the modal characteristics predicted by the finite element models are compared to check the adequacy of the finite element models. Model updating techniques are then used to update certain parameters of the bridge so that the model predicted modal characteristics match the modal characteristics identified by the measured data. Selected results from modal identification and finite element model updating of the bridge are presented in this thesis. In addition, monitoring data of both left and right branch of this bridge were used to compare the dynamic behavior of the two bridges during an intermediate construction phase.

The information for the identified modal models and the updated finite element models is very useful for validating the assumptions used in model development and for improving modelling, analysis and design procedures. The calibrated finite element model will serve as a reference model for continuously monitoring the health of the structure based on vibration measurements provided by a permanently installed monitoring systems.

1.4 Organization of the Thesis

This thesis is organised as follows. In this thesis modal identification methodologies for estimating the dynamic modal characteristics of a representative civil engineering structure, Metsovo Bridge, and finite element model updating techniques have been implemented using ambient vibration measurements.

Chapter 2 presents a detailed description of Metsovo Bridge in order to help the reader understand better the geometry of the structure and the surrounding environment. Then the plan drawings provided by EGNATIA ODOS S.A. were used to create in SoldWorks a three-dimensional solid model of the bridge.

Chapter 3 deals with the finite element modeling of the bridge. Based on the SolidWorks three dimensional model, different types of finite element models of the bridge were developed in COMSOL Multiphysics in order to predict the dynamic behavior of the bridge under two different construction phases. The modal properties of the bridge that are predicted by the various finite element models developed are compared. In addition, the modal properties predicted by the finite element models are compared with the identified modal properties.

In Chapter 4 operational modal identification software is used to obtain the modal characteristics of the bridge for the various sets of available vibration measurements during the two construction phases of both the left and right bridge branches. The modal identification results of the bridge are presented and the adequacy of the measured data provided by a mobile monitoring system consisting of 6 accelearation sensors is discussed.

In Chapter 5 the identified modal characteristics are used to calibrate the finite element models of the bridge. A multi-objective structural identification method is used for estimating the parameters of the finite element structural models based on minimising the modal residuals. The method results in multiple Pareto optimal structural models with variability that depends on the fidelity of the model class employed and the size of measurement errors. The identified Pareto models are used for checking design assumptions, for exploring the adequacy of the different classes of finite element models,

for identifying soil-structure interaction effects, and for estimating the response prediction variability.

Finally, Chapter 6 summarizes the conclusions of this work. Also it presents suggestions for future research on issues related to this thesis.

CHAPTER 2

3-D Design of Metsovo Bridge

2.1 Description of Metsovo Bridge

The new ravine bridge of the west sector of Egnatia Motorway, Metsovo Bridge (Figure 2.1), is the highest bridge of Egnatia Motorway with the height of the taller pier M2 equal to 110m. The total length of the bridge is 537m, the largest beam bridge ever built in Greece. The bridge has 4 spans, of length 44,78m /117,87m /235,00m/140,00m and three piers as it is shown in Figure 2.2 and Figure 2.3. The span is also the highest bridge of any kind ever built in Greece rising approximately 150 m above the Metsovitikos River.

Figure 2.1: General view of Metsovo ravine bridge.

As a consequence of the strong inequality of the heights of the two basic piers of the bridge, M2 and M3 (110m to 35m) and due to the eccentrical position of the key segment, the central span is the longest of the four. Specifically the pier M2 balanced cantilever is 250m long. The key of the central span, shown in Figure 2.4, was not constructed in midspan due to the different heights of the superstructure at its supports to the adjacent piers (13,0m in pier M2 and 11,50 in pier M3) for redistributing mass and load in favor of the short pier M3 and thus relaxing strong structural abnormality. The last was the main reason of this bridge to be designed to resist earthquakes fully elastic (q factor equal to 1).

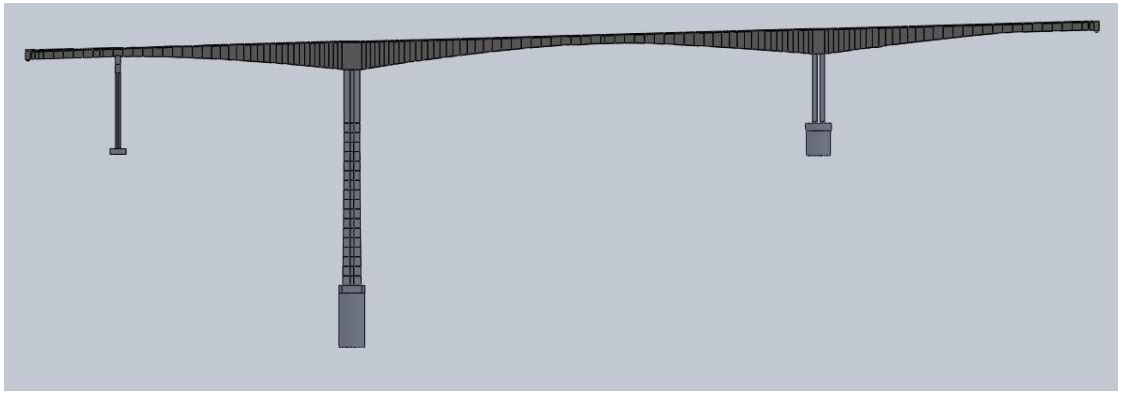

Figure 2.2: Longitudinal section of the solid model of Metsovo ravine bridge.

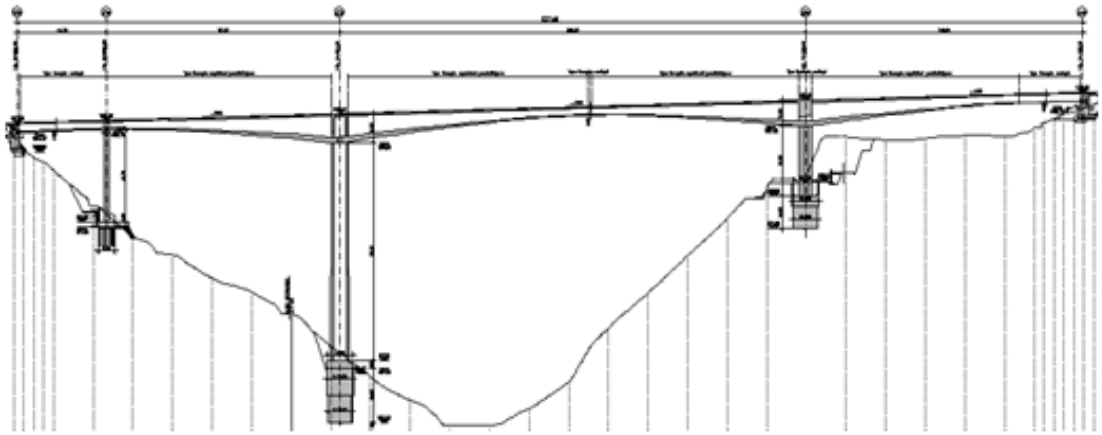

Figure 2.3: Longitudinal section of Metsovo ravine bridge of Egnatia Motorway

Figure 2.4: Key of central span of under construction Metsovo ravine bridge

The bridge has being constructed by the balanced cantilever method of construction, as it is shown in Figure 2.5.The total width of the deck is 13,95m, for each carriageway. The superstructure is limited prestressed of single box beam section, of height varying from the maximum 13,5m in its support to pier M2 to the minimum 4,00m in key section. Piers M2 and M3, the construction of which is shown in Figures 2.6 and 2.7, are founded on huge circular Ø12,0m rock sockets in the steep slopes of the ravine of the Metsovitikos river, in a depth of 25m and 15m, respectively.

Figure 2.5: General view of under construction Metsovo ravine bridge (November 2007)

Figure 2.6: General view of under construction Pier M3of Metsovo ravine bridge

Figure 2.7: Longitudinal section of under construction Pier M3of Metsovo ravine bridge

To better define the characteristics of the bridge, we indicate some details of some parts of which are explained below in more details. The bridge has two branches ,the left and the right. The two branches have almost the same geometry so we will describe one of them, the left branch. In particular, the deck has a total length of 537.65 m, a constant slope of 2.6% along it and its maximum height from the top of deck to the ground is 112.31 m at pier M2. Also the deck has an additional slope across its 168 sections and was built with a maximum step of 5 m, containing in total 14 repeated sections. From these sections only one is constant, while all others are varying in height and thickness.. Also the bridge has three piers of which M1, 45m high, supports the box beam superstructure through pot bearings (movable in both horizontal directions), while M2, M3 piers connect monolithically to the superstructure.

The pier M2, which is the highest of the three piers (99.31 meters), has a variable cross section from its base to the height of 74.80 meters and then it remains constant over that height (from 74.80 until the 99.31 meters). The outer surface of the longitudinal section of pier M2 varies along a circle with a radius of curvature of 4303.877 meters from the base up to a height of 74.80 meters, while the inner surface remains constant. The outer surface of the transverse section of pier M2 varies again along a circle from the base up to a height of 74.80 meters but with a radius of 1398.761 meters. Also, the inner surface of the cross-section follows a circle with a radius of 974,751 meters from the base up to the height of 48.40 meters .

Finally, piers M1 and M3 have relatively simple geometry (rectangular and octagonal, respectively), but there are too many details on all sections of the bridge some of which are mentioned above that highlight the difficulties that were faced during the transition from the two-dimensional design drawings that were provided by EGNATIA ODOS S.A., to the final creation of three-dimensional models of Metsovo Bridge that were necessary for the dynamic analysis of the bridge.

At this point it should be noted that the design program that was preferred for the final creation of the three-dimensional models was SolidWorks among a wide variety of programs like Pro Engineer, AutoCAD, and others. The reason for this choice was that Solidworks cooperates excellent with COMSOL Multiphysics, the software that was used

for the finite element modal analysis of the bridge. COMSOL Multiphysics was preferred among Abaqus and Femtools, because it gave us the opportunity to carry out the finite element model updating using methods and algorithms that have been developed in the System Dynamics Laboratory of the Mechanical Engineering Department (University of Thessaly).

Next, an analysis follows that describes all the individual parts that constitute the superstructure of Metsovo Bridge. These parts are pier M1, pier M2, pier M3 and the deck. Based on the design drawings and the detailed descriptions, a three-dimensional model of the bridge is constructed and shown using SolidWorks. After the detailed description of all parts of the bridge, the assumptions that were made for the better design and analysis of the three-dimensional model are presented.

2.2 Design of Pier M1

The pier M1 is located 44.78 m from the abutment Ao and has a height of 44.1 meters. The base cross section is rectangular (8 x 10 meters) while the cross section of the main body is octagonal with dimensions that are shown in Figure 2.8 that was provided by EGNATIA ODOS S.A. The total height of the pier M1 consists of the base (2.5 meters), the main body of the pier, (35 meters) and of the head which has a height of 6.6 meters, as it is shown in Figures 2.9 and 2.10.

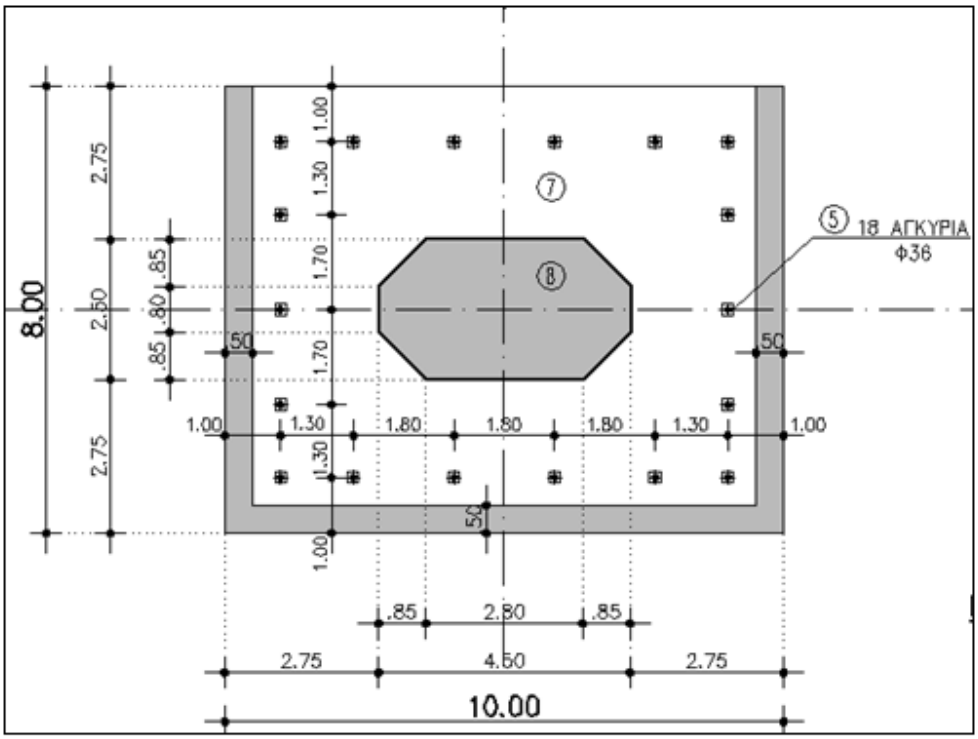

Figure 2.8: Ground plan of pier's M1 base

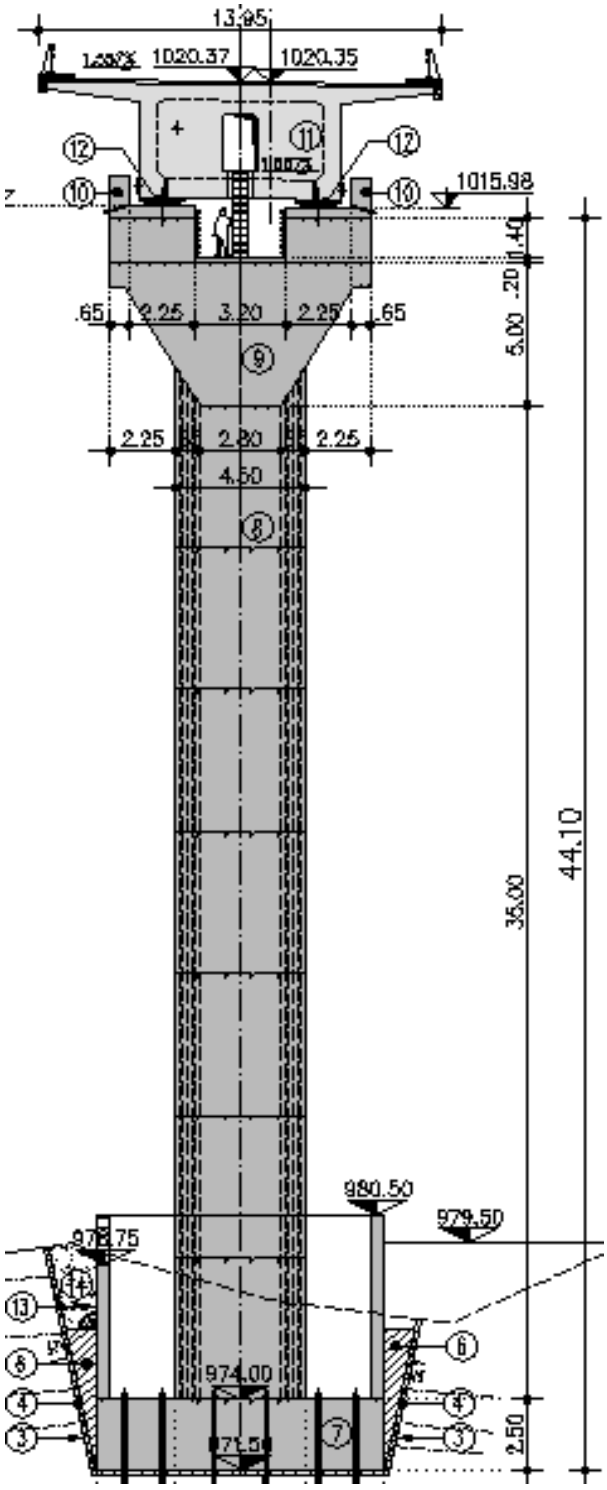

Figure 2.9: Transverse view of pier M1

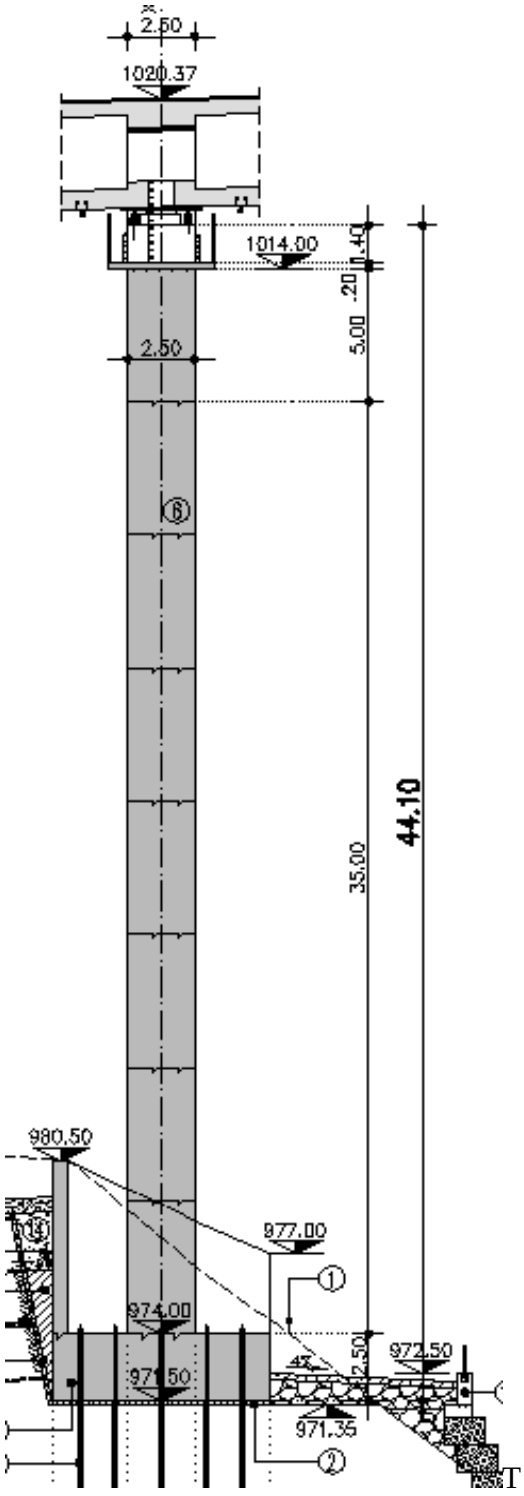

Figure 2.10: Longitudinal view of pier M1

The special characteristic of M1 is that this pier supports the box beam superstructure through pot bearings that allow movement in both horizontal directions, while M2, M3 piers connect monolithically to the superstructure. The full geometry of the pier, of the head, which is connected to the pier through the bearings, as well as of the bearings is presented in detail in the following drawings. More specifically, Figure 2.11 shows a plan view of the head where the precise geometry of the bearings (index 4) is presented in Figure 2.12 that shows the perspective view of the head which was necessary for the better understanding of the overall geometry in order to be able to design it. Finally Figure 2.13 shows a cross section of head showing the exact dimensions as well as the geometry of the body of the deck on the M1.

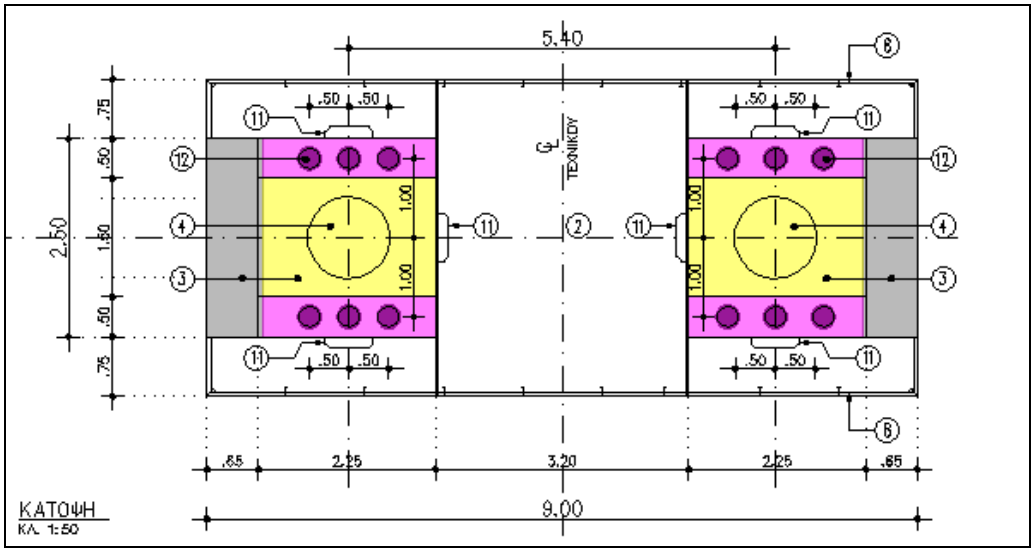

Figure 2.11: Ground plan of pier's M1 head

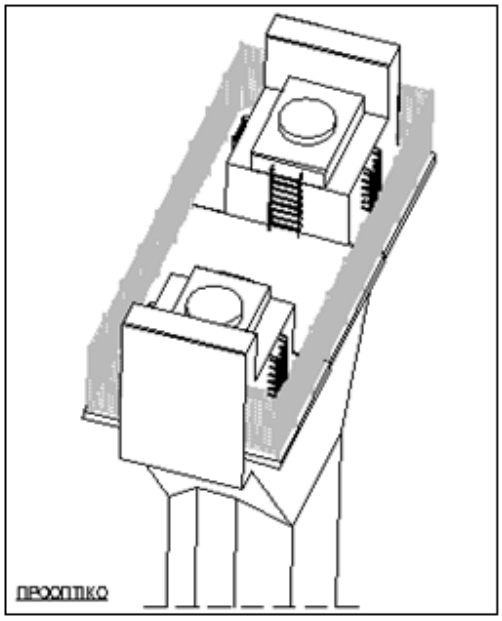

Figure 2.12: Perspective view of pier's M1 head

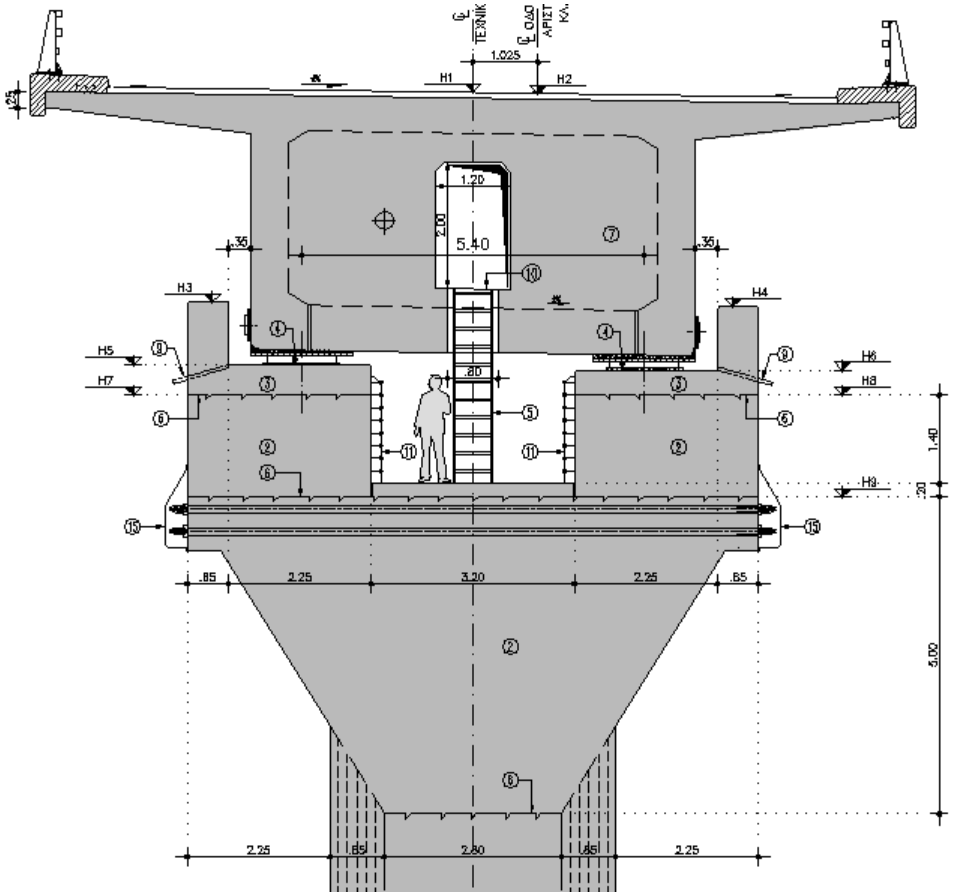

Figure 2.13: Transverse cross section of pier's M1 head

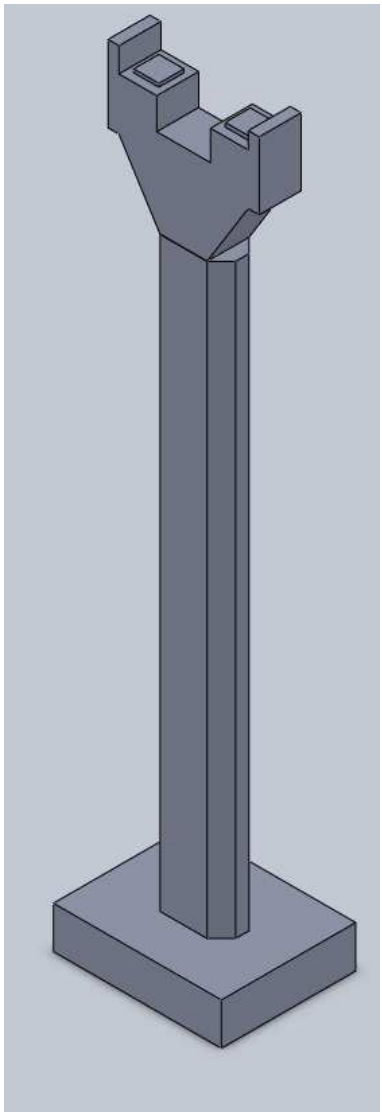

Figure 2.14: Isometric view of the solid model of pier M1 created in Solidworks

The creation of the solid model in Solidworks from the two-dimensional drawings that were provided by EGNATIA ODOS S.A. was conducted as follows. First of all, the base and the body of pier M1 were created as a *Part* in Solidworks and then the head of the pier was created as a separate part. Then the two parts were joined together through the command *Mate* and the *Assembly* of M1 was created in Solidworks. Finally the bearings were added on the final assembly (Figure 2.14) for the purpose of joining the deck with pier M1.

2.3 Design of Pier M2

The pier M2 is located 117.87 m from pier M1 (distance of their center), has a height of 99.31 meters without the height of the deck over the head of M2 which is 13 meters and is the highest structural component of Metsovo Bridge.

Moreover the head of pier M2 has a complex and variable geometry which is described in detail in Section 2.4 that refers to the geometry of the deck. Another feature that made it the most complex of the three piers to be designed is the variable cross-section of its body, or more precisely the change in the thickness of the section both in the transverse and longitudinal direction The outer surface of the longitudinal section of pier M2 varies along a circle with a radius of curvature of 4303.877 meters from the base up to a height of 74.80 meters, while the inner surface remains constant. The outer surface of the transverse section of pier M2 varies again along a circle from the base up to a height of 74.80 meters but with a radius of 1398.761 meters. Also, the inner surface of the cross-section follows circle with a radius of 974,751 meters from the base up to the height of 48.40 meters .

For the better understanding of the geometry of pier M2, the above details are shown in the Figures 2.15 and 2.16. In Figure 2.15 it is shown that in the longitudinal section only the length of the external surface changes, while the interior remains constant with a length of 6.60 meters in the transverse direction. At the left side of Figure 2.15 it is noted that the outer surface of the longitudinal section of pier M2 varies along a circle with a radius of curvature of 4303.877 meters from the base up to a height of 74.80 meters and as a result the length in transverse direction varies from 9.30 m to 8 m. Then it remains constant over that height (from 74.80 until the 99.31 meters). In Figure 2.16 it is shown that in the transverse section change both the interior and the external surface. The outer surface of the transverse section of pier M2 varies again along a circle from the base up to a height of 74.80 meters but with a radius of 1398.761 meters and as a result the length in longitudinal direction varies from 11.50 m to 7.59 m Also, the inner surface of the cross-section follows a circle with a radius of 974,751 meters from the base up to the height of 48.40 meters and as a result the interior longitudinal length varies from 8 m to 5.60 m.

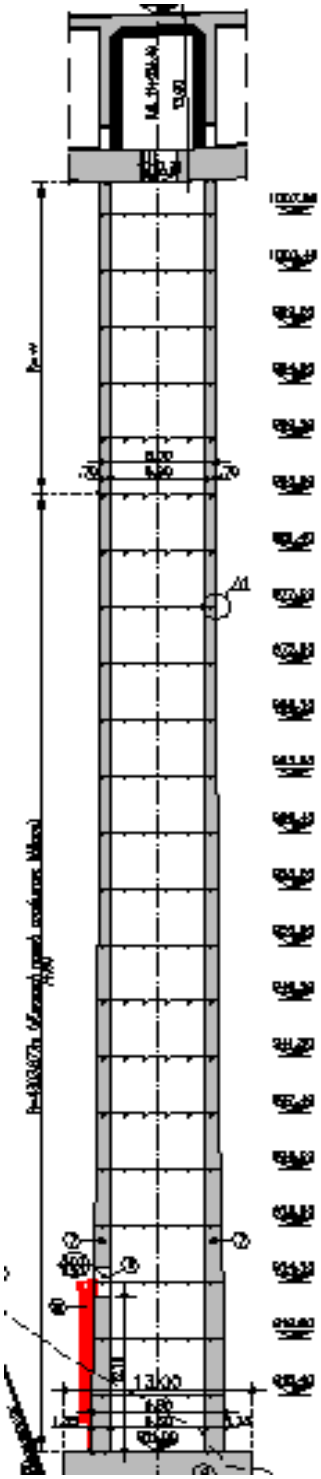

Figure 2.15: Longitudinal view of pier M2a

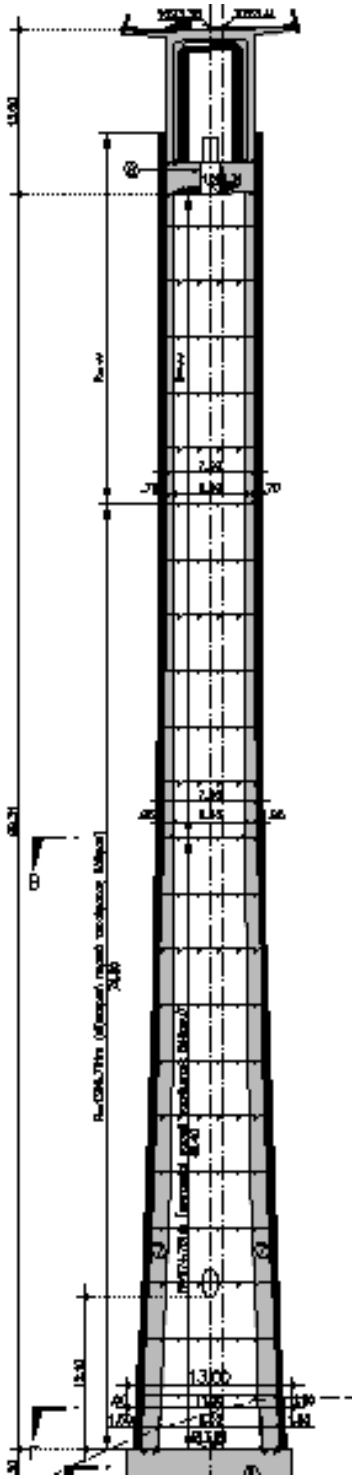

Figure 2.16: Transverse view of pier M2a

At this point it should be noted that we were provided with the drawings of only three cross sections of pier M2 that are shown in the figures below. Figure 2.17 presents the cross section of pier M2 at the base, Figure 2.18 presents that at the height of 48.4 m (over this height the inner surface remains constant) and at the height of 74.8 m. Over that height the cross section remains constant.

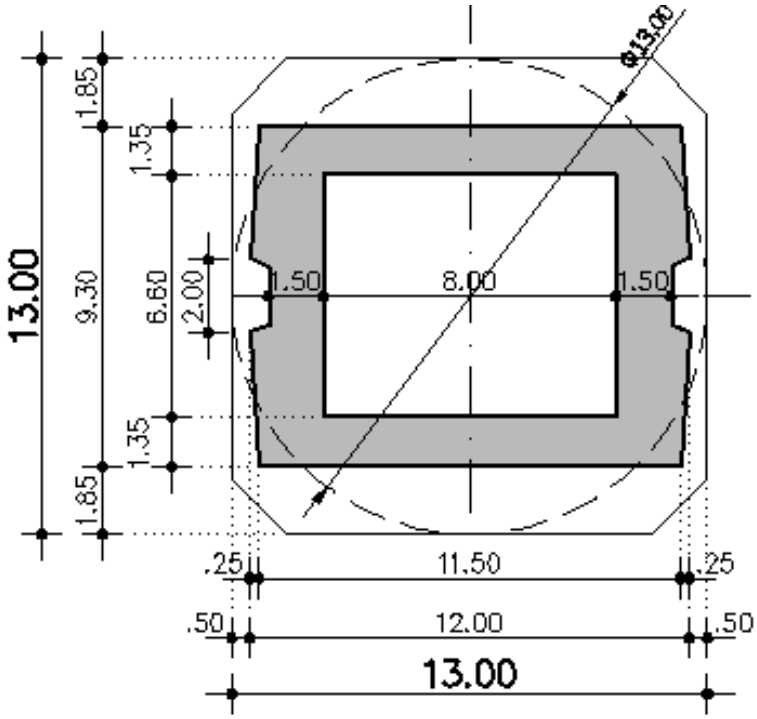

Figure 2.17: Base cross section of pier M2

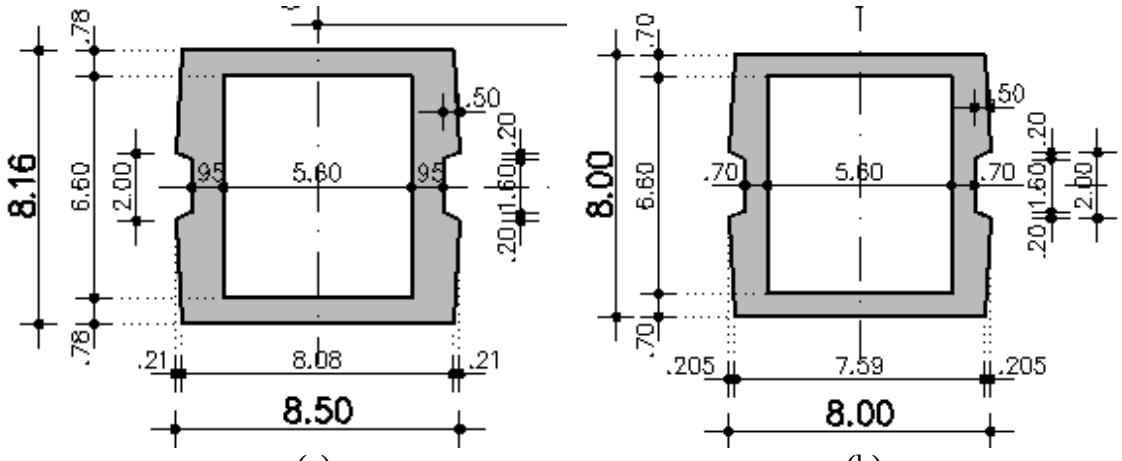

(a) (b)

Figure 2.18: Cross section of pier M2 at the height of (a) 48.4 m, (b) 74.8 m

On the other hand, pier M2 was constructed with step of four meters. So we had to find a way in order to transmit from one section to the other by achieving the best convergence of the nominal solid model to the real bridge. These two events made necessary for the design of the three-dimensional the calculation of all intermediate sections from the base of pier up to the height where the cross-section remains constant. The fact that the design of pier M2 was just like the real construction, resulted in the high accuracy of the solid model of pier M2.

The calculation of these intermediate sections that did not exist in the drawings that we were provided by EGNATIA ODOS S.A. was performed using Matlab. Simple geometric relationships were used to calculate the change of thickness in transverse and longitudinal section were estimated at each step of 4 m in height. More specifically, the the program used has two parts: one for the change in the transverse direction and one for the change in the longitudinal direction. In each iteration loop the height was the parameter that changed and the difference of the length of the interior point of thickness (measured from the center of the circle) from the radius of each circle was calculated.

The relationship that was used to find the thickness of each section is $\delta = R - \sqrt{R^2 + h^2}$ where R is the radius of curvature, h the height and δ the thickness in the next step. The term $\sqrt{R^2 + h^2}$ represents the change in the thickness of each section passing from a higher level to a lower and arises from the geometry of the right triangle that connects the center of the circle and the outer left surfaces of the pier at the points with difference in height in case that $x = R\cos\theta = R\sqrt{1 - \sin^2\theta} = R\sqrt{1 - \frac{h^2}{R^2}} = \sqrt{R^2 + h^2}$

The creation of the solid model from the two-dimensional drawings that were provided by EGNATIA ODOS S.A. was conducted as follows. First of all the command *Lofted Boss* was used to create the various components of the pier (between each section) and then the command *Mate* was used for the union of these individual *Parts*. For the creation of the part of pier that has constant cross section (from the height of 74.8 m and over), the command *Extruded Boss* was used. This command converts a two dimensional sketch of a cross section into a three dimensional Part, by defining only the length of the third dimension. The difference between the first and the last command is that the first is

used to create a three dimensional Part like that shown in Figure 2.19 with variable section. Command *Lofted Boss* joins the points of two sections (regardless of whether they are identical or not) that are designed in parallel planes, filling the intermediate area with solid material.

Finally some information should be mentioned for the geometry as well as for the foundation of pier M2, that appear in Figure 2.20 and Figure 2.21. Figure 2.20 shows a transverse view of the foundation of pier M2. On the other hand Figure 2.21 is a ground plan view of pier M2 in section D of Figure 2.20. Moreover, the foundation of the pier, an isometric view of which is shown in Figure 2.22, is a solid cylinder starting from the ground with diameter thirteen meters (Ø13,0m) and height 25 m. and upon that there is an octagonal geometry with dimensions that are shown in Figure 2.21.

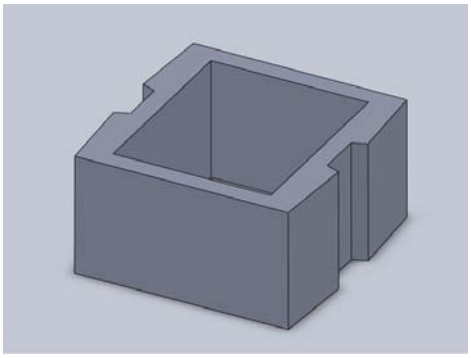

Figure 2.19: Isometric view of a part of pier M2

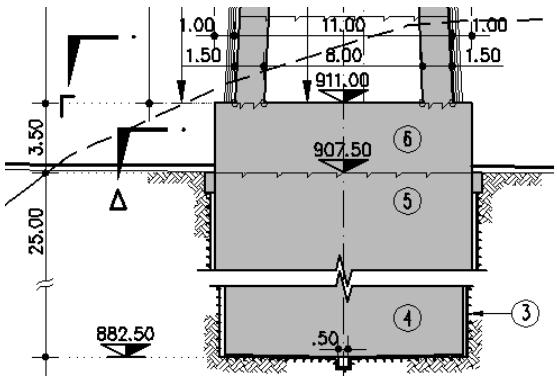

Figure 2.20: Transverse view of the foundation of pier M2

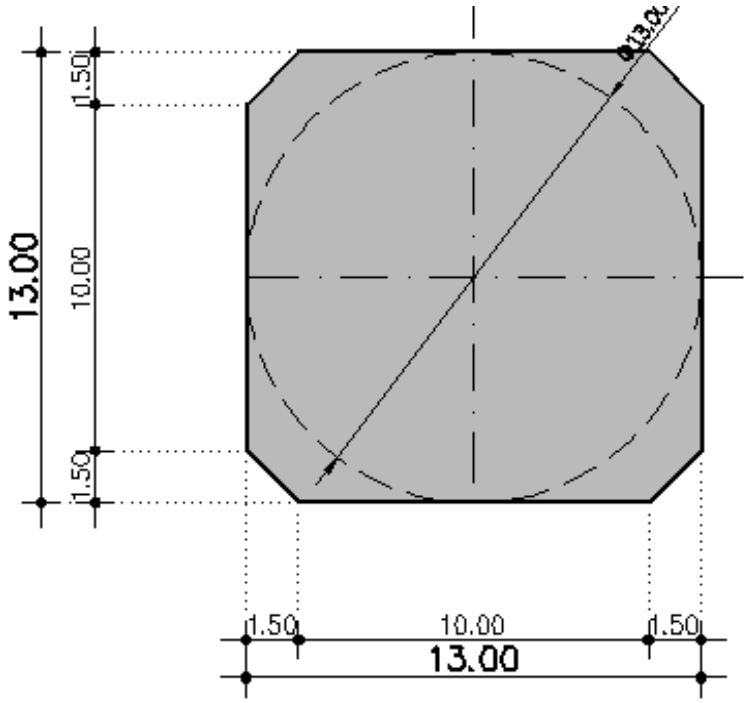

Figure 2.21: Ground plan of the foundation of pier M2

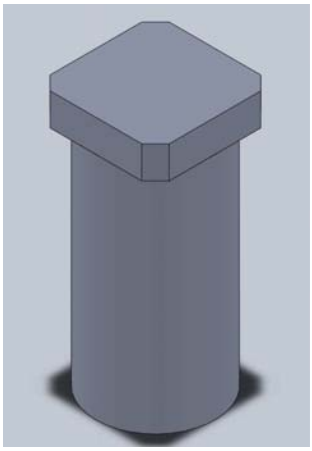

Figure 2.22: Isometric view of the foundation of pier M2

The final design product that resulted from the SolidWorks for pier M2 is presented in Figure 2.23 which shows the pier M2 with the foundation and the part of the deck that is above M2. Pier M2 is analyzed again in Section 2.6 that gives details about the assumptions that were made during the design of the solid model.

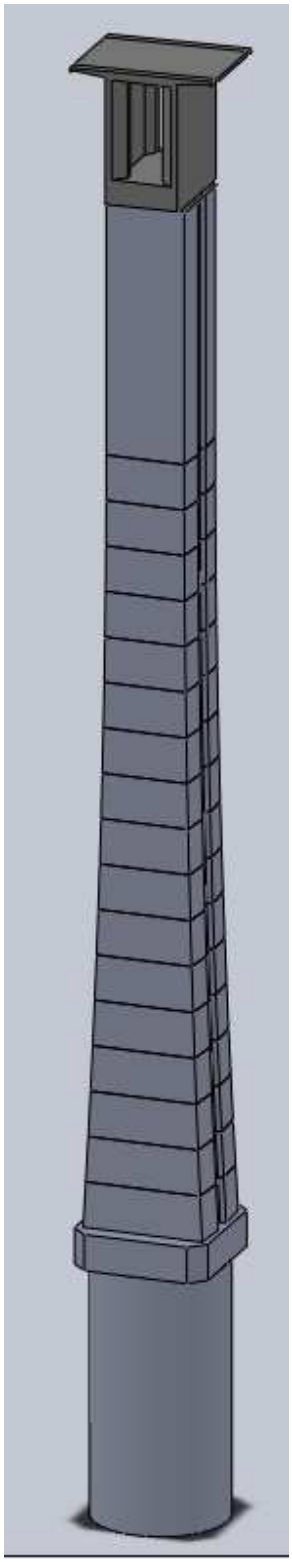

Figure 2.23: Isometric view of the solid model of pier M2 created in Solidworks

2.4 Design of Pier M3

The pier M3 is located 235 m from pier M2 (distance of their center) to the left and 140 m from the abutment A4 to the right. It has a height of 31.92 meters without the height of its base that is 15 meters.

Pier M3 consists of two parallel rectangular piers with dimensions 2.3 m in the longitudinal direction and 8 m in the transverse direction, as it is shown in the ground plan in Figure.2.24. These two sub-piers have a distance of 1.5 meters in the longitudinal direction and are parallel in the transverse direction. Finally the pier's base has a height of 15 meters and consists of two cylinders with diameter 12 and 13 meters each one (Ø12,0m and Ø13,0m respectively).

The construction of the solid model of pier M3 in Solidworks was simple. First of all the ground plan of pier M3 was designed as a rectangular section and then the *Sketch* was converted into a three dimensional *Part* with the command *Extruded Boss* by defining only the length of the third dimension, the height. For defining the geometry of the solid model, Figures 2.25 and Figure 2.26 were also used. The final design product that resulted from the SolidWorks for pier M3 is presented in Figure 2.27 which shows the pier M3 with the foundation and the part of the deck that is above M3

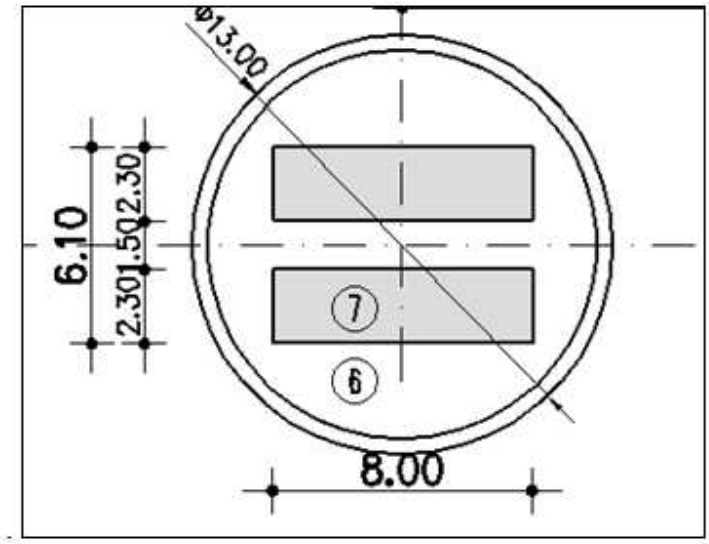

Figure 2.24: Ground plan of the foundation of pier M3

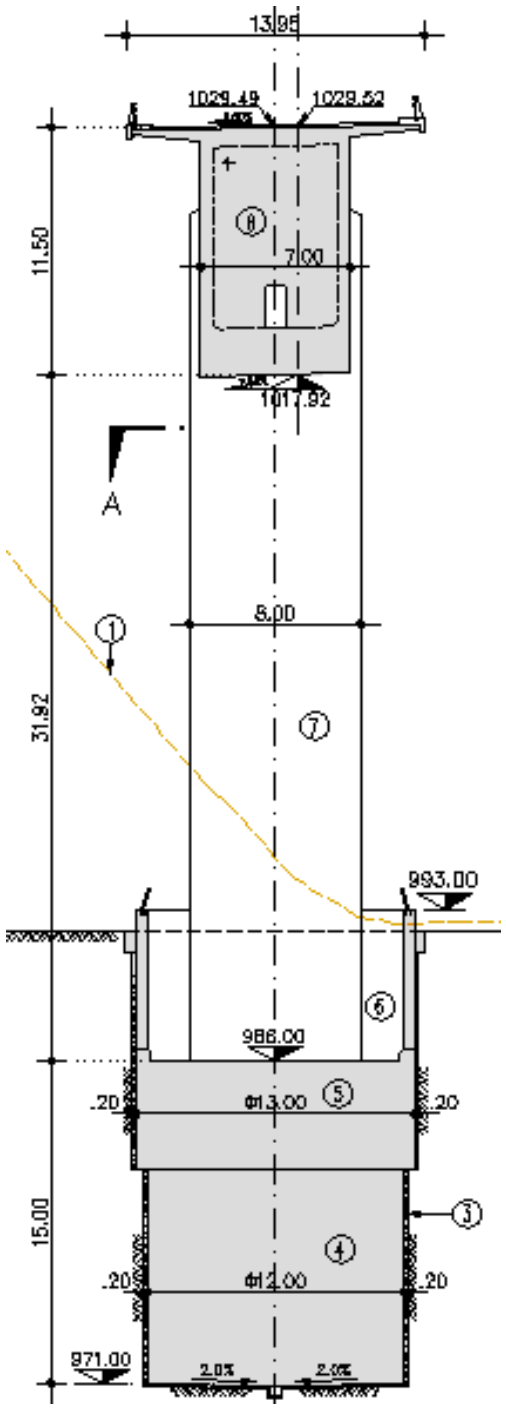

Figure 2.25: Transverse view of pier M3

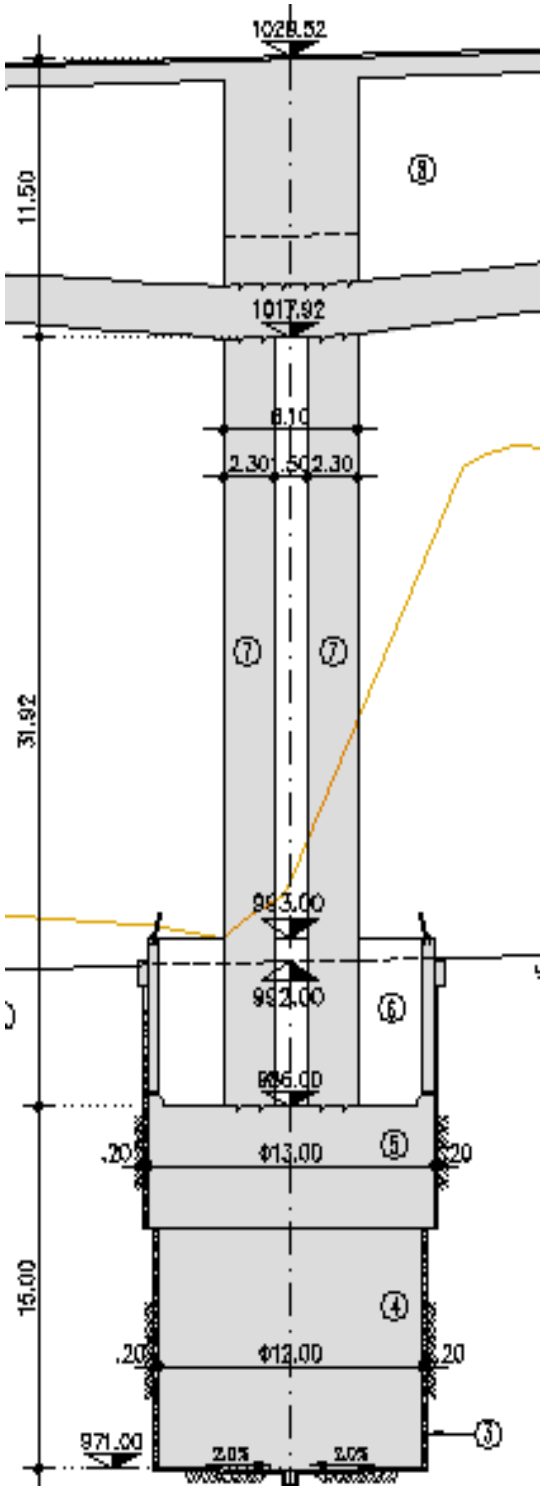

Figure 2.26: Longitudinal view of pier M3

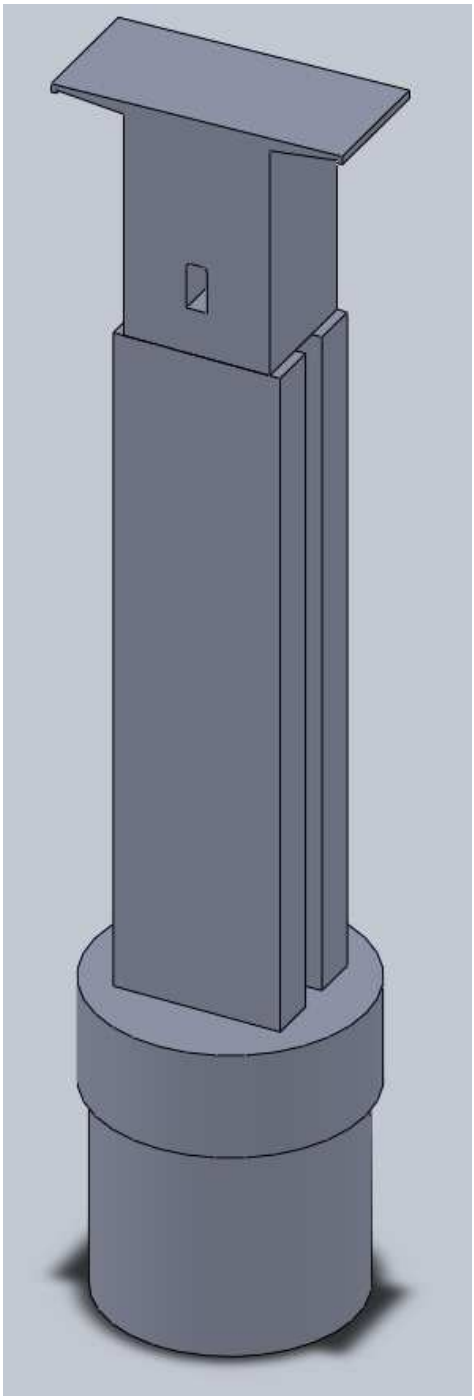

Figure 2.27: Isometric view of the solid model of pier M3 created in Solidworks

2.5 Design of Deck

The deck has a total length of 537.65 m, a constant width of 13.95 m for each carriageway and a constant slope of 2.6% along it. Also the deck has an additional slope across its 168 sections, which varies from 5% at the abutment Ao to 2.5 % at the cross section in distance 85.35 m from abutment Ao and then remains constant and equal to 2.5% until abutment A4. In Figure 2.29 it is shown that the slope in transverse direction changes with rate -0.28 % from abutment Ao (Position: 861.84 m) to distance 60.36 m after abutment Ao (Position: 922.20 m). Then it changes with rate 0.38 % until Position 947.19 m (in distance 85.35 m from abutment Ao). The information about the rate of change in the transverse slopes was derived from the Figure 2.28 that was provided by EGNATIA ODOS S.A.

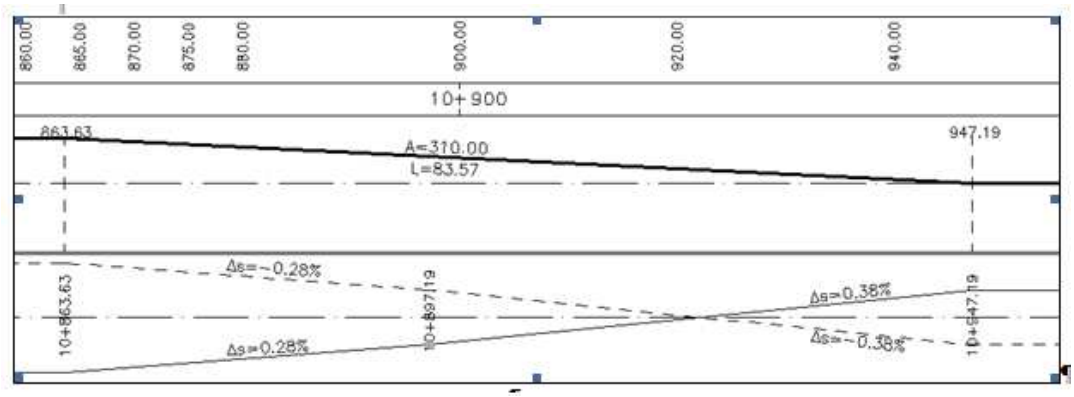

Figure 2.28: Diagram with transverse slopes of deck's cross sections

Another important characteristic of the deck is that it consists of 137 parts and was built with a maximum step of 5 m, containing in total 14 repeated sections. From these sections only one has constant cross section, while all others are varying in height and thickness. This change is shown in the drawings with the cantilevers and the cross sections that are presented below. Also the change in the thickness of the downside of the sections of the bridge resulted in a variable downside of the bridge in a parabolic way while the upside varies linearly with a constant slope of 2.6%. This was shown clearly in Figures 2.2 and 2.3.

The creation of the solid model in Solidworks from the two-dimensional drawings that were provided by EGNATIA ODOS S.A. was conducted as follows. First of all, the deck was divided into 168 sections. For each section the geometry including the height and the width was defined. Then each section was designed as a *Sketch* in Solidworks. The distance between the planes of the sketches was equal to the one that is given in the Diagram with cantilevers, a part of which is shown in Figure 2.29. The Sketches (Figure 2.30) were designed in parallel planes and. Also, the planes were designed in different heights and the difference in height was calculated by multiplying the longitudinal slope (2.6 %) with the distance between the cross sections. Command *Lofted Boss* was then used to join the points of two sections (regardless of whether they were identical or not) filling the intermediate area with solid material. So the *Parts* of the deck,like the one shown in Figure 2.31, were created and command *Mate* was used to create the *Assembly of* the deck by joining all *Parts.*

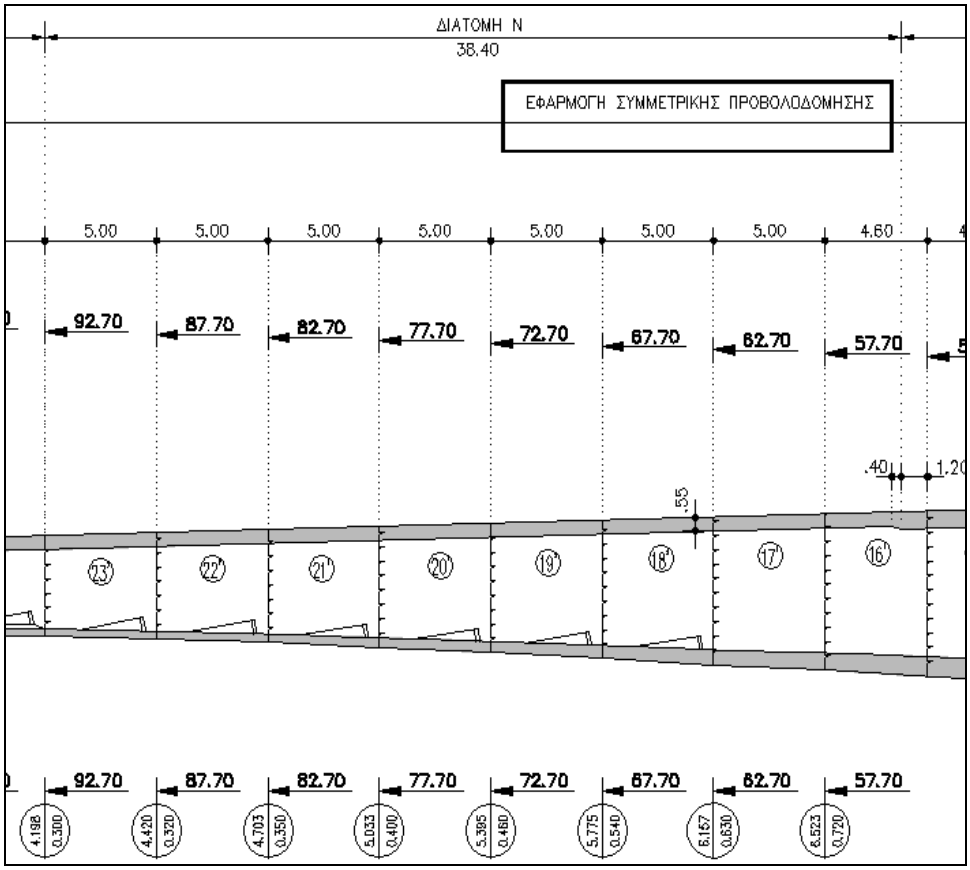

Figure 2.29: Diagram with cantilevers of deck between piers M2 and M3

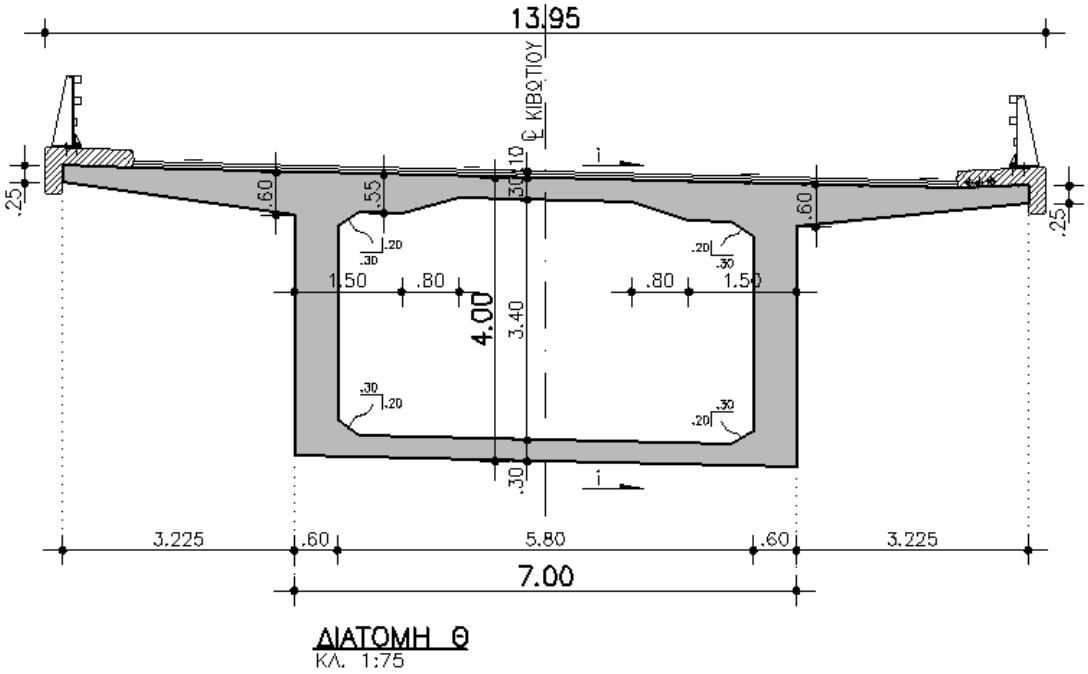

Figure 2.30: Transverse view of cross section Θ

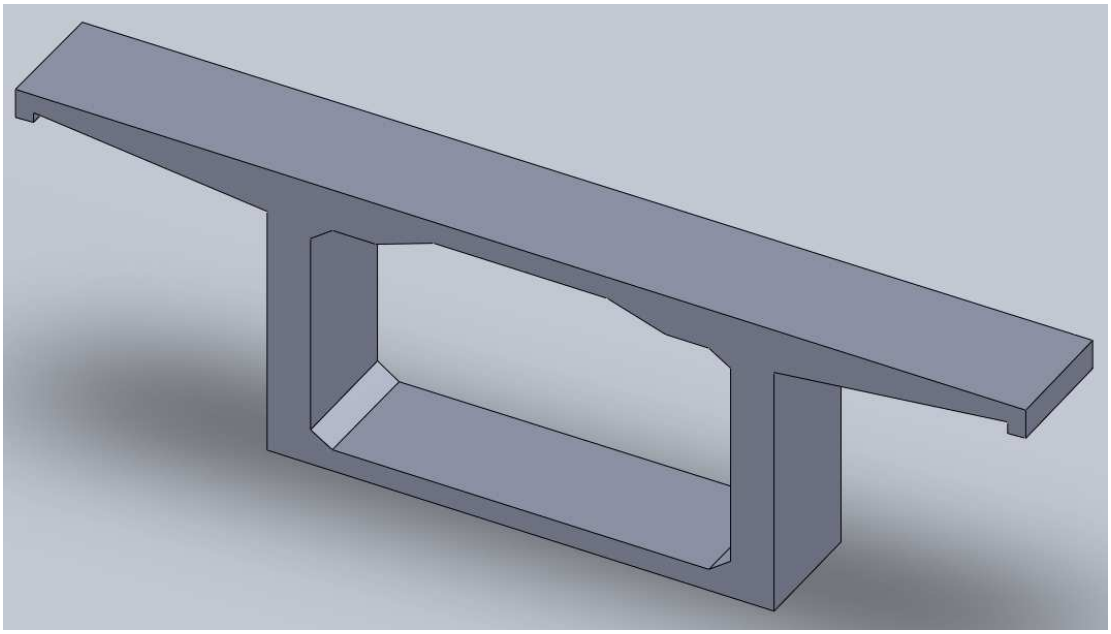

Figure 2.31: Isometric view of cross section Θ at distance 3 m from abutment Ao

The final design product, that resulted from the SolidWorks for the bridge is presented in Figure 2.32 which shows the deck including the abutments Ao and A4 and the piers M1, M2 and M3. Finally the geometry of the two abutments are shown in Figures 2.33-2.38.

Figure 2.32: Isometric view of Metsovo Bridge

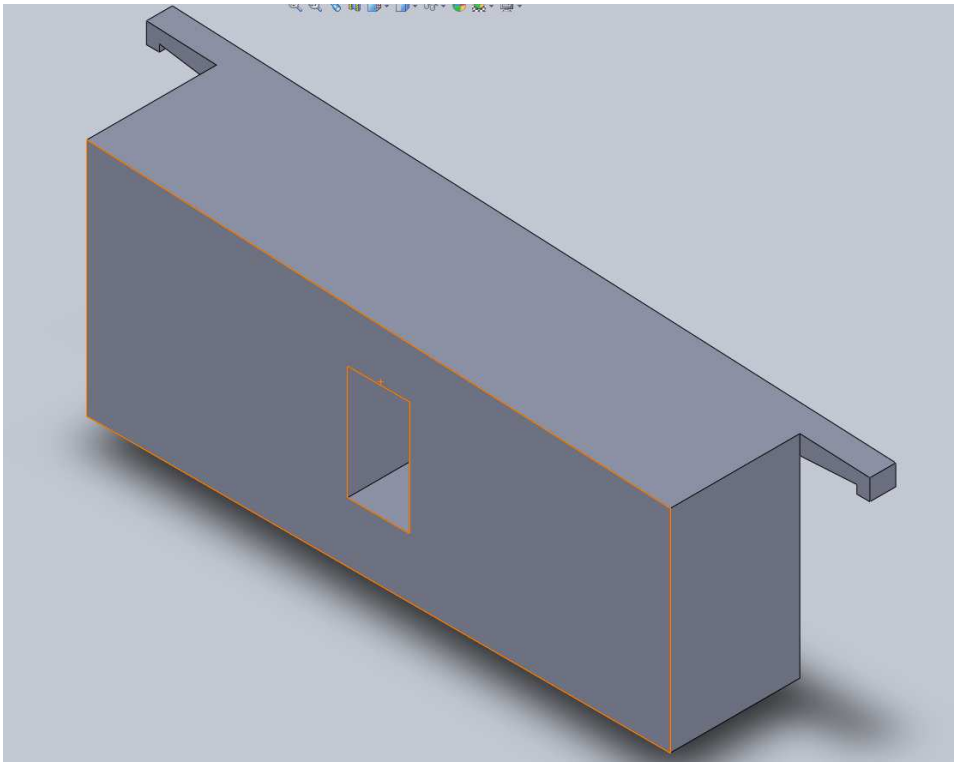

Figure 2.33: Isometric view of Abutment Ao

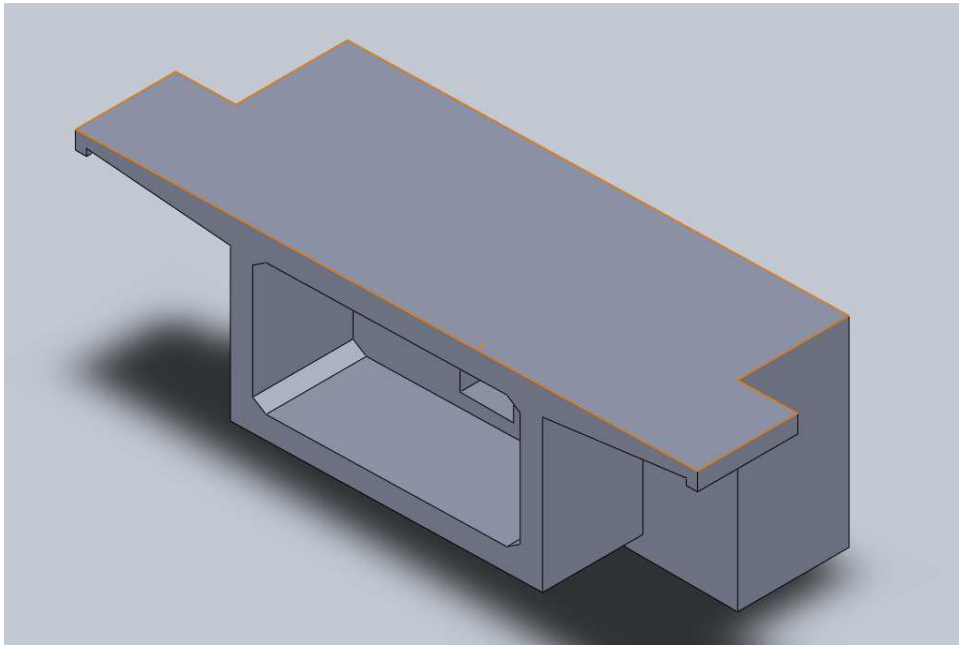

Figure 2.34: Isometric view of Abutment A4

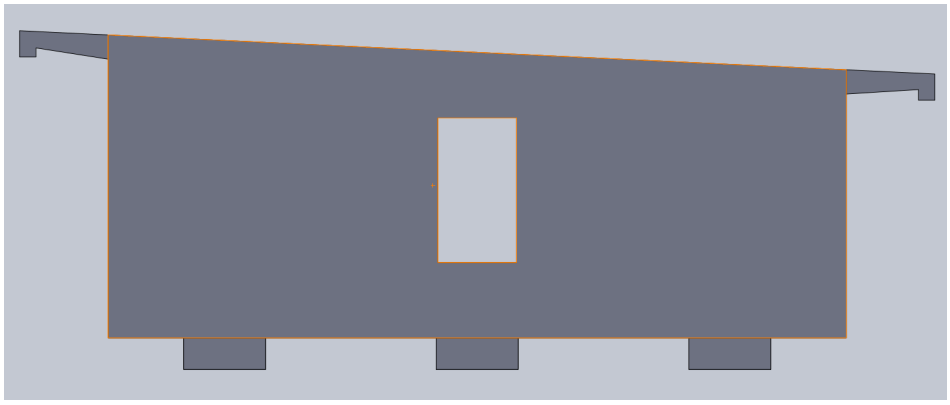

Figure 2.35: Transverse cross section of Abutment Ao

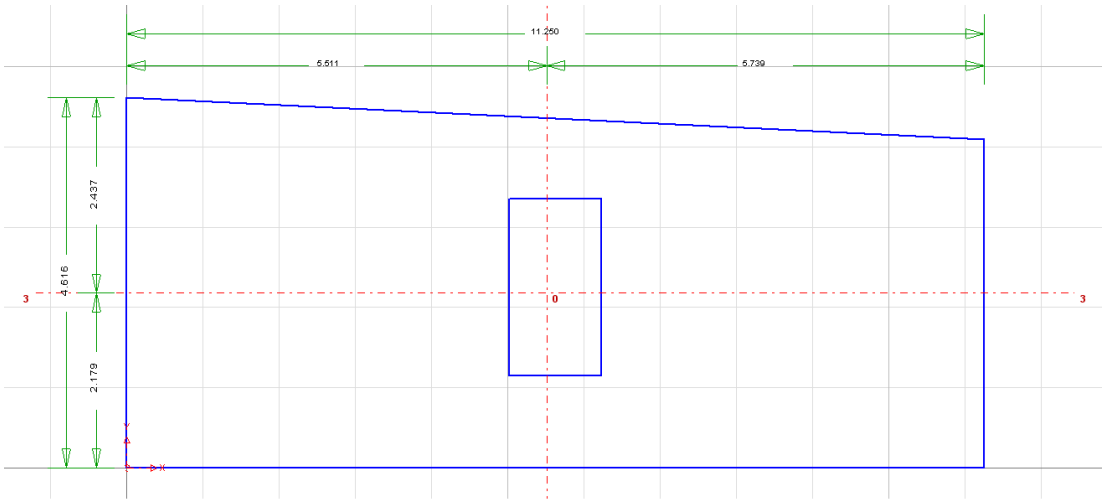

Figure 2.36: Transverse cross section of Abutment Ao in Sketch

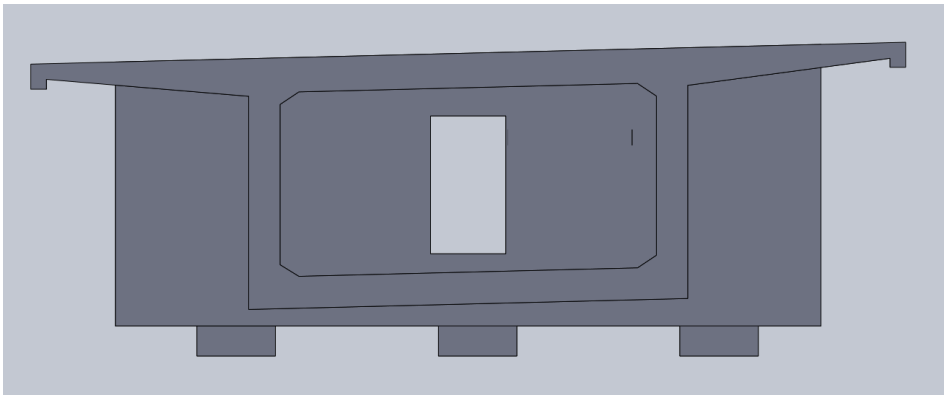

Figure 2.37: Transverse cross section of Abutment A4

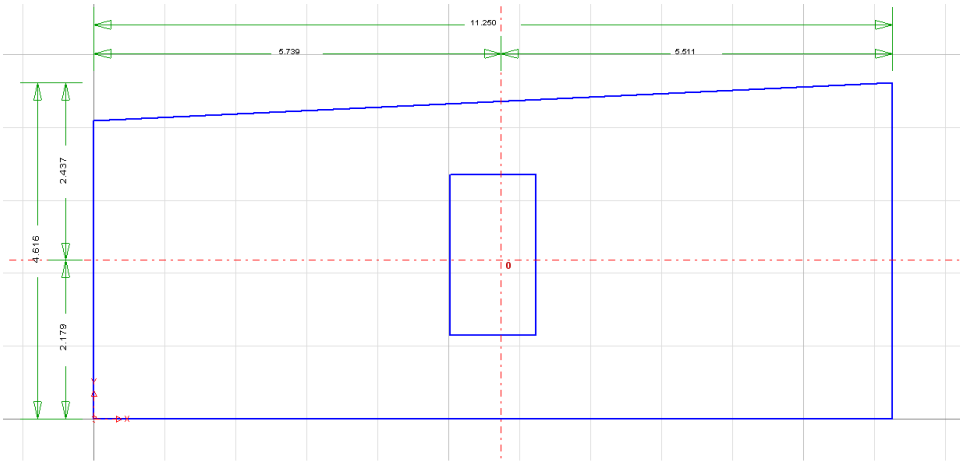

Figure 2.38: Transverse cross section of Abutment A4 in Sketch

2.6 Assumptions for the Creation of the 3-D Solid model of the Bridge

The real geometry of pier M1 is presented in Section 2.2 but during the design of the solid model the following assumption was made [Liokos (2009)]. The bearings were designed on the same level and the underside of the part of deck over the head of pier M1 was designed horizontal. So the transverse slope of the deck at Pier M1 comes only from the transverse slope of the upside of the deck. This assumption is shown clearly in Figure 2.39.

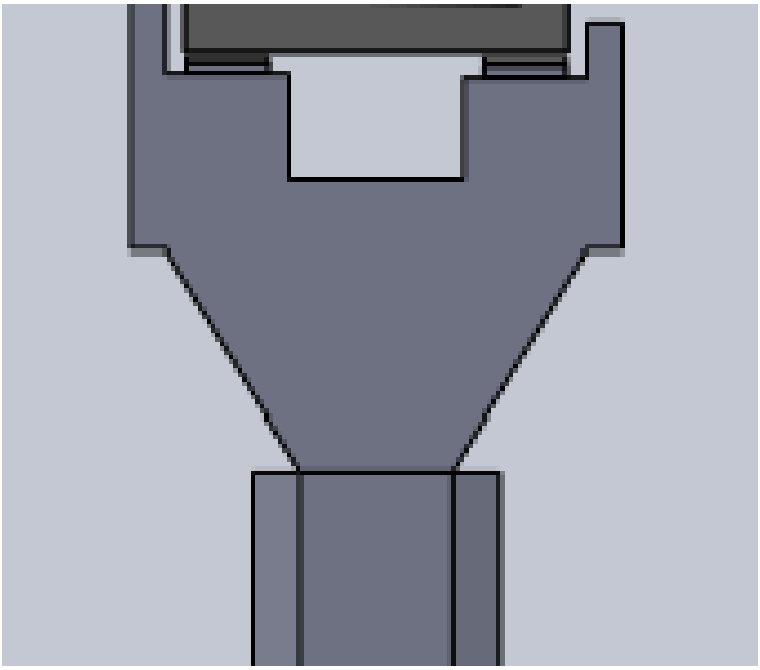

Figure 2.39: Longitudinal cross section of pier M1 that presents the assumption during the creation of the solid model

Also pier M2 has a very complicated geometry and this is the reason that an assumption was made during design again. The real geometry of pier M2 is shown in the following figures and an analysis of the way it was designed is presented. The design of pier M2 was based on Figure 2.40. First of all, the base that is shown in Figure 2.41 was created and then the solid octagonal geometry shown in Figure 2.40. The assumption that was made was the same as in pier M1. The underside of the part of deck over the head of pier M2 was designed horizontal. So the transverse slope of the deck at Pier M2 comes only from the transverse slope of the upside of the deck. For the connection of the deck

and the column at pier M2 an additional intermediate geometry was designed as shown in Figure 2.42.

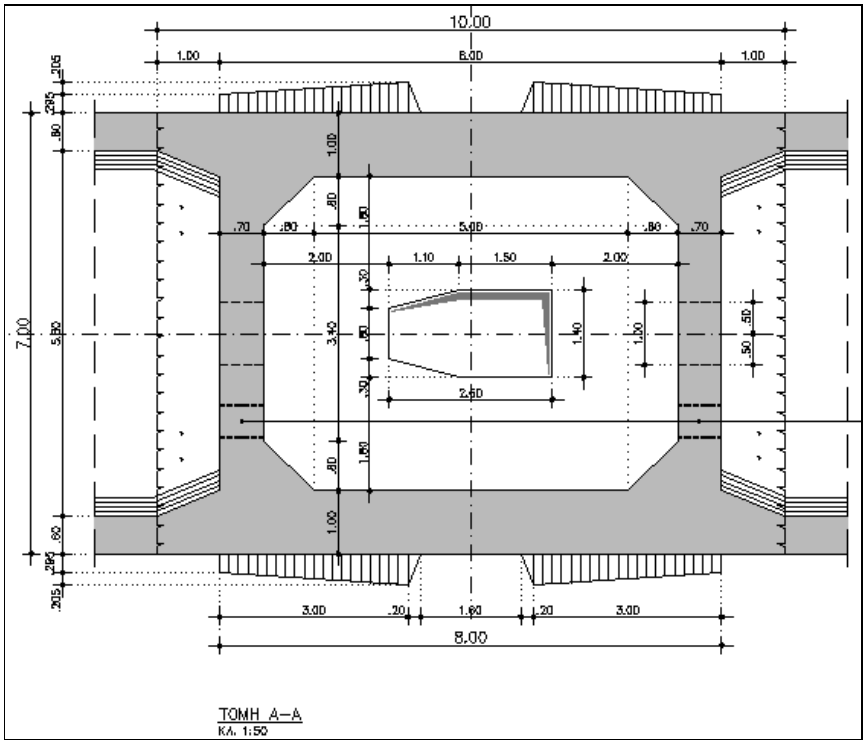

Figure 2.40: Ground Plan of M2's head (section A – A)

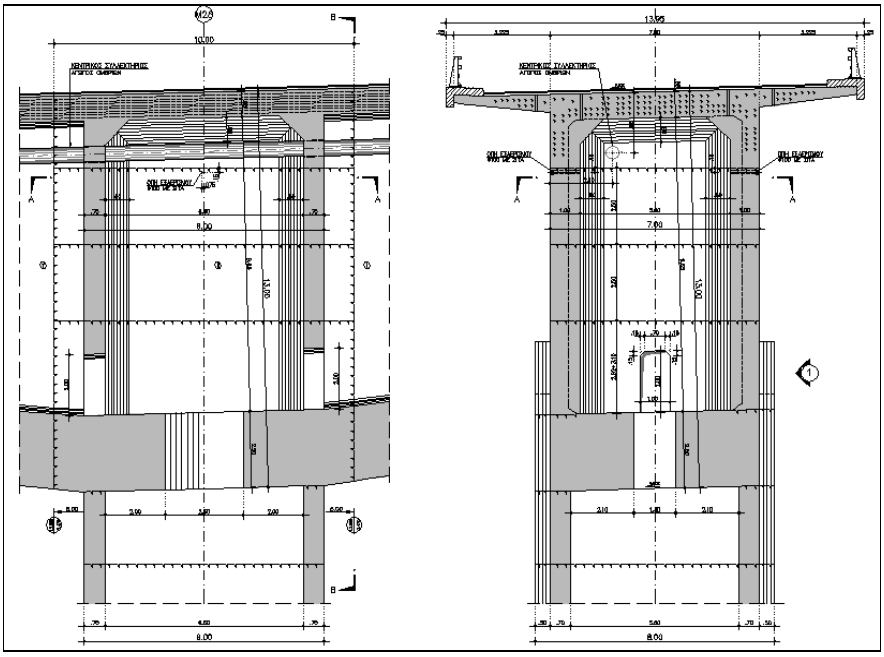

(a) (b)

Figure 2.41: (a)Longitudinal cross section , (b) Transverse cross section

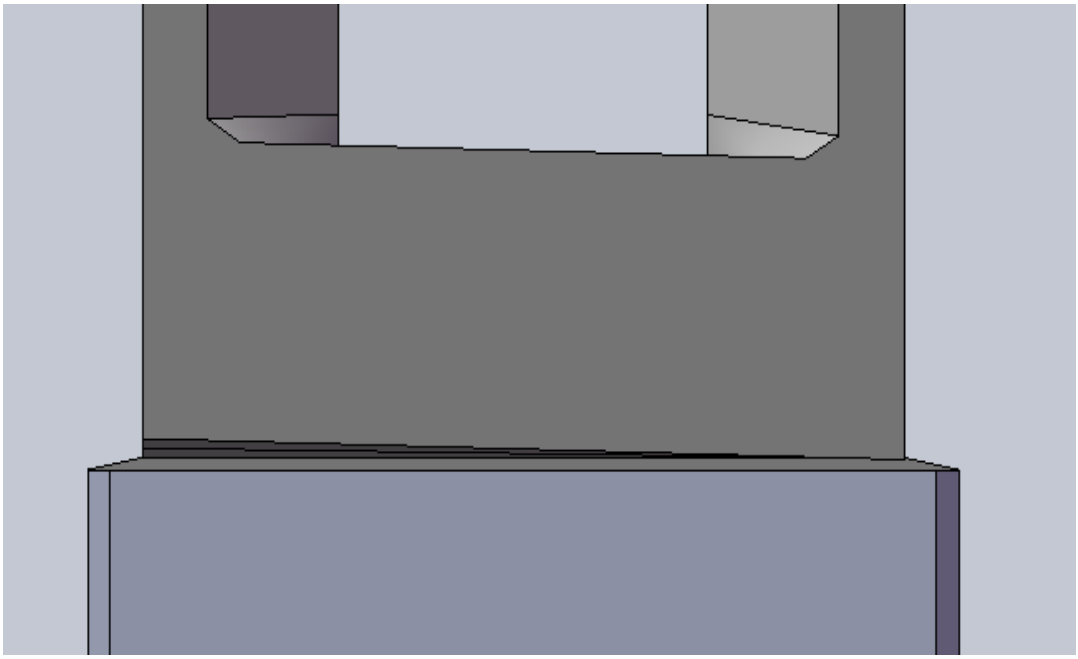

Figure 2.42: Transverse section at the connection of the deck and the column at pier M2 .

This assumption for pier M2 was necessary in order the meshing with finite elements of this assembly in Comsol Multyphysics to be feasible. As a result in the final solid model there exists an additional geometry at the connection of pier M2 and the deck at the pier that joins the two parts but without changing the transverse slope of deck at that point, which is very important.

Finally the geometry of pier M3 was simple enough as it is shown in Section 2.4 and the same assumption as in the other two piers was made.

The above assumptions were made in order for the final solid model to be imported easier to the finite element software Comsol Multyphysics. Moreover, with these assumptions the meshing of the model was better and a lower number of degrees of freedom was achieved. So it is obvious that the analysis time was less and without problems. Finally, it can be said that the simplest the geometry of a solid model is, the better is for the finite element model that is created from it. In any case the design of the solid model must be detailed, something that was absolutely achieved in the case of Metsovo Bridge.

CHAPTER 3

Finite Element Models of Metsovo Bridge

3.1 Finite Element Models of Metsovo Bridge

In order to examine the modal properties of the bridge and the contribution of soil conditions on the dynamic response of the bridge, two different types of finite element models of the bridge were developed to predict the dynamic behavior of the bridge under different construction phases. The first model ignores soil-structure interaction assuming that the bridge is fixed at the foundation bases. The second model considers the effects of soil conditions. In the first model, the bridge was fixed at the base of piers M1, M2 and M3 and at the base of the abutments' bearings. In the second model, the soil under the piers was also simulated by assuming that the foundations are embedded in cylindrical bodies with diameters and height six times higher than the equivalent diameter of the piers' foundation, creating a flexibly supported model of the bridge simulating the behaviour of the subsoil. Also two different construction phases of the bridge were examined: the "M3 Cantilever" construction phase and the completed phase of the bridge.

For bridge modeling, the software package COMSOL Multiphysics was used. The structure was first designed in CAD environment and specifically in Solidworks, as it was described in detail in Chapter 2. Then it was imported in COMSOL Multiphysics modelling environment. COMSOL Multiphysics was preferred among Abaqus and Femtools, because it gave us the opportunity to carry out the finite element model updating, which is presented in Chapter 5, using methods and algorithms that have been developed in the System Dynamics Laboratory of the Mechanical Engineering Department (University of Thessaly).

The models were constructed based on the structural and soil material properties and the geometric details of the structure. After the model was imported in COMSOL Multiphysics, the following process was followed for the dynamic analysis of the bridge. First of all, the boundary conditions were defined with the command *Boundary Settings*

from the group *Physics*. The COMSOL Multiphysics gives the user the ability to define on which parts of the structure a kinematic constraint is imposed and the kind of the constraint. Moreover it gives the user the ability to define the loads that are imposed on a structure. More specifically, in the case of Metsovo bridge the bridge was fixed at the base of piers M1, M2 and M3 and at the base of the abutments' bearings. The other parts of the bridge were set free.

Then the material properties of the components of the bridge were defined through the command *Subdomain Settings* from the group *Physics.* The COMSOL Multiphysics gives the user the ability to define the material properties of a component by loading them from a library or by defining them manually. The Metsovo Bridge is constructed of reinforced concrete. So material "concrete" was loaded from the material library but with the following changes: the density was defined 2548 kg/m^3 and the modulus of Elasticity E was chosen 37 GPa for the deck and 34 GPa for the rest components according to the drawings that we were provided by EGNATIA ODOS S.A.

The final step of the preparation of the model for the analysis was the meshing. The solid model was meshed through the command *Mesh.* In a 3D geometry, COMSOL Multiphysics is possible to create a free mesh containing tetrahedral elements or a swept mesh containing prism elements or hexahedral elements. In the case of Metsovo bridge the free mesh was chosen by selecting from the Mesh menu the option Free Mesh Parameters. With the mesh parameters one can specify the local mesh element sizes and control the element distribution. All mesh parameters aim at prescribing the maximum allowed mesh element size. This means that the size of a mesh element must not be larger than the minimum prescribed local element size determined by all mesh parameters. There is also the choice to select a predefined mesh size that automatically determines the mesh parameters. A predefined mesh size can generate an extremely fine, extra fine, finer, fine, normal, coarse, coarser, extra coarse, or extremely coarse mesh. In order to examine the impact of the density of mesh on the accuracy of the results of the analysis the finite element model of the completed bridge with the soil under the piers (Figure 3.1) was analyzed with different types of mesh.

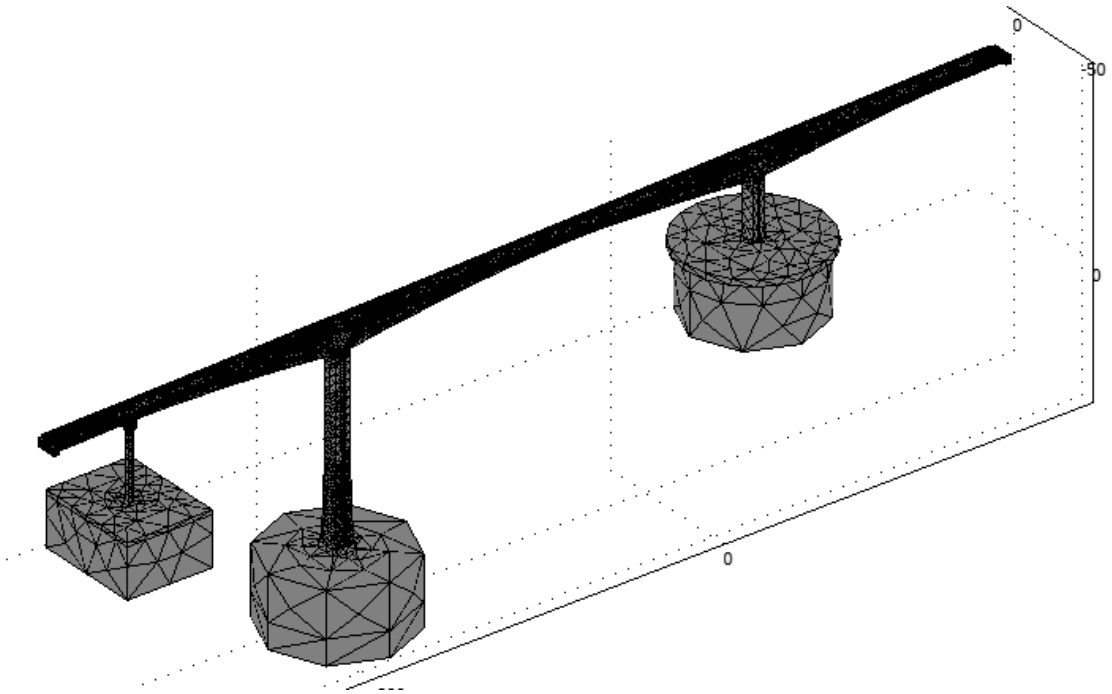

Figure 3.1: Finite Element Model of bridge with soil meshed with extra coarse mesh

Table 3.1 presents the number of degrees of freedom (DOF) and finite elements that were used in each mesh type. It is shown that number of DOFs varies from 573.372 for the extra coarse mesh to 2.347.786 for the fine mesh. It is a fact that the larger the number of DOFs is, the more time consuming the analysis is. So it is preferable to choose a coarser mesh but under the condition that it does not affect the accuracy of the results. Due to space limitations, twenty of the identified modal frequencies are presented in Table 3.2 and only the error between fine and extra coarse mesh are calculated. It can be seen from the results in Table 3.2 that the error due to a coarser mesh type varies from 0.22% (1st Mode) to 2.22% (18th Mode). The average error is 0.59% and is obvious that it can be ignored since it does not affect the accuracy of the results.

Table 3.1: Number of DOF and elements for each mesh type

Mesh Type	Extra Coarse	Coarser	Coarse	Normal	Fine
No of DOF	573.372	844.614	1.169.091	1.729.374	2.347.786
No of elements	99.787	148.700	208.578	315.778	436.340

Table 3.2: Error due to coarser mesh type

No of Mode	Mesh Type				Error (%) Between Fine and Extra Coarse Mesh
	Extra Coarse	Coarse	Normal	Fine	
1	0.3133	0.3126	0.3122	0.3122	0.35
2	0.6034	0.6014	0.6004	0.6004	0.50
3	0.6337	0.6314	0.6297	0.6297	0.63
4	0.9616	0.9579	0.9552	0.9552	0.67
5	1.081	1.078	1.076	1.076	0.46
6	1.131	1.127	1.125	1.125	0.53
7	1.458	1.454	1.451	1.451	0.48
8	1.644	1.639	1.636	1.636	0.49
9	1.861	1.858	1.856	1.856	0.27
10	2.226	2.215	2.209	2.209	0.76
11	2.259	2.253	2.249	2.249	0.44
12	2.492	2.481	2.475	2.475	0.68
13	2.732	2.729	2.726	2.726	0.22
14	3.006	2.999	2.995	2.995	0.37
15	3.046	3.037	3.030	3.030	0.53
16	3.492	3.482	3.475	3.475	0.49
17	3.784	3.776	3.772	3.772	0.32
18	3.891	3.828	3.804	3.804	2.24
19	4.294	4.285	4.280	4.280	0.33
20	4.361	4.326	4.312	4.312	1.12

The maximum error is observed at 18th mode (3.891 Hz) which is a pure bending mode with intensive local bending of pier M1 as shown in Figure 3.2.

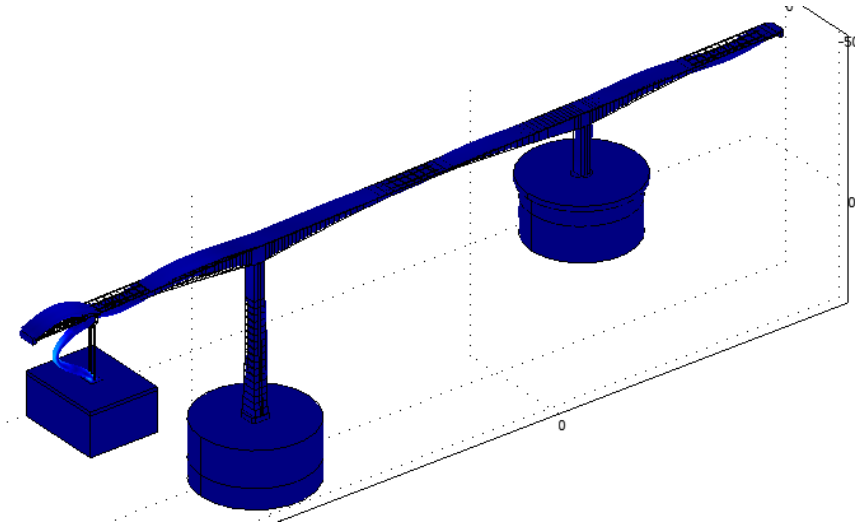

Figure 3.2: The 18th mode of Finite Element Model of bridge with soil

As a result of the above conclusions, the finite element models for the bridge were created using three dimensional tetrahedron solid finite elements to model the whole structure with extra coarse mesh. Finite element models were developed for both the left and right branch of the bridge. Since the two branches have almost the same geometry, details for the model are presented in Sections 3.2 and 3.3 for the left branch. The construction of this branch was completed first and a permanent monitoring system has been placed on it after completion of its construction, to monitor its behavior under wind, traffic and earthquake loads. The system consists of 12 acceleration sensors, 16 strain sensors, 12 temperature sensors and one wind velocity sensor. The data are collected remotely through internet connection. In addition, monitoring during the construction phases of the bridge was also performed using a mobile system of six acceleration sensors.

Section 3.2 presents the fixed base model and the flexibly supported model for the “M3 Cantilever” construction phase of the bridge, while Section 3.3 presents the fixed base model and the flexibly supported model for the complete bridge. Also, in Sections 3.2 and 3.3 the modal properties predicted by the finite element models are compared to those identified using vibration measurements from the mobile monitoring system. Finally, in Section 3.4 the modal properties predicted for the two branches are compared to each other to identify similarities in the dynamic characteristics of the two branches since these two branches are geometrically similar.

3.2 Finite Element Model for Construction Phase: “M3 Cantilever”

This phase corresponds to the pier M3 balanced cantilever (Figure 3.3) that has been instrumented after the construction of all its segments and before the construction of the key segment that joins with the balanced cantilever of pier M2. At this state the total length of M3 cantilever was 215m while its total height was 35m. Moreover the same number of segments were completed on both sides of pier M3 (26 parts of deck on each side) due to the symmetry of the construction method (balanced cantilevering). Also at the time of data collection, two trucks, as shown in Figure 3.3, of total mass 85t, were located at the two edges, each one supported the edge parts of each side. In the bridge finite element modeling, this amount of mass was distributed to the last two parts.

Figure 3.3: M3 Cantilever construction phase on 9/7/2007

For this construction phase the first detailed finite element model was constructed. The mass of the two trucks was simulated by changing the density for the last two parts that were supported from 2548 kg/m^3, that was taken for the other parts, to 3876,9 kg/m^3. The modulus of Elasticity E was chosen 37 GPa for the deck and 34 GPa for pier

M3. Also cantilever M3 was fixed at the base of pier M3 and no other kinematic constraints were imposed on the remaining components. Then the model was meshed with extra coarse mesh. So, the fixed base model shown in Figure 3.4 consists of 33.402 finite elements and has 195.120 DOF.

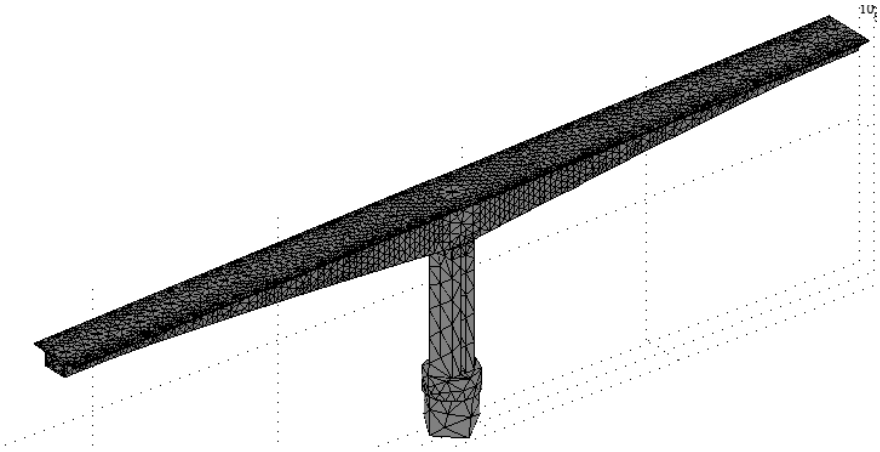

Figure 3.4: Fixed base Finite Element Model of “M3 Cantilever”

In order to examine the contribution of soil conditions on the dynamic response of the cantilever portion of the bridge, a flexibly supported finite element model of the cantilever was developed to predict the dynamic behavior. While the first model ignores soil-structure interaction assuming that the bridge is fixed at the foundation base of pier M3, the second model shown in Figure 3.5 considers the effects of soil conditions.

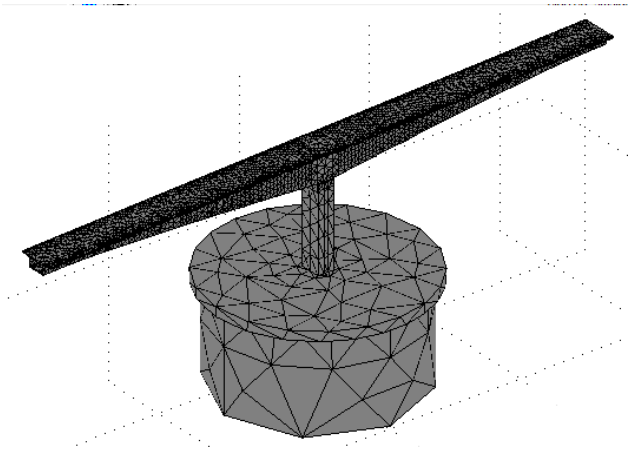

Figure 3.5: Flexibly supported Finite Element Model of “M3 Cantilever”

In Figure 3.5 it is shown that in the second model, the soil under the piers was also simulated by assuming that the foundation of pier is embedded in a cylindrical body with diameter and height six times higher than the equivalent diameter of the pier's foundation, creating a flexibly supported model of the bridge simulating approximately the behaviour of the subsoil [Panetsos et al. (2010)]. Specifically, the pier's base consists of two cylinders with diameter 12 and 13 meters each one (Ø12,0m and Ø13,0m respectively) and soil was simulated with two cylindrical bodies with diameter 72 and 78 meters, respectively. The material properties of the deck and pier M3 were taken the same with the properties of the fixed base model and for soil the modulus of elasticity E was chosen 2880 MPa while for specific gravity γ =25 KN/m^3 the density was calculated to be 2548 kg/m^3. Then the model was meshed with extra coarse mesh and the flexibly supported model consists of 34.654 finite elements and has 200.631 degrees of freedom.

The lowest modal frequencies of the left branch of the "M3 Cantilever" construction phase of the bridge, predicted by the design (nominal) FE models, are reported in Table 3.3. In Table 3.3, the modal frequencies predicted by the design (nominal) FE models are compared to those identified using vibration measurements. The measured modal characteristics were estimated using the Modal Identification Toolbox (MI-Tool) developed by the System Dynamics Laboratory in the University of Thessaly. The identification of the modal properties was conducted using measurement data collected from a 6-acceleration sensors mobile monitoring system on 22/11/2007. Specifically, six uniaxial accelerometers were installed inside the box beam cantilever M3 of the left carriageway of Metsovo ravine bridge. Due to the symmetry of the construction method (balanced cantilevering) and as the same number of segments were completed on both sides of pier M3, the instrumentation was limited to the right cantilever of pier M3 along the vertical, transverse and longitudinal directions. It should be noted that the recorded responses are mainly due to wind loads and loads induced by construction activities, such as the crossing of light vehicles, placing the prestressing cables inside the tendon tubes, etc.

Table 3.3: Modes of left branch of "M3 Cantilever" construction phase

No	Type of Mode	Measured Properties		FEM (fixed base)	FEM (with soil)	Fixed vs with soil
		Frequency Hz	Damping ζ%	Modal frequencies	Modal frequencies	% difference
1	Pure torsion of column	0.159	1.06	0.155	0.158	-1.94
2	1st pure bending of column	0.305	0.48	0.280	0.283	-1.08
3	1st transverse and bending of column in transverse direction	0.623	0.61	0.570	0.553	3.07
4	2nd bending of column and deck deformation	0.686	0.38	0.639	0.640	-0.16
5	3rd bending of deck without deck deformation	0.908	0.59	0.858	0.822	4.20
6	2nd transverse and deck deformation in opposite direction of transverse	1.31	1.28	1.27	1.23	3.14
7	3rd transverse	1.46	0.87	-	-	
8	4th bending and column deformation	2.29	0.41	2.19	2.12	3.20
9	4th transverse and column slightly deformed	2.38	1.29	2.43	2.33	4.12
10	bending	3.24	0.32	3.14	3.00	4.66
11	transverse	4.63	0.35	4.36	4.19	3.90
12	1st rotational, x axis	4.94	0.61	5.01	4.80	4.19

It can be seen from the results in Table 3.3 that soil contribution varies from 0.16% (4th Mode) to 4.66% (10th Mode). The average soil contribution is 3.06% and is obvious that the effect of soil-structure interaction on dynamic response of Metsovo Bridge cannot be ignored. Also, it is obvious that modal frequencies predicted by the Cantilever model including the contribution of soil are, as expected, lower than the ones for the fixed base Cantilever. Finally representative mode shapes predicted by the fixed base finite element model are also shown in Figure 3.6.

"1st Mode" (0.155 Hz)

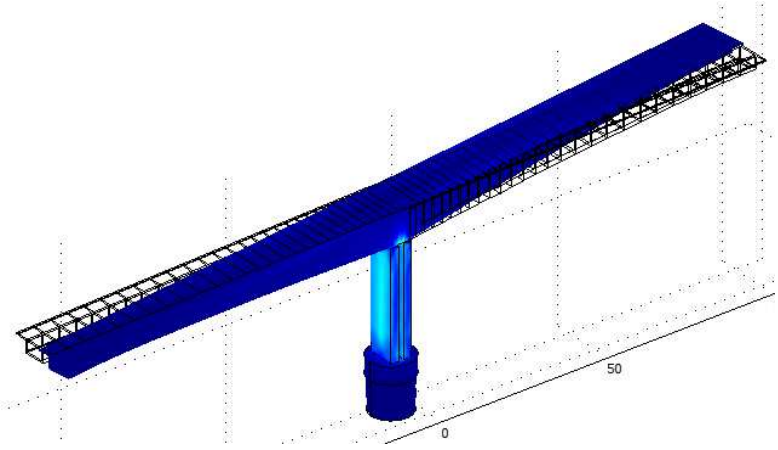

Isometric View

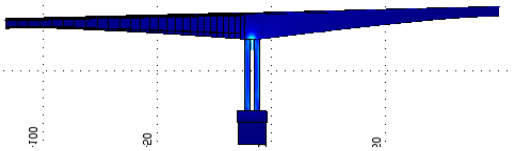

Side View

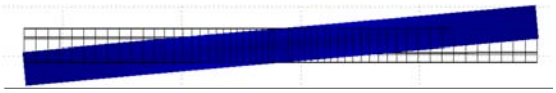

Top View

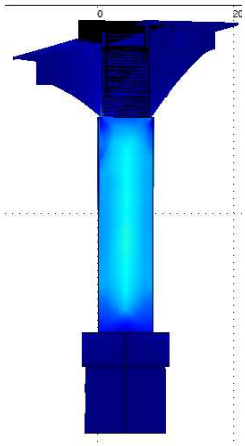

Front View

Figure 3.6: The first 12 mode shapes of "M3 Cantilever" predicted by the fixed base finite element model

"2nd Mode" (0.279 Hz)

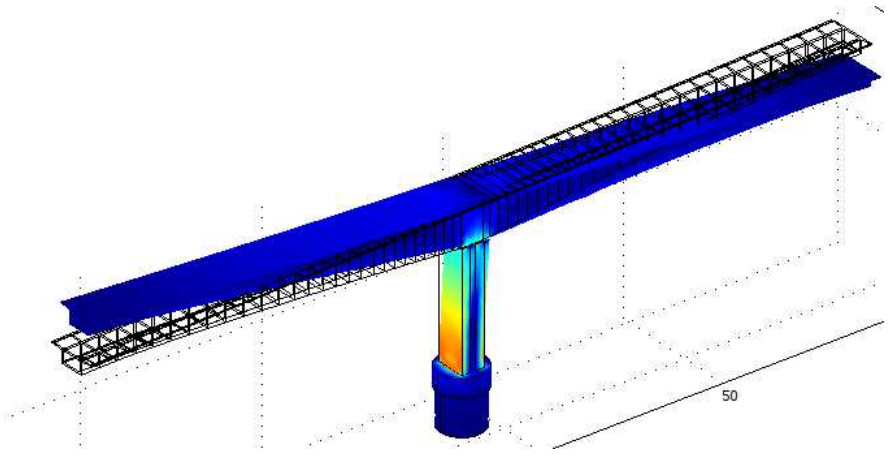

Isometric View

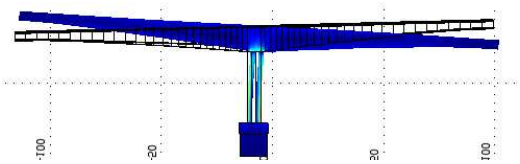

Side View

Top View

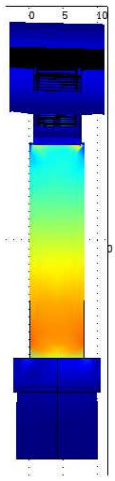

Front View

Figure 3.6: The first 12 mode shapes of "M3 Cantilever" predicted by the fixed base finite element model

"3rd Mode" (0.570 Hz)

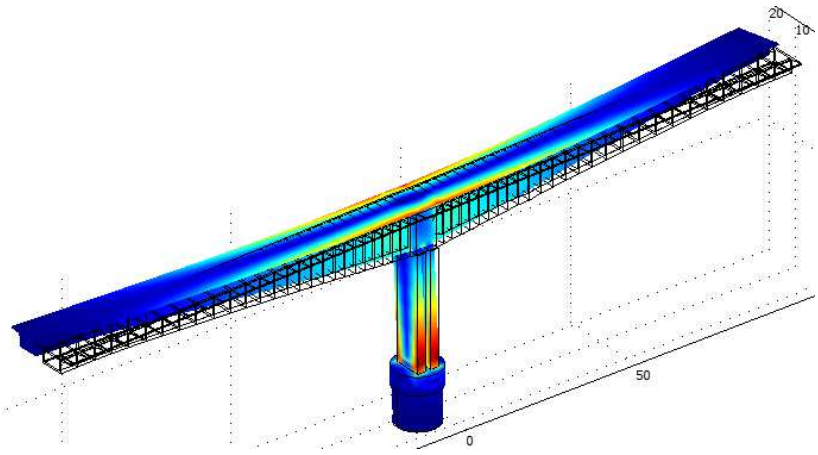

Isometric View

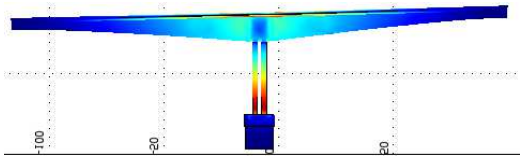

Side View

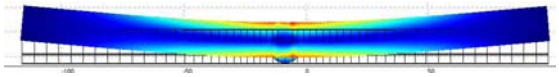

Top View

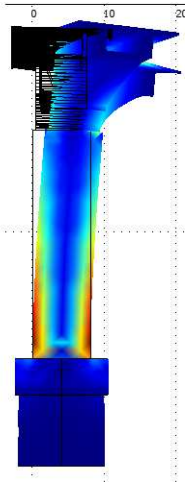

Front View

Figure 3.6: The first 12 mode shapes of "M3 Cantilever" predicted by the fixed base finite element model

"4th Mode" (0.639 Hz)

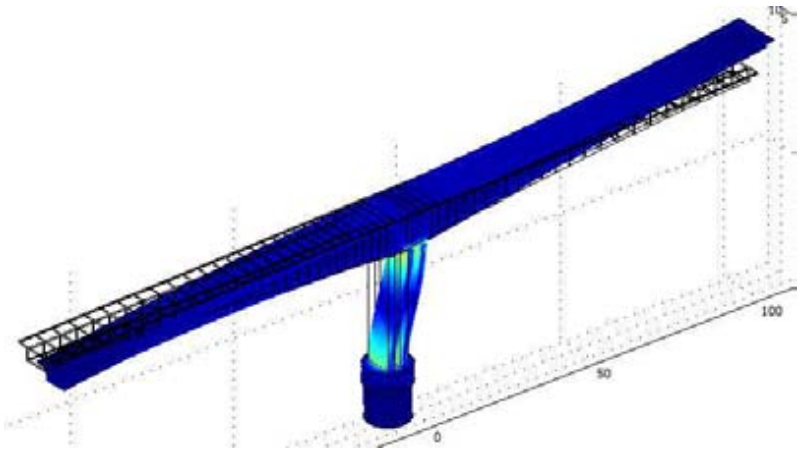

Isometric View

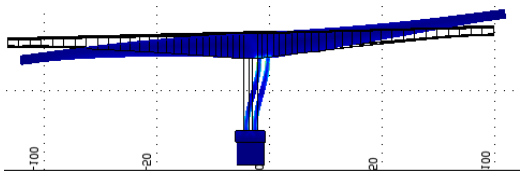

Side View

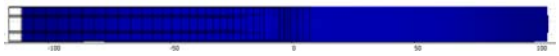

Top View

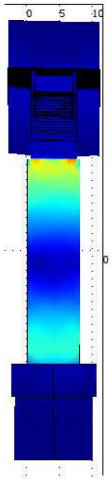

Front View

Figure 3.6: The first 12 mode shapes of "M3 Cantilever" predicted by the fixed base finite element model

"5th Mode" (0.857 Hz)

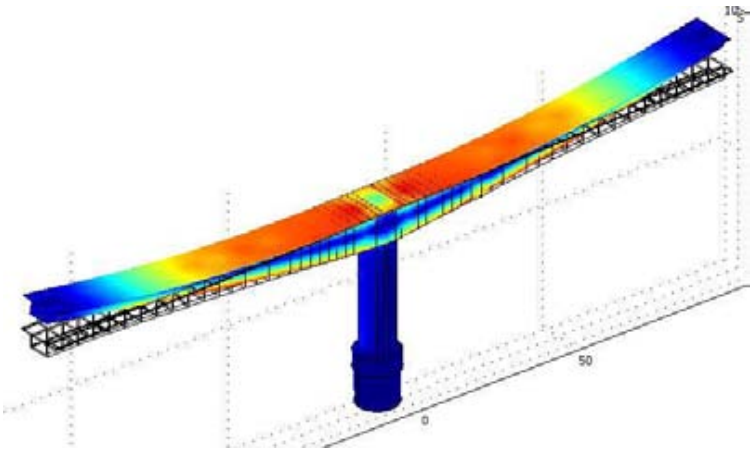

Isometric View

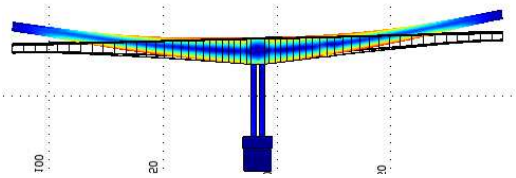

Side View

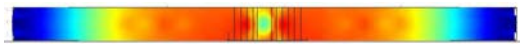

Top View

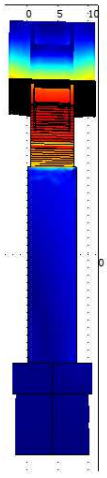

Front View

Figure 3.6: The first 12 mode shapes of "M3 Cantilever" predicted by the fixed base finite element model

"6th Mode" (1.274 Hz)

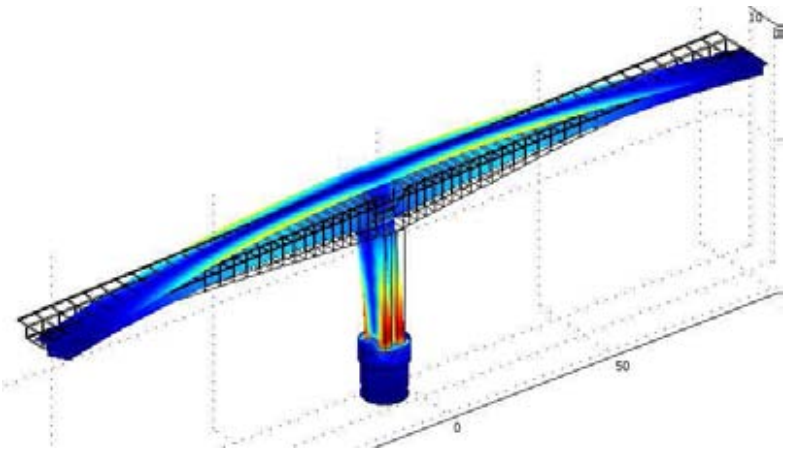

Isometric View

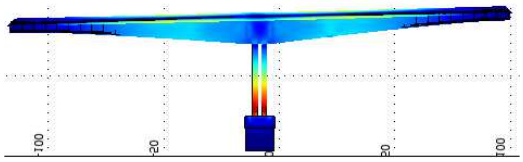

Side View

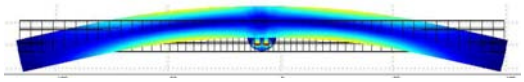

Top View

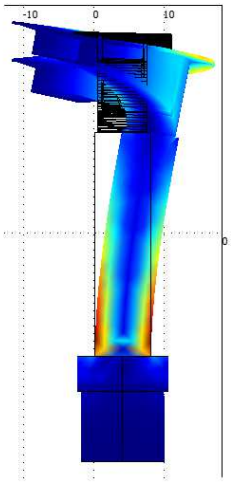

Front View

Figure 3.6: The first 12 mode shapes of "M3 Cantilever" predicted by the fixed base finite element model

“8th Mode” (2.194 Hz)

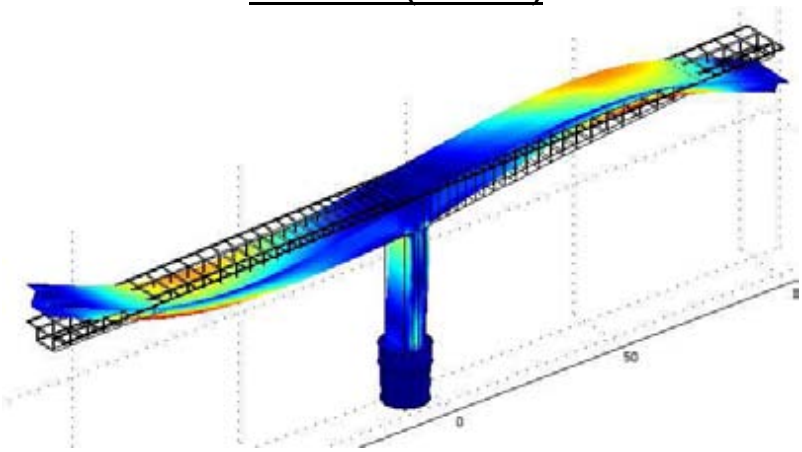

Isometric View

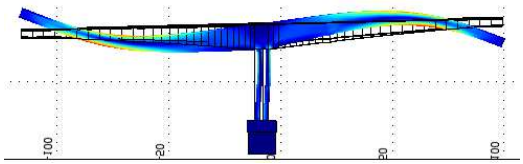

Side View

Top View

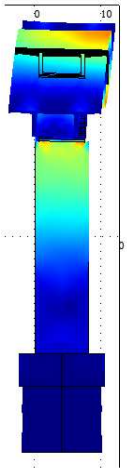

Front View

Figure 3.6: The first 12 mode shapes of “M3 Cantilever” predicted by the fixed base finite element model

“9th Mode” (2.429 Hz)

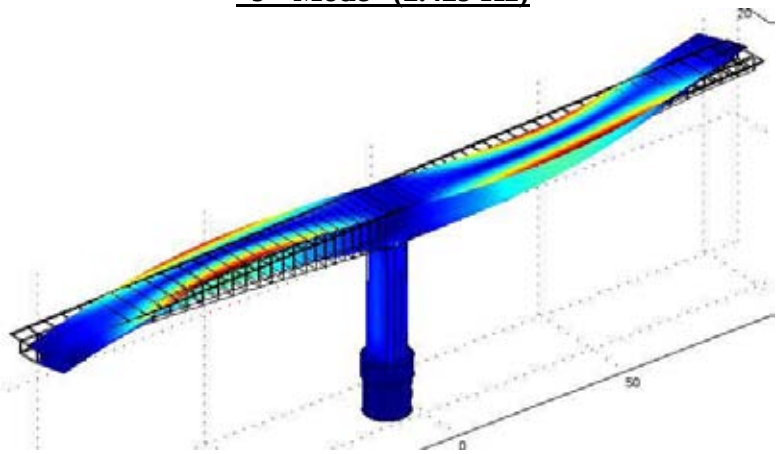

Isometric View

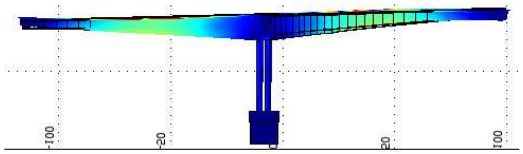

Side View

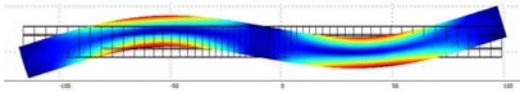

Top View

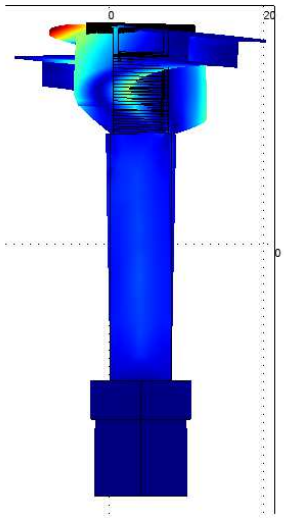

Front View

Figure 3.6: The first 12 mode shapes of “M3 Cantilever” predicted by the fixed base finite element model

“10th Mode” (3.132 Hz)

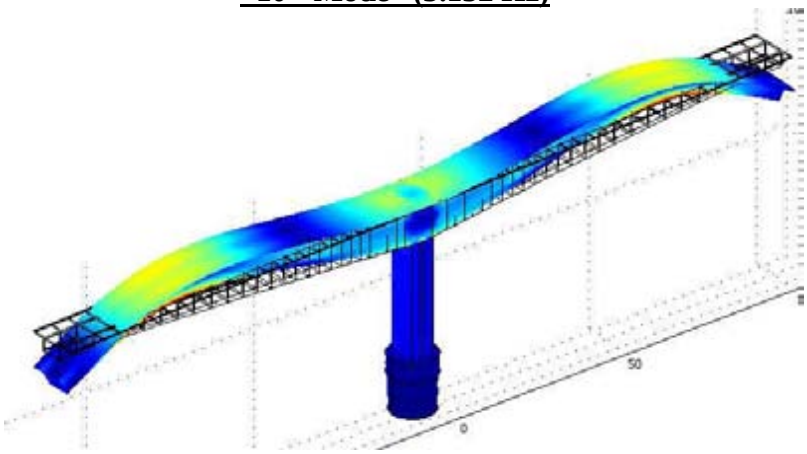

Isometric View

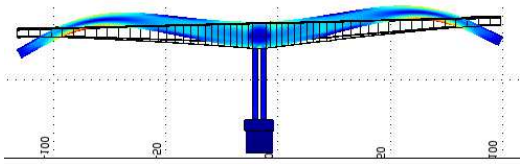

Side View

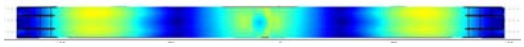

Top View

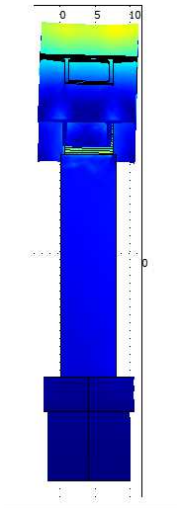

Front View

Figure 3.6: The first 12 mode shapes of “M3 Cantilever” predicted by the fixed base finite element model

“11th Mode” (4.366 Hz)

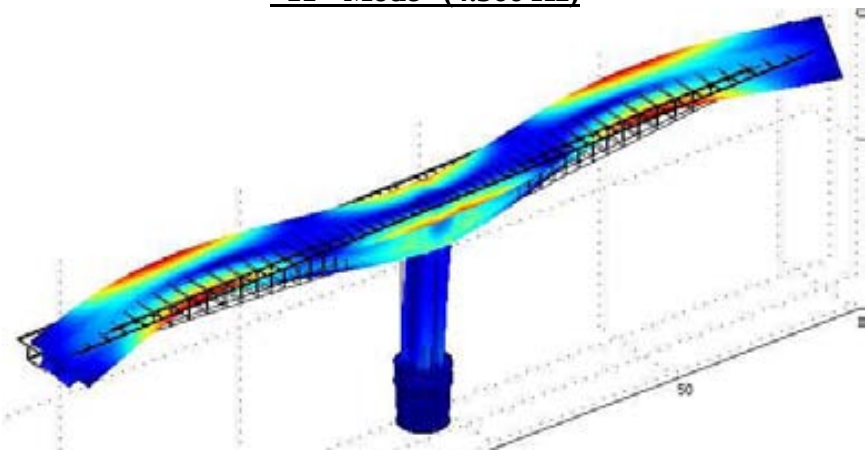

Isometric View

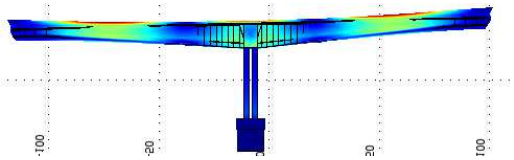

Side View

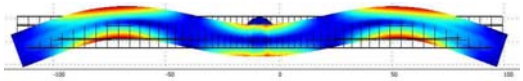

Top View

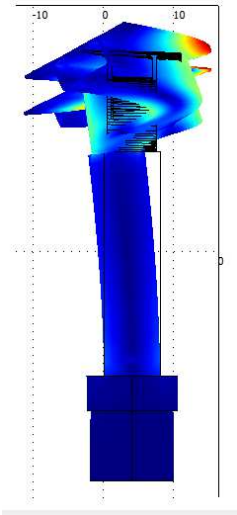

Front View

Figure 3.6: The first 12 mode shapes of “M3 Cantilever” predicted by the fixed base finite element model

“12th Mode” (5.006 Hz)

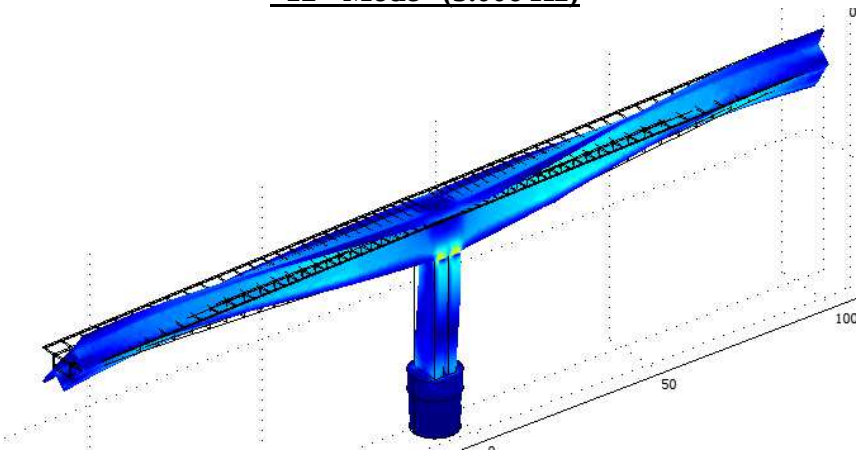

Isometric View

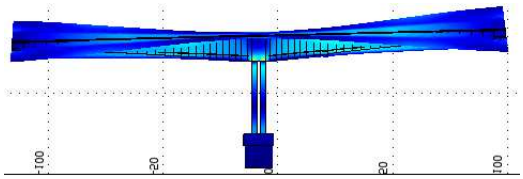

Side View

Top View

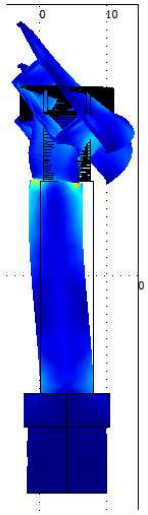

Front View

Figure 3.6: The first 12 mode shapes of “M3 Cantilever” predicted by the fixed base finite element model

In Figure 3.6 the first 12 mode shapes of “M3 Cantilever” are presented only for the fixed base model because although the modal frequencies predicted by the fixed base model are slightly higher than those predicted by the model simulating the effects of soil, the mode shapes predicted by the two models are identical. This is evident in Figure 3.7 by comparing a representative bending and a representative transverse mode shape of “M3 Cantilever” predicted by the two models.

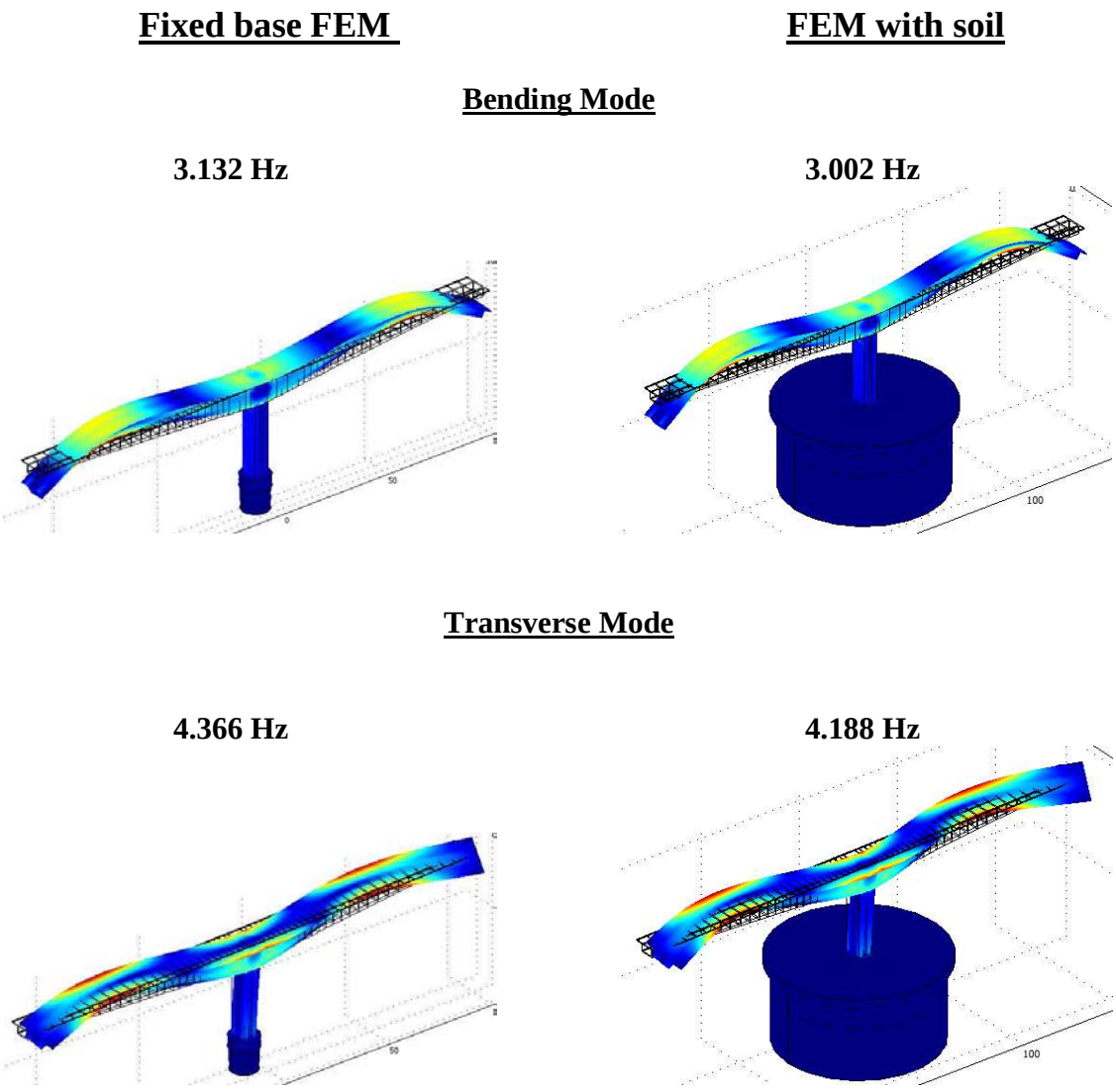

Figure 3.7: Representative bending and transverse mode shapes of “M3 Cantilever” predicted by the fixed base and the flexibly supported model

Finally, in Figure 3.8 the first ten mode shapes identified with MI-Tool are compared to those predicted by the fixed base finite element model.

"1st Mode" (0.155 Hz)

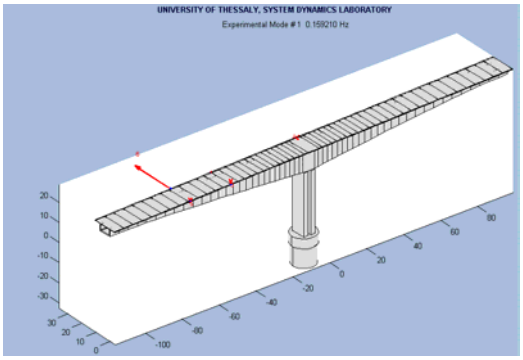

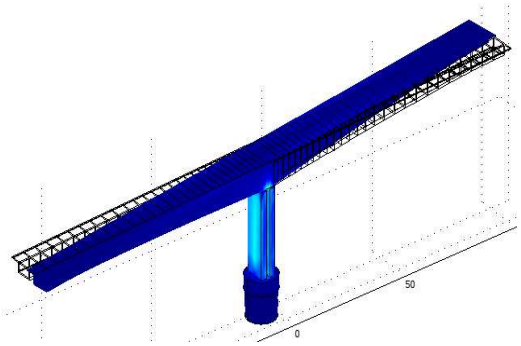

"2nd Mode" (0.279 Hz)

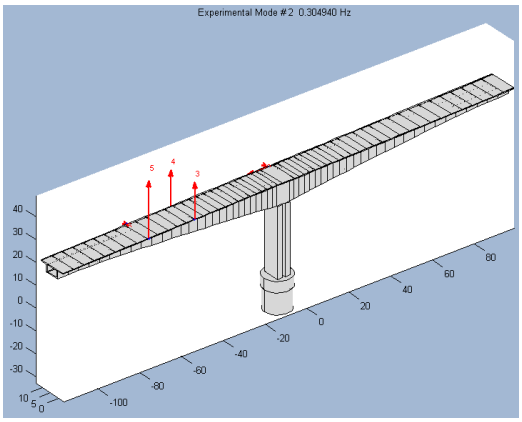

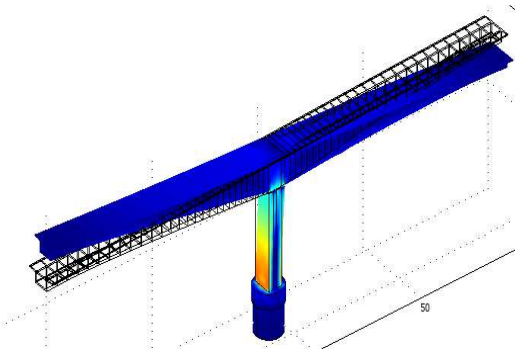

"3rd Mode" (0.571 Hz)

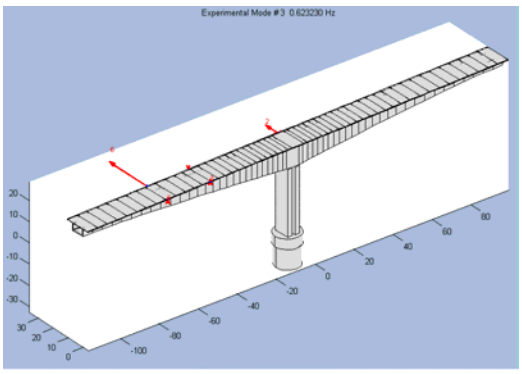

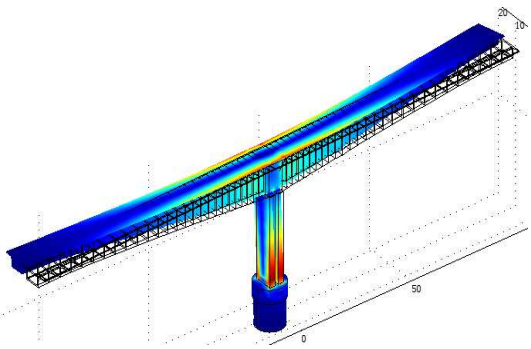

“4th Mode” (0.639 Hz)

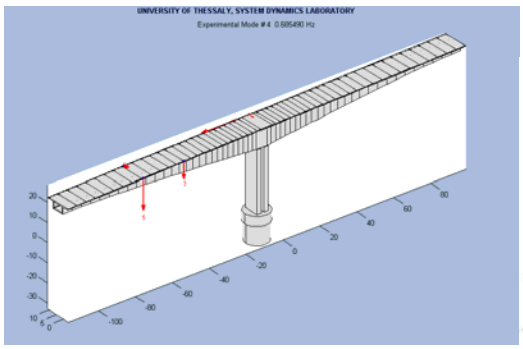

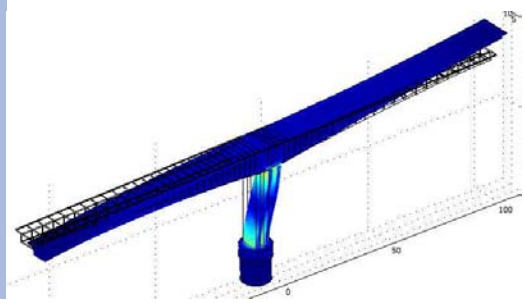

“5th Mode” (0.858 Hz)

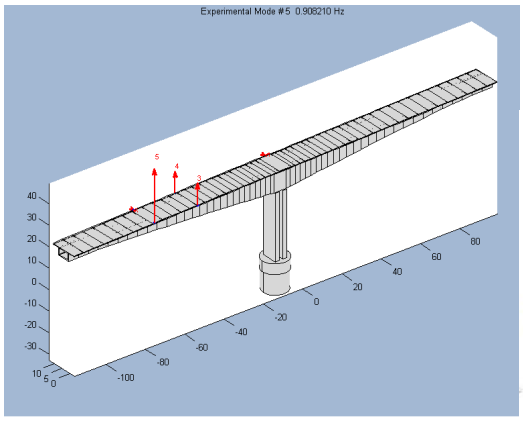

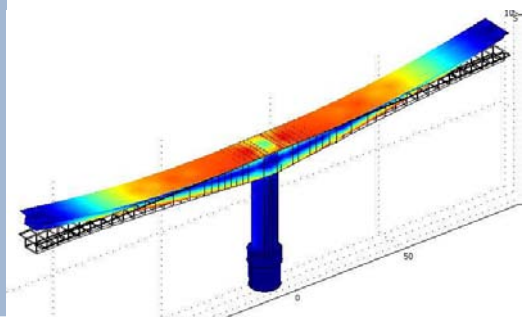

“6th Mode” (1.275 Hz)

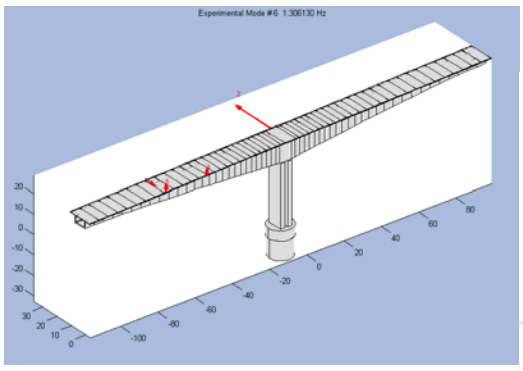

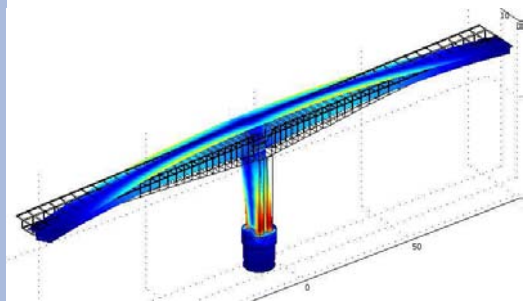

"7th Mode" (1.460 Hz)

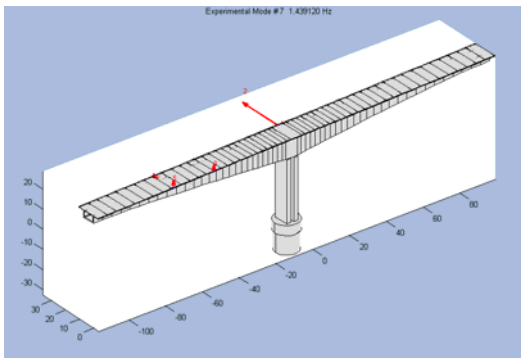

It was not predicted by FEM

"8st Mode" (0.155 Hz)

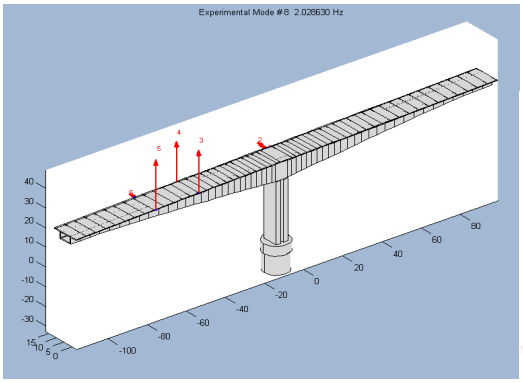

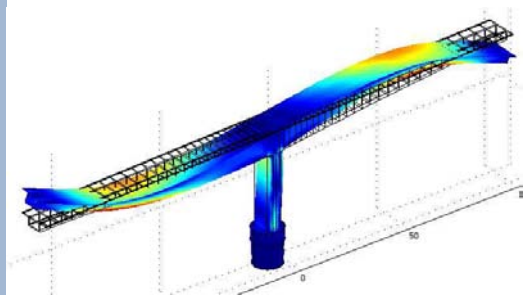

"9th Mode" (2.430 Hz)

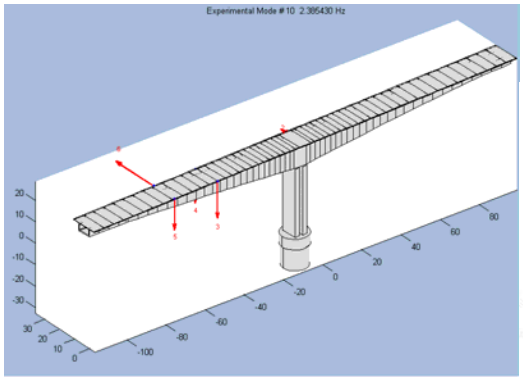

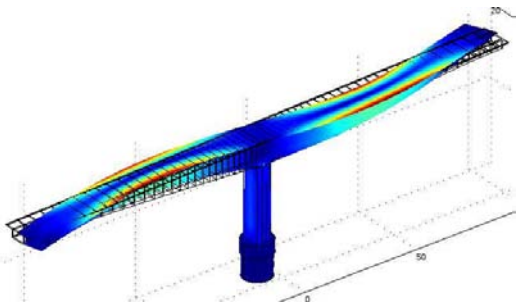

“10th Mode” (3.132 Hz)

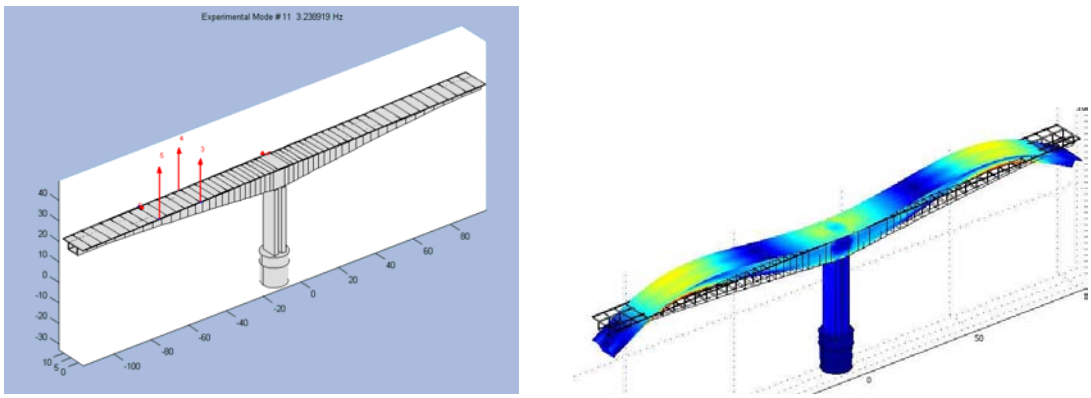

Figure 3.8: The first ten mode shapes of “M3 Cantilever” identified using vibration measurements compared to those predicted by the fixed base and the flexibly supported model

3.3 Finite Element Model for the Complete Bridge

This is the final construction phase that refers to the state that the left branch of Metsovo bridge has been constructed with all its segments. For this state two finite elements have been developed: the fixed base model and the flexibly supported model. The fixed base model ignores soil-structure interaction assuming that the bridge is fixed at the foundation bases. The second model considers the effects of flexible soil conditions. In the first model, the bridge was fixed at the base of piers M1, M2 and M3 and at the base of the abutments' bearings. In the second model, the soil under the piers was simulated by assuming that the foundations are embedded in cylindrical bodies with diameters and height six times higher than the equivalent diameter of the piers' foundation, creating a flexibly supported model of the bridge simulating the behaviour of the subsoil.

For the complete bridge the material properties for both models were taken to be the same. Specifically, the modulus of Elasticity E was chosen 37 GPa for the deck and 34 GPa for the remaining parts. Moreover, the density was chosen to be 2548 kg/m^3 as the bridge is constructed from reinforced concrete. The bridge was fixed at the base of piers M1, M2 and M3 and at the base of the abutments' bearings and no other kinematic constraints were imposed on the remaining components. Then the model was meshed with extra coarse mesh. So, the fixed base model shown in Figure 3.9 consists of 97.636 finite elements and has 563.586 DOF.

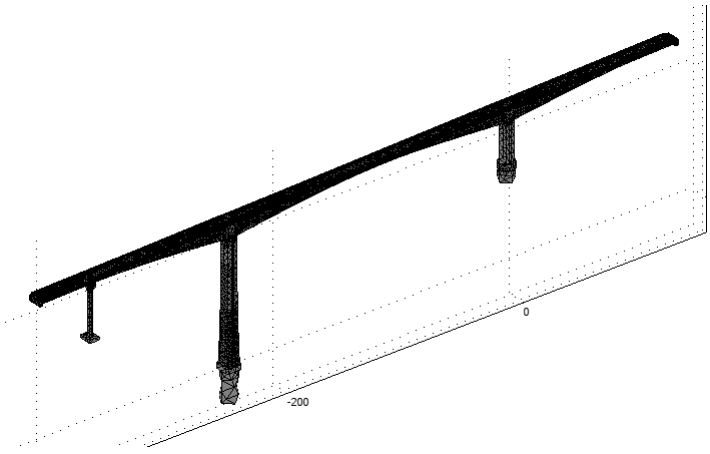

Figure 3.9: Fixed base Finite Element Model of left branch of Metsovo bridge

In the flexibly supported model, the soil under the piers was also simulated by assuming that the foundation of each pier is embedded in a solid body with diameter and height six times higher than the equivalent diameter of the pier's foundation, creating a flexibly supported model of the bridge simulating approximately the behaviour of the subsoil.The material properties of the deck and piers were taken the same with the properties of the fixed base model and the modulus of elasticity E for soil was chosen 2880 MPa while for specific gravity γ =25 KN/m^3 the density was calculated to be 2548 kg/m^3. Then the model was meshed with extra coarse mesh and the flexibly supported model shown in Figure 3.10 consists of 99.787 finite elements and has 573.372 DOF .

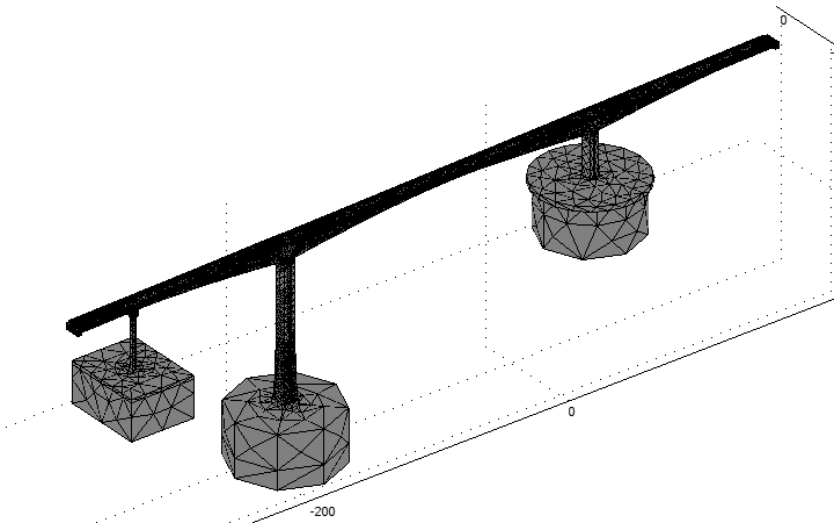

Figure 3.10: Flexibly supported Finite Element Model of left branch of Metsovo bridge

The lowest modal frequencies of the left branch of the completed phase of the bridge, predicted by the design (nominal) FE models, are reported in Table 3.4. Due to space limitations, the first twenty of the identified modal frequencies are presented in Table 3.4. The mode shapes of the left branch of Metsovo Bridge predicted by the fixed base model are presented in Appendix I and are compared to those predicted by the flexibly supported model. It can be seen from the results in Table 3.4 that soil contribution varies from 0.48% (1st Mode) to 4.05% (17th Mode). The average soil contribution is 3.30% and is obvious that the effect of soil-structure interaction on dynamic response of Metsovo

Bridge cannot be ignored. Finally, it is obvious that modal frequencies predicted by the bridge model including the contribution of soil are, as expected, lower than the ones for the fixed base bridge models.

Table 3.4: Identified modes of the left branch of Metsovo Bridge

No	Type of Mode	Low amplitude response		High amplitude response		FEM (fixed base)	FEM (with soil)	Fixed vs with soil
		Frequency Hz	Damping ζ%	Frequency Hz	Damping ζ%	Modal frequencies	Modal frequencies	% difference
1	1st transverse	0.281	0.29	0.278	0.47	0.318	0.313	-0.48
2	transverse	0.439	0.53	0.441	0.60	-	-	-
3	transverse	0.567	1.08	-	-	-	-	-
4	2nd transverse	0.636	1.07	0.623	0.90	0.621	0.603	2.93
5	1st bending	0.656	0.55	0.656	0.23	0.645	0.634	1.81
6	transverse	0.713	0.31	0.713	0.40	-	-	-
7	3rd transverse	1.03	0.46	1.02	1.23	0.989	0.962	2.76
8	2nd bending	1.09	0.51	1.47	2.15	1.11	1.08	2.65
9	4th transverse	-	-	-	-	1.17	1.13	3.51
10	3rd bending	1.48	0.52	1.61	0.19	1.51	1.46	3.69
11	5th transverse	1.69	0.43	1.69	0.33	1.71	1.64	3.88
12	4th bending	1.86	0.75	1.85	0.91	1.93	1.86	3.72
13	5th bending	2.08	0.37	2.01	2.75	2.31	2.23	3.72
14	6th transverse	2.3578	0.325	2.3581	1.2770	2.3506	2.2590	3.90
15	6th bending	2.8329	0.614	2.8323	0.4674	2.8378	2.7323	3.72
16	7th transverse	3.0951	0.365	3.0932	0.4177	3.1306	3.0062	3.97
17	7th bending	3.1993	0.769	3.2179	0.9178	3.1743	3.0456	4.05
18	bending	3.6015	0.378	3.6023	0.3665	3.6344	3.4921	3.92
19	transverse	3.8850	3.845	0.217	0.2476	3.9423	4.0133	1.80
20	bending	4.3241	0.177	4.2839	0.3296	4.4609	4.2941	3.74

3.4 Comparison of the Left and Right Branch of Metsovo Bridge

Since the two branches of Metsovo Bridge have almost the same geometry, the comparison of the mode shapes and modal frequencies predicted by the finite element models is of great interest. The three-dimensional models for the two branches of the bridge were created independently by two different engineers in SolidWorks. Thus, slight differences exists due to the assumptions made during the creation of the three-dimensional models from the two-dimensional design drawings. The finite element models were then created in COMSOL Multiphysics using extra coarse tetrahedral finite elements. The comparison between the finite element models is carried out only for the fixed base model because as it was proved and above the mode shapes of the two types of models are exactly the same and the modal frequencies have slight differences due to the small differences in the geometry. Finally the comparison is carried out for both construction phases.

3.4.1 Finite Element Models of the Construction Phase: "M3 Cantilever"

The lowest modal frequencies of the left and right branch of the "M3 Cantilever" construction phase of the bridge, predicted by the design (nominal) FE models, are reported in Table 3.5. In Table 3.5, the frequencies predicted by the design (nominal) FE models are compared to each other and to those identified by the Modal Identification Toolbox (MI-Tool) [Ntotsios (2008)]. As it was mentioned in Section 3.2 the identification of the modal properties was conducted using measurement data collected from a mobile monitoring system on 22/11/2007 for the left branch and on 10/9/2008 for the right branch. Finally, in both branches the recorded responses are mainly due to wind loads and loads induced by construction activities, such as the crossing of light vehicles, placing the prestressing cables inside the tendon tubes, etc.

It can be seen from the results in Table 3.5 that the difference in modal frequencies between the left and right branch of the "M3 Cantilever" varies from 0.00% to 0.69% The average difference is 0.36% and is obvious that this difference can be ignored. This is evident in Figure 3.11 by comparing a representative bending and a representative transverse mode shape of "M3 Cantilever" predicted by the two models.

Table 3.5: Comparison between modes of left (LB) and right (RB) branches of "M3 Cantilever" construction phase

No	Type of Mode	Measured Frequencies Hz		Measured Damping ζ%		FEM (fixed base)	FEM (fixed base)	L.B vs R.B
		LB	RB	LB	RB	LB	RB	% diff.
1	Pure torsion of column	0.159	0.159	1.06	0.35	0.155	0.154	0.65
2	1st pure bending of column	0.305	0.305	0.48	0.47	0.280	0.279	0.36
3	1st transverse and bending of column in transverse direction	0.623	0.621	0.61	0.32	0.570	0.569	0.18
4	2nd bending of column and deck deformation	0.686	0.686	0.38	0.22	0.639	0.635	0.63
5	3rd bending of deck without deck deformation	0.908	0.906	0.59	0.40	0.858	0.856	0.23
6	2nd transverse and deck deformation in opposite direction of transverse	1.31	1.31	1.28	0.48	1.27	1.28	0.79
7	3rd transverse	1.46	1.47	0.87	1.25	-	-	-
8	4th bending and column deformation	2.29	2.29	0.41	0.39	2.19	2.19	0.00
9	4th transverse and column slightly deformed	2.38	2.38	1.29	0.94	2.43	2.43	0.00
10	bending	3.24	3.24	0.32	0.47	3.13	3.13	0.00
11	transverse	4.63	4.63	0.35	0.61	4.36	4.39	0.69
12	1st rotational, x axis	4.94	4.91	0.61	0.54	5.01	5.02	0.20

Left Branch **Right Branch**

Bending Mode

3.132 Hz **3.131 Hz**

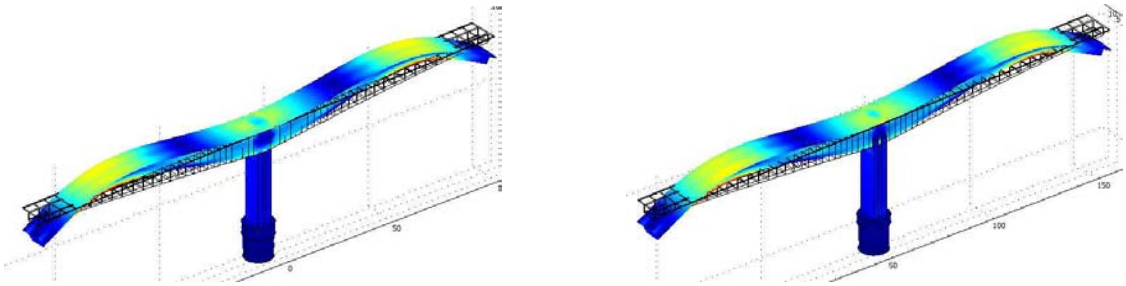

Transverse Mode

4.366 Hz **4.396 Hz**

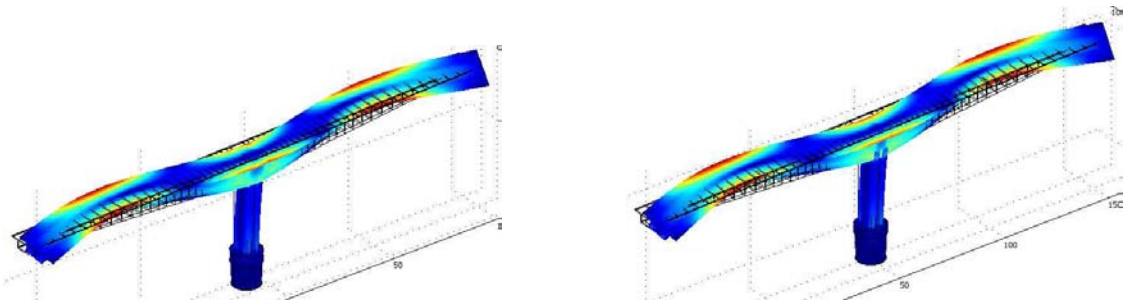

Figure 3.11: Representative bending and transverse mode shapes of “M3 Cantilever” predicted by the fixed base models of left and right branchl

3.4.2 Finite Element Models of The Complete Bridge

The lowest modal frequencies of the left and right branch of the complete bridge predicted by the design (nominal) FE models, are reported in Table 3.6. In Table 3.6, the frequencies predicted by the design (nominal) FE models are compared to each other and to those identified with the Modal Identification Toolbox (MI-Tool). As it was mentioned in Section 3.3, the identification of the modal properties was conducted using measurement data collected from a mobile monitoring system on 4/8/2008 for the left branch. Measurement data for the right branch are not available. Finally, the recorded responses are mainly due to wind loads and loads induced by construction activities, such as the crossing of light vehicles, placing the prestressing cables inside the tendon tubes, etc.

Table 3.6:. Comparison between identified modes of the left and right branch of the Metsovo bridge

No	**Type of Mode**	**Measured Frequencies Hz**		**Measured Damping ζ%**		**FEM (fixed base)**	**FEM (fixed base)**	**L.B vs R.B**
		Low amplitude response		**High amplitude response**		**L.B**	**R.B**	**% diff.**
1	1st transverse	0.281	0.278	0.29	0.47	0.318	0.3216	1.12
2	transverse	0.439	0.441	0.53	0.60	-	-	-
3	transverse	0.567	-	1.08	-	-	-	-
4	2nd transverse	0.636	0.623	1.07	0.90	0.621	0.6397	3.01
5	1st bending	0.656	0.656	0.55	0.23	0.645	0.6549	1.53
6	transverse	0.713	0.713	0.31	0.40	-	-	-
7	3rd transverse	1.03	1.02	0.46	1.23	0.989	1.0014	1.25
8	2nd bending	1.09	1.47	0.51	2.15	1.11	1.1229	1.16
9	4th transverse	-	-	-	-	1.17	1.2048	2.98
10	3rd bending	1.48	1.61	0.52	0.19	1.51	1.5295	1.29
11	5th transverse	1.69	1.69	0.43	0.33	1.71	1.7613	3.00
12	4th bending	1.86	1.85	0.75	0.91	1.93	1.9561	1.35
13	5th bending	2.08	2.01	0.37	2.75	2.31	2.3497	1.71
14	6th transverse	2.3578	2.3581	0.325	1.2770	2.3506	2.3985	2.04
15	6th bending	2.8329	2.8323	0.614	0.4674	2.8378	2.8572	0.68
16	7th transverse	3.0951	3.0932	0.365	0.4177	3.1306	3.1884	1.85
17	7th bending	3.1993	3.2179	0.769	0.9178	3.1743	3.2089	1.09
18	bending	3.6015	3.6023	0.378	0.3665	3.6344	3.6540	0.54
19	transverse	3.8850	3.8415	0.217	0.2476	3.9423	4.0133	1.80
20	bending	4.3241	4.2839	0.177	0.3296	4.4609	4.6329	3.86

It can be seen from the results in Table 3.6 that the difference in modal frequencies between the left and right branch of the complete bridge varies from 0.54% to 3.86% The average difference is 1.78%. These differences may be due to the slight differences in geometry of the two branches as well as the different assumptions made by the independent engineers in the creation of the two three-dimensional models in SolidWorks. Comparing the values of the modal frequencies for the left and right branch it is evident that the dynamic characteristics of the two different branches are very close validating the mechanical similarities of the two different branches. Moreover, comparing the identified modal frequencies in the above Tables with the modal frequencies obtained by the nominal FE models it is observed that the identified values are fairly close to the model based values.

Finally, in Appendix II the fifteen most representative mode shapes predicted by the fixed base finite element models for the two branches are presented. It is obvious that the mode shapes of the two branches are identical.

Chapter 4

Modal Identification of Metsovo Bridge

4.1 Monitoring System of Metsovo Bridge

Modal identification software is used to estimate the modal characteristics of the Metsovo bridge during various construction phases and after the bridge was completed. The identification was carried out using output-only measurements which were processed by the operational modal identification toolbox of the MI-Tool software [Ntotsios (2008)] developed in System Dynamics Laboratory of the Department of Mechanical Engineering (University of Thessaly). The modal characteristics to be identified are the modal frequencies, the modal damping ratios and the mode shapes.

During the various construction phases of both left and right branches of the bridge, monitoring data were collected from a 6-acceleration sensors mobile monitoring system. Specifically, during the "M3 Cantilever" construction phase of the bridge, six uniaxial accelerometers were installed inside the box beam cantilever M3 of the left carriageway of Metsovo ravine bridge. The accelerometer locations are shown in Figure 4.1.

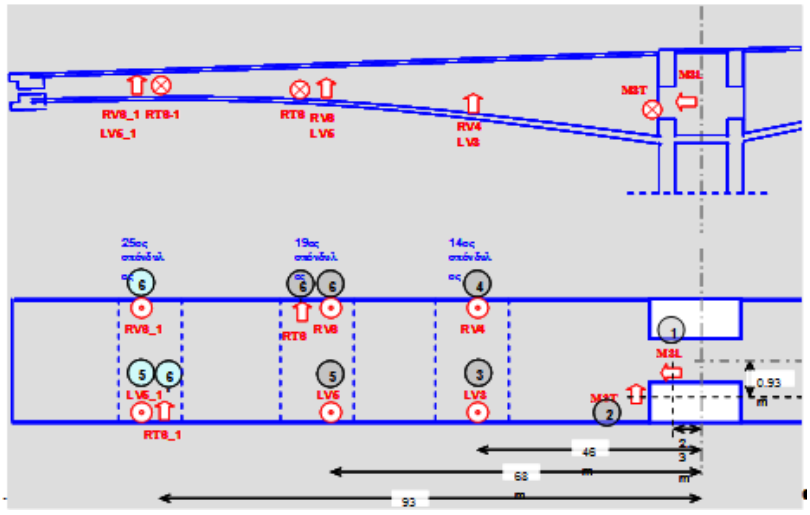

Figure 4.1: Sensor configuration for the "M3 cantilever" construction phase

Due to the symmetry of the construction method (balanced cantilevering) and as the same number of segments were completed on both sides of pier M3, the instrumentation was limited to the right cantilever of pier M3, following two basic sensor configurations. According to the 1st sensor configuration two (2) sensors were placed on the head of pier M3, one measuring longitudinal and the other transverse accelerations (M3L, M3T), while the remaining four (4) accelerometers were placed on the right and the left internal sides of the box beam's webs, two (2) at a distance of 46m and two (2) at a distance of 68m from M3 axis, respectively (LV3, RV4, LV5, RV6). All four sensors measure vertical acceleration. According to the 2nd sensor configuration the last two sensors of the 1st sensor configuiration were fixed in a section near the cantilever edge, at a distance 93m from M3 axis, while the other four remain in the same positions. In both arrangements the sixth sensor was adjusted to alternatively measure both in vertical and in transverse horizontal direction (RV6 or RT6).

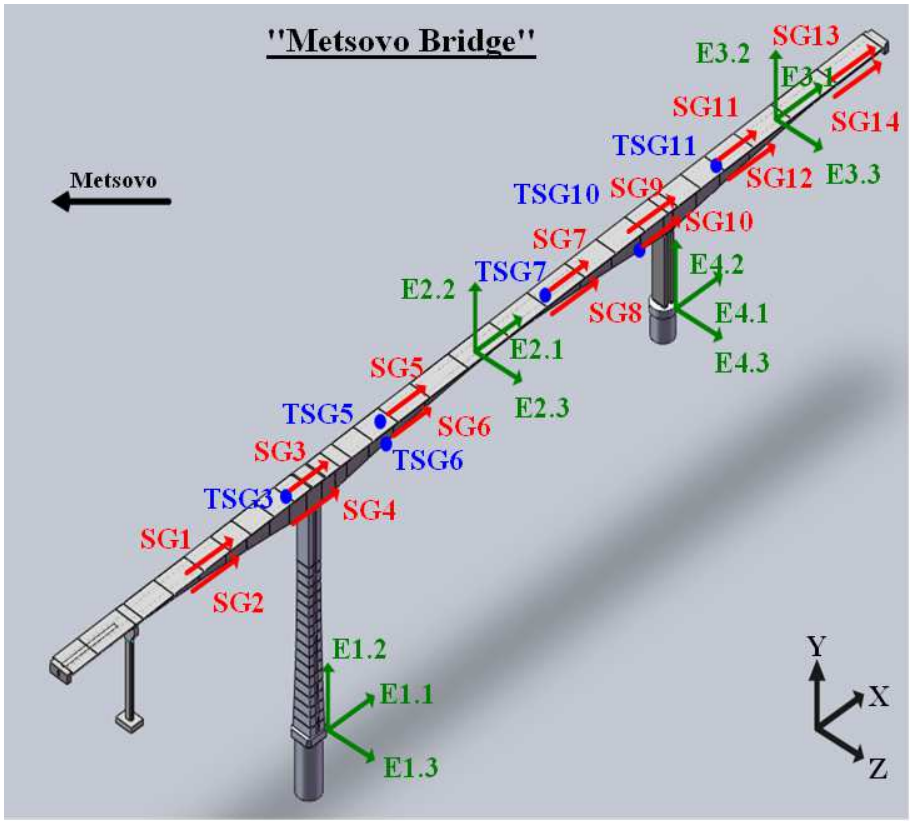

Figure 4.2: Sensor configuration for the complete left branch of Metsovo bridge.

After completion of its construction a permanent monitoring system, consisting of 12 acceleration sensors (E1.1 to E4.3), 14 strain sensors (SG1 to SG14), 6 temperature sensors (TSG3, TSG5,TSG6,TSG7,TSG10 and TSG11) and one wind velocity sensor has been placed on the left branch of the bridge to monitor its behavior under wind, traffic and earthquake loads. The data are collected remotely through internet connection. The sensor array is shown in Figure 4.2. However, the measurements from the permanent monitoring system are not used in this thesis to evaluate the modal characteristics of the bridge. Instead, the mobile monitoring system consisting of six acceleration sensors is used to collect ambient vibration measurements.

4.2 Modal Identification Software using Ambient Vibration Measurements

The acceleration time histories recorded by the aforementioned monitoring system are used to identify the modes of the bridge under the different construction phases. The recorded responses are mainly due to wind loads and loads induced by construction activities, such as the crossing of light vehicles placing the prestressing cables inside the tendon tubes, etc. The Modal Identification Toolbox (MI-Tool) that has been developed by the System Dynamics Laboratory in the University of Thessaly is used to identify the modal properties of the bridge.

MI-Tool software for modal identification was originally developed in MATLAB 7.0 (R14) environment. The software includes Graphical User Interface (GUI) in order to be simple in use and easily comprehensible even to unspecialized persons. It allows the full exploration and analysis of signals that are measured on specific points on a structure when it is excited for an Experimental Modal Identification, Operational Modal Identification or identification using earthquake induced vibrations, and it is fully adaptable to satisfy the user's requirements by allowing the resetting of most of its operational parameters. More details about the software and its capabilities can be found in the work by Ntotsios (2008).

4.3 Modal Identification Results for the “M3 Cantilever” Construction Phase

4.3.1 Left Branch of Metsovo Bridge

The response of the cantilever structure subjected to ambient loads such as the wind, and loads induced by construction activities such as the crossing of light vehicles placing the prestressing cables inside the tendon tubes, was as expected of very low intensity (0,6% of the acceleration of gravity) as shown in Figure 4.3.

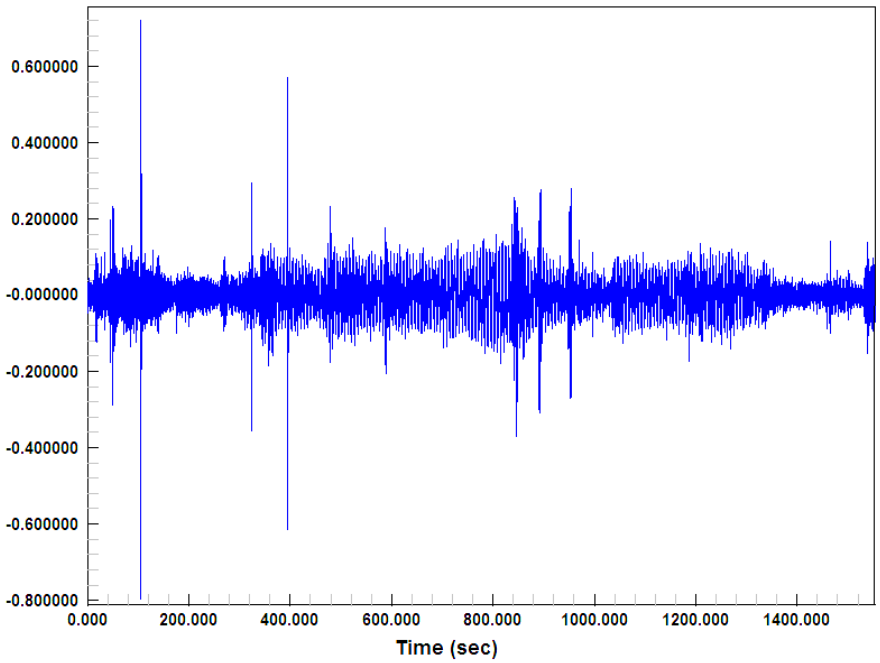

Figure 4.3: Acceleration time histories (cm/sec^2) in channel RT6

Using the acceleration response time histories measured from the 6 channel mobile system, the lowest modal frequencies, mode shapes and damping ratios of the bridge were identified. The identified type and values of the modal frequencies and the corresponding values of the damping ratios are shown in Table 4.1. It is observed that the values of damping are of the order of 0.2% to 2.9%. Due to the small number of available sensors (six), the type of some of the mode shapes were not identified with confidence. Three indicative mode shapes are presented in Figure 4.4. The arrows are placed in the measuring points and their length is proportional to the respective value of the normalized modal component.

Table 4.1: Identified modes of left branch (LB) of "M3 Cantilever" construction phase of the Metsovo Bridge

No	Type of Mode	Measured Frequencies Hz	Measured Damping ζ%
1	Pure torsion of column	0.159	1.06
2	1st pure bending of column	0.305	0.48
3	1st transverse and bending of column in transverse direction	0.623	0.61
4	2nd bending of column and deck deformation	0.686	0.38
5	3rd bending of deck without deck deformation	0.908	0.59
6	2nd transverse and deck deformation in opposite direction of transverse	1.31	1.28
7	3rd transverse	1.46	0.87
8	4th bending and column deformation	2.29	0.41
9	4th transverse and column slightly deformed	2.38	1.29
10	bending	3.24	0.32
11	transverse	4.63	0.35
12	1st rotational, x axis	4.94	0.61

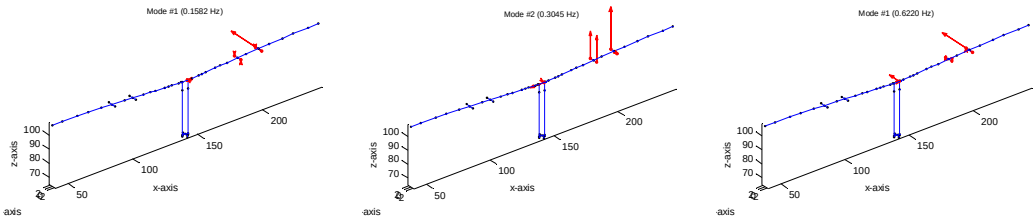

Figure 4.4: The three first identified modeshapes of Metsovo bridge.

The accuracy in the estimation of the modal characteristics is shown in Figure 4.5 which compares the measured with the modal model predicted cross power spectral density (CPSD). As it is seen, the fit between the measured and the modal model predicted cross power spectral densities is very good which validates the effectiveness of the proposed modal identification software based on ambient vibrations.

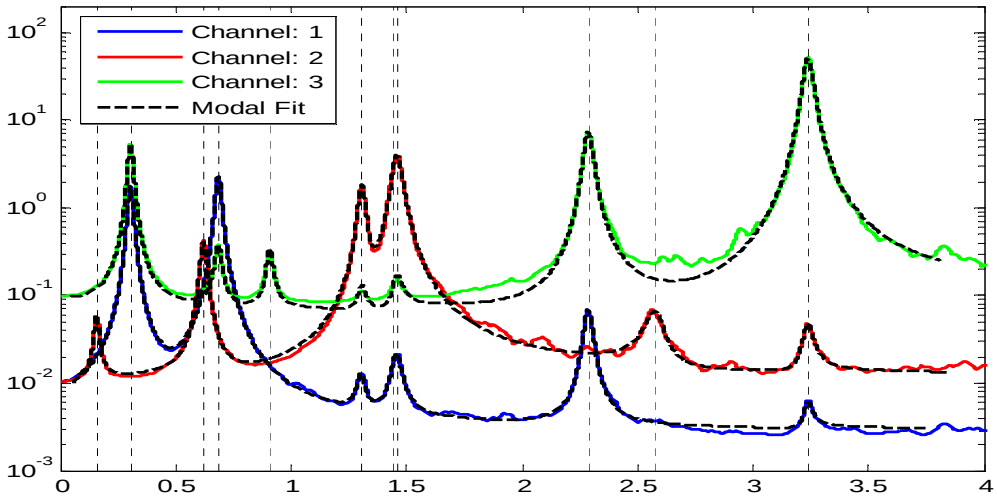

Figure 4.5: Comparison between measured and modal model predicted CPSD.

4.3.2 Right Branch of Metsovo Bridge

A similar analysis for identifying the modal characteristics of the right branch of the Metsovo bridge was also performed using measurements collected from the 6-sensor mobile system on 10/9/2008. The measurements were conducted when the M3 Cantilever Construction phase was completed. This phase corresponds to the construction of pier M3 with its cantilever segments and before the construction of the key segment that joins with the balanced cantilever of pier M2. Moreover, 26 parts of deck on each side of pier M3 were completed. Also two trucks of total mass 85t were located at the two edges, each one supported the edge parts of each side as in the left branch. This amount of mass was distributed to the last two parts. It is obvious that this construction phase of right branch is exactly the same with that of left branch during the measurement on 22/11/2007 that was analysed in Section 4.3.1.

For the right branch, more than the first 12 mode shapes were identified because of the good quality of signal that was of low noise. The identified type and values of the modal frequencies and the corresponding values of the damping ratios are shown in Table 4.2. It is observed that the values of damping are of the order of 0.2% to 1.2%.

Table 4.2: Modes of right branch of "M3 Cantilever" construction phase of the Metsovo bridge

No	**Type of Mode**	**Measured Frequencies Hz**	**Measured Damping ζ%**
1	Pure torsion of column	0.1584	0.31
2	1st pure bending of column	0.3049	0.19
3	1st transverse and bending of column in transverse direction	0.6206	0.46
4	2nd bending of column and deck deformation	0.6864	0.41
5	3rd bending of deck without deck deformation	0.9059	0.27
6	2nd transverse and deck deformation in opposite direction of transverse	1.3049	0.40
7	-	1.4655	1.25
8	-	2.2865	0.39
9	-	2.3876	0.55
10	-	2.5914	0.94
11	-	3.2378	0.47
12	-	3.5558	0.40
13	-	4.6247	0.60
14	-	4.9107	0.54
15	-	5.1568	0.63
16	-	5.9685	0.67
17	-	6.1184	0.69
18	-	6.8663	2.00

Due to the limited number of available sensors (six) the type of only the first 6 modes were identified with confidence and matched with those of left branch as it is shown in Table 4.3 .

Table 4.3: Comparison between modes of left and right branch of "M3 Cantilever" construction phase of the Metsovo bridge

No	Type of Mode	Measured Frequencies Hz		Measured Damping ζ%		L.B vs R.B
		LB	RB	LB	RB	% diff.
1	Pure torsion of column	0.1592	0.1584	1.05	0.35	0.50
2	1st pure bending of column	0.3049	0.3049	0.48	0.47	0.00
3	1st transverse and bending of column in transverse direction	0.6232	0.6206	0.60	0.32	0.42
4	2nd bending of column and deck deformation	0.6855	0.6864	0.38	0.22	-0.13
5	3rd bending of deck without deck deformation	0.9082	0.9059	0.59	0.40	0.25
6	2nd transverse and deck deformation in opposite direction of transverse	1.3061	1.3049	1.28	0.48	0.09

The differences in the modal frequencies between the two branches are of the order of 0,5% or even smaller. These differences are considered to be very small and they may be mostly due to temperature differences or data processing errors. So, the above results testify that the two branches of Metsovo bridge have as it was expected identical modal characteristics for at least the first 6 modes.

4.4 Modal Identification Results for the Left Branch of Metsovo Bridge

4.4.1 Measurement Data Collected on 4/8/2008

For the left branch of Metsovo bridge the first 22 mode shapes, shown in Table 4.4, were identified, when the left branch was completed (4/8/2007).

Table 4.4:. Identified modes of the left branch of the Metsovo bridge

No	Type of Mode	Low amplitude response		High amplitude response	
		Frequency Hz	Damping ζ%	Frequency Hz	Damping ζ%
1	transverse	0.2809	0.29	0.2783	0.47
2	transverse	0.4390	0.53	0.4406	0.60
3	transverse	0.5671	1.08	-	-
4	transverse	0.6363	1.07	0.6228	0.90
5	bending	0.6559	0.55	0.6561	0.23
6	transverse	0.7129	0.31	0.7129	0.40
7	transverse	1.0292	0.46	1.0189	1.23
8	bending	1.0906	0.45	1.0745	0.75
9	bending	1.4757	0.51	1.4677	2.15
10	transverse	1.6234	0.52	1.6077	0.19
11	transverse	1.6934	0.43	1.6878	0.33
12	bending	1.8568	0.75	1.8545	0.91
13	bending	2.0795	0.37	2.0089	2.75
14	transverse	2.3578	0.33	2.3581	1.27
15	bending	2.8329	0.62	2.8323	0.47
16	transverse	3.0951	0.37	3.0932	0.42
17	bending	3.1993	0.77	3.2179	0.92
18	bending	3.6015	0.38	3.6023	0.37
19	transverse	3.8850	0.22	3.8415	0.25
20	bending	4.2814	0.23	4.1728	0.62
21	bending	4.3241	0.18	4.2839	0.33
22	bending	4.5950	0.43	-	-

The modal identification was conducted using two data sets. The first data set contains low amplitude vibration measurements. In Figure 4.6 the transverse acceleration time history in channel RV4 during the measurement on 4/8/2008 is presented. The response is of very low intensity, 0.01% - 0.05% of the acceleration of gravity. The second data set contains high amplitude vibration measurements. In Figure 4.7 the transverse acceleration time history in channel RV4 during the measurement on 4/8/2008

is presented. Now the response is of higher intensity, 0.1% - 0.8% of the acceleration of gravity.

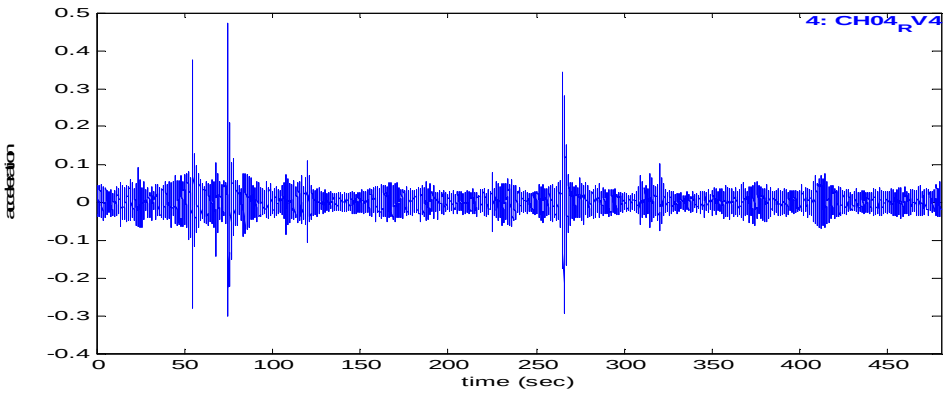

Figure 4.6: Acceleration time histories (cm/sec^2) in channel RV4 from low amplitude vibration

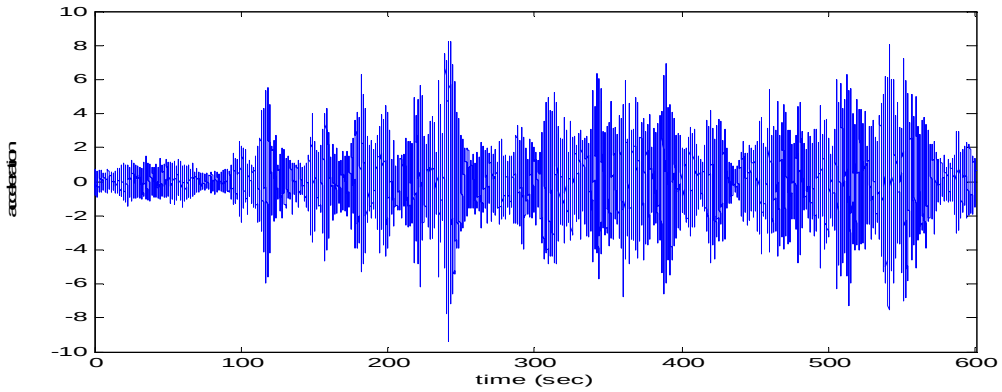

Figure 4.7: Acceleration time histories (cm/sec^2) in channel RV4 from high amplitude vibration

In Figure 4.8 the CPSD functions estimated from the measured output acceleration time histories and the CPSD functions predicted by the modal model are compared for four sensor channels. Specifically, in the frequency range [0,1] Hz the CPSD functions are presented for the sensor RV6 in vertical direction, sensors M3T and RT6 in transverse direction and sensor M3L in longitudinal direction. A very good fit between measured and modal model predicted CPSD is observed.

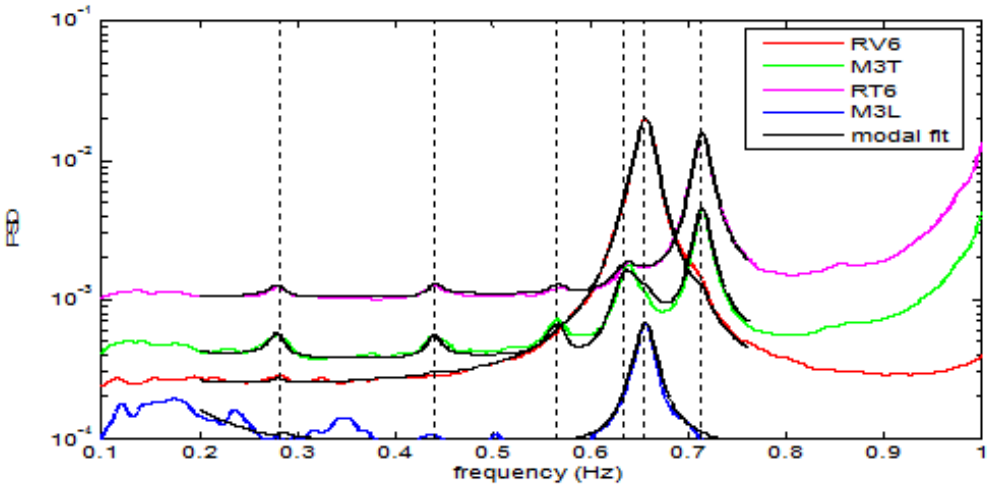

Figure 4.8: Comparison between measured and modal model predicted CPSDs.

In Figure 4.9 the CPSD functions estimated from the measured output acceleration time histories and the CPSD functions predicted by the modal model are compared for two sensor channels. Specifically, in the frequency range [0,3] Hz the CPSD functions are presented for the sensor M3T in transverse direction and sensor LV3 in bending direction. Finally, it is obvious that the fit between the measured power spectral density and that predicted by the modal model is very good, validating the effectiveness of the modal identification software based on ambient vibration and the high quality of measurement setups.

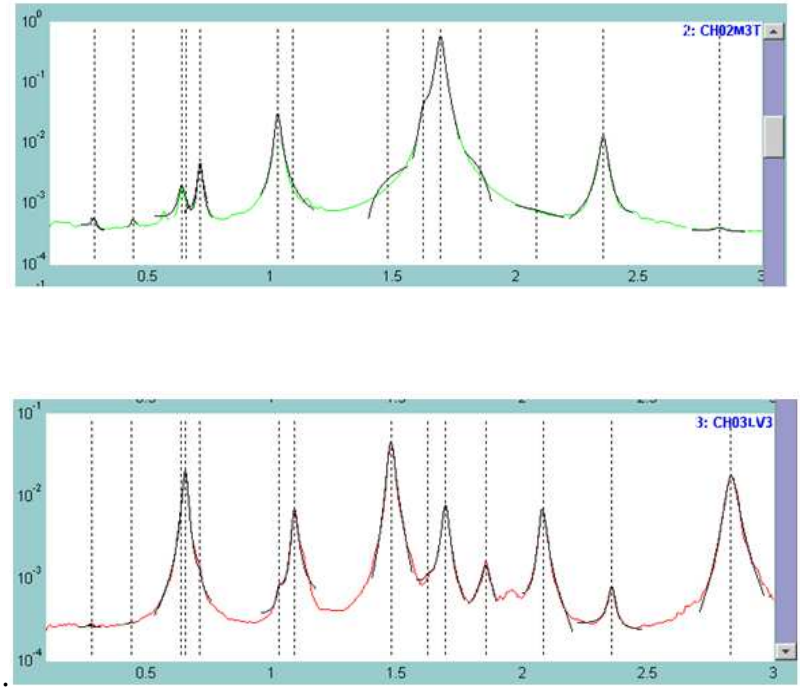

Figure 4.9: Comparison between measured and modal model predicted CPSDs for two sensor channels

4.4.2 Measurement Data Collected on 5/5/2010 and 8/6/2010

In order to identify the modal characteristics of the left branch of Metsovo Bridge and monitor its dynamic behavior two years after its construction, two measurements were conducted on 5/5/2010 and 8/6/2010. The first measurement includes six setups and the second five setups. The sensors locations during the 11 measurement data sets are presented in Appendix III. The identified type of modes, values of the modal frequencies and the corresponding values of the damping ratios are shown in Table 4.5. The results of the modal identification presented in Table 4.5came out from the analysis of the first five measurement setups.

Table 4.5: Identified modes of the LB of Metsovo bridge using first five setups

No	Type of Mode	FEM Fixed Base Model	Measurement 4/8/2008		Measurement 5/5/2010				
			Low Amplitude Response	High Amplitude Response	Set 1 JQ003	Set 2 JQ004	Set 3 JQ005	Set 4 JQ006	Set 5 JR002
1	1st transverse	0.3178	0.281	0.278	0.32435	-	0.32166	0.32131	0.32131
2	transverse	-	0.439	0.441	-	-	-	-	-
3	transverse	-	0.567	-	-	-	-	-	-
4	2nd transverse	0.6215	0.636	0.623	0.62868	-	0.62038	0.61702	0.63048
5	1st bending	0.6455	0.656	0.656	0.63847	0.63228	0.63829	0.63822	0.65140
6	transverse	-	0.713	0.713	-	-	-	-	-
7	3rd transverse	0.9890	1.03	1.02	-	0.97588	-	0.97893	-
8	2nd bending	1.1109	1.09	1.47	1.07187	1.07068	1.07060	1.07465	1.07664
9	4th transverse	1.1720	-	-	1.17181	1.16987	1.16476	1.16013	1.16878
10	3rd bending	1.5141	1.48	1.61	1.44925	1.44373	1.43283	1.44884	1.44273
11	5th transverse	1.7103	1.69	1.69	1.73976	1.75086	-	1.72521	1.73568
12	4th bending	1.9327	1.86	1.85	1.87176	1.85836	1.84551	-	-
13	5th bending	2.3117	2.08	2.01	-	2.05536	1.95125	1.96144	2.04793
14	6th transverse	2.3506	2.3578	2.3581	2.40908	2.40617	2.36215	-	2.38349
15	6th bending	2.8378	2.8329	2.8323	2.75976	2.75032	2.75649	2.74097	2.75061
16	7th transverse	3.1306	3.0951	3.0932	3.14860	3.15582	3.14644	3.15731	3.15951
17	7th bending	3.1743	3.1993	3.2179	-	-	-	3.17573	-
18	bending	3.6344	3.6015	3.6023	3.56289	3.54481	3.56754	3.56038	3.56951

In Table 4.5 the identified modal frequencies are compared to those identified using the measurement data set collected on 4/8/2008 and to those predicted by the finite element model. As it is seen, small differences were found between the values of modal frequencies identified using the two measurements. For the second set of measurements

collected on 8/6/2010, the modal characteristics that were identified with MI-Tool are presented for the 6th Measurement JS003, that is the most representative data set, in Table 4.6. The modal frequencies and modal damping ratios identified by the MI-Tool are also compared to the modal frequencies and modal damping ratios identified from two other software available in the literature, the operational modal identification software developed by Au's group [Siu Kui Au (2010)] and the DP software [De Roeck (2009)] developed by the Department of Civil Engineering in Katholieke Universiteit Leuven.

Table 4.6:. Identified modes of the left branch of Metsovo bridge using setup JS003

No	Type of Mode	FEM Fixed Base Model	MI-Tool		Software By Siu-Kui Au		Software DP Algorithm	
			Frequency Hz	Damping Ratio %	Frequency Hz	Damping Ratio %	Frequency Hz	Damping Ratio %
1	transverse	0.3178	0.3136	0.83	0.3124	0.80	0.3127	0.76
2	transverse	0.6215	0.6265	0.95	0.6220	1.36	0.6264	0.97
3	bending	0.6455	0.6343	0.89	0.6292	1.07	-	-
4	transverse	0.9890	0.9399	0.95	-	-	-	-
5	bending	1.1109	1.0693	3.15	1.0606	3.60	1.1084	3.21
6	transverse	1.1720	1.1335	2.10	1.1513	2.57	-	-
7	-	-	-	-	1.1788	1.25	-	-
8	bending	1.5141	1.4288	1.12	1.4297	2.80	1.4289	2.10
9	transverse	1.7103	-	-	1.5701	2.50	1.6495	1.95
10	-	-	-	-	1.6032	1.65	-	-
11	bending	1.9327	1.9247	2.01	1.9640	2.69	1.9669	2.61
12	bending	2.3117	1.9542	0.47	2.3186	3.96	2.5587	0.40
13	transverse	2.3506	2.3728	0.76	2.3736	1.13	-	-
14	bending	2.8378	2.7263	1.01	2.7251	1.49	2.7252	0.98
15	transverse	3.1306	3.0657	0.16	-	-	-	-
16	bending	3.1743	3.1515	0.18	3.1329	0.67	3.1526	0.23
17	bending	3.6344	3.5053	1.72	3.5217	0.89	3.4894	1.13

As it is seen in Table 4.6, the modal frequencies and modal damping ratios identified with MI-Tool are very close to those identified by the other two software and those predicted by the finite element model. The results confirm the effectiveness and accuracy of the MI-Tool modal identification software developed by the System Dynamics Laboratory in University of Thessaly.

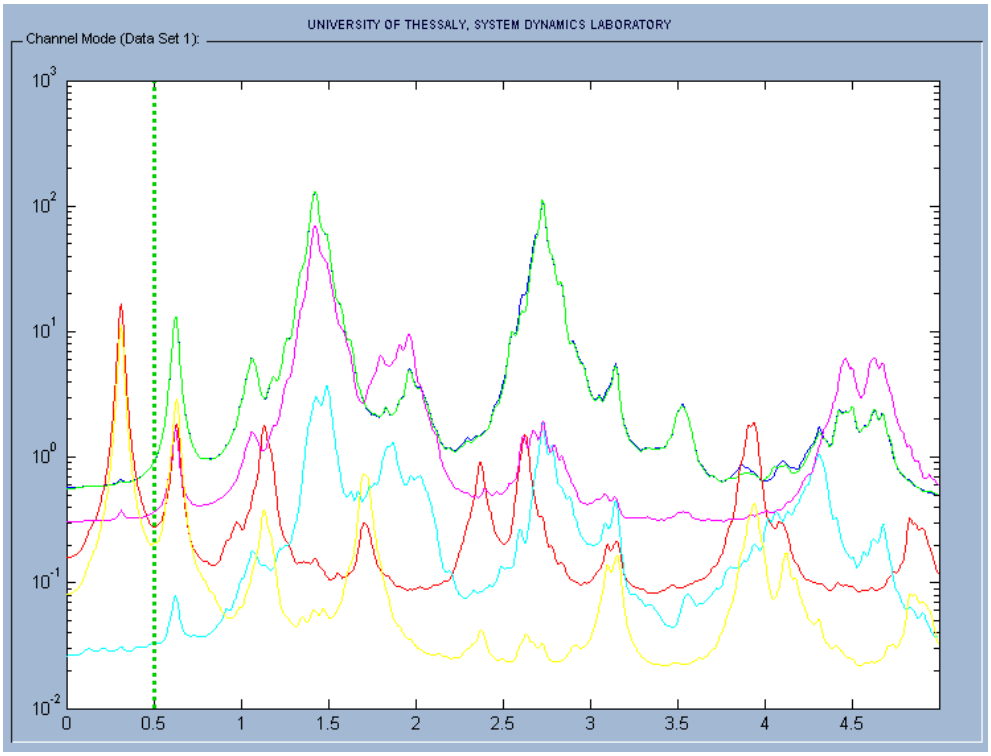

Figure 4.10: Cross Power Spectral Density functions for the six sensor channels during Measurement JS003

It is worth mentioning that one of the problems that we faced during the modal identification is finding the transverse modes and especially the 9th mode (1.71 Hz) when we used the acceleration time histories from all the six sensors. This happened due to the fact that for some frequency bands like this between 1.64-1.71 Hz the signal collected from the sensors in bending direction: “CHO2_LV2” and “CH05_RV63”, presented with green and pink color respectively in Figure 4.10, was of higher order of that collected from sensors in the transverse direction. When we used only the transverse sensors it was easier for us to find the transverse modes and the fit of the measured power spectral density was very good. Also the fit for the transverse modes was very good when we multiplied the acceleration time histories measured only for the transverse modes. This problem is mainly due to the fact that the quality of measurement data collected on 4/6/2010 was not good, containing high levels of noise. For this reason, new measurements are going to be collected in March 2011. But for the given quality of measurement data, the modal identification analysis was conducted with the best possible

accuracy as it is shown from the good fit between the measured and the modal predicted model in Figure 4.11.

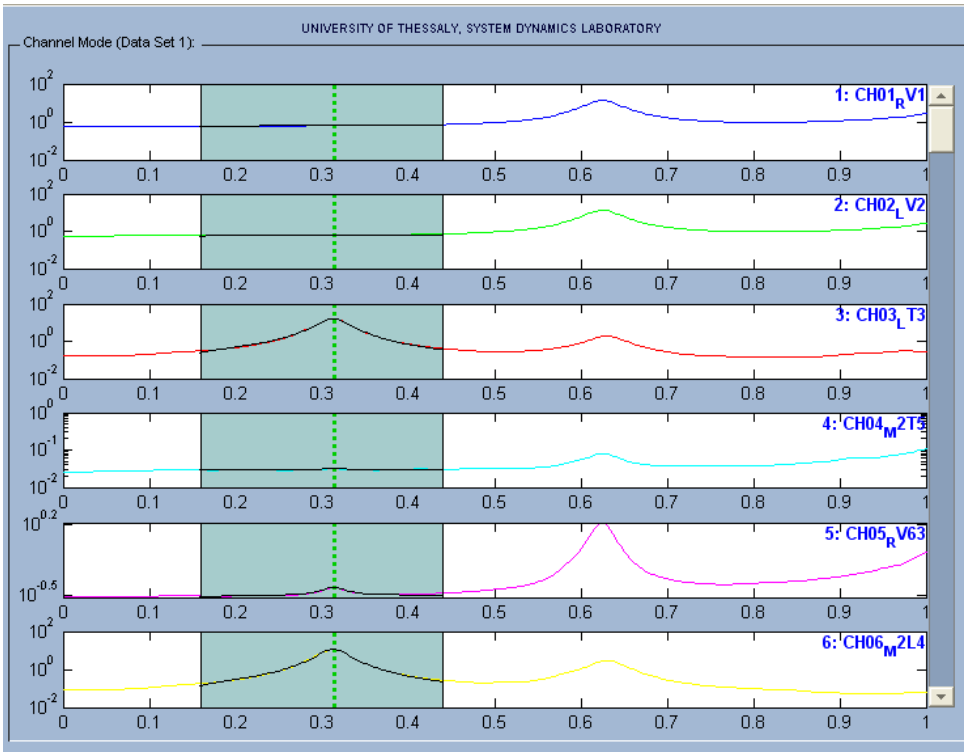

Figure 4.11: Comparison between measured and modal model predicted CPSDs for the six sensor channels during Measurement JS003

Finally in Appendix IV the mode shapes identified with MI-Tool are presented and compared to those identified by Au's modal identification method [Siu Kui Au (2010)].

4.5 Mode Shape Assembling from Multiple Data

Due to limited instrumentation budget and practical difficulties in deploying a large array of sensors, full mode shapes with a large number of measured DOFs are often assembled from partial (local) ones identified from individual setups, each covering a different part of the structure. Common reference DOFs must be present across different setups in order to allow their mode shapes to be assembled. The reference DOFs must have significant frequency response in the modes of interest. There must also be at least one common reference DOF across any two setups. The choice of the reference setup can affect the quality of results if the identified mode shape is of poor quality. If there is no reference DOF present in all setups, multiple reference setups need to be used for scaling. Methods [Siu Kui Au (2010)] have been developed to properly assemble full mode shapes from partial ones identified from individual setups. A modified version of the method described by Au (2010) is applied to assemble eight identified mode shapes of Metsovo Bridge using nine of the eleven available setups each one involving 6 sensor locations. The assembled mode shapes cover 22 DOFs that are shown in Figure 4.12.

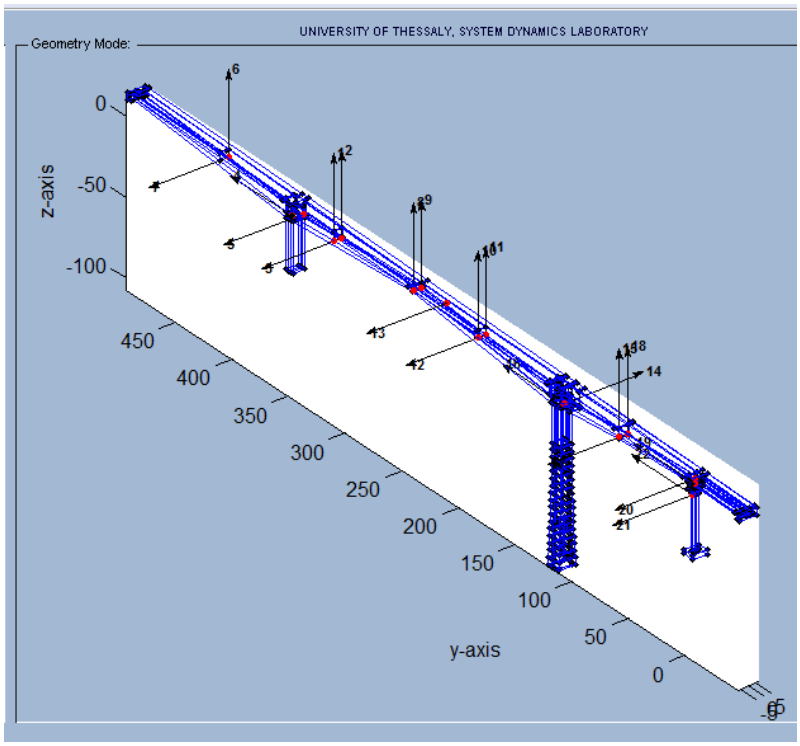

Figure 4.12: The 22 degrees of freedom of which mode shapes are identified

The relationship between the twenty two degrees of freedom covered with mode assembling and the degrees of freedom from the individual setups is presented in Table 4.7 As it is seen, there is no reference DOF that is measured in all setups because reference locations needed to be changed across the setups due to the limited cable lengths. However, there is at least one common reference DOF measured between any two setups, which is essential for assembling the full mode shapes. As the setups proceeded, the sensor locations migrated from Pier M1 to Pier M3.

Table 4.7: Relation of DOFs of assembled mode shapes to those of individual setups

Dir*	DOF	Setup 1	Setup 2	Setup 4	Setup 5	Setup 6	Setup 7	Setup 9	Setup 10	Setup 11
v	1	1	1	1						
v	2	2	2	2						
t	3	3	3	3						
l	4	4								
t	5	5	5	5						
v	6	6	6							
t	7		4							
v	8			6	6					
v	9			4	4					
v	10				1	1	1			
v	11				2	2	2			
t	12				3	3				
t	13				5					
t	14					4	4			
v	15					5	5	3	3	3
l	16					6	6			
t	17						3			
v	18							5	5	5
l	19							2	2	2
t	20							1	1	1
t	21							4	4	
l	22									4

*t= transverse
l=longitudinal
v= vertical

Specifically, the mode shape assembling technique was implemented for eight identified mode shapes: 1st, 2nd, 3rd, 8th, 14th, 15th, 16th and 17th as they are noticed in Table 4.7. The following nine measurement setups were used: JQ003 (Setup 1), JQ004 (Setup 2), JQ006 (Setup 4), JR002 (Setup 5), JS003 (Setup 6), JS005 (Setup 7), JW003 (Setup 9), JW005 (Setup 10), JW006 (Setup 11). The eight assembled mode shapes are presented in Table 4.8.

Table 4.8: Eight representative assembled mode shapes of left branch of Metsovo bridge

DOF	Mode 1	Mode 2	Mode 3	Mode 8	Mode 15	Mode 16	Mode 17	Mode 18
1	0.00017	-0.0800	0.1980	-0.6154	-0.9345	-0.0063	0.4413	-0.9882
2	-0.00059	-0.0717	0.2275	-0.6258	-0.9412	-0.0076	0.4037	-1.0000
3	-0.01120	0.1191	0.4194	0.0252	0.0824	0.0285	0.6012	0.0316
4	-0.00016	-0.0193	0.0308	0.1224	-0.0795	-0.0047	0.1747	0.2713
5	-0.00250	0.0332	0.1217	-0.0251	-0.0234	-0.0091	-0.1819	-0.0302
6	-0.00036	0.1088	-0.1069	-0.7672	-0.7362	0.0065	0.0300	0.2427
7	0.00180	-0.0068	-0.0773	0.0388	0.0920	0.0309	1.0000	-0.0268
8	-0.00430	-0.2253	0.7946	-0.9981	0.8514	-0.0396	0.2644	0.1367
9	-0.00076	-0.2270	0.7899	-1.0000	0.8287	-0.0266	0.1745	0.1471
10	-0.04960	-0.4250	0.3996	0.5477	-1.0000	0.0777	0.0999	-0.7830
11	0.05100	-0.4382	0.3821	0.5494	-0.9997	0.0679	0.1380	-0.7812
12	1.00000	0.1481	0.3251	0.0146	0.0225	-0.0438	0.1186	0.00053
13	0.97840	0.2207	0.7673	0.0111	-0.0280	0.1835	-0.4750	-0.0061
14	0.01280	-0.0381	0.0165	-0.0630	0.1244	0.0368	-0.0354	-0.0543
15	-0.06110	0.1952	-0.0296	-0.4241	-0.0600	-0.1262	-0.0037	-0.1382
16	0.81920	-0.4080	-0.5126	0.0053	-0.0019	-0.0339	0.2096	-0.0053
17	0.68360	-1.0000	-1.0000	-0.0150	-0.0235	0.0838	-0.7534	0.0166
18	0.14820	0.2194	-0.0023	-0.4196	-0.0036	-0.1019	-0.00041	-0.1289
19	0.00650	-0.0100	-0.00001	-0.1047	0.0094	0.2752	0.00045	-0.0823
20	-0.62400	-0.3140	-0.0113	-0.0183	0.0289	-1.0000	0.00071	0.0124
21	-0.56040	-0.2668	-0.0067	-0.0217	0.0376	-0.9051	0.00095	0.0104
22	-0.01030	-0.0101	-0.0012	-0.1687	0.0170	0.4517	-0.00003	-0.0691

Finally, the mode shapes are plotted on the structure and compared to those predicted by the finite element model in Comsol Multiphysics. This comparison is presented in Appendix V. In Figure 4.13 two representative mode shapes are presented. For some modes, the assembled mode shapes are found to be quite reasonable and of high quality, fact that validates the effectiveness and accuracy of the above proposed technique of mode assembling. However, for other modes the assembling procedure did not yield reasonable results due to the fact that the reference DOFs do not have significant

frequency response in these modes. Based on the results, it is concluded that in order to improve the quality of the assembled mode shapes, the sensor configurations setups have to be re-examined and new setups have to be proposed. In the future it is planned to use alternative setups and repeat the measurements and the mode shape identification procedure in an effort to improve the quality of the assembled mode shapes for all modes of interest.

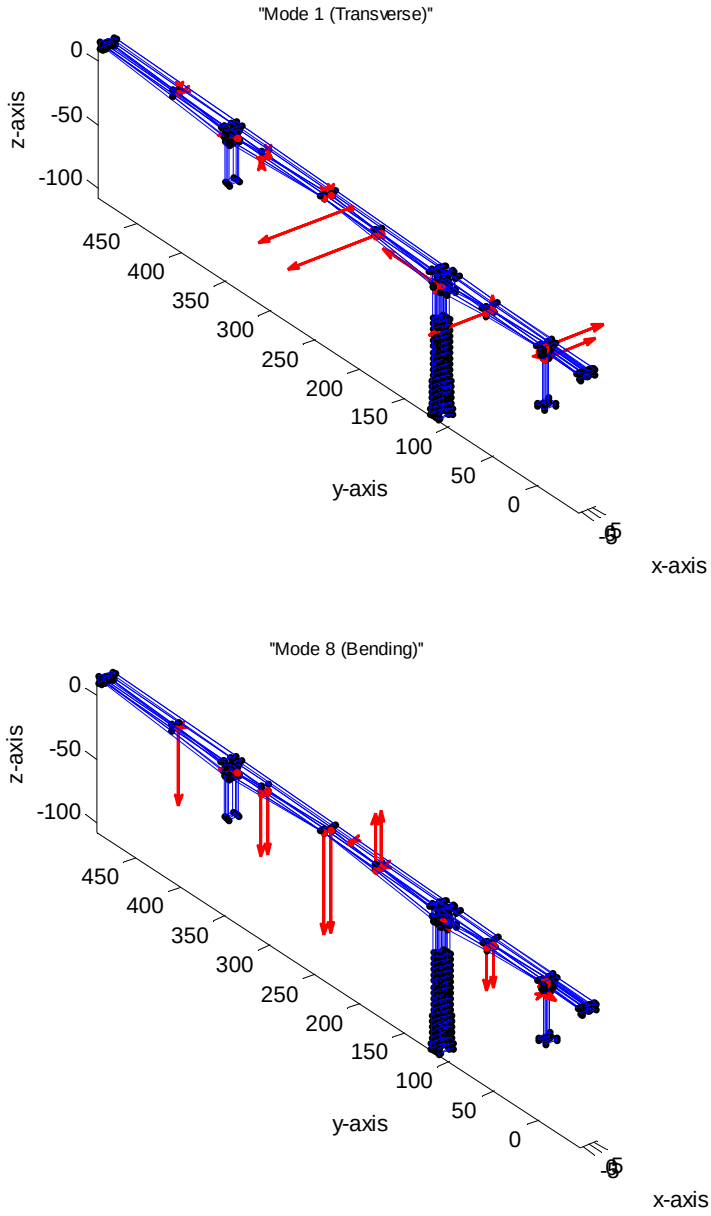

Figure 4.13 One bending and one transverse assembled mode shape

Chapter 5

Finite Element Model Updating of Metsovo Bridge

5.1 Finite Element Model Updating Theory

Structural model updating methods have been proposed in the past to reconcile mathematical models, usually discretized finite element models, with experimental data. The estimate of the optimal model from a parameterized class of models is sensitive to uncertainties that are due to limitations of the mathematical models used to represent the behavior of the real structure, the presence of measurement and processing error in the data, the number and type of measured modal or response time history data used in the reconciling process, as well as the norms used to measure the fit between measured and model predicted characteristics. The optimal structural models resulting from such methods can be used for improving the model response and reliability predictions [Papadimitriou (2001)] ,structural health monitoring applications and structural control [Yuen (2003)].

Structural model parameter estimation problems based on measured data, such as modal characteristics [Fritzen et al. (2001); Teughels and De Roeck (1998); Vanik et al. (2000); Ntotsios et al. (2008)] or response time history characteristics [Beck and Katafygiotis (1998)], are often formulated as weighted least-squares problems in which metrics, measuring the residuals between measured and model predicted characteristics, are build up into a single weighted residuals metric formed as a weighted average of the multiple individual metrics using weighting factors. Standard optimization techniques are then used to find the optimal values of the structural parameters that minimize the single weighted residuals metric representing an overall measure of fit between measured and model predicted characteristics. Due to model error and measurement noise, the results of the optimization are affected by the values assumed for the weighting factors.

The model updating problem has also been formulated in a multi-objective context [Haralampidis et al. (2005)] that allows the simultaneous minimization of the multiple metrics, eliminating the need for using arbitrary weighting factors for weighting the

relative importance of each metric in the overall measure of fit. The multi-objective parameter estimation methodology provides multiple Pareto optimal structural models consistent with the data and the residuals used in the sense that the fit each Pareto optimal model provides in a group of measured modal properties cannot be improved without deteriorating the fit in at least one other modal group.

Theoretical and computational issues arising in multi-objective identification have been addressed and the correspondence between the multi-objective identification and the weighted residuals identification has been established [Christodoulou and Papadimitriou (2007); Christodoulou et al. (2008)]. Emphasis was given in addressing issues associated with solving the resulting multi-objective and single-objective optimization problems. For this, efficient methods were also proposed for estimating the gradients and the Hessians [Ntotsios and Papadimitriou (2008)]of the objective functions using the Nelson's method [Nelson (1976)] for finding the sensitivities of the eigenproperties to model parameters.

In this Chapter, the structural model updating problem using modal residuals is formulated as single- and multi-objective optimization problems with the objective formed as a weighted average of the multiple objectives using weighting factors. The model updating methodologies are applied to update two different model classes of finite element models of the Metsovo bridge using ambient vibration measurements. Emphasis is given in investigating the variability of the Pareto optimal models from each model class.

5.2 Model Updating Based on Modal Residuals

Let $D = \{\hat{w}_r^{(k)}, \hat{\underline{f}}_r^{(k)} \Xi R^{N_0},\ r = 1,\cdots,m,\ k = 1,\cdots,N_D\}$ be the measured modal data from a structure, consisting of modal frequencies $\hat{w}_r^{(k)}$ and mode shape components $\hat{\underline{f}}_r^{(k)}$ at N_0 measured degrees of freedom (DOF), where m is the number of observed modes and N_D is the number of modal data sets available. Consider a parameterized class of linear structural models used to model the dynamic behavior of the structure and let $\underline{q} \Xi R^{N_q}$ be the set of free structural model parameters to be identified using the measured modal data. The objective in a modal-based structural identification methodology is to estimate the values of the parameter set $\underline{q}$ so that the modal data $\{w_r(\underline{q}), \underline{f}_r(\underline{q}) \Xi R^{N_d}, r = 1,\cdots,m\}$, where N_d is the number of model DOF, predicted by the linear class of models best matches, in some sense, the experimentally obtained modal data in D. For this, let

$$e_{w_r}(\underline{q}) = \frac{w_r^2(\underline{q}) - \hat{w}_r^2}{\hat{w}_r^2} \qquad \text{and} \qquad e_{\underline{f}_r}(\underline{q}) = \frac{\left\| b_r(\underline{q}) L\underline{f}_r(\underline{q}) - \hat{\underline{f}}_r \right\|}{\left\| \hat{\underline{f}}_r \right\|} \tag{5.1}$$

$r = 1,\cdots,m$, be the measures of fit or residuals between the measured modal data and the model predicted modal data for the r-th modal frequency and mode shape components, respectively, where $\| \underline{z} \|^2 = \underline{z}^{\mathrm{T}} \underline{z}$ is the usual Euclidean norm, and $b_r(\underline{q}) = \hat{\underline{f}}_r^T L\underline{f}(\underline{q})_r / \left\| L\underline{f}_r(\underline{q}) \right\|^2$ is a normalization constant that guaranties that the measured mode shape $\hat{\underline{f}}_r$ at the measured DOFs is closest to the model mode shape $b_r(\underline{q}) L\underline{f}_r(\underline{q})$ predicted by the particular value of $\underline{q}$. The matrix $L \Xi R^{N_0 \times N_d}$ is an observation matrix comprised of zeros and ones that maps the N_d model DOFs to the N_0 observed DOFs.

In order to proceed with the model updating formulation, the measured modal properties are grouped into two groups. The first group contains the modal frequencies while the second group contains the mode shape components for all modes. For each group, a norm is introduced to measure the residuals of the difference between the

measured values of the modal properties involved in the group and the corresponding modal values predicted from the model class for a particular value of the parameter set $\underline{q}$. For the first group the measure of fit $J_1(\underline{q})$ is selected to represent the difference between the measured and the model predicted frequencies for all modes. For the second group the measure of fit $J_2(\underline{q})$ is selected to represents the difference between the measured and the model predicted mode shape components for all modes. Specifically, the two measures of fit are given by

$$J_1(\underline{q}) = \sum_{r=1}^{m} e_{w_r}^2(\underline{q}) \quad \text{and} \quad J_2(\underline{q}) = \sum_{r=1}^{m} e_{f_r}^2(\underline{q}) \tag{5.2}$$

The aforementioned grouping scheme is used in the next subsections for updating the finite elment models of the Metsovo bridge. demonstrating the features of the proposed model updating methodologies.

5.2.1 Multi Objective Identification

The problem of identifying the model parameter values $\underline{q}$ that minimize the modal or response time history residuals can be formulated as a multi-objective optimization problem stated as follows [Papadimitriou et. al (2005)]. Find the values of the structural parameter set $\underline{q}$ that simultaneously minimizes the objectives

$$\underline{y} = \underline{J}(\underline{q}) = (J_1(\underline{q}), J_2(\underline{q})) \tag{5.3}$$

subject to parameter constrains $\underline{q}_{low} \le \underline{q} \le \underline{q}_{upper}$, where $\underline{q} = (q_1, \cdots, q_{N_q}) \in Q$ is the parameter vector, Q is the parameter space, $\underline{y} = (y_1, \cdots, y_n) \in Y$ is the objective vector, Y is the objective space and $\underline{q}_{low}$ and $\underline{q}_{upper}$ are respectively the lower and upper bounds of the parameter vector . For conflicting objectives $J_1(\underline{q})$ and $J_2(\underline{q})$ there is no single optimal solution, but rather a set of alternative solutions, known as Pareto optimal solutions, that are optimal in the sense that no other solutions in the parameter space are superior to them when both objectives are considered. The set of objective vectors $\underline{y} = \underline{J}(\underline{q})$ corresponding to the set of Pareto optimal solutions $\underline{q}$ is called Pareto optimal

front. The characteristics of the Pareto solutions are that the residuals cannot be improved in one group without deteriorating the residuals in the other group.

The multiple Pareto optimal solutions [Zitzler and Thiele (1999)] are due to modelling and measurement errors. The level of modelling and measurement errors affect the size and the distance from the origin of the Pareto front in the objective space, as well as the variability of the Pareto optimal solutions in the parameter space. The variability of the Pareto optimal solutions also depends on the overall sensitivity of the objective functions or, equivalently, the sensitivity of the modal properties, to model parameter values $\underline{q}$. Such variabilities were demonstrated for the case of two-dimensional objective space and one-dimensional parameter space in the work by Christodoulou and Papadimitriou (2007).

5.2.2 Weighted Modal Residuals Identification

The parameter estimation problem is traditionally solved by minimizing the single objective

$$J(\underline{q};\underline{w}) = w_1 J_1(\underline{q}) + w_2 J_2(\underline{q}) \tag{5.4}$$

formed from the multiple objectives $J_i(\underline{q})$ using the weighting factors $w_i \geq 0$, $i = 1,2$, with $w_1 + w_2 = 1$. The objective function $J(\underline{q};\underline{w})$ represents an overall measure of fit between the measured and the model predicted characteristics. The relative importance of the residual errors in the selection of the optimal model is reflected in the choice of the weights. The results of the identification depend on the weight values used. Conventional weighted least squares methods assume equal weight values, $w_1 = w_2 = 1/2$. This conventional method is referred herein as the equally weighted modal residuals method.

The single objective is computationally attractive since conventional minimization algorithms can be applied to solve the problem. However, a severe drawback of generating Pareto optimal solutions by solving the series of weighted single-objective optimization problems by uniformly varying the values of the weights is that this procedure often results in cluster of points in parts of the Pareto front that fail to provide an adequate representation of the entire Pareto shape. Thus, alternative algorithms

dealing directly with the multi-objective optimization problem and generating uniformly spread points along the entire Pareto front should be preferred. Formulating the parameter identification problem as a multi-objective minimization problem, the need for using arbitrary weighting factors for weighting the relative importance of the residuals $J_i(q)$ of a modal group to an overall weighted residuals metric is eliminated. An advantage of the multi-objective identification methodology is that all admissible solutions in the parameter space are obtained. Special algorithms are available for solving the multi-objective optimization problem [Papadimitriou and Ntotsios (2009)]. A very efficient algorithm for solving the multi-objective optimization problem is the Normal-Boundary Intersection (NBI) method [Das and Denis (1998)].

5.3 Selected Applications on the Models of Metsovo Bridge

The model updating methodologies were applied to three finite element models of Metsovo bridge during "M3 Cantilever" Construction Phase: the fixed base model, the model with soil stiffness $E_{soil} = 1$ GPa and the model with soil stiffness $E_{soil} = 7$ GPa. The soil stiffness values selected are based on geotechnical studies. The five lowest identified modal frequencies were used in the identification. The purpose of the identification was to update the stiffness values of the piers and the deck.

Results are next presented for the "M3 cantilever" construction phase. The three parameterized finite element models have two parameters θ_1 and θ_2. The first parameter θ_1 accounts for the modulus of elasticity of the cantilever deck and the second parameter θ_2 accounts for the modulus of elasticity of the pier M3. These parameters multiply the values of the selected model properties that describe, such as the values of $\theta_1 = \theta_2 = 1$ correspond to the initial design (nominal) model.

The results from the multi-objective identification methodology for the three solid element models are shown in Figure 5.1. Figure 5.1(a) shows the Pareto front and Figure 5.1(b) shows the Pareto optimal solutions. The non-zero size of the Pareto front and the non-zero distance of the Pareto front from the origin are due to modeling and measurement errors. Specifically, the distance of the Pareto points along the Pareto front from the origin is an indication of the size of the overall measurement and modeling error. The size of the Pareto front depends on the size of the model error and the sensitivity of the modal properties to the model parameter values. The optimal structural models corresponding to the equally weighted (EWM) and the optimally weighted modal residuals methods [Christodoulou and Papadimitriou (2007)] for the three finite element models are also shown in Figure 5.1. It can be seen that these optimal models are points along the Pareto front, as it should be expected.

It is observed that a wide variety of Pareto optimal solutions are obtained for the three different model classes that are consistent with the measured data and the objective functions used. Comparing the Pareto optimal solutions, it can be said that there is no Pareto solution that improves the fit in both modal groups simultaneously. Thus, all

Pareto solutions correspond to acceptable compromise structural models trading-off the fit in the modal frequencies involved in the first modal group with the fit in the mode shape components involved in the second modal groups.

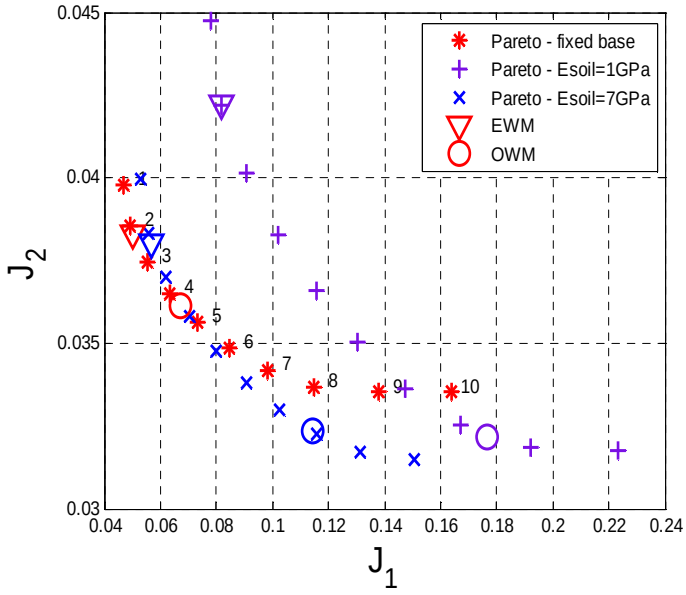

(a)

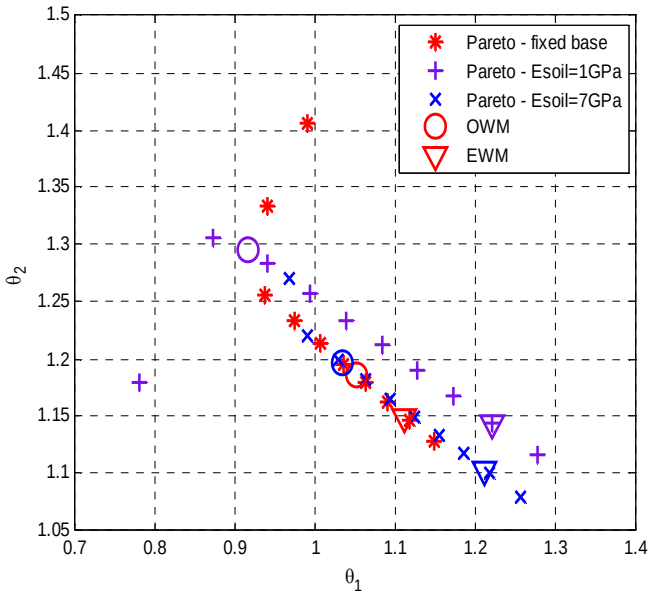

(b)

Figure 5.1: Pareto front and Pareto optimal solutions, (a) objective space and (b) parameter space.

From Figure 5.1 it is obvious the model with stiffer soil fits better the identified modal frequencies and mode shapes since the Pareto front is closer to the origin and shorter in size than the Pareto front corresponding to the model with softer soil. The fixed base model gives better results than the model with stiffer soil for part of the Pareto front that corresponds to the best fit in the modal frequencies, while it gives worse results for the Pareto front that corresponds to the best fit in the mode shapes. Results indicate that soil stiffness has a contribution to the behavior of the bridge. Finally, the parameter values vary considerably for all three models. In particular for the model with the stiffer soil, the deck stiffness varies from 0.93 to 1.27 times while the pier stiffness varies from 1.08 to 1.26 times the nominal values.

Table 5.1: Relative error between experimental and Finite element model predicted modal frequencies

Mode	Relative frequency error(%)					
	Nominal Model	Equally Weighted	Optimally Weighted	Pareto solution		
				1	5	10
1	-2.4487	4.4396	5.6346	3.6894	5.9363	13.5328
2	-8.2059	-1.7962	-0.8774	-2.3922	-0.6527	5.8426
3	-8.5170	-2.7699	-3.6006	-2.3791	-3.8554	-2.1596
4	-6.7234	-0.2568	0.5559	-0.7903	0.7529	7.0779
5	-5.5702	-0.4009	-3.1220	1.1943	-3.8471	-5.8935

Table 5.2: MAC values between experimental and finite element model predicted modeshapes

Mode	MAC Value					
	Nominal Model	Equally Weighted	Optimally Weighted	Pareto solution		
				1	5	10
1	0.9851	0.9851	0.9851	0.9851	0.9851	0.9852
2	0.9968	0.9969	0.9972	0.9967	0.9972	0.9978
3	0.9730	0.9751	0.9799	0.9718	0.9810	0.9878
4	0.9999	0.9999	0.9995	0.9999	0.9993	0.9960
5	0.9991	0.9991	0.9992	0.9990	0.9993	0.9995

For the fixed base model, the percentage error between the experimental (identified) values of the modal frequencies and the values of the modal frequencies predicted by the Pareto optimal solutions 1, 5 and 10, the equally weighted solution, and the optimally weighted solution are reported in Table 5.1. Table 5.2 reports the corresponding MAC values. It is observed that for the modal frequencies the difference between the experimental values and the values predicted by the Pareto optimal model vary between 0.75 % and 13.53%. Specifically, for the Pareto solution 1 that corresponds to the one that minimizes the errors in the modal frequencies (first objective function), the modal frequency errors vary from 0.8% to 3.7%. Higher modal frequency errors are observed as one moves towards Pareto solution 10 (ranging from 2.1% to 13.5% for Pareto solution 10) since such solutions are based more on minimizing the errors in the mode shapes than the error in the modal frequencies. Moreover, the errors observed for the nominal model are not much higher than the errors from the Pareto, which means that the nominal model was well designed. The MAC values between the experimental mode shapes and the mode shapes predicted by the Pareto optimal model are very close to one because of the small number of measured DOF available.

5.3 The Component Mode Synthesis

The implementation of the above finite element model updating techniques on the complex structure of the complete left branch of Metsovo Bridge remains a challenge due to the high number of model degrees of freedom which varies from 573.372 dofs for extra coarse meshing to 2.347.786 for fine meshing. To overcome the computational problems that arise with these models with very large number of DOFs, component mode synthesis methods are proposed to be used in future work.

Component mode synthesis (CMS) is a process that involves separating a structure into substructures, or components, calculating component mode shapes which describe the displacement of points within the substructures, and assembling, or synthesizing, this information into a reduced-order model of the full structure. These are the three basic steps of this process, depicted in Figure 5.2.

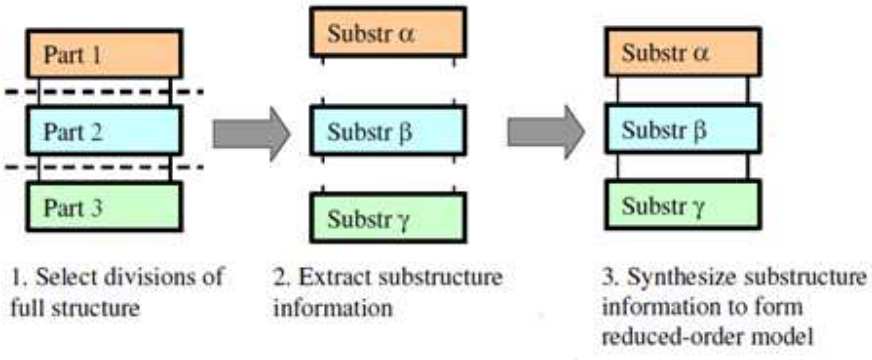

Figure 5.2: The three basic steps of Component Mode Synthesis.

Structural analysts have used CMS, also commonly referred to as substructuring, since the 1960s to solve very large structural dynamics models, such as those of aircraft. Craig [Craig (2000)] has discussed the history of CMS and provided an overview of the terminology and methods employed since the earliest developments .CMS has provided analysts with many advantages. It provided a method of reducing the size of the mathematical problem, so that analysts could obtain answers in less time or with limited computer resources. The division of the structure into substructures facilitated concurrent work by different analysts on different parts of the structure. The analysts of

subassemblies could feed reduced-order models of these subassemblies to the analysts responsible for the top-level structure. This was done by choosing to retain only those component modes that had significant influence on the response of the top-level structure. The analysts of the top-level structure would assemble these reduced-order substructure models into a reduced-order top-level model. They would realize even greater efficiency if any of these substructures were used multiple times. So, structural analysts have used component mode synthesis (CMS) for decades to divide large structural models into smaller, more manageable models, and to reduce the size of the associated mathematical problem. Applying CMS can also reduce the front-end effort to build models, even models that are smaller than those for which CMS has typically been applied.

Three methods of Component Mode Synthesis have been identified:

(a) Fixed Interface Methods: Where composite structural dynamic characteristics are developed using normal mode shapes and constraint modes of substructures.

(b) Free Interface Methods: Where composite structural dynamic characteristics are developed using normal mode shapes and attachment modes of substructures.

(c) Hybrid Methods: Where composite structural dynamic characteristics are developed from mixed or hybrid component modes , that is modes obtained with some interface coordinates free and other constrained.

Among these three methods, the fixed interface method, presented in 1968 by Craig and Bampton [Craig and Bampton (1968)], is one of the most straightforward and widely-implemented CMS methods. It is planned to use this method for reducing the computational burden involved in the finite element model updating and structural damage detection methodologies applied on models with very large number of DOFs. One example is the Metsovo bridge which is a complex structure with a finite element model consisting of a high number of degrees of freedom. Such modeling reduction techniques are important and left for future work.

Chapter 6

Conclusions and Future Work

The main objective of this thesis has been the identification of the modal characteristics of the Metsovo bridge, the development of a detailed finite element model of the bridge and the calibration of the model based on vibration measurements collected during two construction phases of the bridge. First of all, based on the design drawings and the material properties that were provided by EGNATIA ODOS S.A., detailed finite element models of the left branch of the bridge were constructed for two construction phases. In order to estimate the dynamic modal characteristics of the Metsovo bridge during various construction phases and after the bridge was completed, monitored data were collected by a mobile monitoring system. The measured response data were processed using MI-Tool software for the estimation of the modal characteristics. The identified modal frequencies and mode shapes were then used for the calibration of the corresponding finite element models introduced to simulate the bridge behaviour. A multi-objective structural identification method was used for updating the detailed finite element models based on minimizing two groups of the experimentally identified modal residuals, one associated with the modal frequencies and the other with the mode shapes. The identified modal characteristics of the bridge and the calibrated finite element models are useful for continually monitoring the structural health of the bridge.

The conclusions arising from the aforementioned three-dimensional modeling, modal identification and finite element model updating are next summarized.

Concerning the modal identification process, the identified modal characteristics and the modal characteristics predicted by the finite element models were compared to check the adequacy of the finite element models. Specifically, in order to examine the modal properties of the bridge and the contribution of soil conditions on the dynamic response of the bridge, two different types of finite element models of the bridge were developed, one fixed base model and one simulating soil-structure interaction. Comparing the changes in modal frequencies predicted by the two models, it has been found that soil

contribution affects the values of the modal frequencies from 0.16% to 4.66%. It is obvious that the effect of soil-structure interaction on the dynamic response of the Metsovo Bridge cannot be ignored. Moreover, the difference in modal predicted frequencies between the left and right branch of the “M3 Cantilever” varies from 0.00% to 0.69% while for the complete bridge varies from 0.54% to 3.86% , thus validating the fact that slight changes in the modal frequencies of the left and right branch are very small. The estimated differences may have been caused by the different assumptions made during the creation of the three-dimensional models from the two-dimensional design drawings by two different engineers in SolidWorks. So comparing the values of the modal frequencies for the two branches it is evident that the dynamic characteristics of the two different branches are very close validating the mechanical similarity of the two almost geometrically identical branches and validating design assumptions. Moreover, comparing the identified modal frequencies obtained by the nominal FE models to the identified values of the modal frequencies, it is observed that they are fairly close, thus confirming the high accuracy of the finite element models.

It is worth mentioning that one of the problems that we faced during the modal identification of the complete left branch of the bridge is finding the transverse modes due to the fact that the quality of measurement data collected on 4/6/2010 was not good, containing high levels of noise and the reference DOFs of the measurement setups did not have significant response in these modes. In the future it is planned to use alternative setups and repeat the measurements and the mode shape identification procedure in an effort to improve the quality of the assembled mode shapes for all modes of interest.

Concerning the model updating of the “M3 Cantilever” bridge, three different finite element models were updated: a fixed base model and two models that include the effect of soil. All estimated Pareto optimal models are shown to provide good fit to the lowest measured modal properties. The finite element model with stiffer soil was found to provide the best fit, indicating the role that soil stiffness plays on the dynamics of the structure. The derived finite element models are representative of the initial structural condition of the “M3 Cantilever” construction phase of the bridge.

Regarding the model updating of the complete left branch of the bridge, model updating results were not presented in this thesis. This is due to the fact that the computational effort is extremely high due to the large number of repeated finite element analyses required in the multi-objective finite element model updating methodology.

The implementation of the finite element model updating techniques on the complex structure of the complete left branch of Metsovo bridge is a challenge due to the high number of model degrees of freedom (573.372 DOFs for extra coarse meshing and 2.347.786 DOFs for fine mesh). An efficient solution strategy for this problem can be to integrate with finite element model updating methodology with component mode synthesis techniques. Such techniques involve separating a structure into substructures, or components, calculating component mode shapes which describe the displacement of points within the substructures, and assembling, or synthesizing, this information into a significantly reduced-order model of the full structure. This will significantly reduce by order of magnitudes the number of model DOFs, thus allowing the finite element model updating to be carried out efficiently with the minimum computational effort. Future work will concentrate on developing finite element model updating techniques based on component mode synthesis methods.

Appendix I

Comparison of Fixed Base and with Soil FEM for the LB of Metsovo Bridge

Fixed base FEM

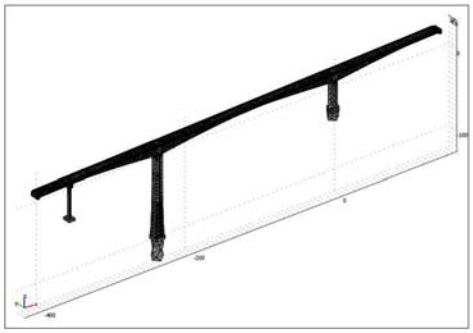

97.636 finite elements
563.586 DOF

FEM with soil

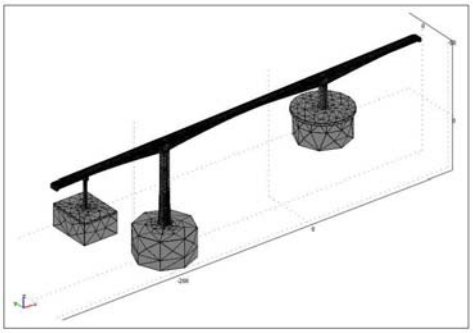

99.787 finite elements
573.372 DOF

"TRANSVERSE MODESHAPES"

Fixed base FEM **FEM with soil**

1st transverse

0.318 Hz

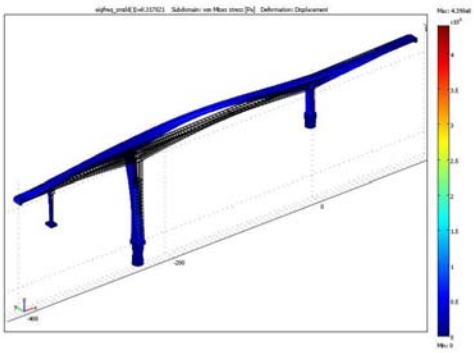

0.313 Hz

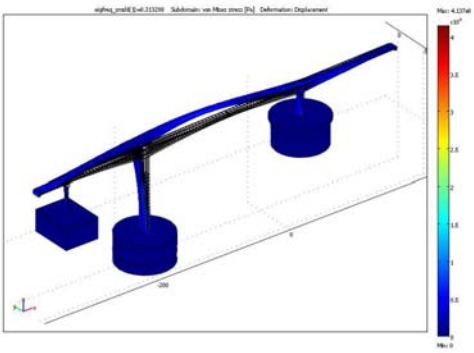

2nd transverse

0.621 Hz

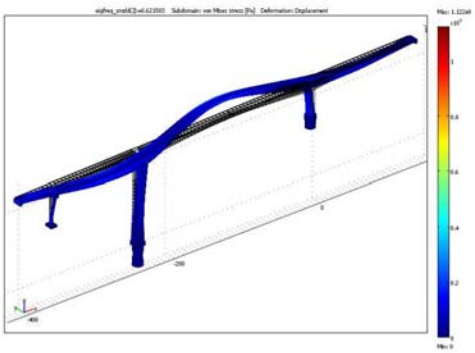

0.603 Hz

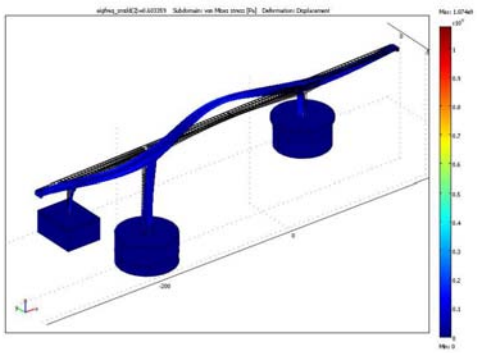

3rd transverse

0.989 Hz

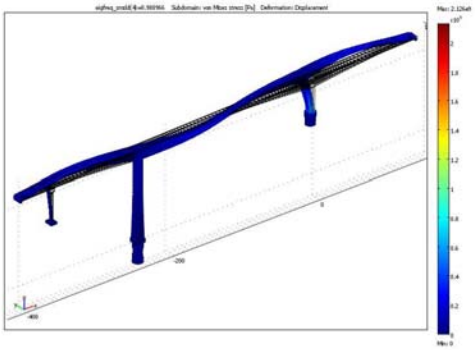

0.962 Hz

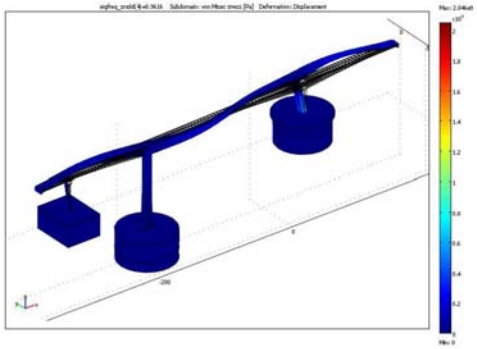

4th transverse

1.172 Hz

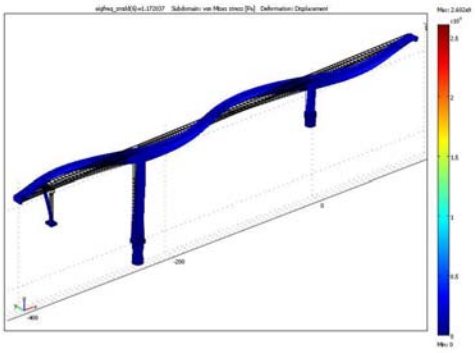

1.13 Hz

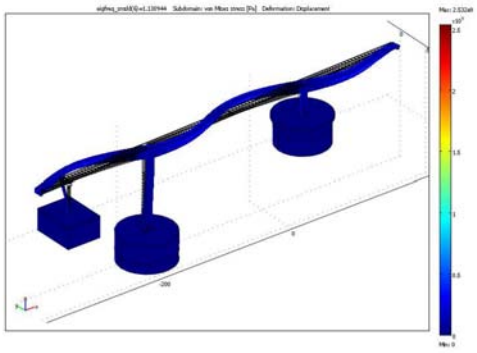

5th transverse

1.71 Hz

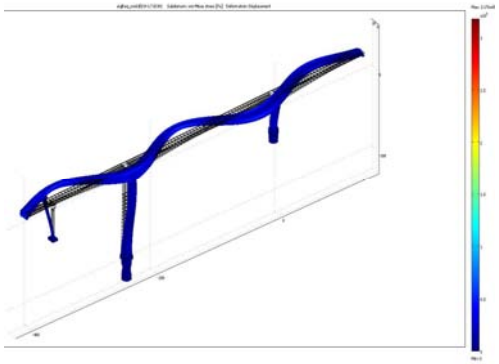

1.64 Hz

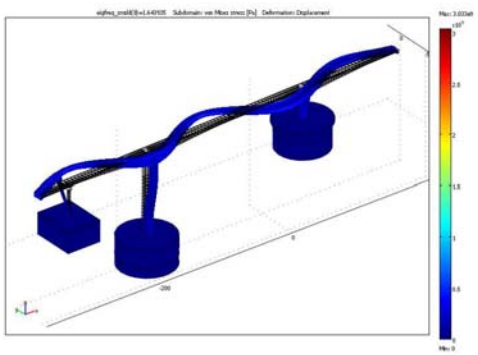

6th transverse

2.35 Hz

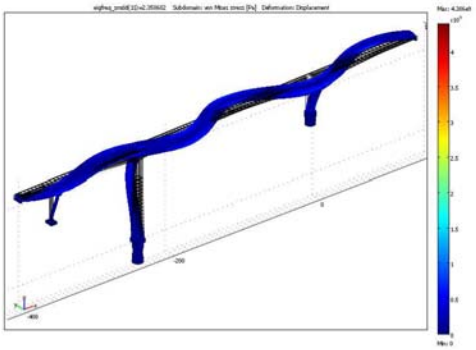

2.26 Hz

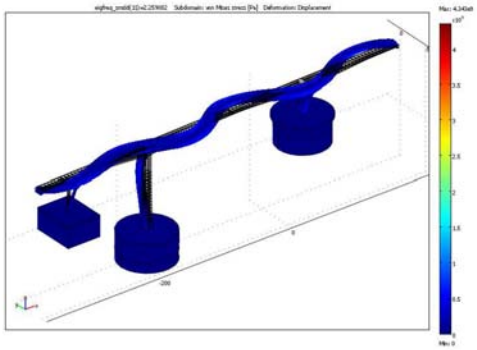

7th transverse

3.13 Hz

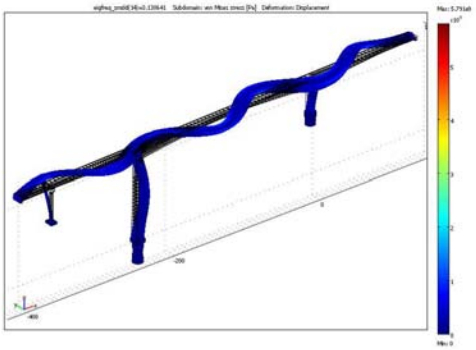

3.01 Hz

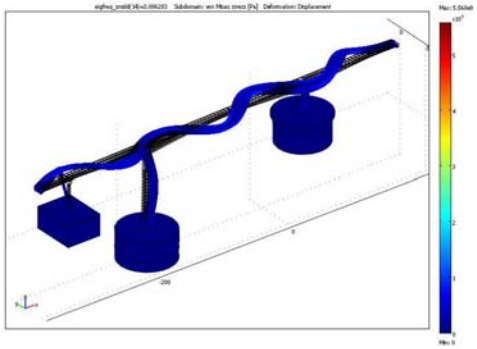

“BENDING MODESHAPES”

Fixed base FEM **FEM with soil**

1st bending

0.645 Hz

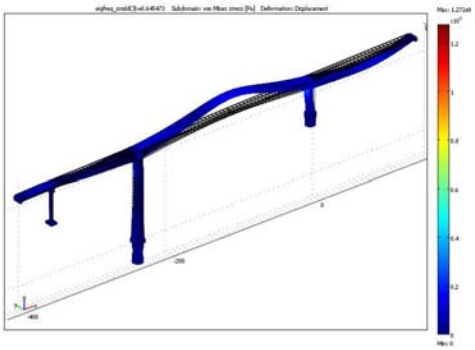

0.634 Hz

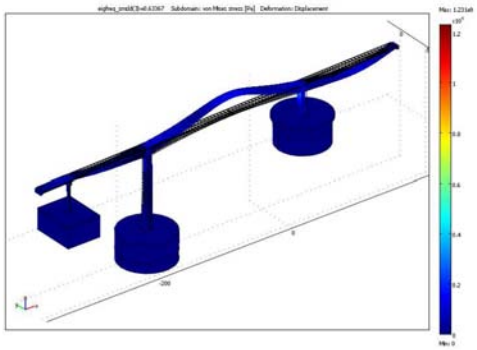

2nd bending

1.11 Hz

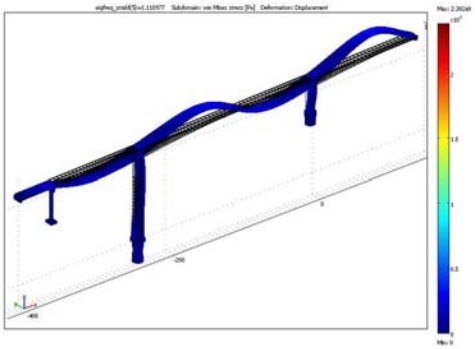

1.08 Hz

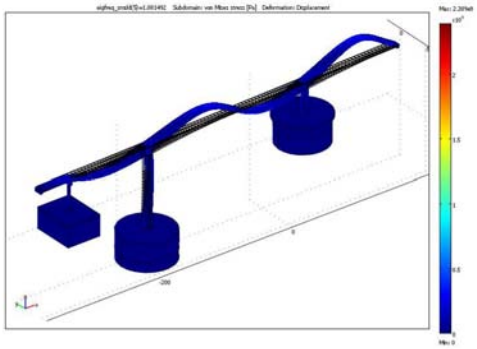

3rd bending

1.51 Hz

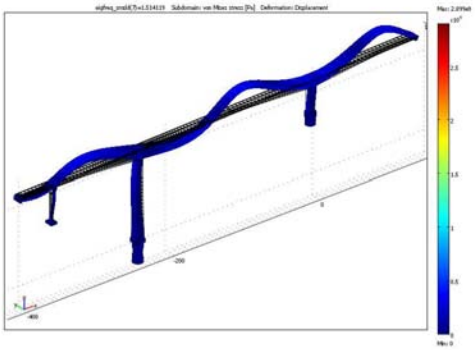

1.46 Hz

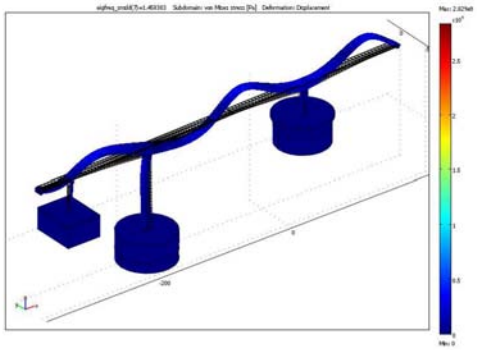

4th bending

1.93 Hz

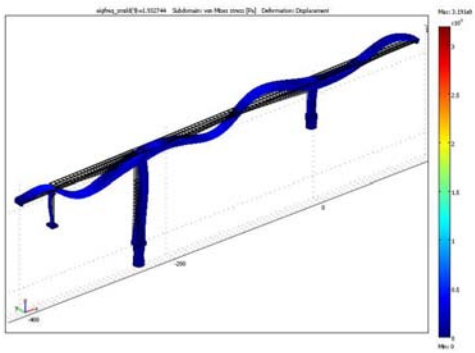

1.86 Hz

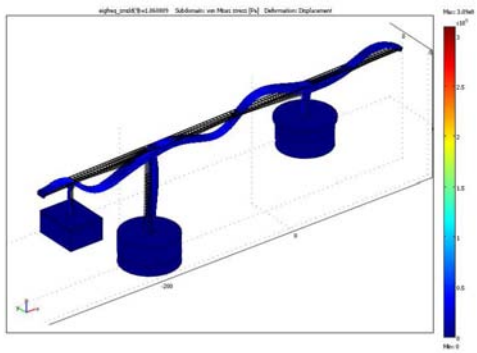

5th bending

2.31 Hz

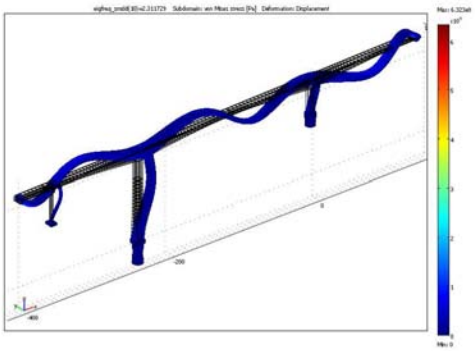

2.23 Hz

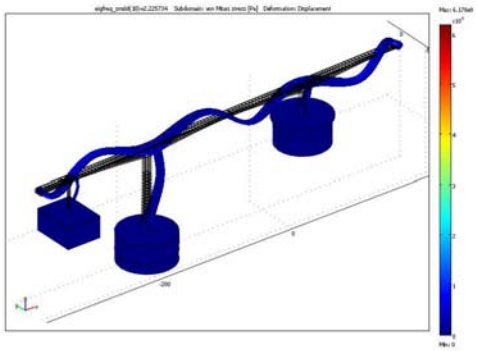

6th bending

2.83 Hz

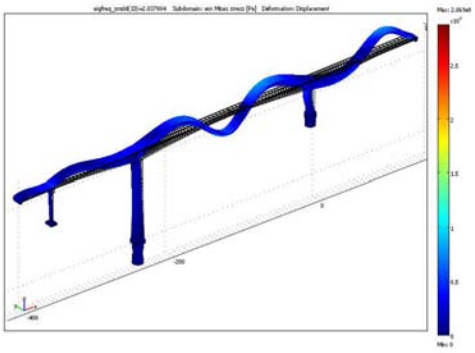

2.73 Hz

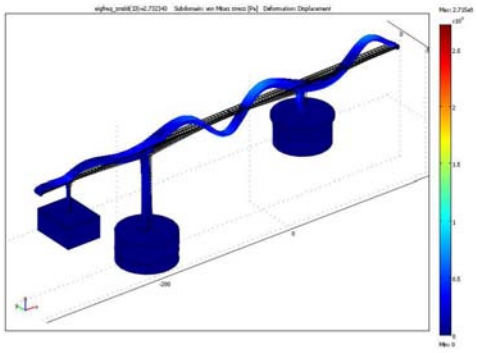

7th bending

3.17 Hz

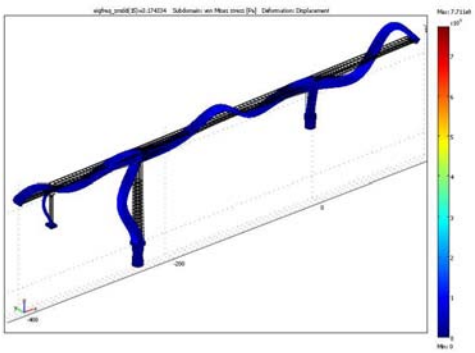

3.05 Hz

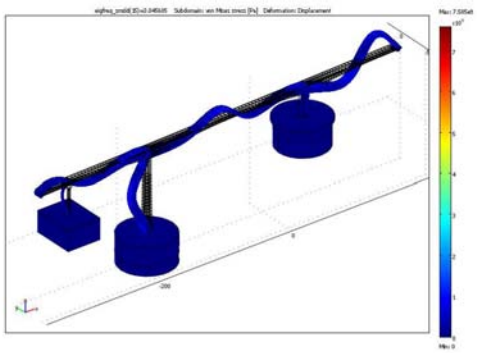

8th bending

3.63 Hz

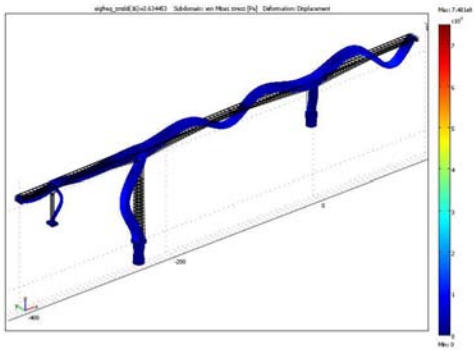

3.49 Hz

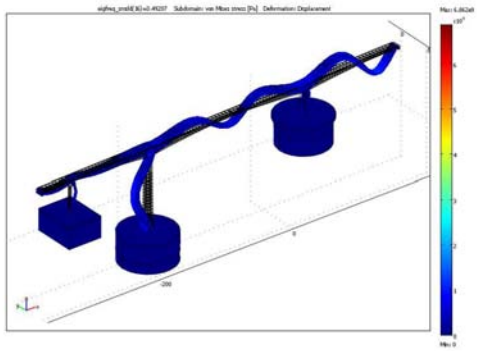

Appendix II

Comparison of LB and RB Fixed Base FEM of Metsovo Bridge

"1st Mode"
(1st transverse)

Left Branch(0.318 Hz)

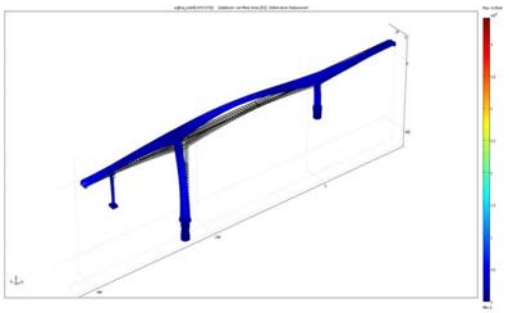

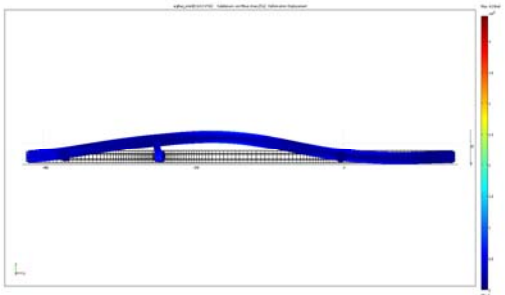

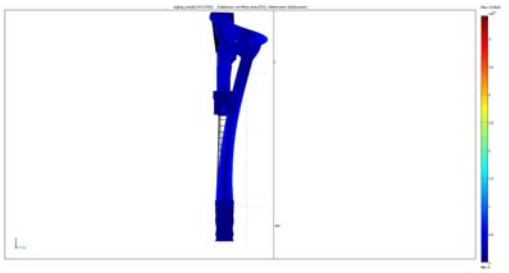

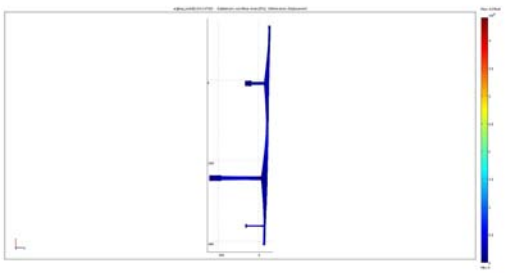

“1st Mode'”
(1st transverse)

Right Branch(0.322 Hz)

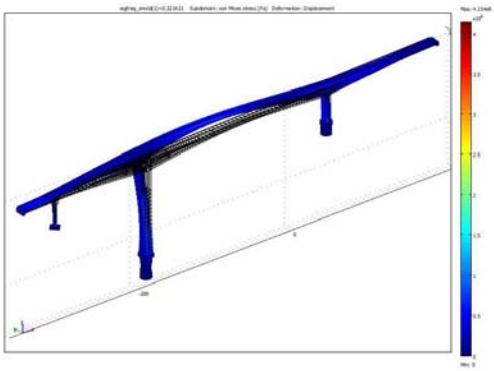

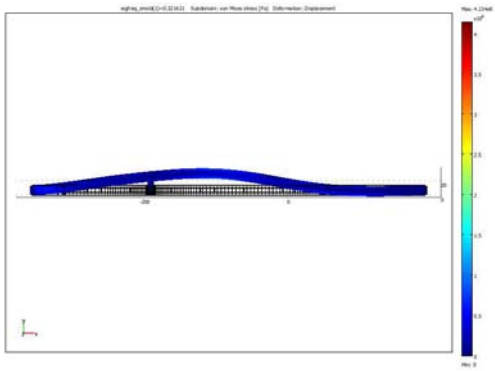

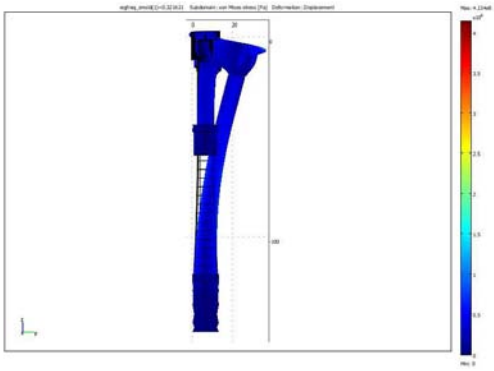

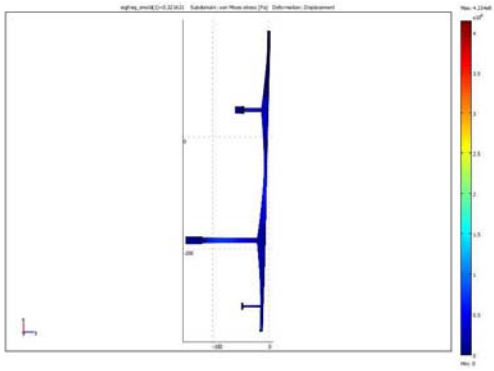

“4th Mode”
(2nd transverse)

Left Branch(0.622 Hz)

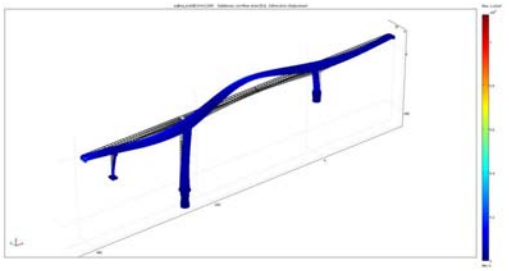

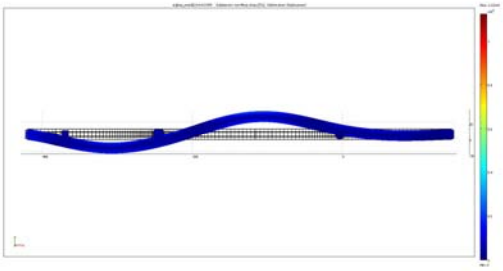

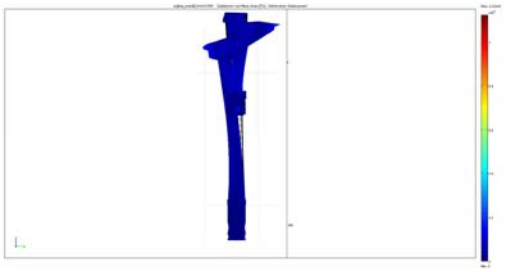

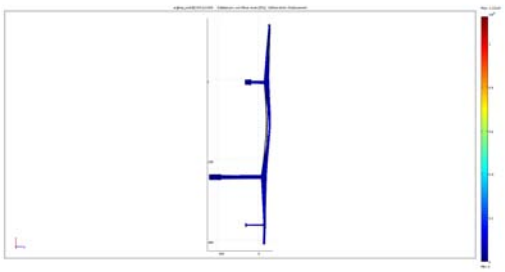

“4th Mode”
(2nd transverse)

Right Branch(0.640 Hz)

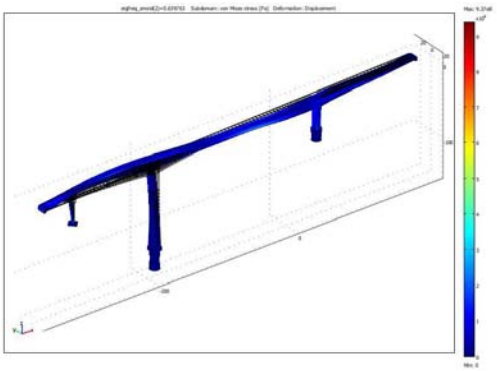

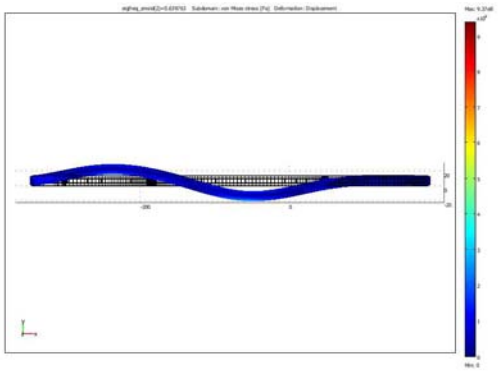

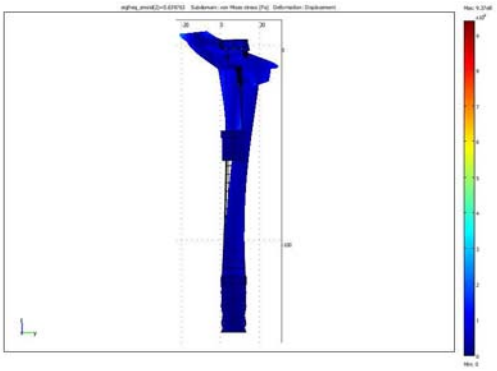

“5th Mode”
(1st bending)

Left Branch(0.645 Hz)

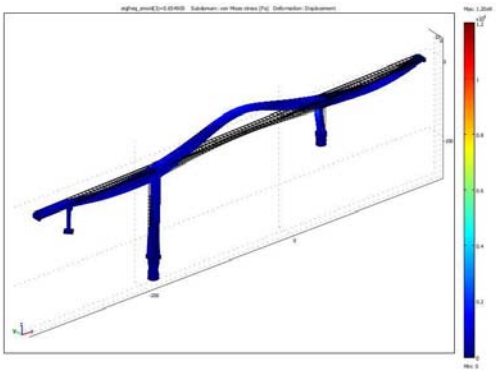

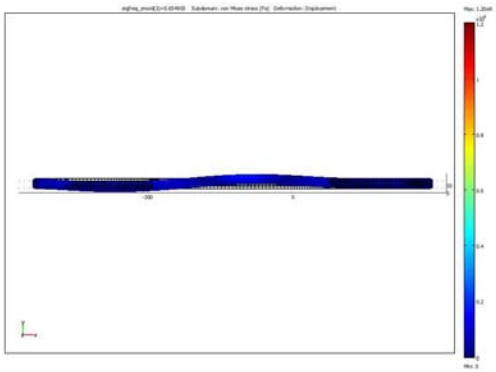

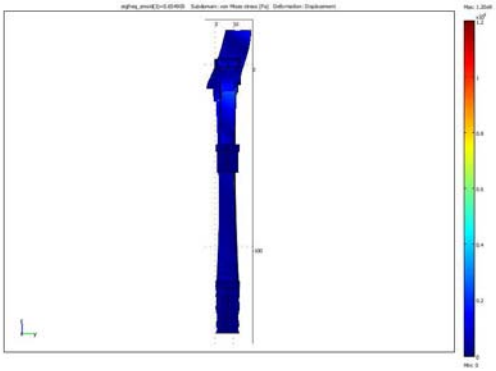

“5th Mode”
(1st bending)

Right Branch(0.655 Hz)

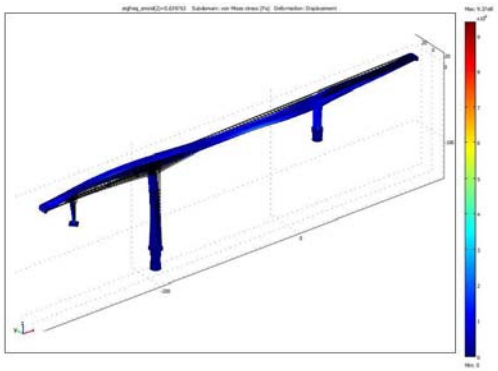

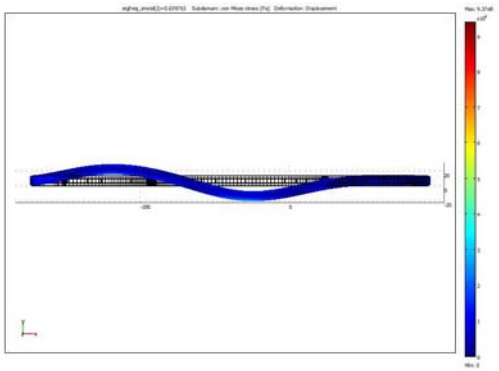

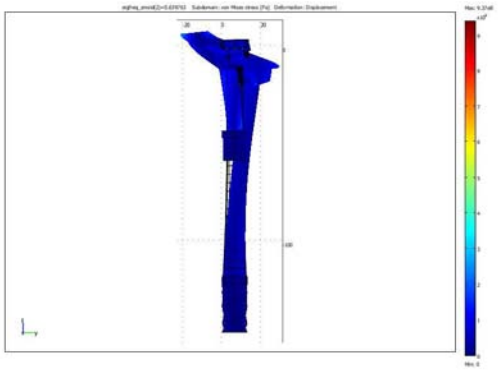

“7th Mode”
(3rd transverse)

Left Branch(0.989 Hz)

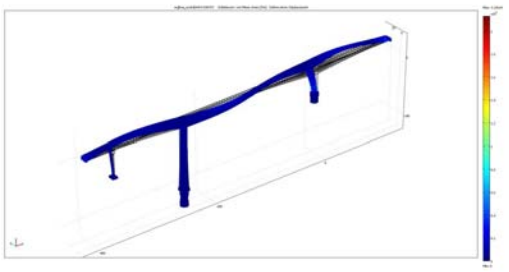

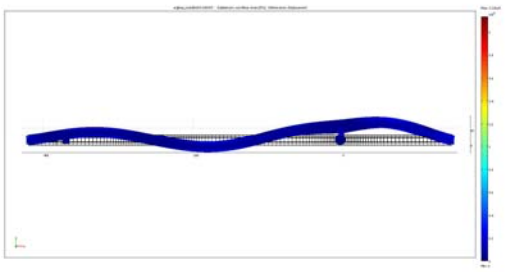

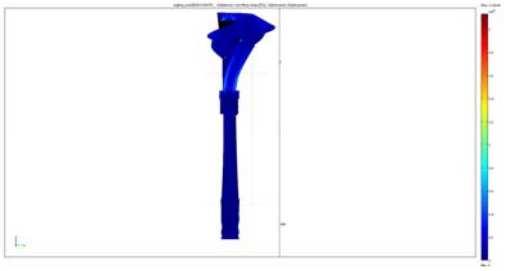

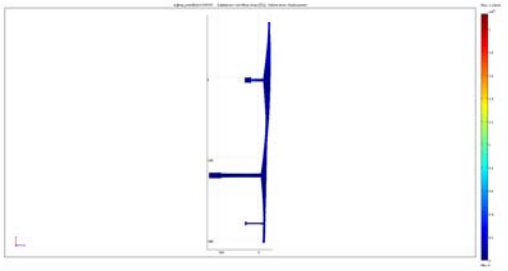

“7th Mode”
(3rd transverse)

Right Branch(1.001 Hz)

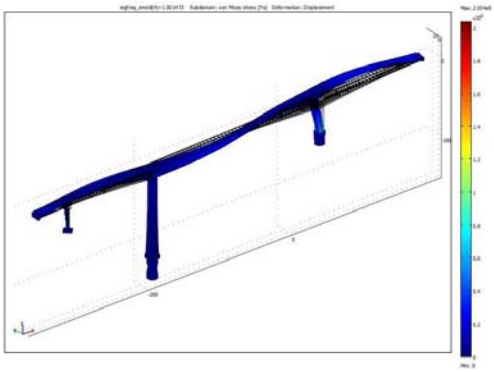

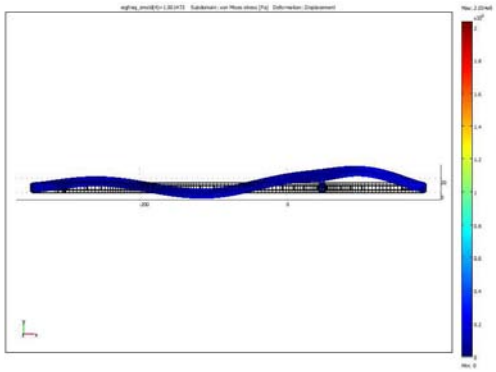

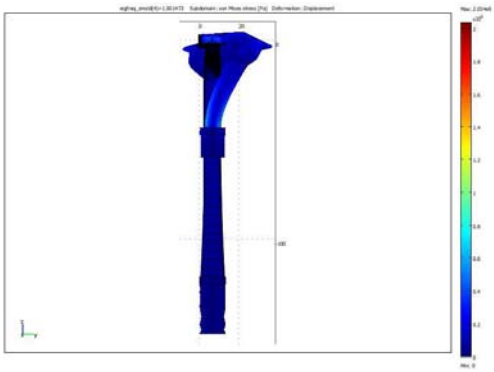

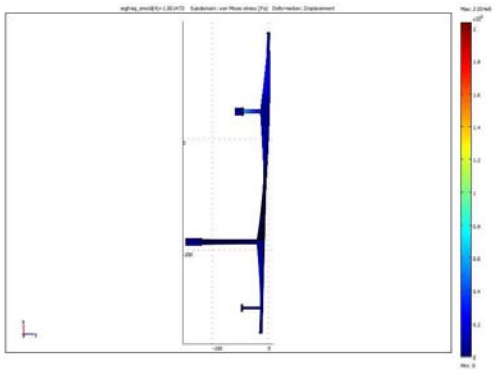

“8th Mode”
(2nd bending)

Left Branch(1.111 Hz)

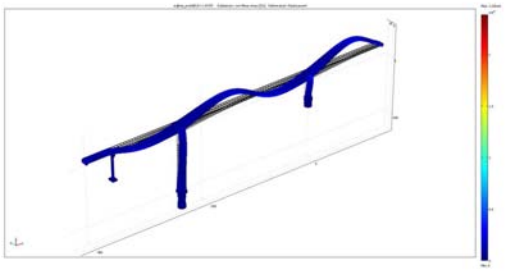

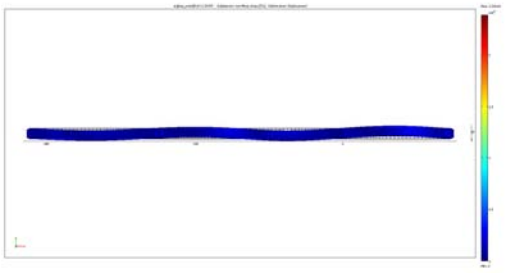

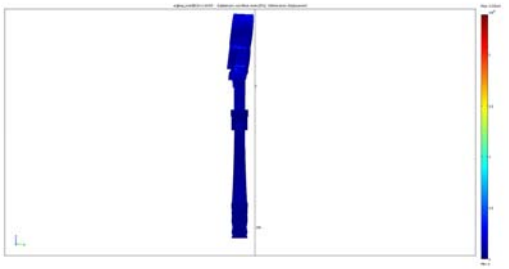

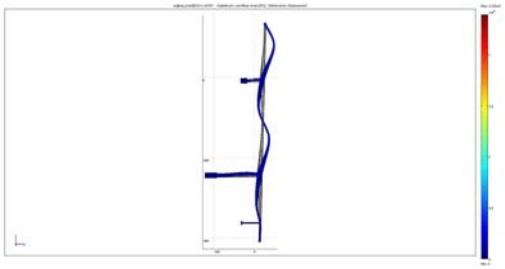

“8th Mode”
(2nd bending)

Right Branch(1.123 Hz)

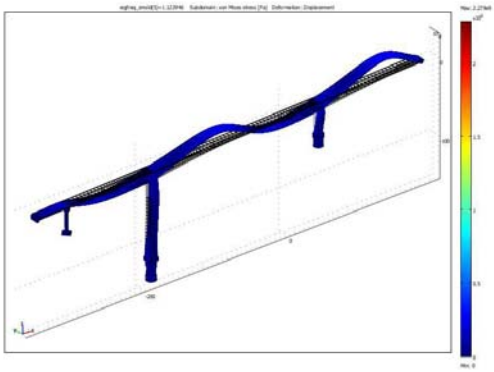

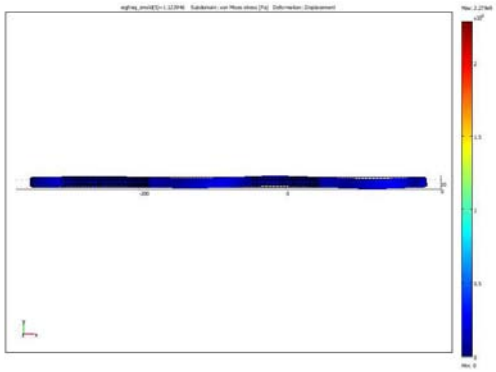

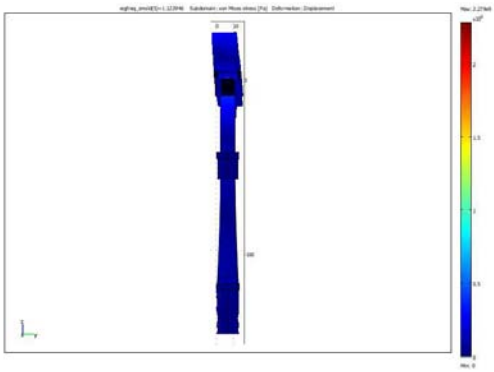

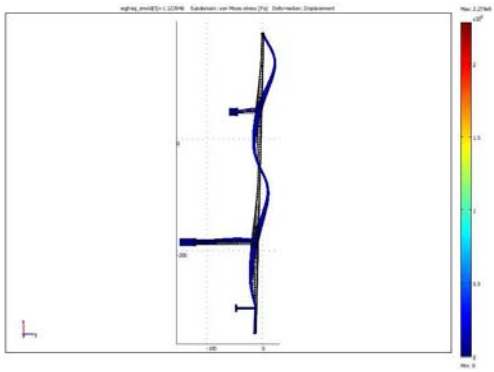

“9th Mode”
(4th transverse)

Left Branch(1.172 Hz)

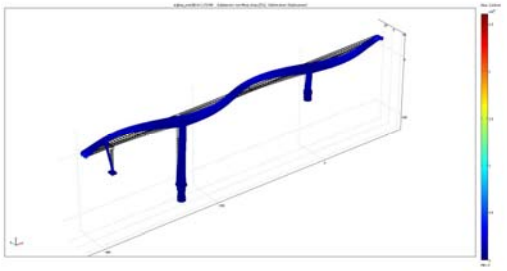

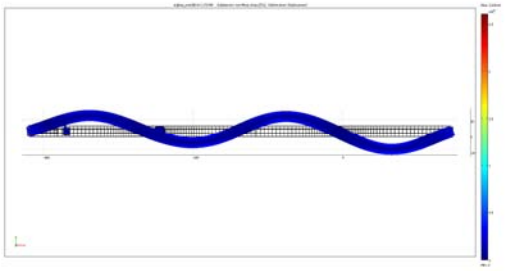

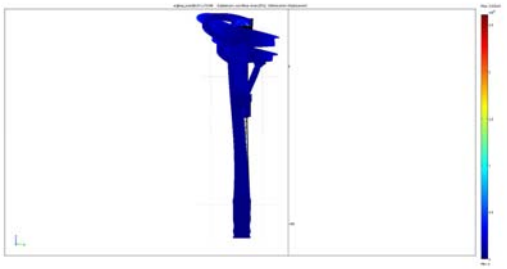

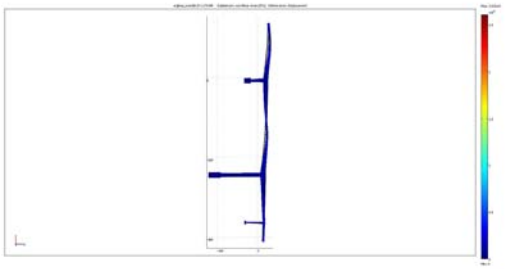

“9th Mode”
(4th transverse)

Right Branch(1.205 Hz)

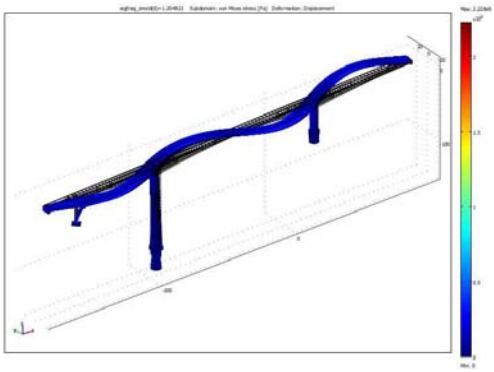

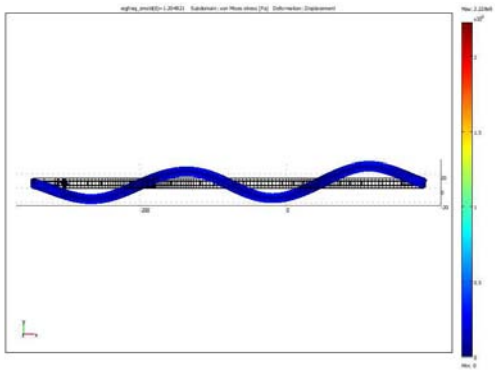

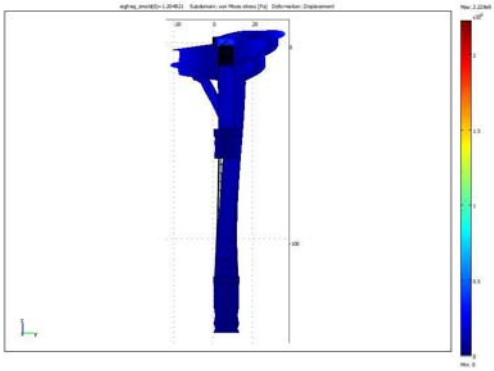

“10th Mode”
(3rd bending)

Left Branch(1.514 Hz)

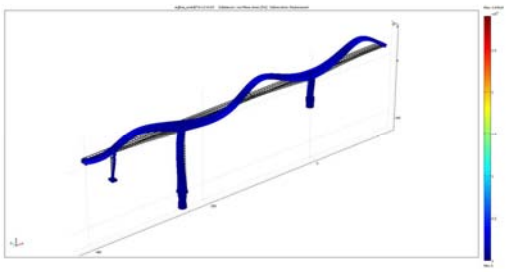

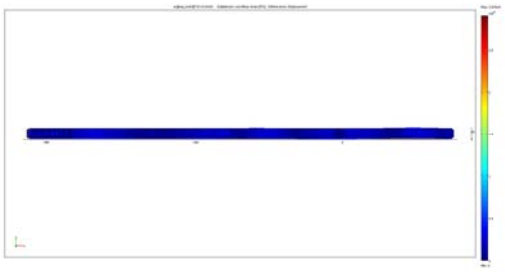

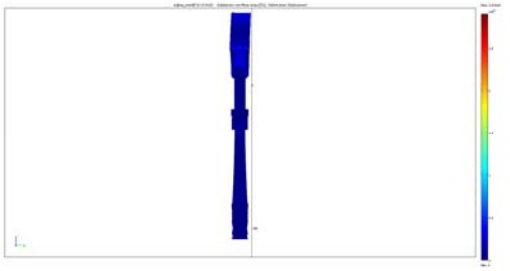

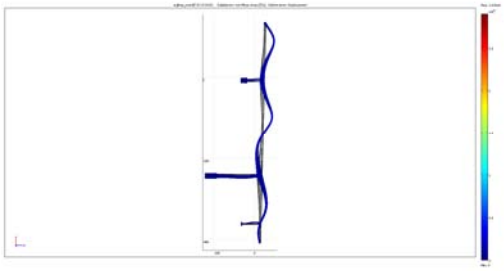

“10th Mode”
(3rd bending)

Right Branch(1.530 Hz)

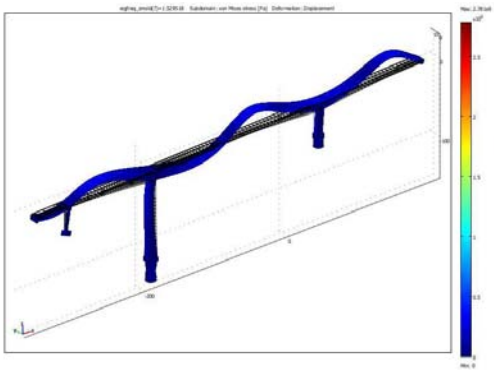

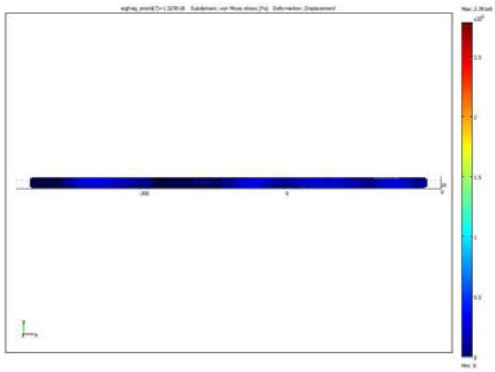

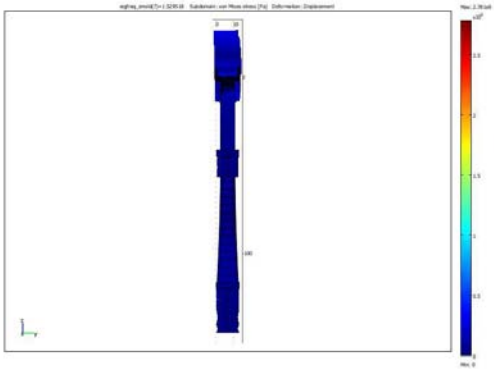

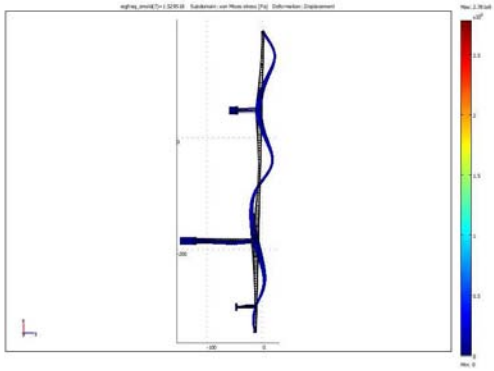

“11th Mode”
(5th transverse)

Left Branch(1.710 Hz)

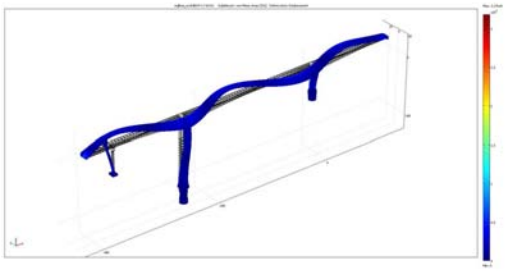

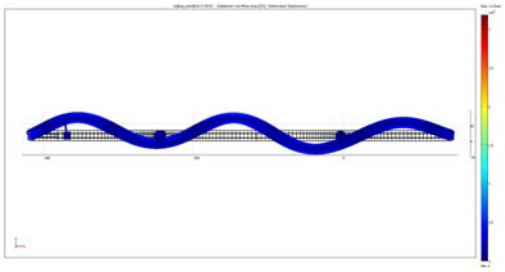

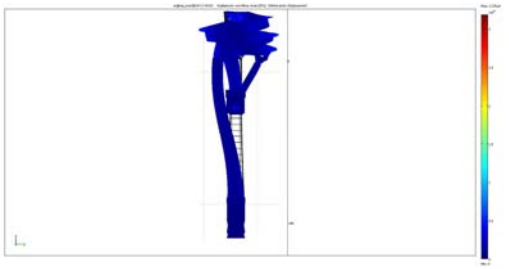

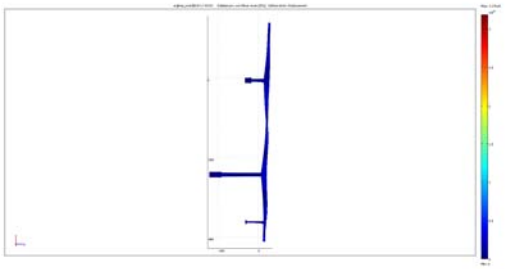

“11th Mode”
(5th transverse)

Right Branch(1.761 Hz)

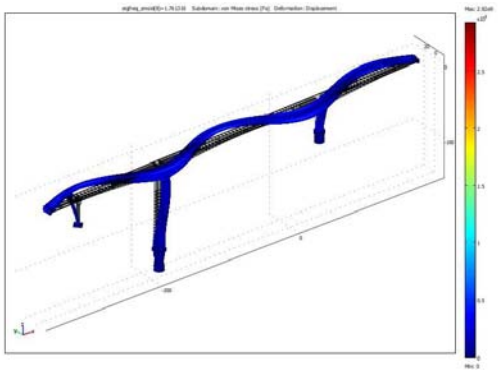

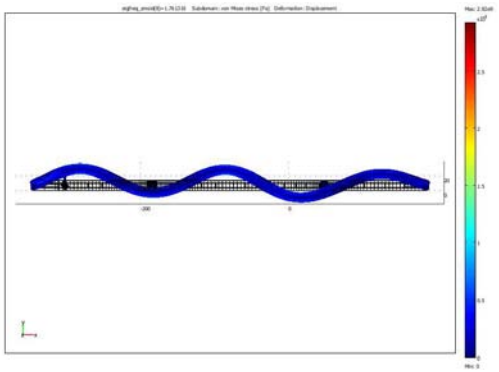

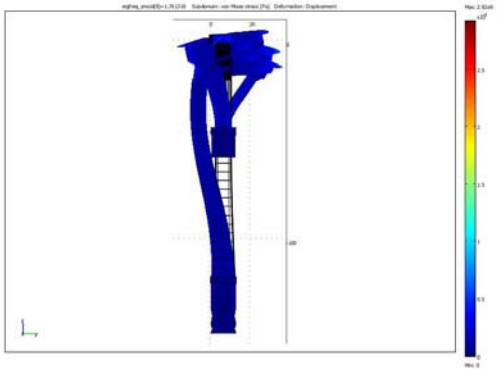

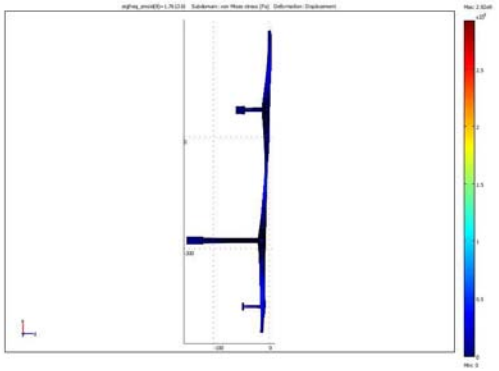

“12th Mode”
(4th bending)

Left Branch(1.933 Hz)

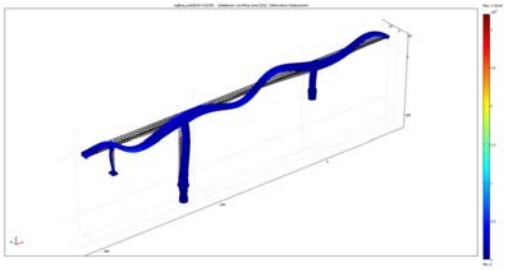

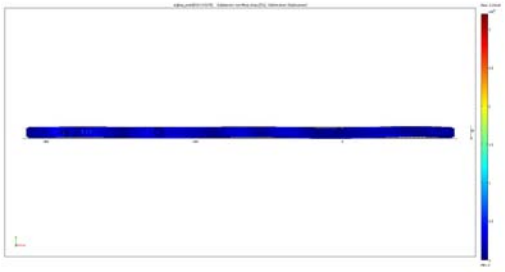

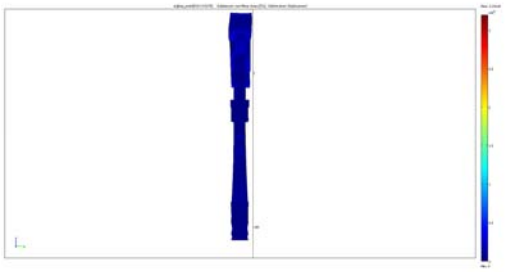

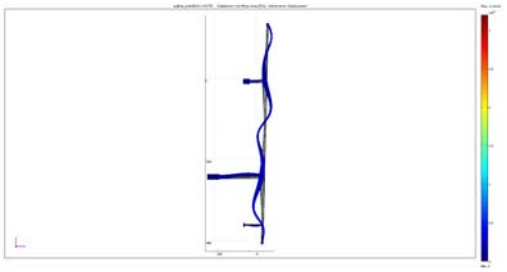

“12th Mode”
(4th bending)

Right Branch(1.956 Hz)

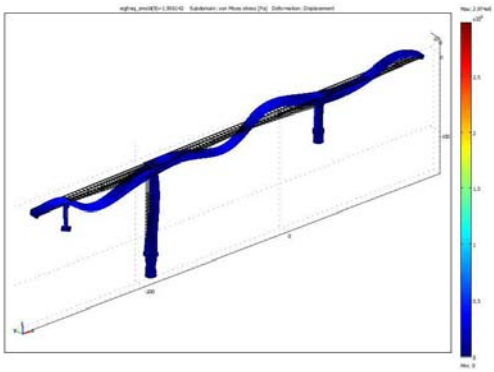

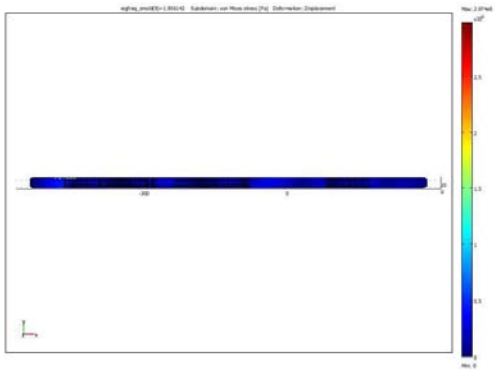

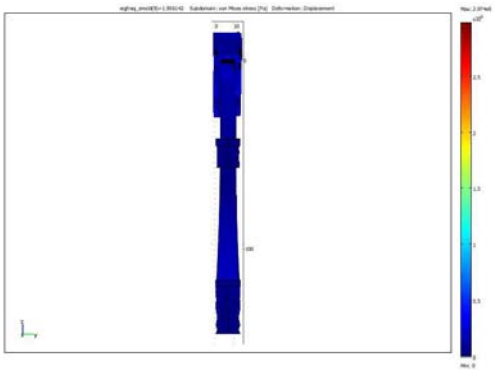

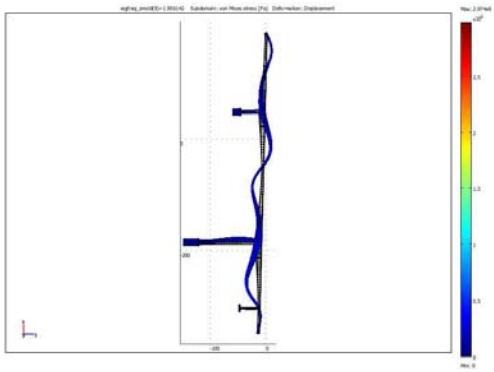

“13th Mode”
(5th bending)

Left Branch(2.312 Hz)

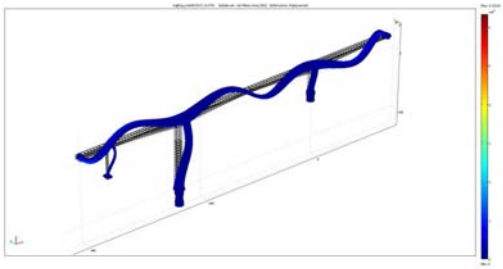

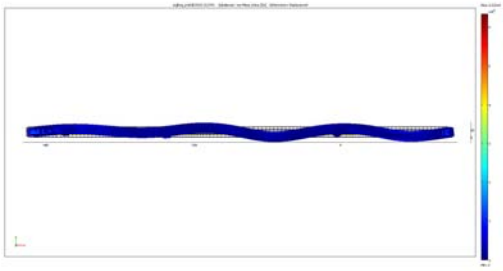

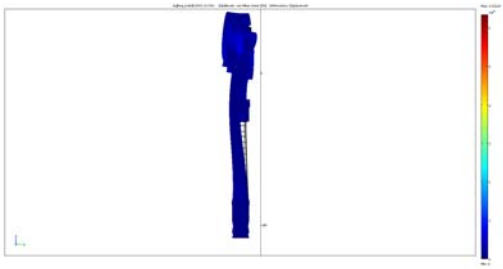

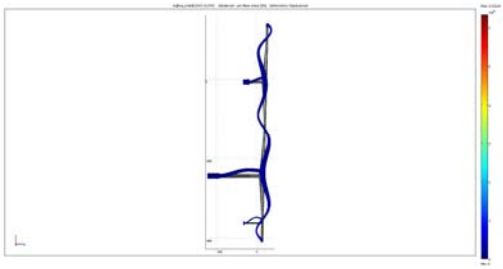

“13th Mode”
(5th bending)

Right Branch(2.350 Hz)

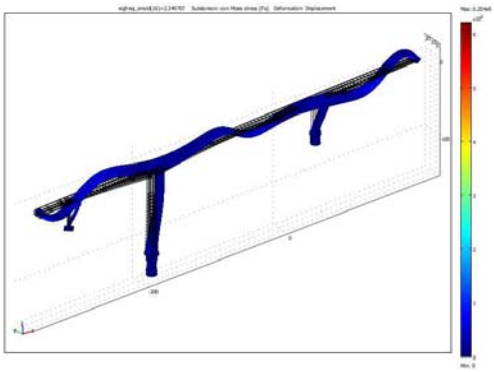

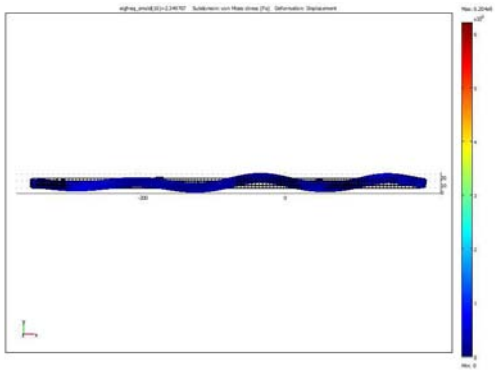

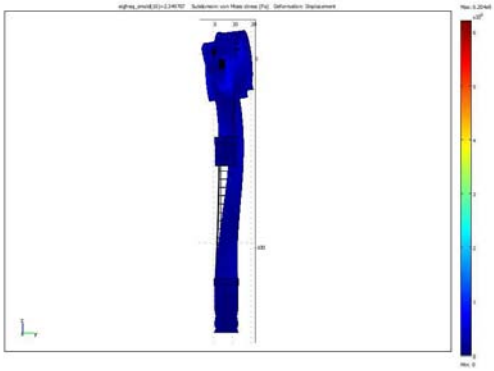

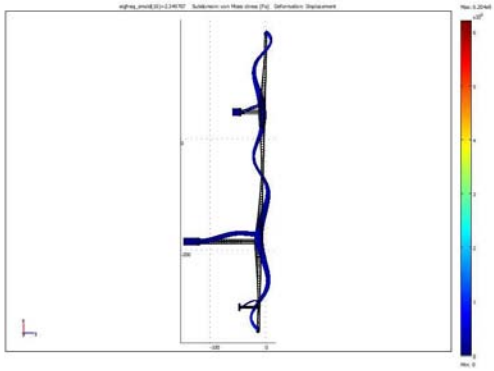

“14th Mode”
(6th transverse)

Left Branch(2.351 Hz)

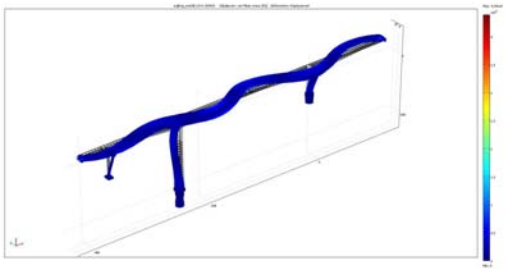

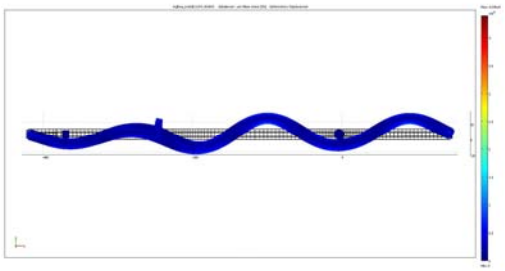

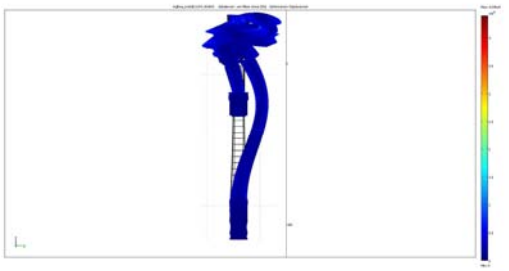

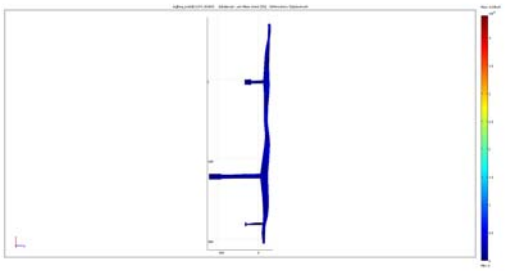

“14th Mode”
(6th transverse)

Right Branch(2.399 Hz)

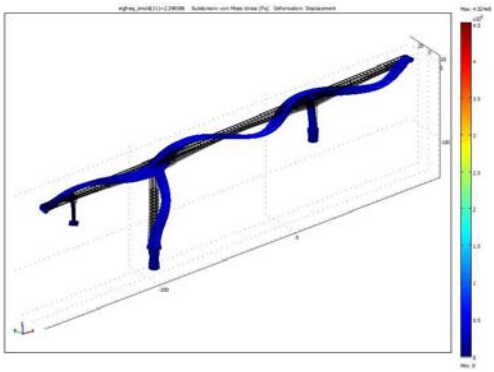

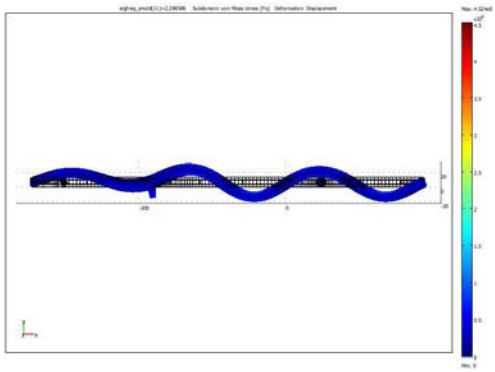

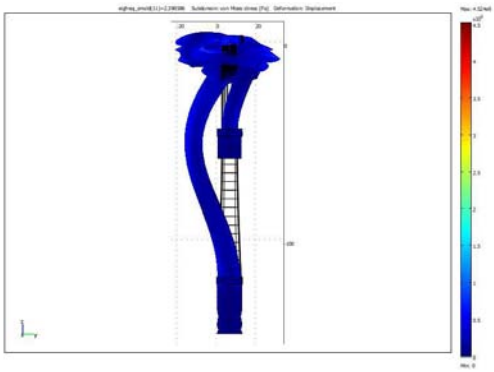

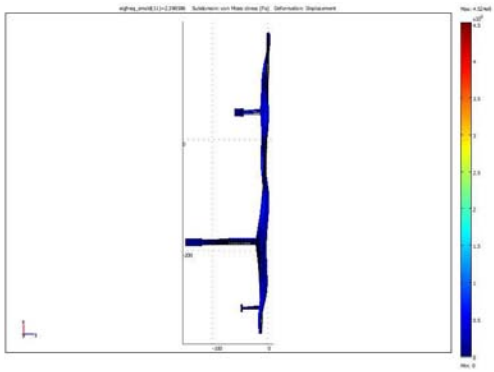

“15th Mode”
(6th bending)

Left Branch(2.838 Hz)

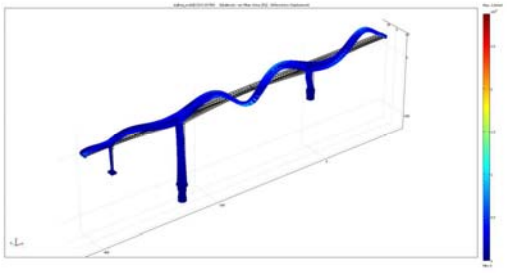

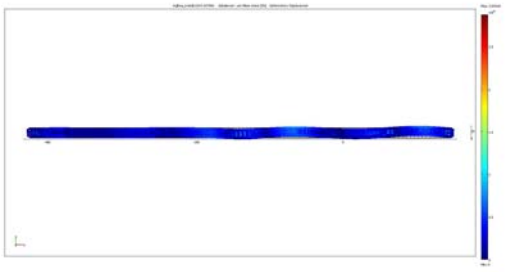

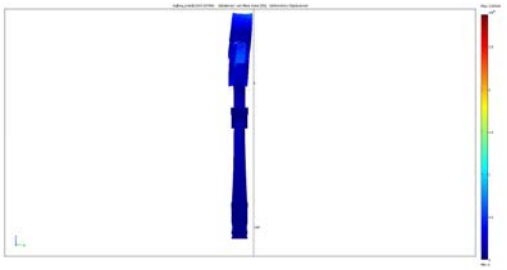

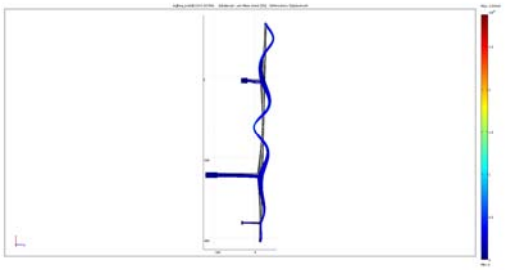

“15th Mode”
(6st bending)

Right Branch(2.857 Hz)

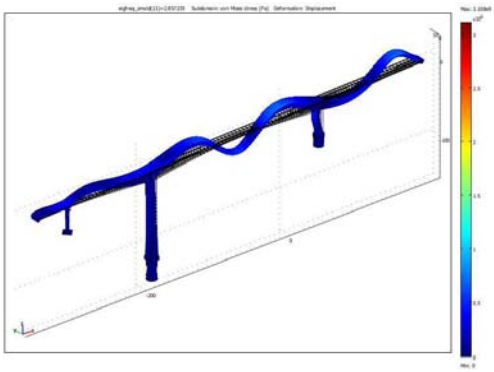

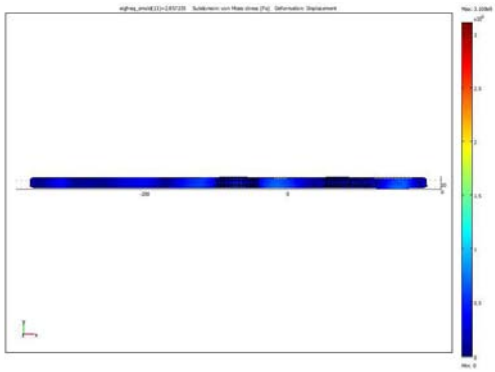

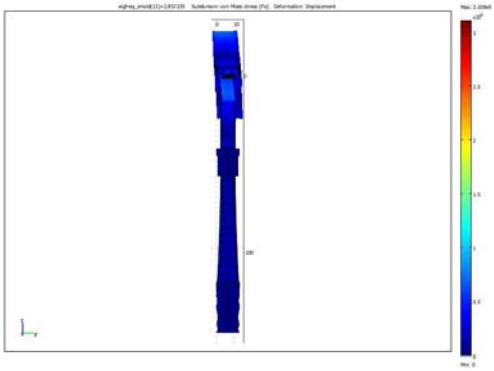

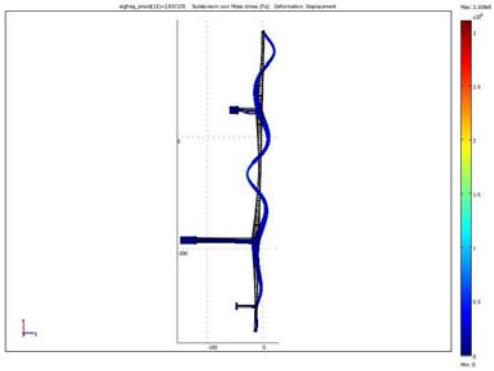

“16th Mode”
(7th transverse)

Left Branch(3.131 Hz)

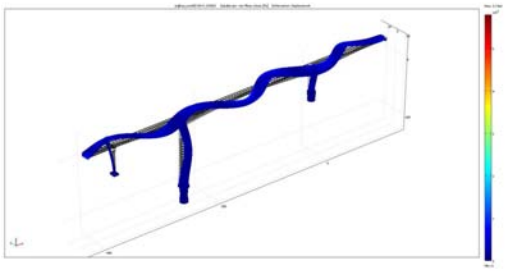

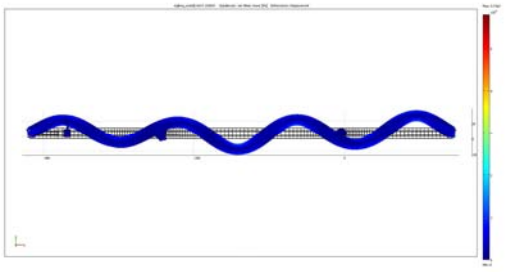

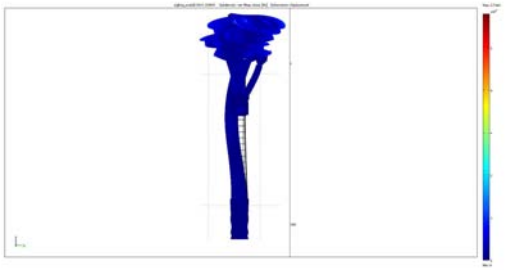

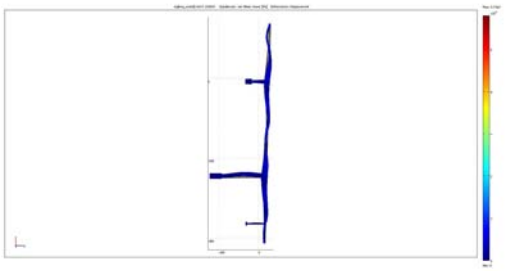

“16th Mode”
(7th transverse)

Right Branch(3.188 Hz)

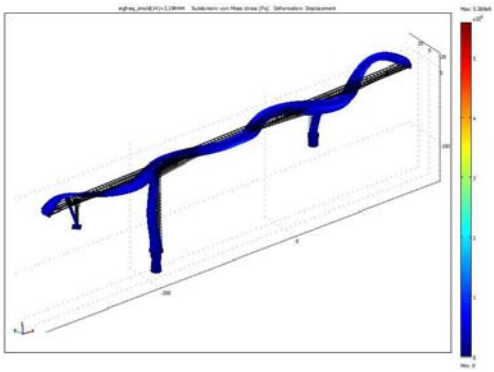

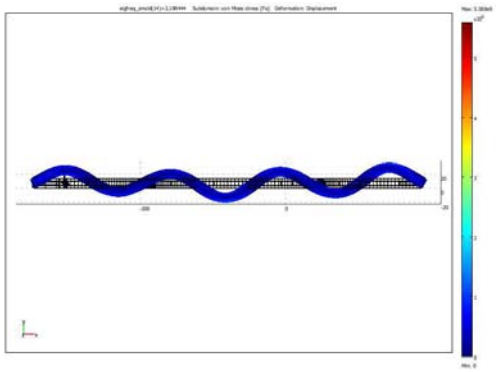

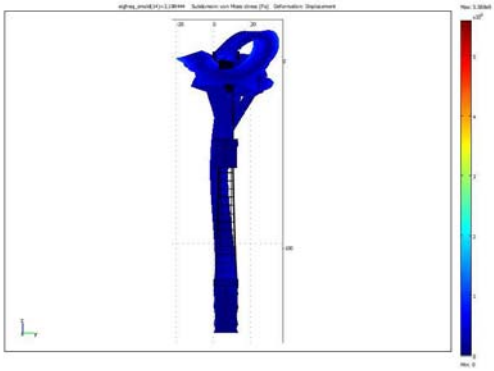

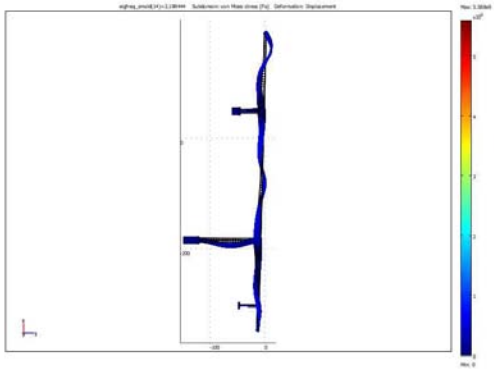

“17th Mode”
(7th bending)

Left Branch(3.174 Hz)

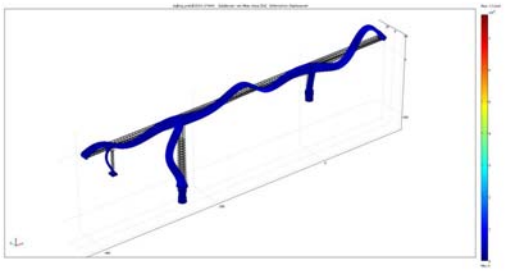

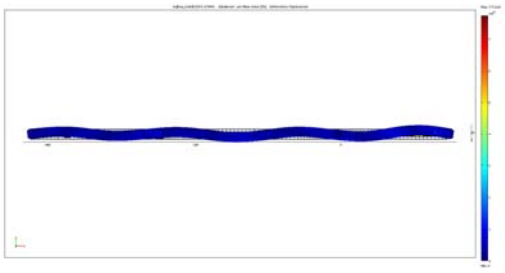

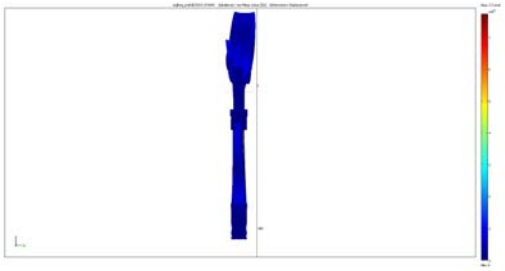

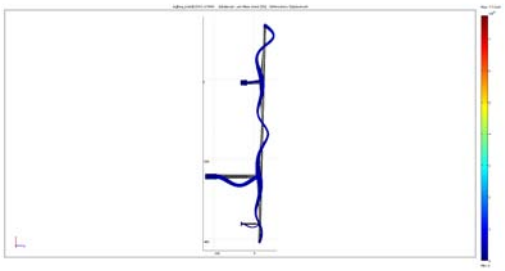

“17th Mode”
(7th bending)

Right Branch(3.209 Hz)

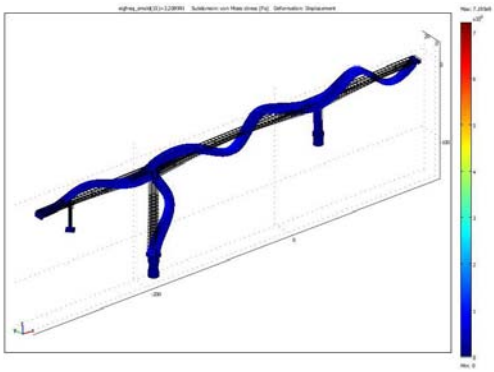

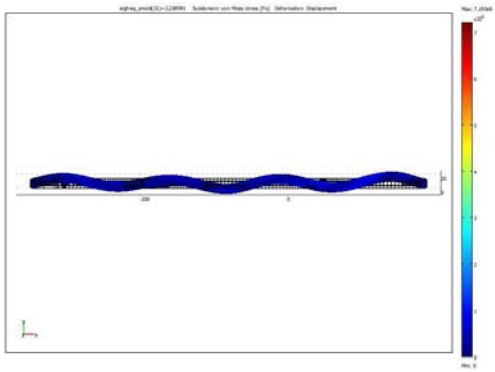

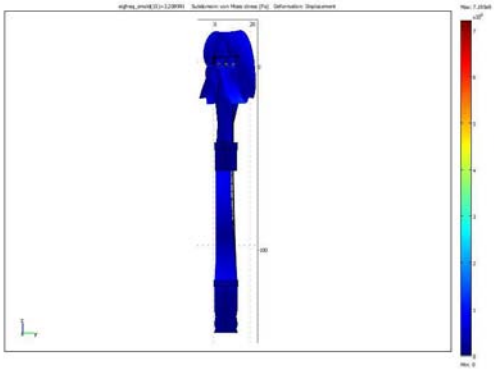

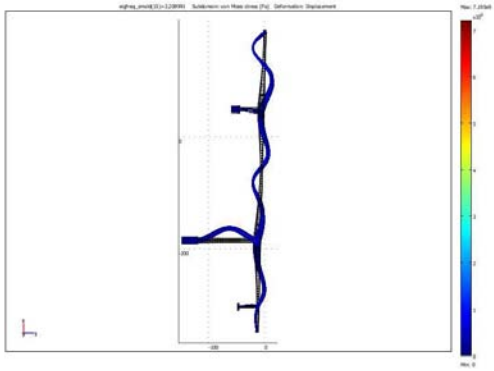

Appendix III

Sensor Locations on LB of Metsovo Bridge During 11 Setups

"1st Setup" (JQ003)

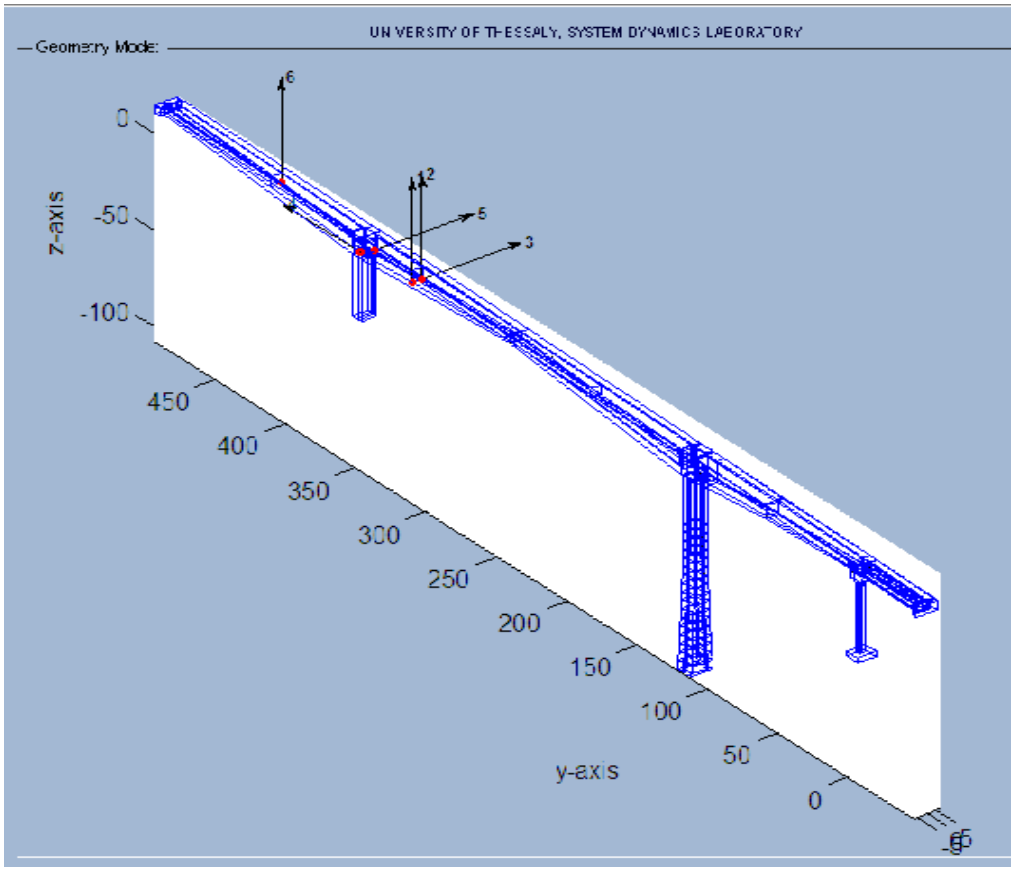

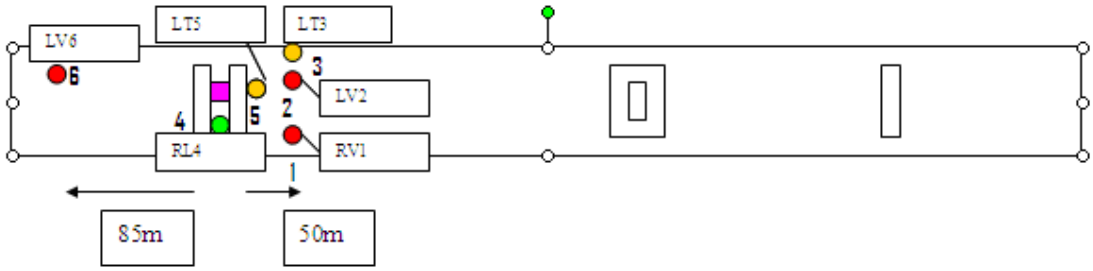

Sensor1: 'CH01_RV1' (vertical)
Sensor2: 'CH02_LV2'(vertical)
Sensor3: 'CH03_LT3' (transverse)
Sensor4: 'CH04_RL4'(longitudinal)
Sensor5: 'CH05_LT5'(transverse)
Sensor6: 'CH06_LV6'(vertical)

"2nd Setup" (JQ004)

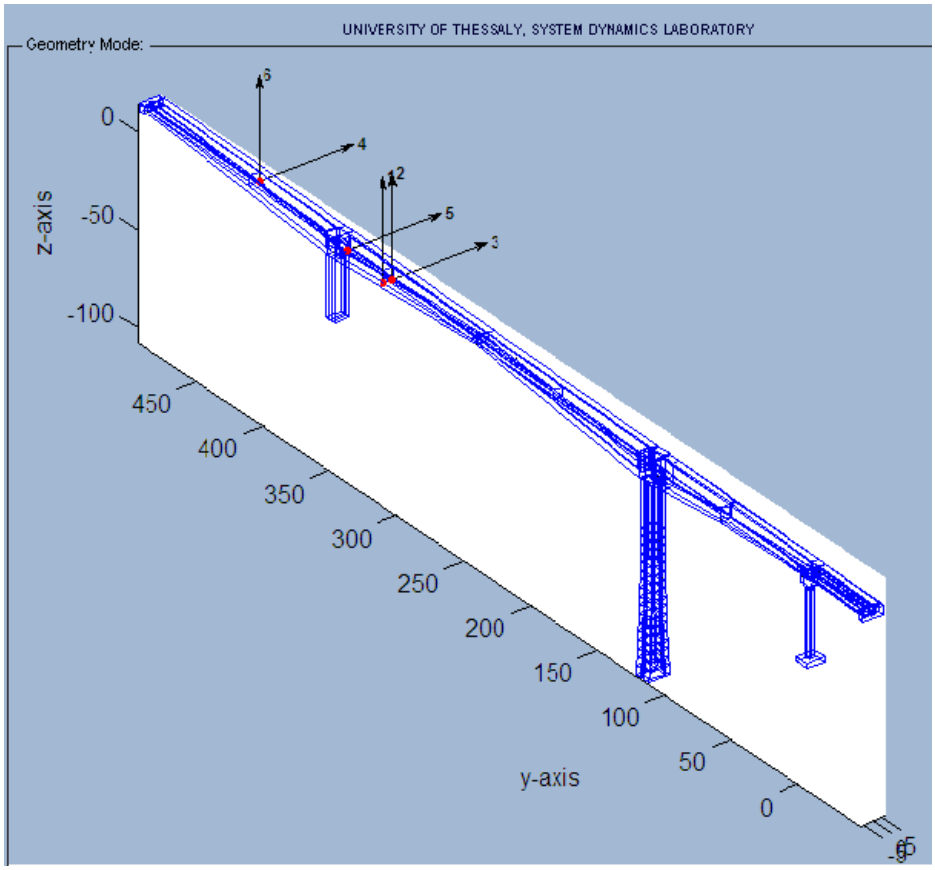

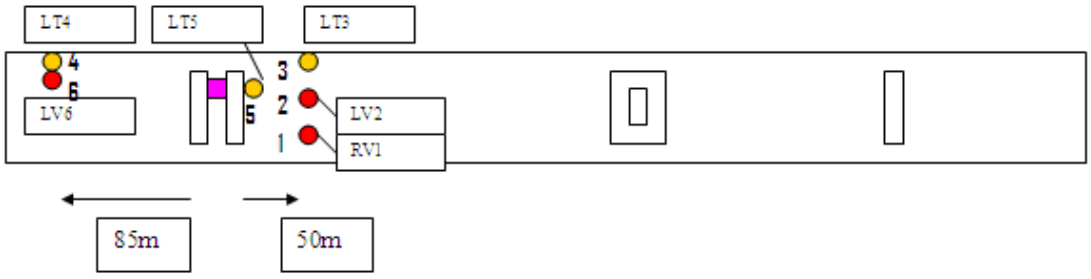

Sensor1: 'CH01_RV1' (vertical)
Sensor2: 'CH02_LV2'(vertical)
Sensor3: 'CH03_LT3' (transverse)
Sensor4: 'CH04_LT41'(transverse)
Sensor5: 'CH05_LT5'(transverse)
Sensor6: 'CH06_LV6'(vertical)

"3rd Setup" (JQ005)

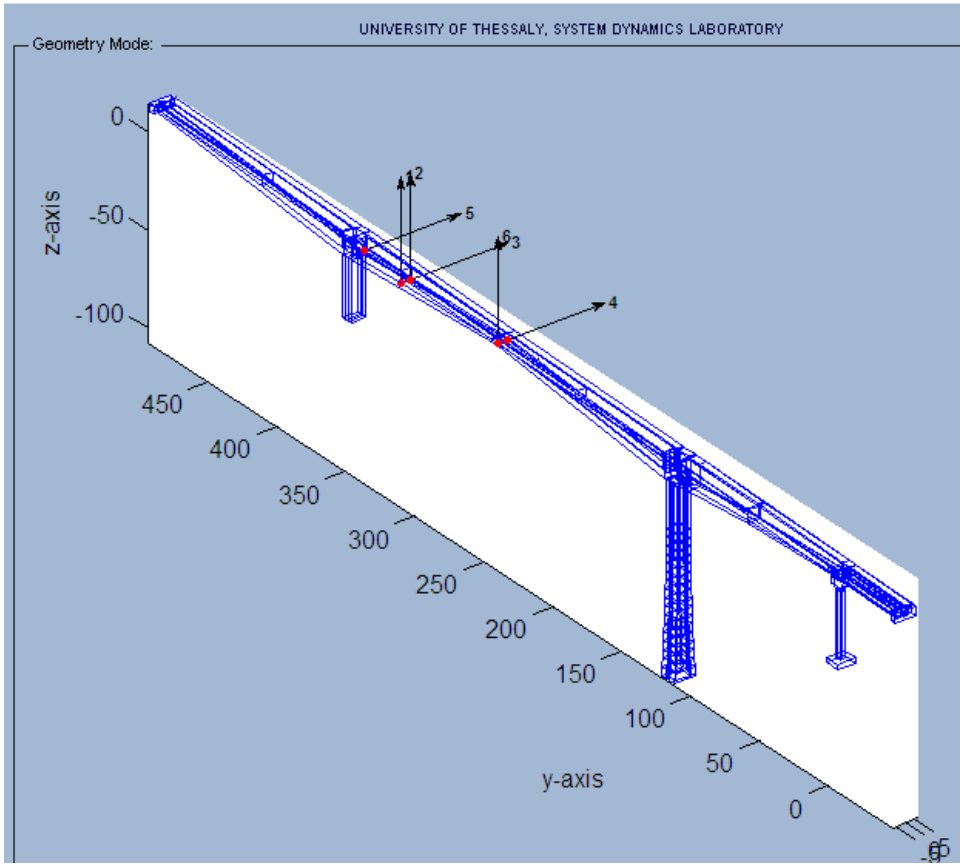

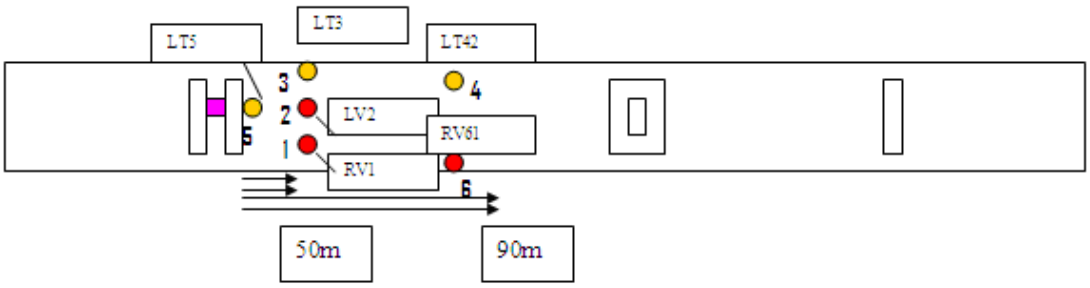

Sensor1: 'CH01_RV1' (vertical)
Sensor2: 'CH02_LV2'(vertical)
Sensor3: 'CH03_LT3' (transverse)
Sensor4: 'CH04_LT42'(transverse)
Sensor5: 'CH05_LT5'(transverse)
Sensor6: 'CH06_RV61'(vertical)

"4th Setup" (JQ006)

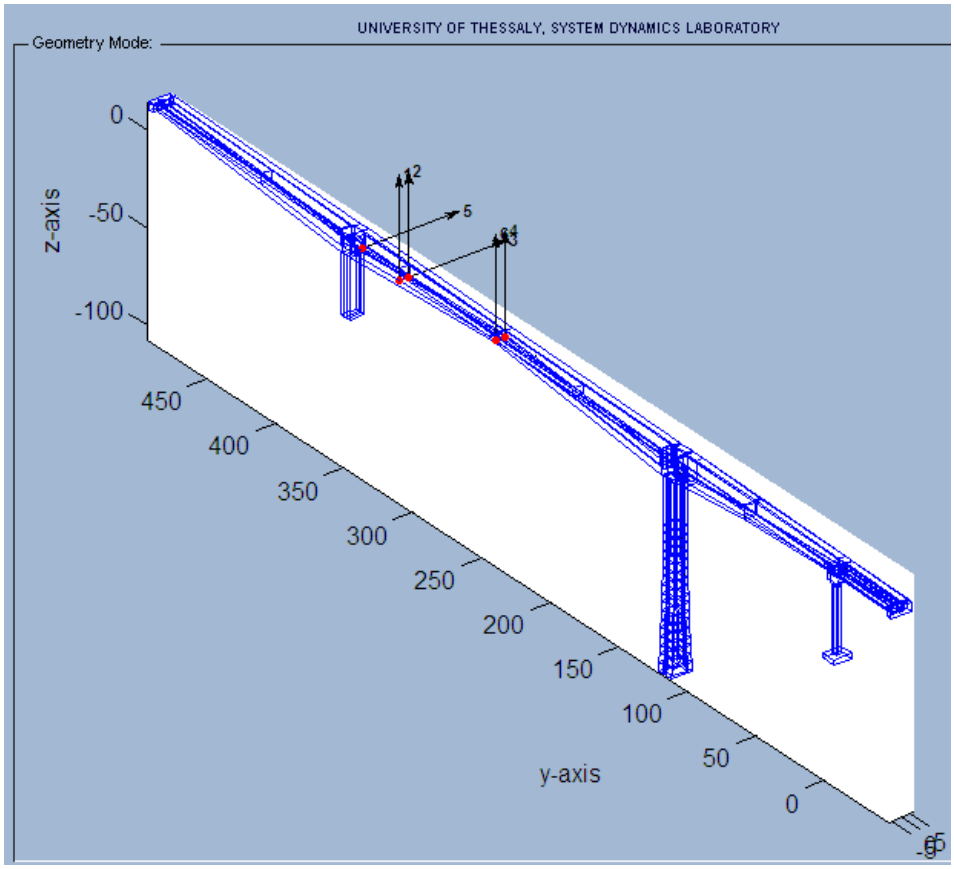

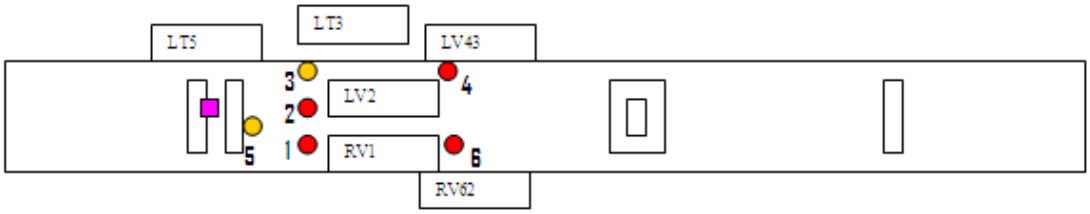

Sensor1: 'CH01_RV1' (vertical)
Sensor2: 'CH02_LV2'(vertical)
Sensor3: 'CH03_LT3' (transverse)
Sensor4: 'CH04_LV43' (vertical)
Sensor5: 'CH05_LT5'(transverse)
Sensor6: 'CH06_RV61'(vertical)

"5th Setup" (JR002)

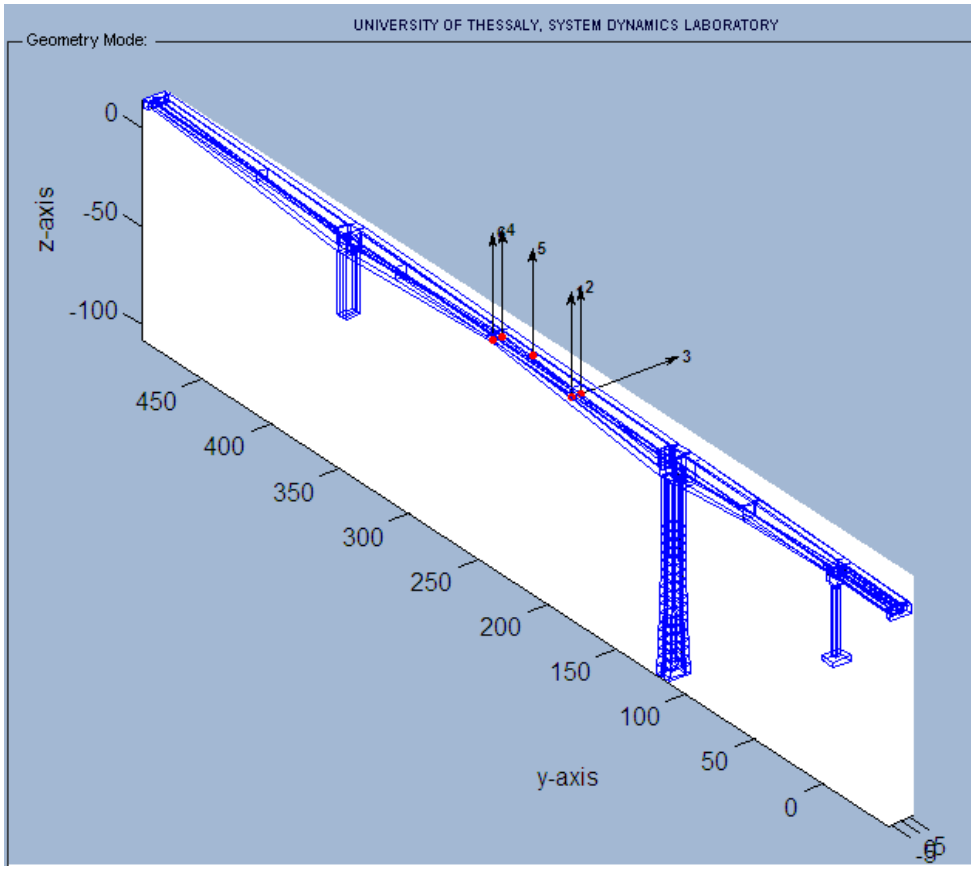

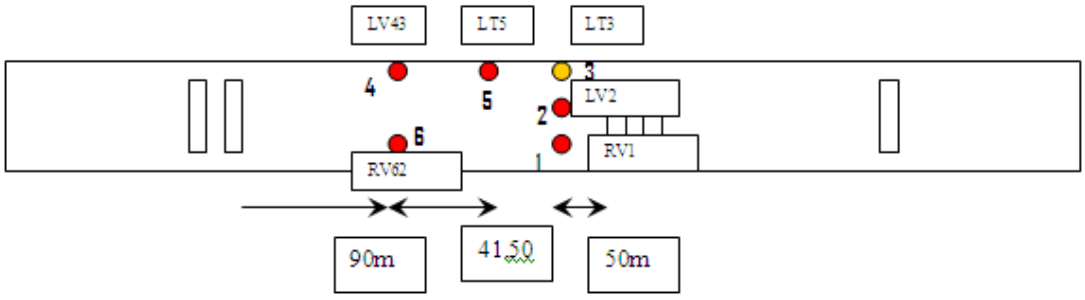

Sensor1: 'CH01_RV1' (vertical)
Sensor2: 'CH02_LV2'(vertical)
Sensor3: 'CH03_LT3' (transverse)
Sensor4: 'CH04_LV44'(vertical)
Sensor5: 'CH05_LT5'(vertical)
Sensor6: 'CH06_RV62'(vertical)

"6th Setup" (JS003)

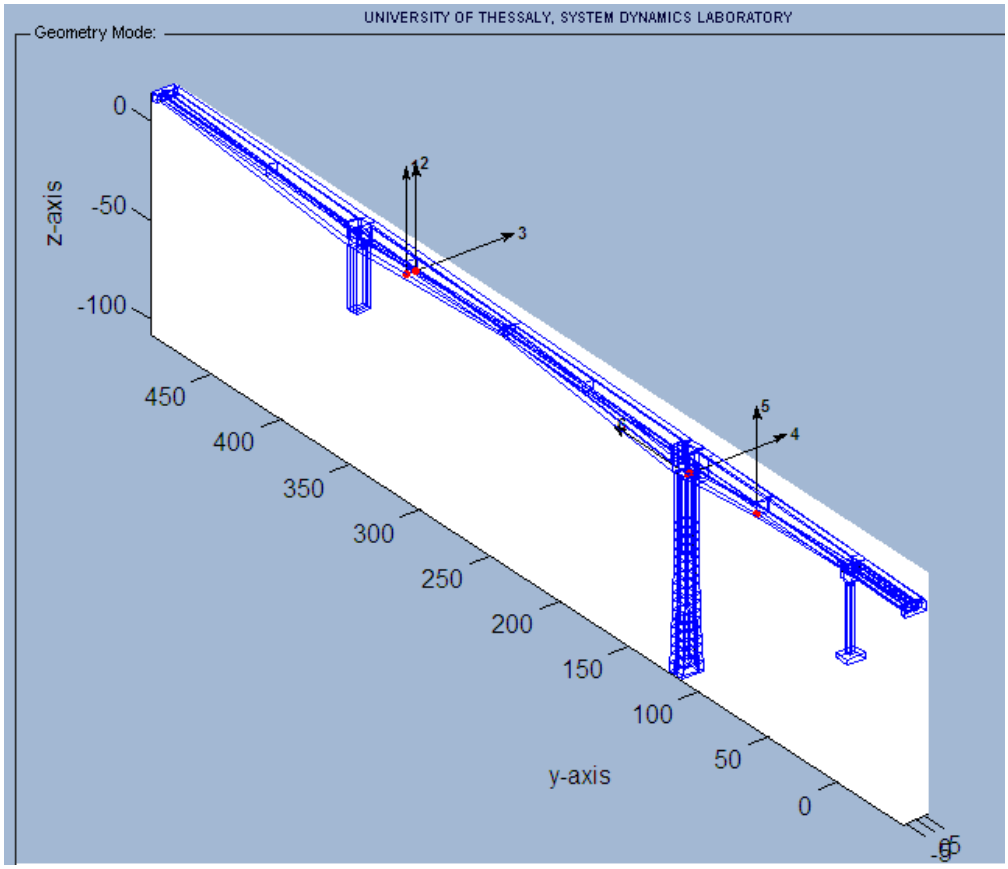

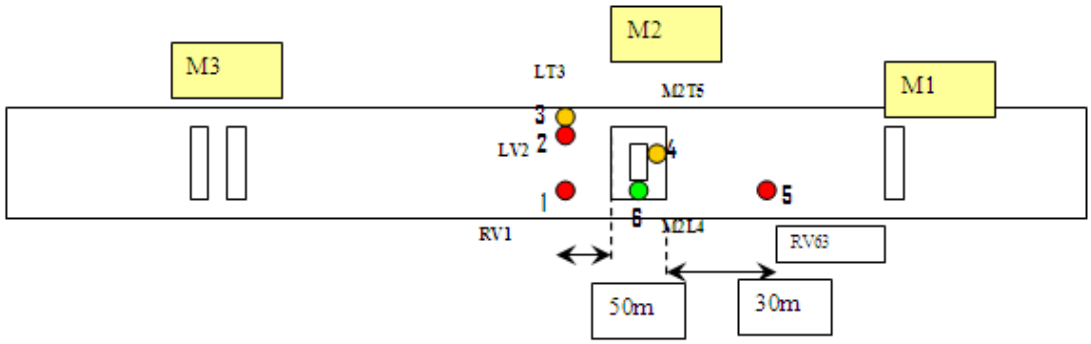

Sensor1: 'CH01_RV1' (vertical)
Sensor2: 'CH02_LV2'(vertical)
Sensor3: 'CH03_LT3' (transverse)
Sensor4: 'CH04_M2T5'(transverse)
Sensor5: 'CH05_RV63'(vertical)
Sensor6: 'CH06_M2L4'(longitudinal)

"7th Setup" (JS005)

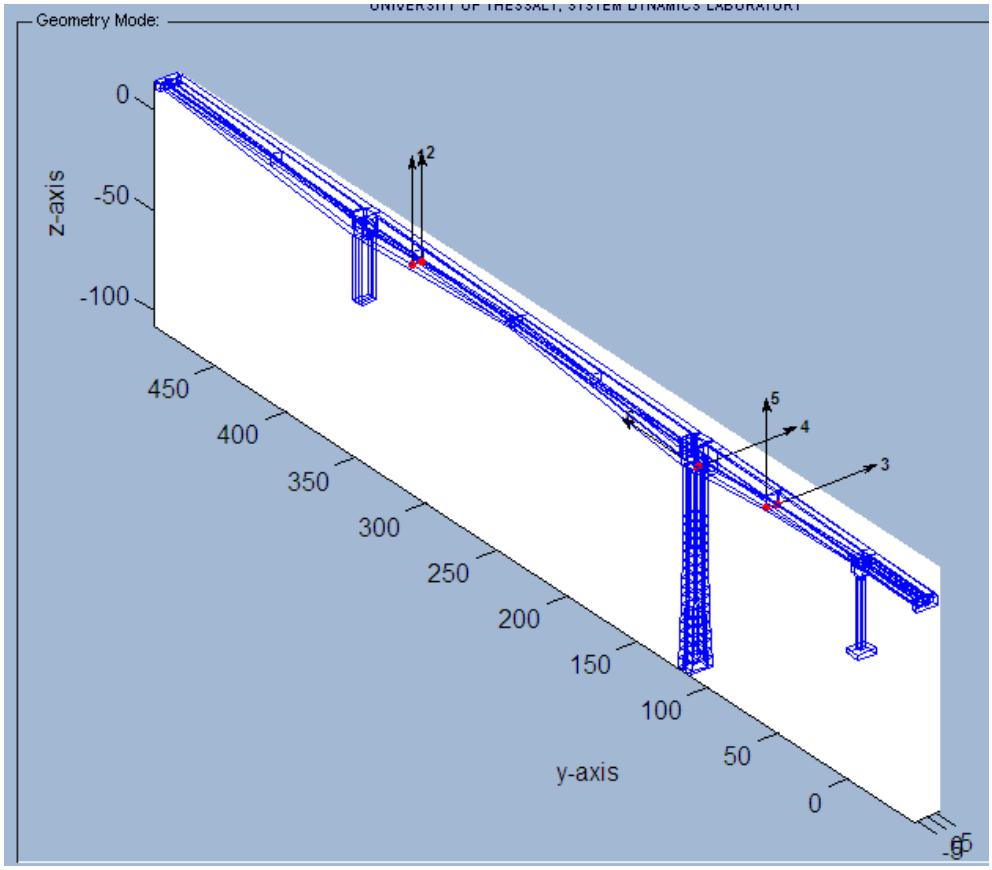

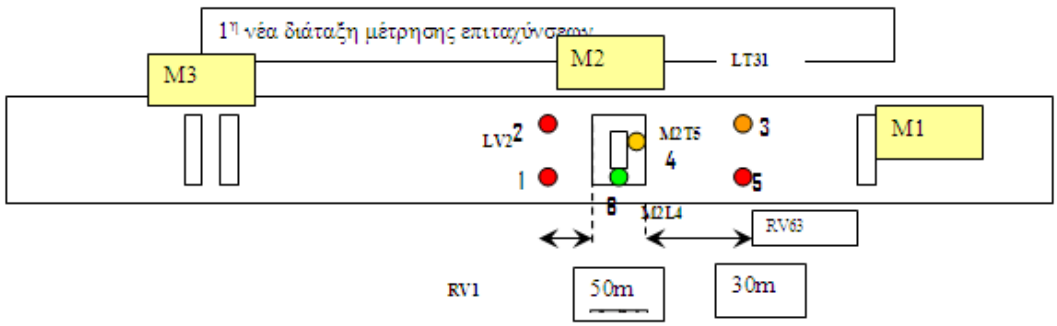

Sensor1: 'CH01_RV1' (vertical)
Sensor2: 'CH02_LV2'(vertical)
Sensor3: 'CH03_LT31' (transverse)
Sensor4: 'CH04_M2T5'(transverse)
Sensor5: 'CH05_RV63'(vertical)
Sensor6: 'CH06_M2L4'(longitudinal)

"8th Setup" (JT003)

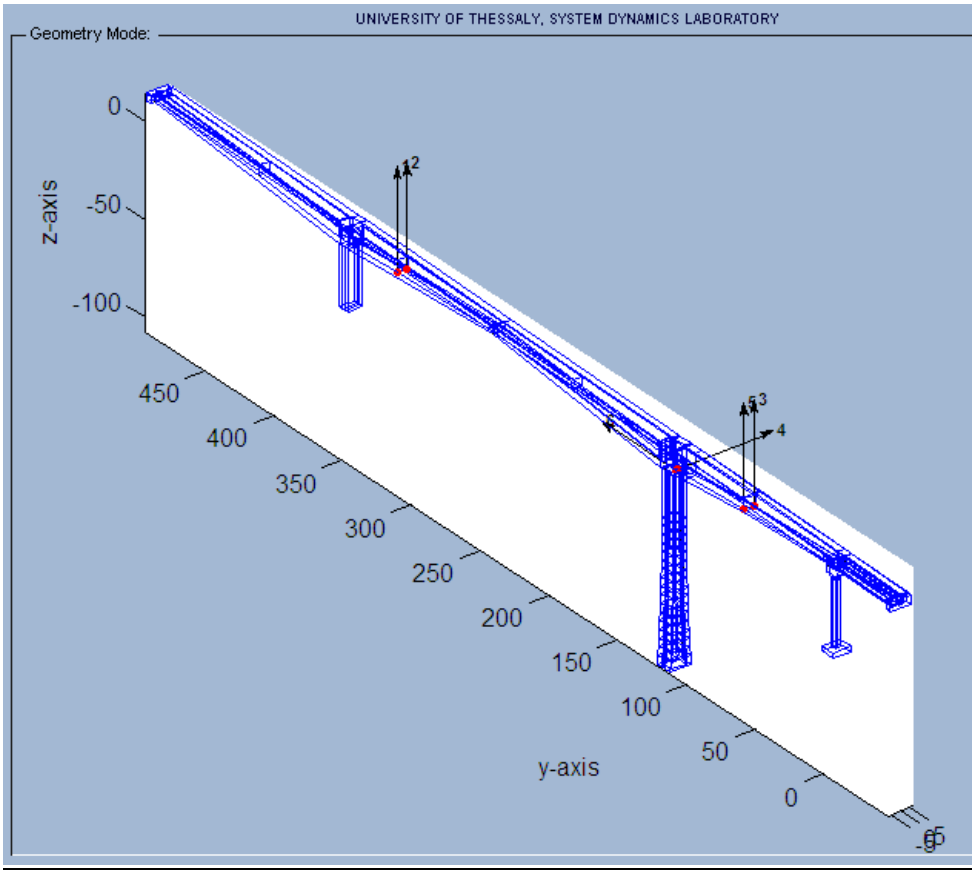

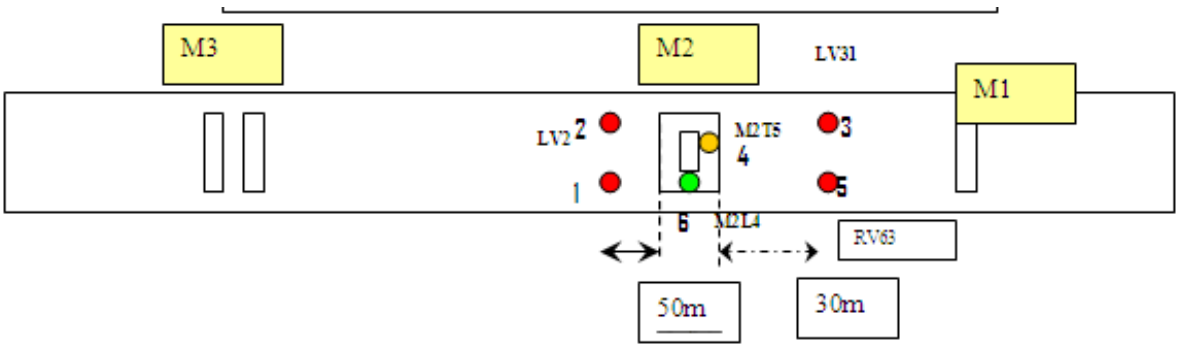

Sensor1: 'CH01_RV1' (vertical)
Sensor2: 'CH02_LV2'(vertical)
Sensor3: 'CH03_LV31' (vertical)
Sensor4: 'CH04_M2T5'(transverse)
Sensor5: 'CH05_RV63'(vertical)
Sensor6: 'CH06_M2L4'(longitudinal)

"9th Setup" (JW003)

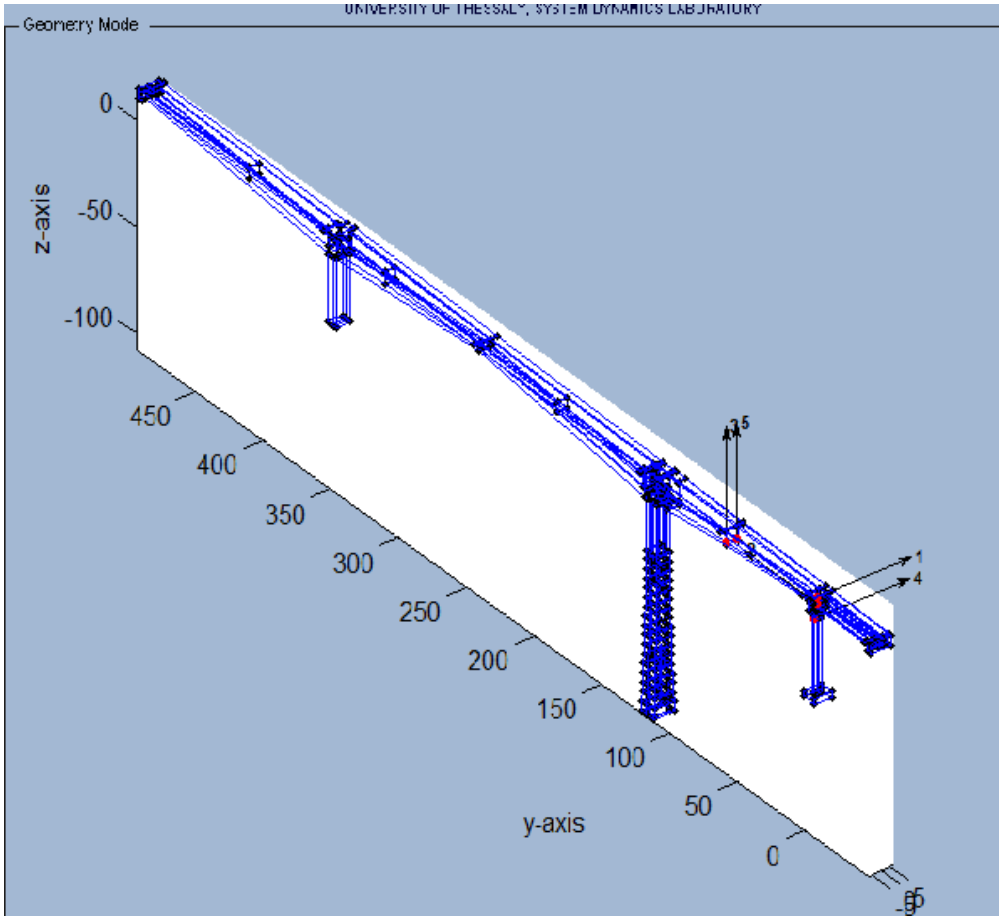

Sensor1: 'CH01_M2T4' (transverse)
Sensor2: 'CH02_M1L3' (longitudinal)
Sensor3: 'CH03_RV1' (vertical)
Sensor4: 'CH05_U2T5' (transverse)
Sensor5: 'CH06_LV2' (vertical)

"10th Setup" (JW005)

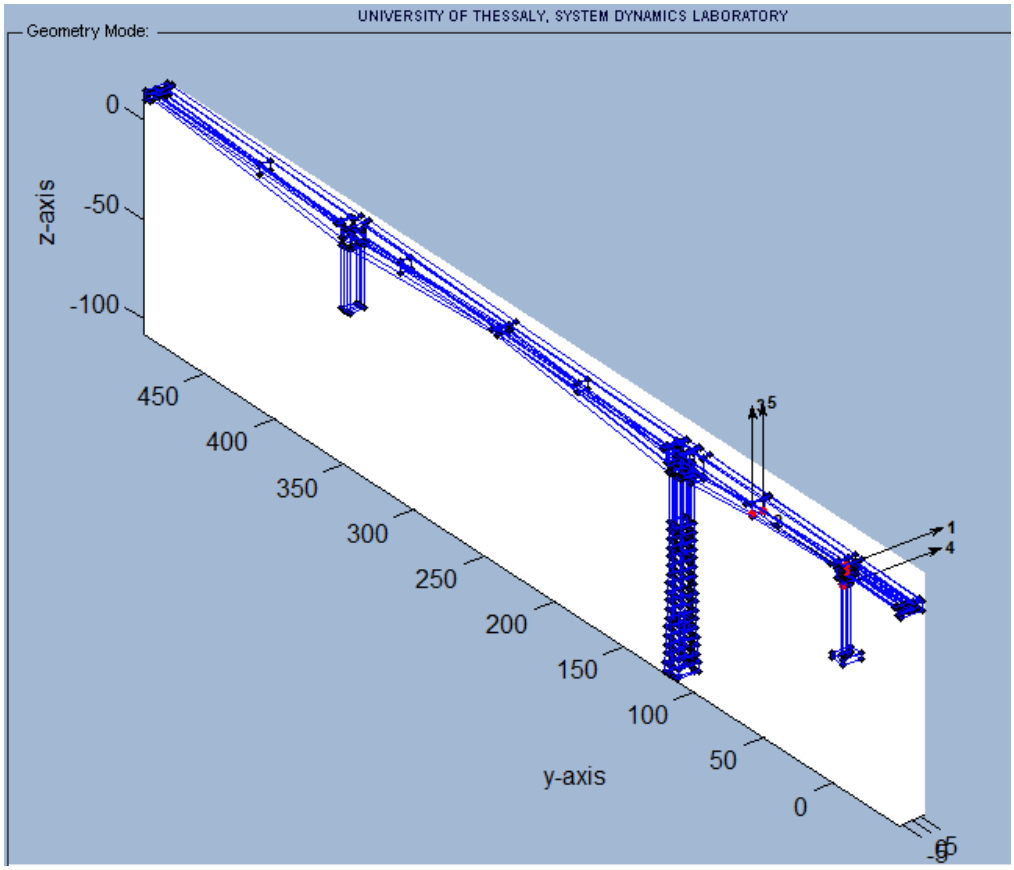

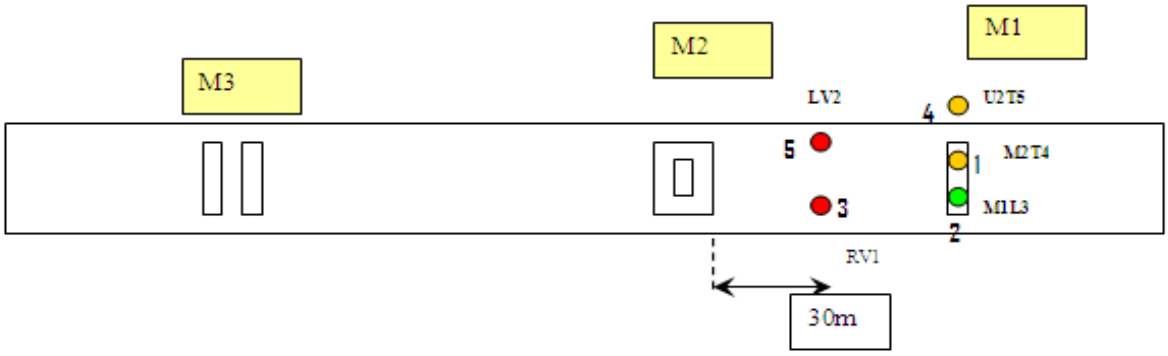

Sensor1: 'CH01_M2T4' (transverse)
Sensor2: 'CH02_M1L3' (longitudinal)
Sensor3: 'CH03_RV1' (vertical)
Sensor4: 'CH05_U2T5' (transverse)
Sensor5: 'CH06_LV2' (vertical)

“11th Setup” (JW006)

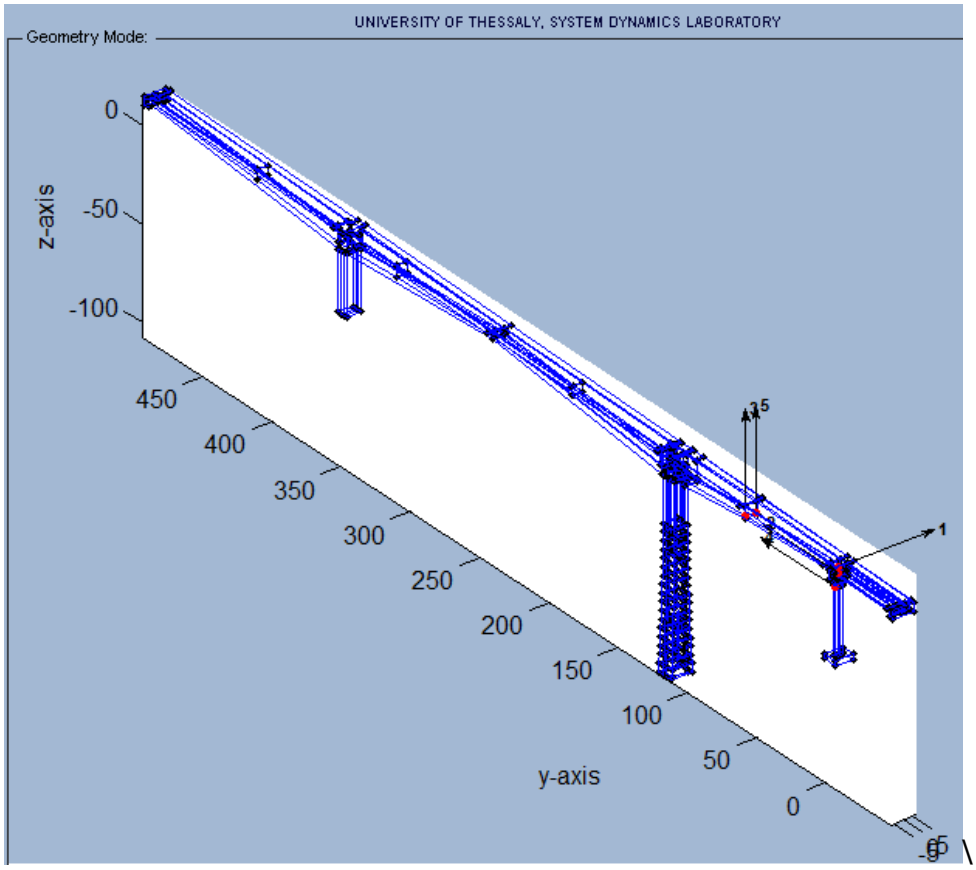

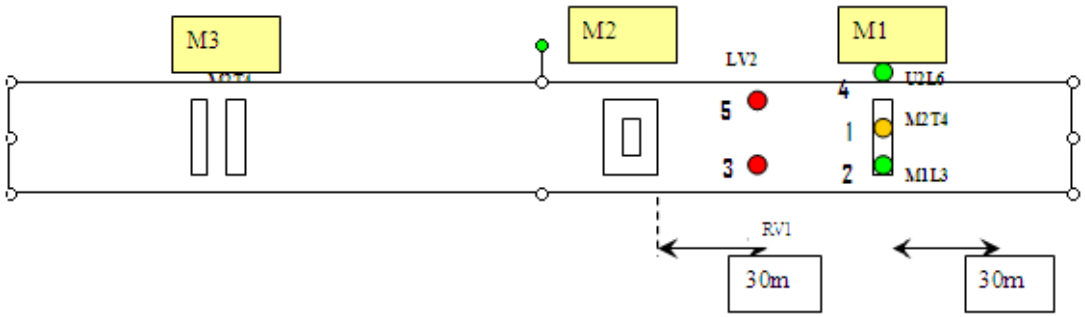

Sensor1: 'CH01_M2T4' (transverse)
Sensor2: 'CH02_M1L3' (longitudinal)
Sensor3: 'CH03_RV1' (vertical)
Sensor4: 'CH05_U2L6' (longitudinal)
Sensor5: 'CH06_LV2' (vertical)

Appendix IV

Identified Mode shapes of LB of Metsovo Bridge Using 6th Setup (JS003)

"1st Mode"
(transverse)

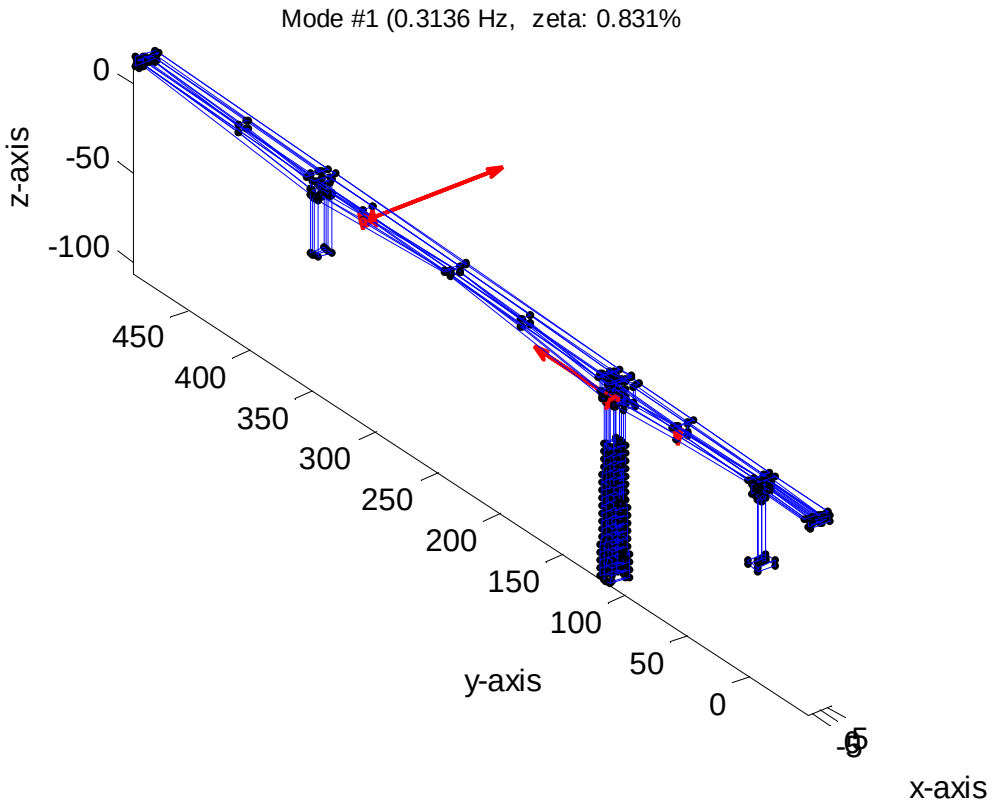

Modal Frequency	0.3136 Hz	0.3124 Hz
Mode Components	MI-Tool	Au's Method
'CH01_RV1' (vertical)	-0.05397	-0.0551
'CH02_LV2'(vertical)	0.04815	0.0436
'CH03_LT3' (transverse)	1.00000	1.0000
'CH04_M2T5'(transverse)	0.01377	0.0138
'CH05_RV63'(vertical)	-0.06067	-0.0611
'CH06_M2L4'(longitudinal)	0.81820	0.8188

“2nd Mode” (bending)

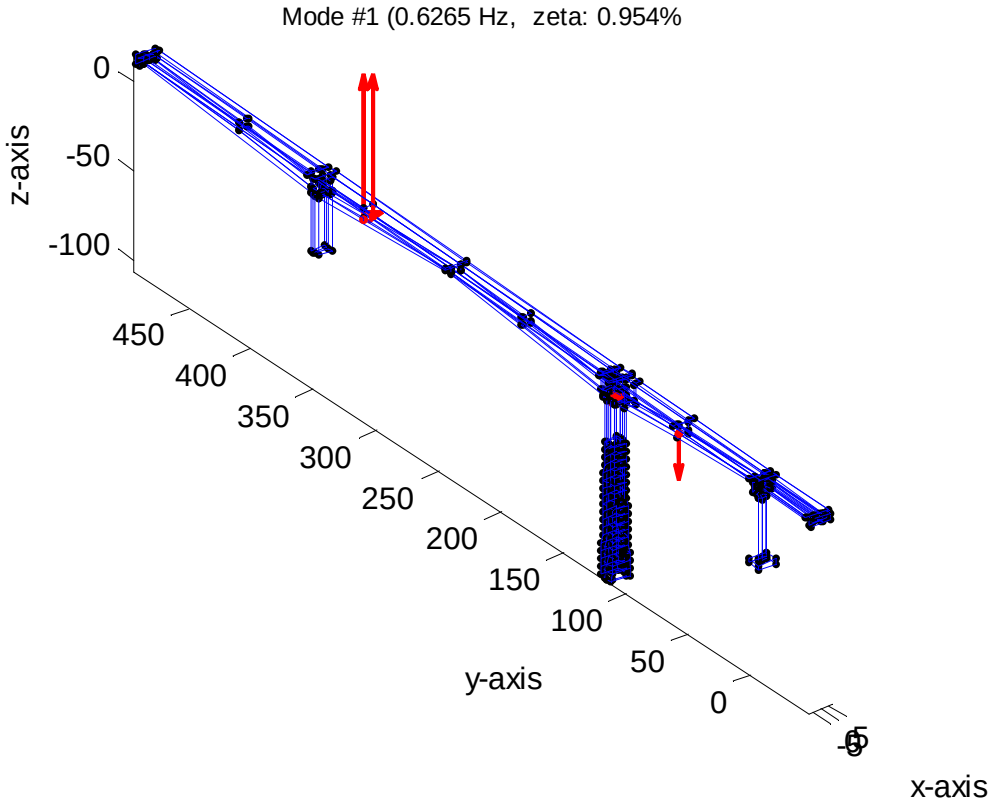

Modal Frequency	0.6265 Hz	0.6220 Hz
Mode Components	MI-Tool	Au’s Method
'CH01_RV1' (vertical)	1.00000	-0.9724
'CH02_LV2'(vertical)	0.99076	-1.0000
'CH03_LT3' (transverse)	0.08169	0.3942
'CH04_M2T5'(transverse)	0.05115	-0.0695
'CH05_RV63'(vertical)	-0.32235	0.4044
'CH06_M2L4'(longitudinal)	-0.03452	-0.5949

“3rd Mode”
(bending)

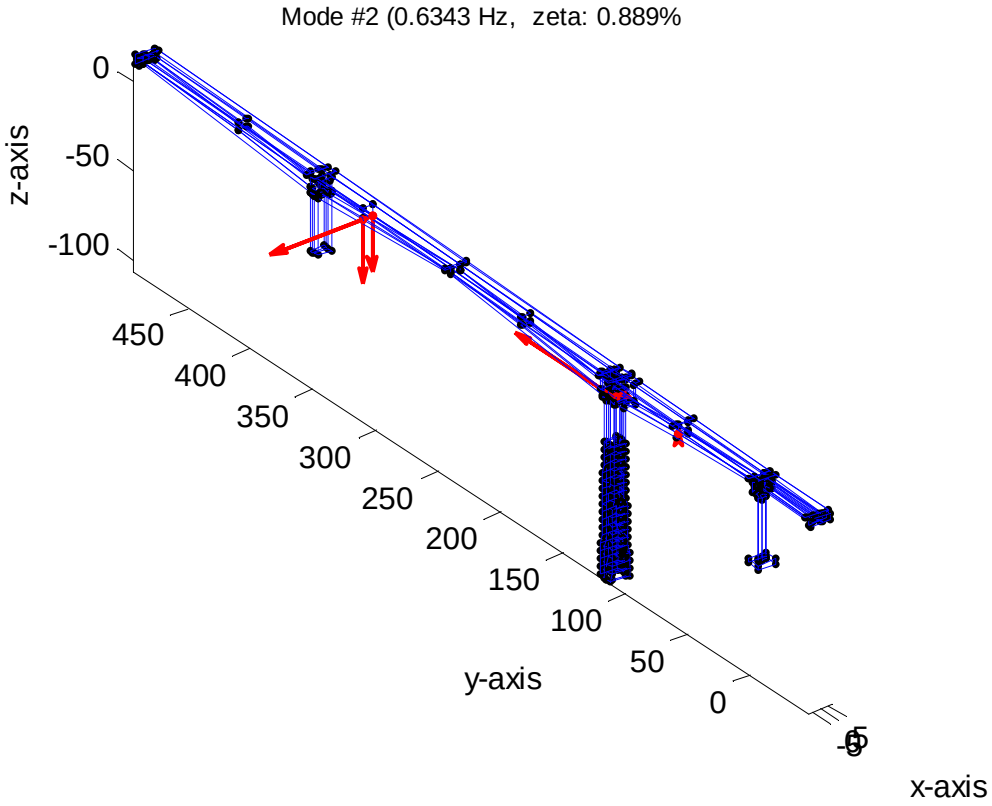

Modal Frequency	0.6343 Hz	0.6292 Hz
Mode Components	MI-Tool	Au’s Method
'CH01_RV1' (vertical)	-0.44779	-0.9724
'CH02_LV2'(vertical)	-0.39716	-1.0000
'CH03_LT3' (transverse)	-0.77097	0.3942
'CH04_M2T5'(transverse)	-0.02425	-0.0695
'CH05_RV63'(vertical)	0.02794	0.4044
'CH06_M2L4'(longitudinal)	1.00000	-0.5949

“4th Mode”
(bending)

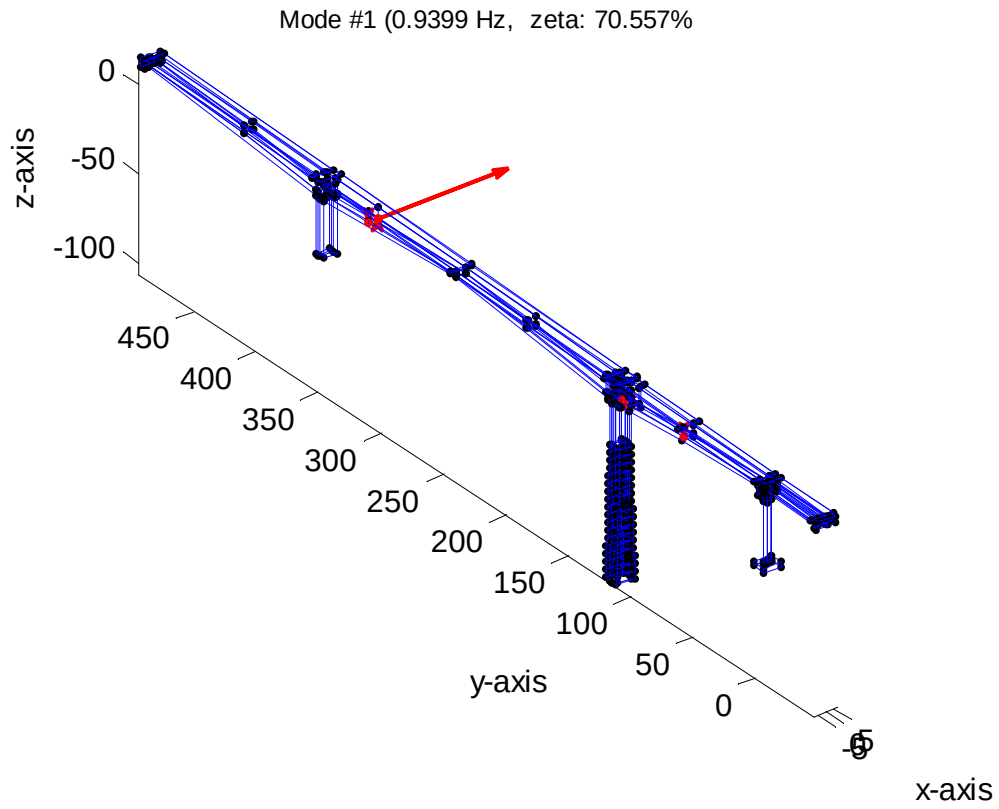

Modal Frequency	0.9399 Hz	Not Identified
Mode Components	MI-Tool	Au’s Method
'CH01_RV1' (vertical)	-0.02437	
'CH02_LV2'(vertical)	0.01978	
'CH03_LT3' (transverse)	1.00000	
'CH04_M2T5'(transverse)	0.10186	
'CH05_RV63'(vertical)	-0.00334	
'CH06_M2L4'(longitudinal)	0.25090	

“5th Mode”
(bending)

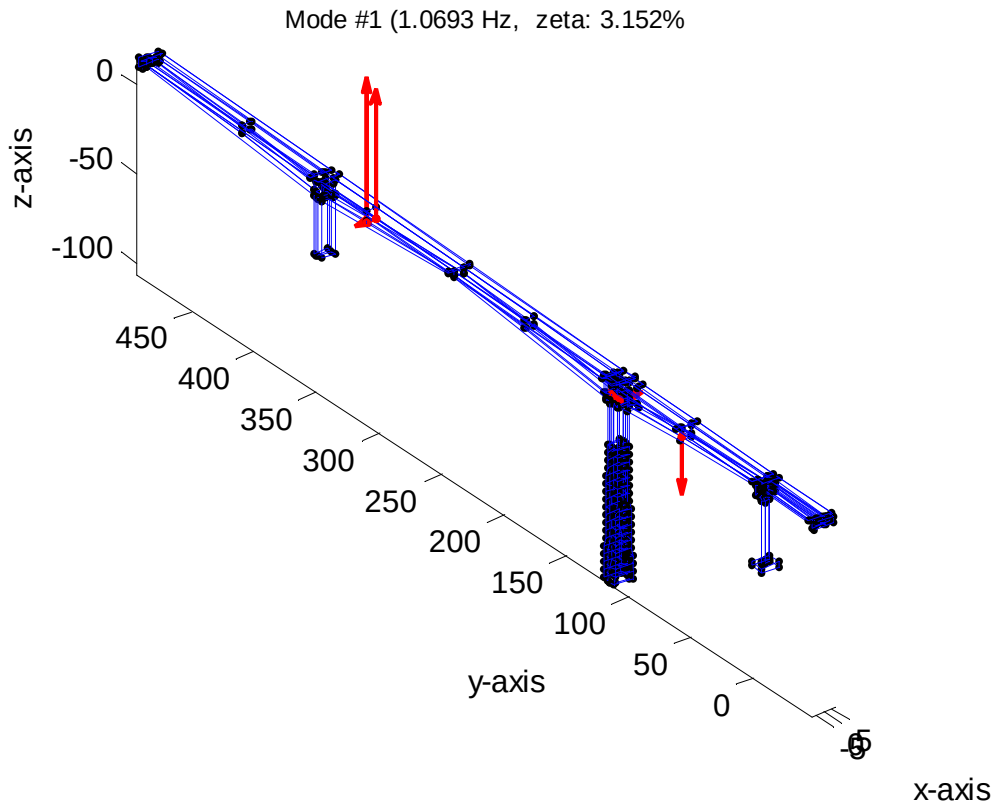

Modal Frequency	1.0693 Hz	1.0606 Hz
Mode Components	MI-Tool	Au’s Method
'CH01_RV1' (vertical)	1.00000	-1.0000
'CH02_LV2'(vertical)	0.90616	-0.9959
'CH03_LT3' (transverse)	-0.15780	0.1347
'CH04_M2T5'(transverse)	0.17017	-0.1519
'CH05_RV63'(vertical)	-0.39893	0.4406
'CH06_M2L4'(longitudinal)	-0.01323	0.0422

“6th Mode”
(transverse)

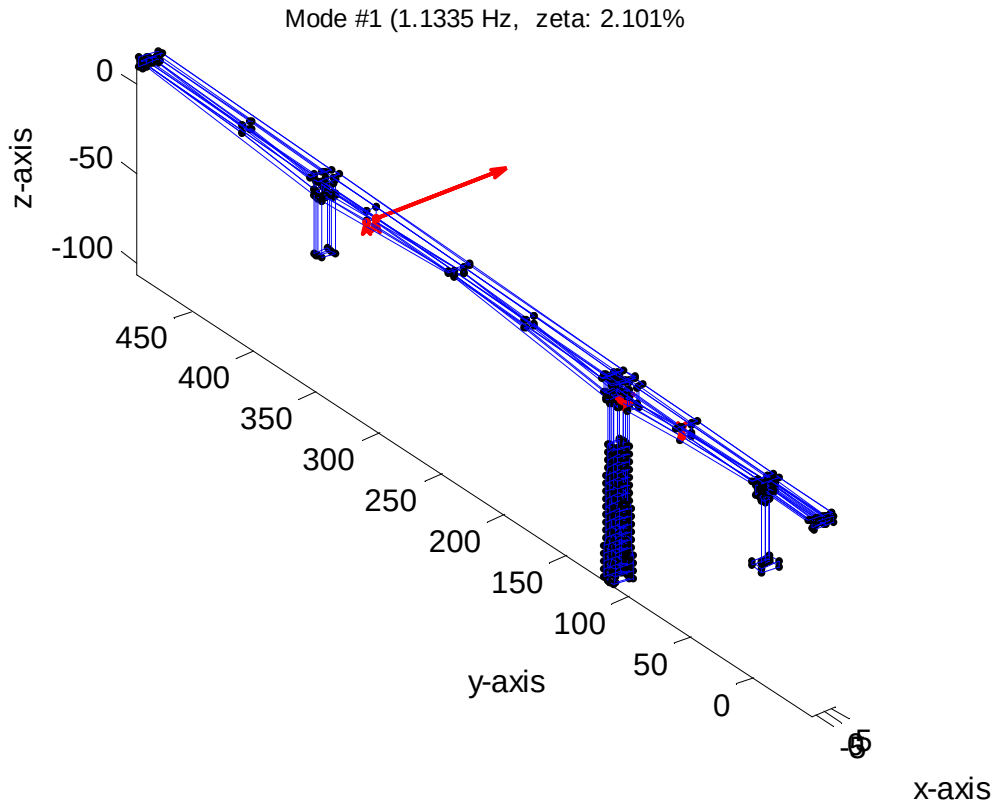

Modal Frequency	1.1335 Hz	1.1513 Hz
Mode Components	MI-Tool	Au’s Method
'CH01_RV1' (vertical)	0.02113	0.1007
'CH02_LV2'(vertical)	0.0120	0.1375
'CH03_LT3' (transverse)	1.0000	1.0000
'CH04_M2T5'(transverse)	0.11703	0.1126
'CH05_RV63'(vertical)	-0.00419	-0.0084
'CH06_M2L4'(longitudinal)	0.4523	0.4265

“8th Mode”
(bending)

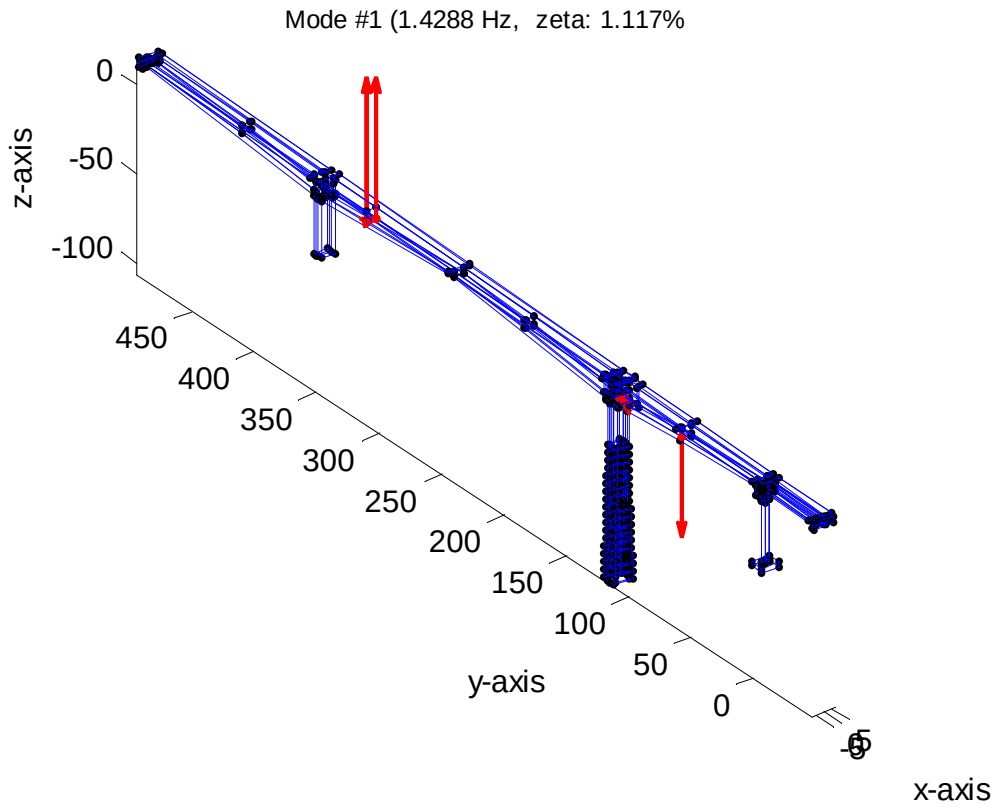

Modal Frequency	1.4288 Hz	1.4297 Hz
Mode Components	MI-Tool	Au’s Method
'CH01_RV1' (vertical)	1.00000	-1.0000
'CH02_LV2'(vertical)	0.90616	-0.9959
'CH03_LT3' (transverse)	-0.15780	0.1347
'CH04_M2T5'(transverse)	0.17017	-0.1519
'CH05_RV63'(vertical)	-0.39893	0.4406
'CH06_M2L4'(longitudinal)	-0.01323	0.0422

"11th Mode" (bending)

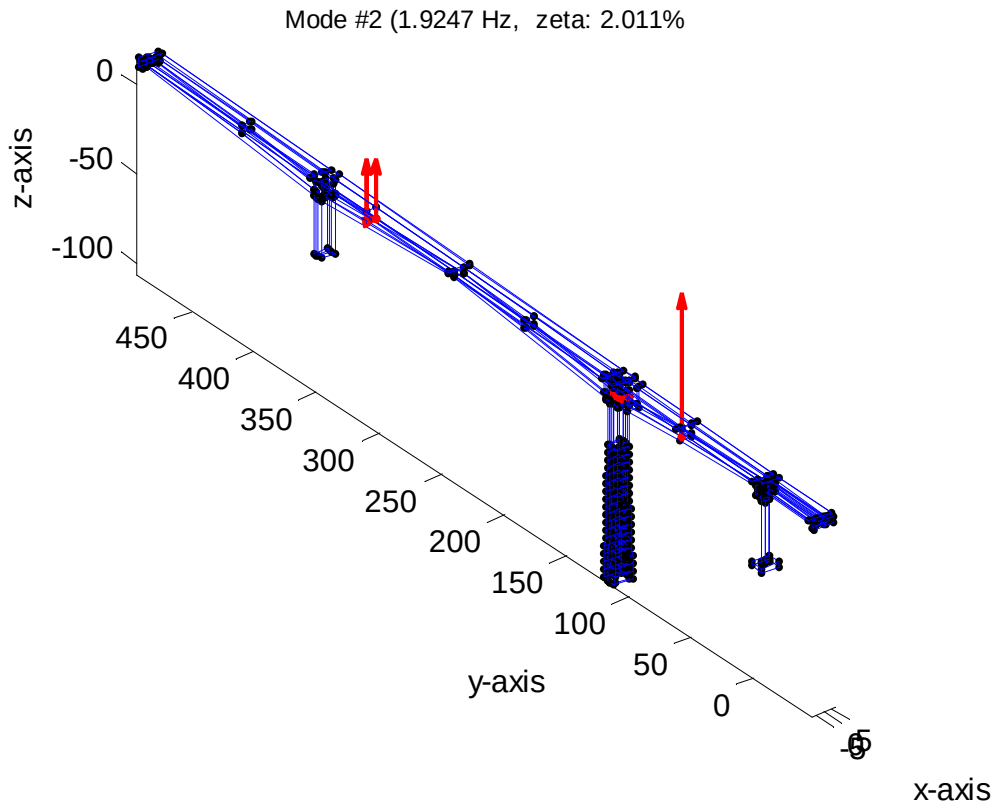

Modal Frequency	1.9247 Hz	1.9640 Hz	
Mode Components	MI-Tool	Au's Method	
'CH01_RV1' (vertical)	0.44105	-0.2379	-0.7248
'CH02_LV2'(vertical)	0.41112	-0.2470	-0.7174
'CH03_LT3' (transverse)	0.01963	-0.0601	-0.0012
'CH04_M2T5'(transverse)	0.09734	0.3073	-0.1405
'CH05_RV63'(vertical)	1.00000	-1.0000	-1.0000
'CH06_M2L4'(longitudinal)	-0.02042	0.0366	0.0092

“12th Mode” (bending)

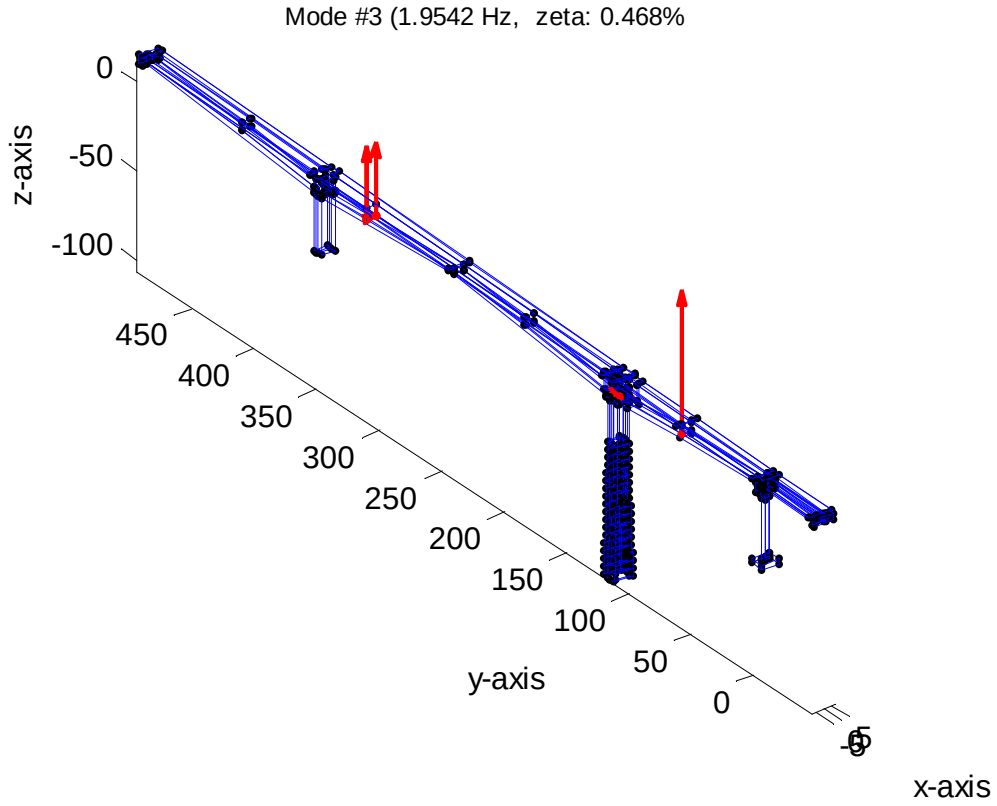

Modal Frequency	1.9542 Hz	2.3186 Hz
Mode Components	MI-Tool	Au’s Method
'CH01_RV1' (vertical)	0.50497	1.0000
'CH02_LV2'(vertical)	0.51139	0.8955
'CH03_LT3' (transverse)	0.01887	-0.2450
'CH04_M2T5'(transverse)	-0.02084	0.1160
'CH05_RV63'(vertical)	1.00000	0.3797
'CH06_M2L4'(longitudinal)	-0.01125	0.0448

“13th Mode”
(transverse)

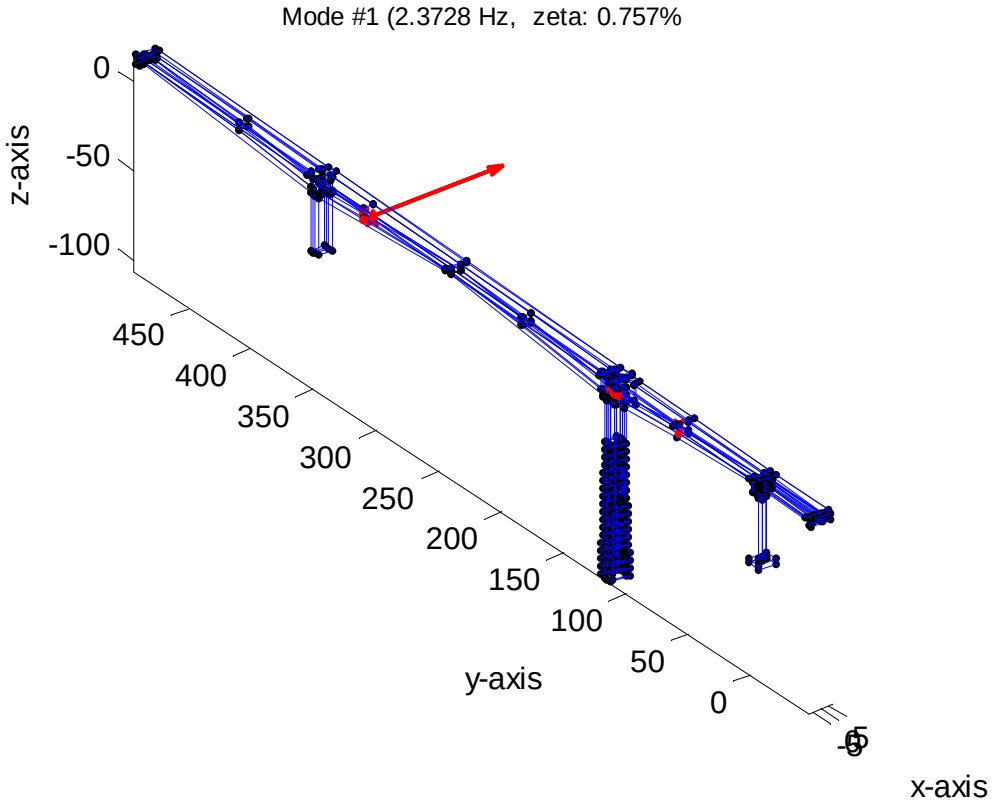

Mode Components	MI-Tool	Au’s Method
'CH01_RV1' (vertical)	-0.02844	0.1321
'CH02_LV2'(vertical)	0.04021	-0.1940
'CH03_LT3' (transverse)	1.00000	-1.0000
'CH04_M2T5'(transverse)	-0.04979	0.0272
'CH05_RV63'(vertical)	-0.01586	0.0775
'CH06_M2L4'(longitudinal)	-0.1532	0.1531

“14th Mode” (bending)

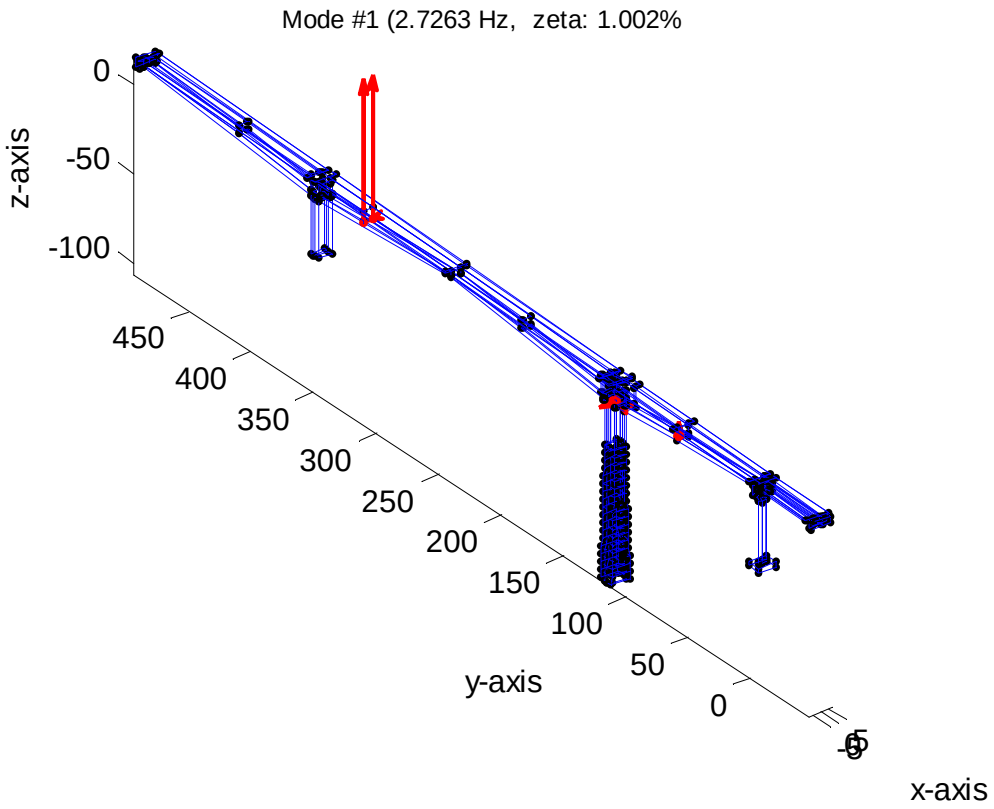

Modal Frequency	2.7263 Hz	2.7251 Hz
Mode Components	MI-Tool	Au’s Method
'CH01_RV1' (vertical)	0.98764	-1.0000
'CH02_LV2'(vertical)	1.00000	-0.9827
'CH03_LT3' (transverse)	-0.03651	0.0096
'CH04_M2T5'(transverse)	-0.13566	0.1135
'CH05_RV63'(vertical)	0.11329	-0.1284
'CH06_M2L4'(longitudinal)	0.00582	-0.0004

“15th Mode” (transverse)

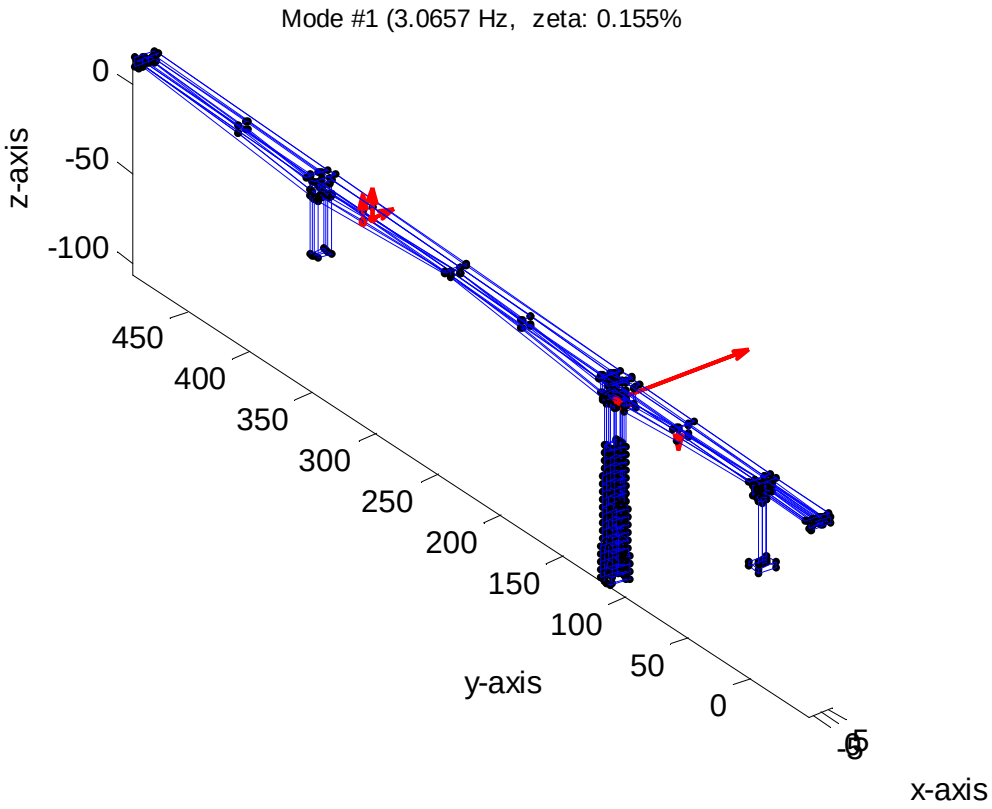

Modal Frequency	3.0657 Hz	Not Found
Mode Components	MI-Tool	Au’s Method
'CH01_RV1' (vertical)	0.18991	
'CH02_LV2'(vertical)	0.21339	
'CH03_LT3' (transverse)	0.17098	
'CH04_M2T5'(transverse)	1.0000	
'CH05_RV63'(vertical)	-0.08945	
'CH06_M2L4'(longitudinal)	0.2720	

“16th Mode” (bending)

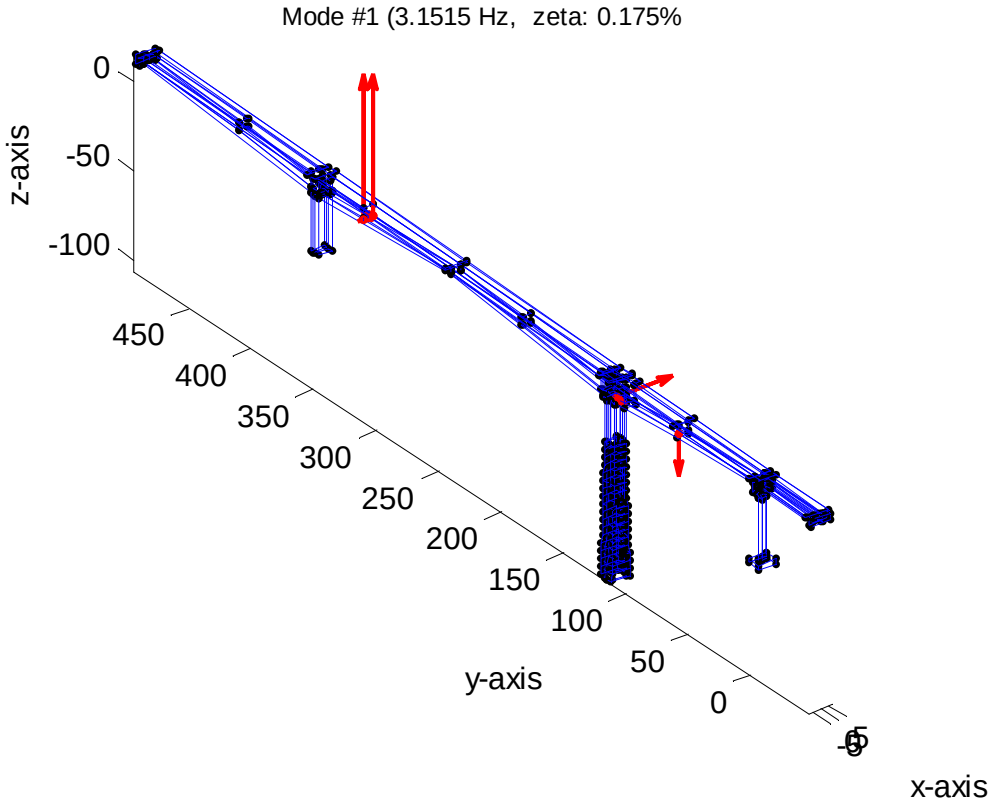

Modal Frequency	3.1515Hz	3.1329 Hz
Mode Components	MI-Tool	Au’s Method
'CH01_RV1' (vertical)	1.00000	-1.0000
'CH02_LV2'(vertical)	0.98735	-0.9767
'CH03_LT3' (transverse)	-0.11456	0.0731
'CH04_M2T5'(transverse)	0.42639	-0.2285
'CH05_RV63'(vertical)	-0.29634	0.1620
'CH06_M2L4'(longitudinal)	-0.09343	0.0523

“17th Mode” (bending)

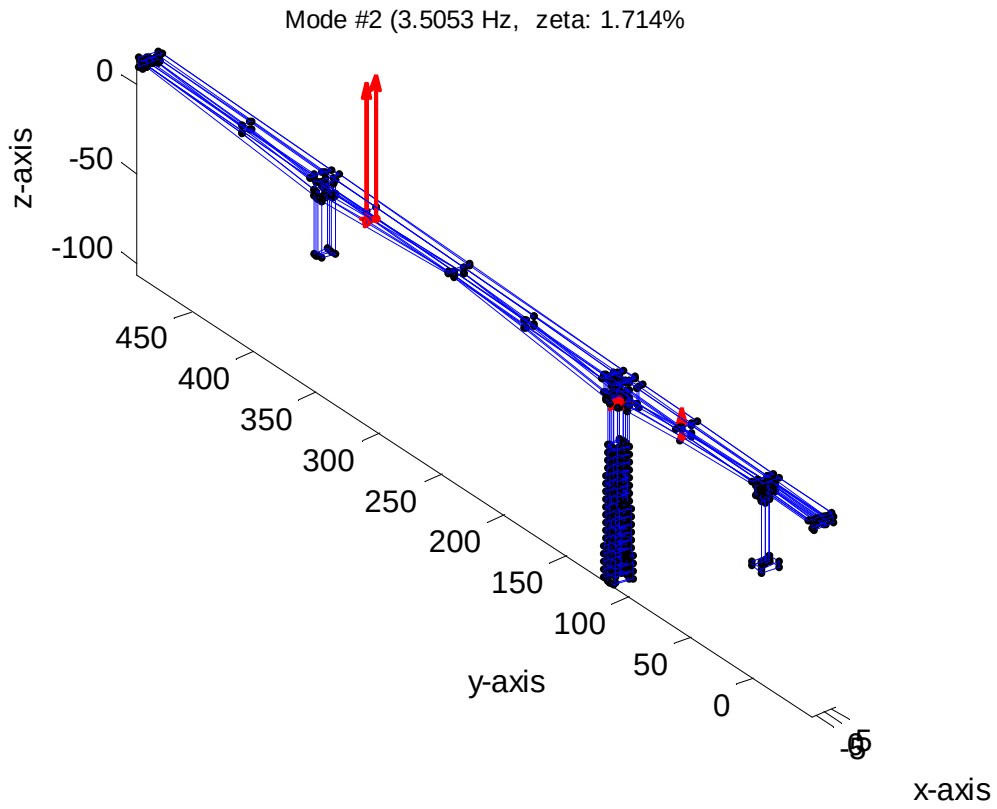

Modal Frequency	3.5053Hz	3.5217 Hz
Mode Components	MI-Tool	Au’s Method
'CH01_RV1' (vertical)	0.96536	-1.0000
'CH02_LV2'(vertical)	1.00000	-0.9976
'CH03_LT3' (transverse)	0.01726	-0.0052
'CH04_M2T5'(transverse)	0.02120	-0.0886
'CH05_RV63'(vertical)	0.21283	-0.1909
'CH06_M2L4'(longitudinal)	0.03352	-0.0070

Appendix V

Assembled Mode shapes of LB of Metsovo Bridge

“1st Mode” (transverse)

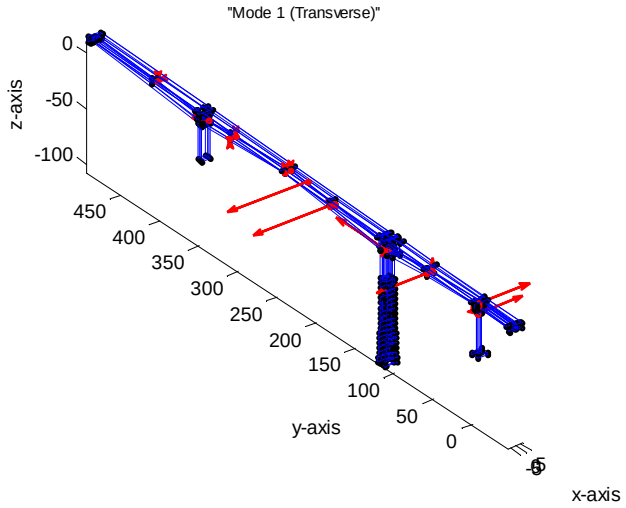

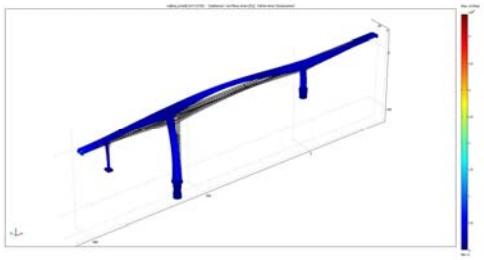

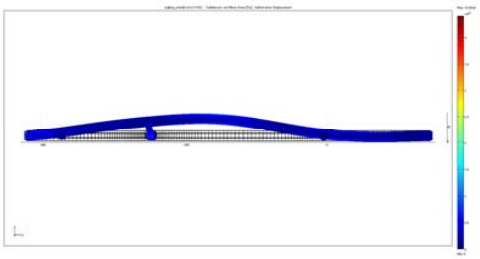

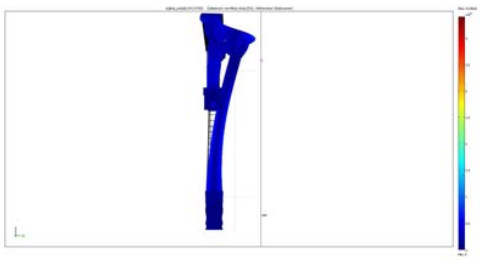

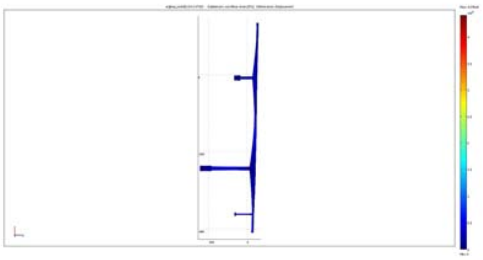

“2nd Mode” (transverse)

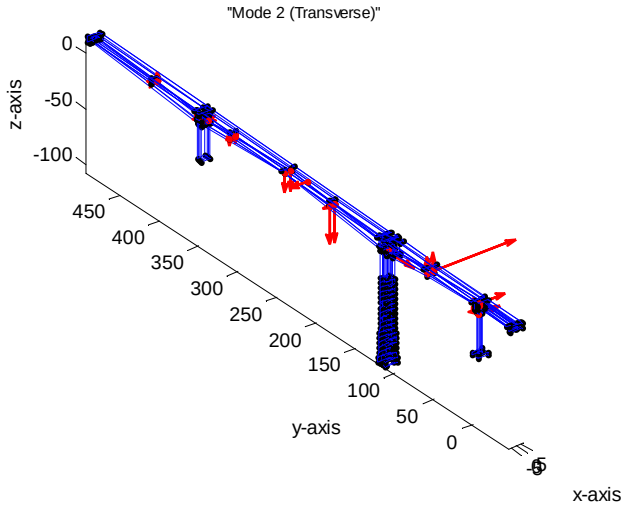

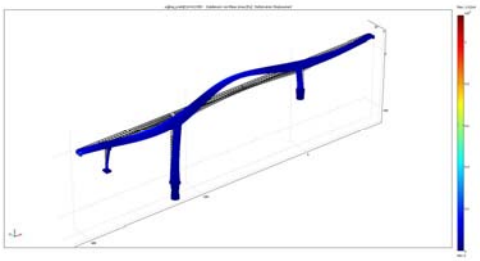

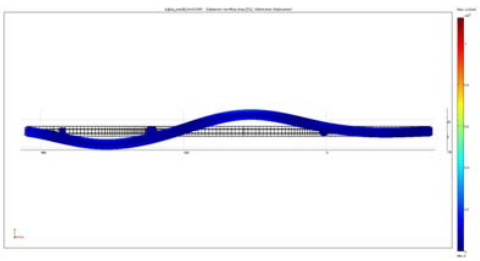

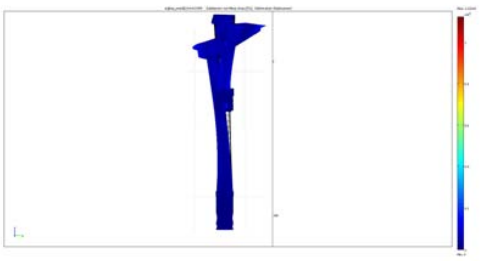

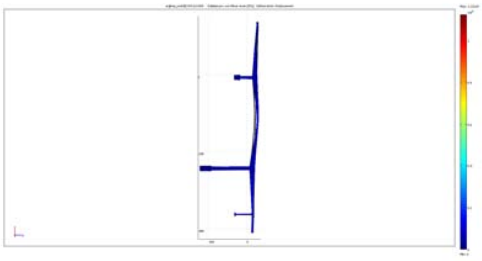

“3rd Mode”
(transverse&bending)

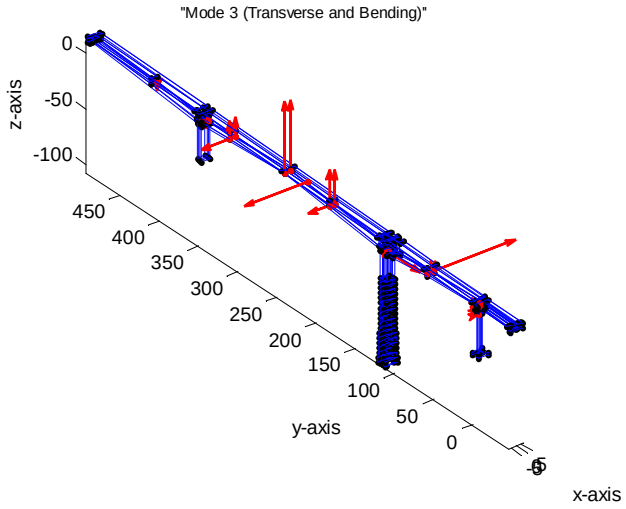

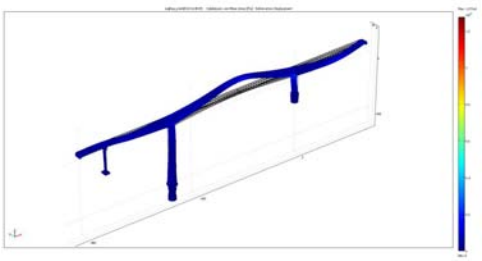

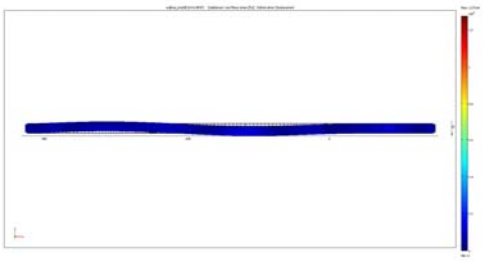

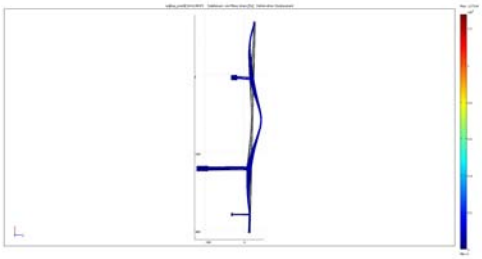

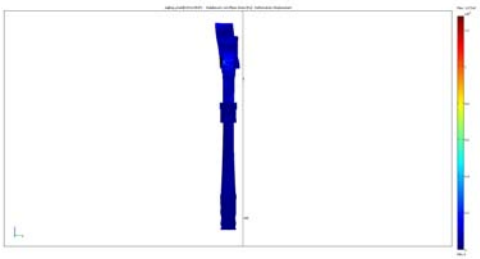

“8th Mode” (bending)

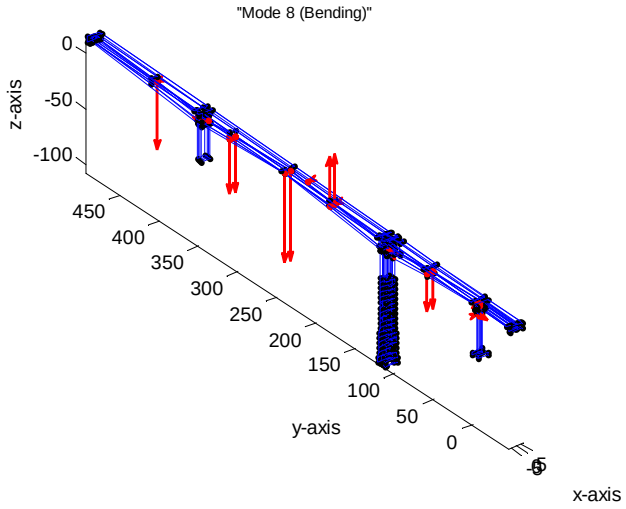

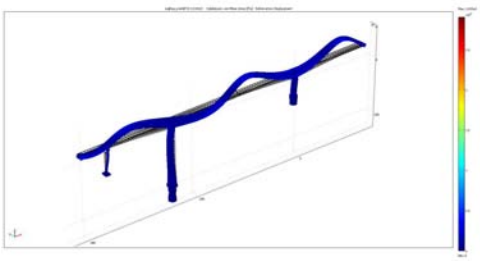

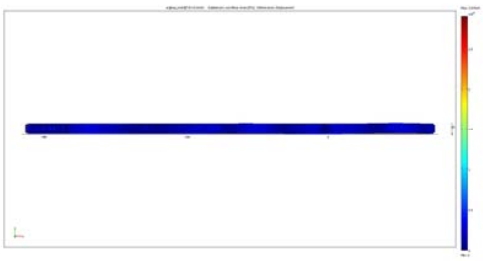

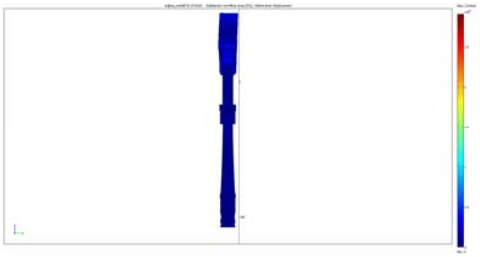

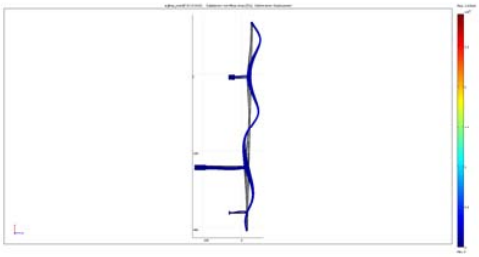

“14th Mode” (bending)

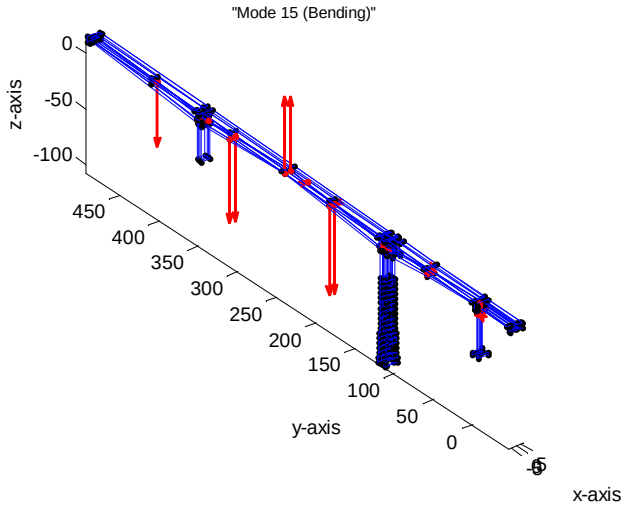

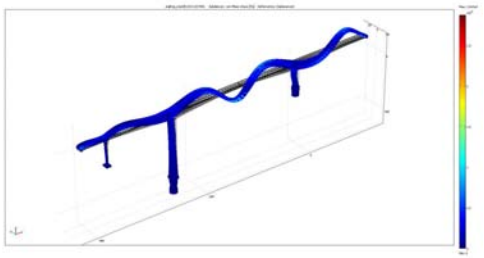

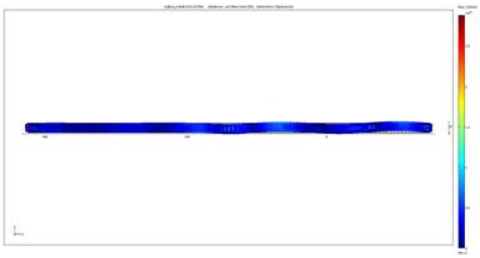

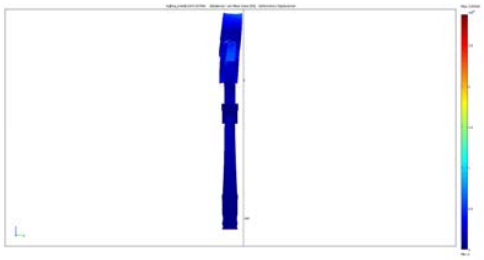

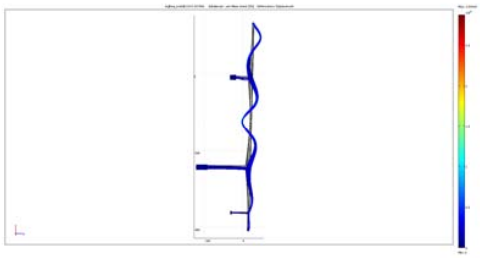

“15th Mode” (transverse)

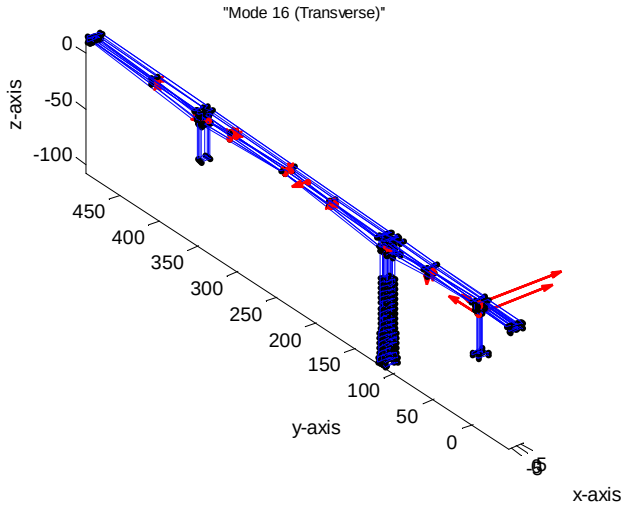

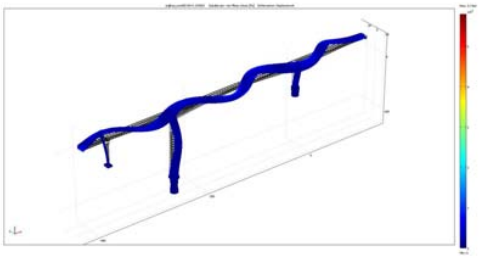

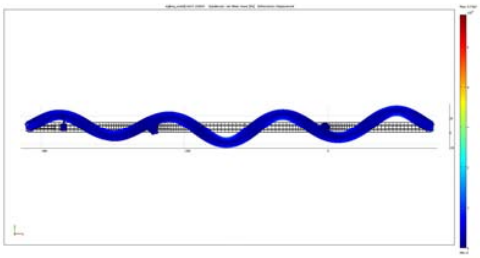

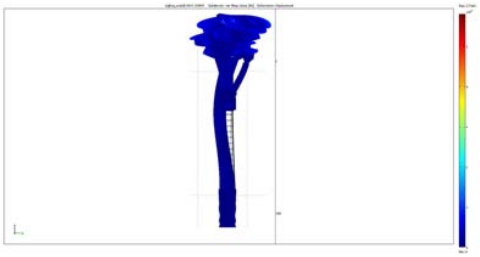

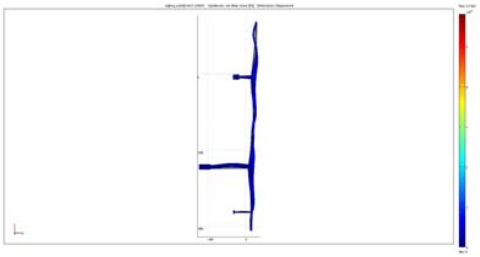

“16th Mode” (transverse)

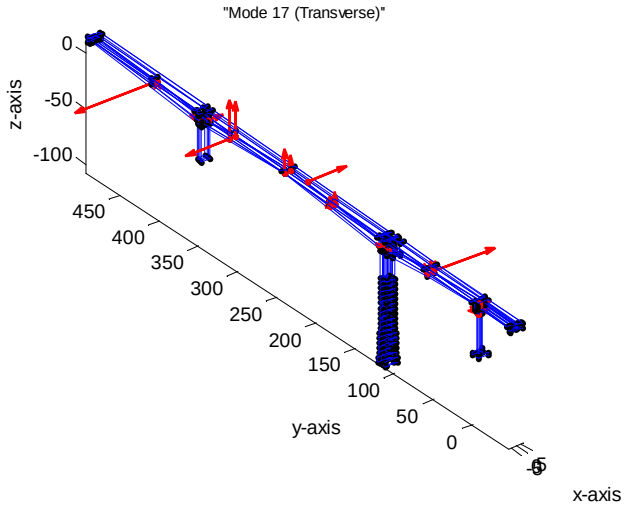

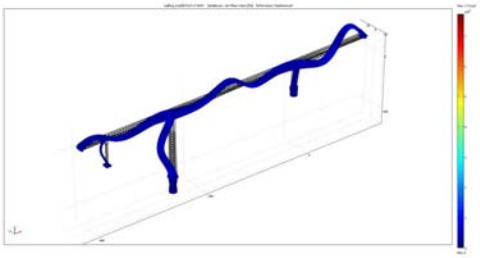

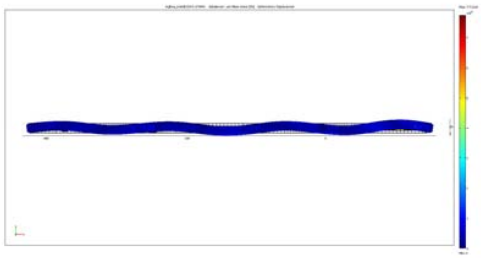

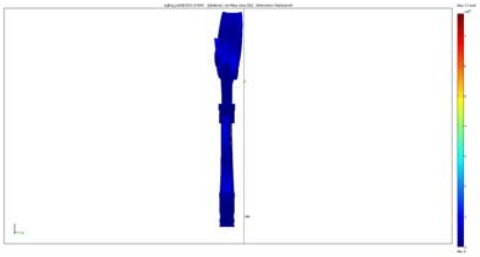

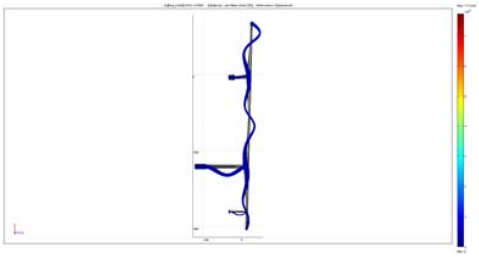

“17th Mode” (bending)

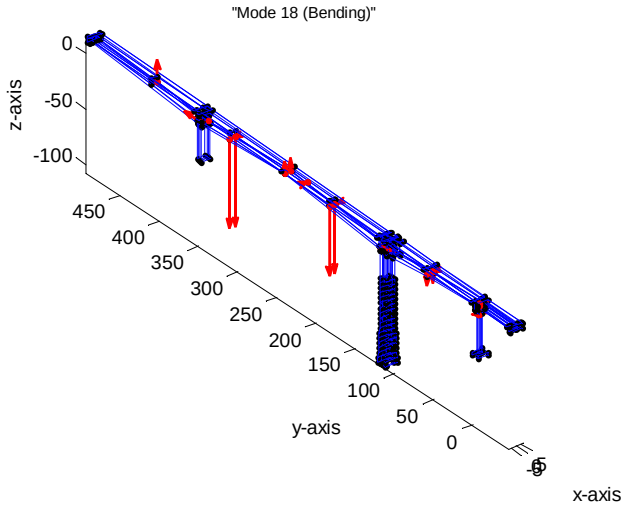

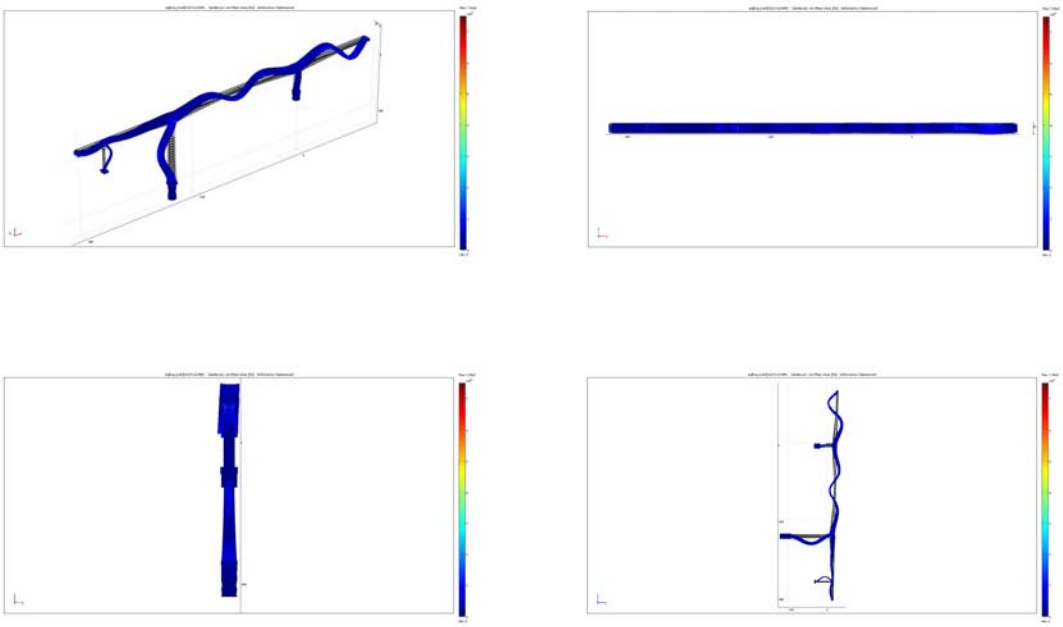

References

[1] Beck J.L., Katafygiotis L.S. (1998), *"Updating models and their uncertainties- I: Bayesian statistical framework."* Journal of Engineering Mechanics (ASCE), 124 **(**4), 455-461.

[2] Craig R, Bampton M.C.C (1968), *"Coupling of Substructures for Dynamic Analysis."* AIAA Journal, 6 (7), 1313-1319.

[3] Craig R. (2000), *"Coupling of Substructures for Dynamic Analysis: An Overview."* AIAA Dynamics Specialists Conference, Atlanta, GA.

[4] Christodoulou K., Ntotsios E., Papadimitriou C., Panetsos P. (2008), *"Structural model updating and prediction variability using Pareto optimal models."* Computer Methods in Applied Mechanics and Engineering, 198 (1), 138-149.

[5] Christodoulou K., Papadimitriou C. (2007), *"Structural identification based on optimally weighted modal residuals."* Mechanical Systems and Signal Processing, 21, 4-23.

[6] COMSOL AB (2005), *"Comsol Multyphysics user's guide"* [www.comsol.com/].

[7] Das I., Dennis J.E. Jr. (1998), *"Normal-Boundary Intersection: A new method for generating the Pareto surface in nonlinear multi-criteria optimization problems."* SIAM Journal of Optimization, 8, 631-657.

[8] Fritzen C.P., Jennewein D., Kiefer T. (1998*), "Damage detection based on model updating methods."*Mechanical Systems and Signal Processing, 12 (1), 163-186.

[9] Haralampidis Y., Papadimitriou C., Pavlidou M. (2005), *"Multi-objective framework for structural model identification."*, Earthquake Engineering and Structural Dynamics, 34 (6), 665-685.

[10] Katafygiotis L.S. and Yuen K.V. (2001), *"Bayesian spectral density approach for modal updating using ambient data."* Earthquake Engineering and Structural Dynamics , 30 (8), 1103-1123.

[11] Liokos N.A. (2009), "*Design and Response Identification of Structures*" Diploma Thesis Report, Department of Mechanical and Industrial Engineering, University of Thessaly.

[12] Lourens, E., Lombaert, G., De Roeck, G., Degrande, G. (2009), *"Reconstructing dynamic moving loads using an extended dynamic programming algorithm and eigenvalue reduction."* 2nd International Conference on Computational Methods in Structural Dynamics and Earthquake Engineering COMPDYN 2009, Rhodes, Greece.

[13] Nelson R.B. (1976), *"Simplified calculation of eigenvector derivatives."*AIAA Journal, 14 (9), 1201-1205.

[14] Ntotsios E., Christodoulou K., Papadimitriou C. (2006), *"Optimal Experimental Design in Structural Dynamics."* 5th International Conference on Computational Stochastic Mechanics, Rhodes, Greece.

[15] Ntotsios E.(2008), *"Experimental modal analysis using ambient and earthquake vibrations: Theory, Software and Applications*." MS Thesis Report No. SDL-08-1, Department of Mechanical and Industrial Engineering, University of Thessaly.

[16] Ntotsios E., Papadimitriou C., Panetsos P, Karaiskos G, Perros K., Perdikaris Ph (2008), *"Bridge health monitoring system based on vibration measurements."* Bulletin of Earthquake Engineering, doi: 10.1007/s10518-008-9067-4.

[17] Ntotsios E., Papadimitriou C. (2008), *"Multi-objective optimization framework for finite element model updating and response prediction variability."* Inaugural International Conference of the Engineering Mechanics Institute (EM08), Department of Civil Engineering University of Minnesota, Minneapolis, Minnesota.

[18] Panetsos P., Ntotsios E., Papadioti D.-C., Papadimitriou C., Dakoulas P**.** (2010), *"Health Monitoring of Metsovo Bridge using Ambient Vibrations"* 5th European Workshop on Structural Health Monitoring, Sorrento, Italy.

[19] Panetsos P , Ntotsios E., Liokos N.A, Papadimitriou C. (2009), *"Identification of Dynamic Models of Metsovo Bridge Using Ambient Vibration Measurements."* 2nd International Conference on Computational Methods in Structural Dynamics and Earthquake Engineering COMPDYN 2009, Rhodes, Greece.

[20] Panetsos P , Lambropoulos S. (2005), *"Bridge Health Monitoring for Egnatia Odos Bridge Management System."* 5th International Workshop on Structural Health Monitoring, Stanford, USA .

[21] Papadimitriou, C., Ntotsios, E. (2009), *"Structural Model Updating using Vibration Measurements."* 2nd International Conference on Computational Methods in Structural Dynamics and Earthquake Engineering COMPDYN 2009, Rhodes, Greece.

[22] Papadimitriou C., Beck J.L., Au S.K. (2000), *"Entropy-Based Optimal Sensor Location for Structural Model Updating."*, Journal of Vibration and Control, 6 (5),781-800.

[23] Papadimitriou C. (2005), *"Pareto Optimal Sensor Locations for Structural Identification."*Computer Methods in Applied Mechanics and Engineering, 194 (12-16), 1655-1673.

[24] Papadimitriou C., Beck J.L, Katafygiotis L.S. (2001), *"Updating robust reliability using structural test data."* Probabilistic Engineering Mechanics, 16, 103-113.

[25] Siu Kui Au. (2011), *"Assembling mode shapes by least squares."* Mechanical Systems and Signal Processing, 25, 164-179.

[26] SOLIDWORKS 2009 SPO.O, *"Solidworks user's guide"* [www.solidworks.com/].

[27] Teughels A., De Roeck G. (2005), *"Damage detection and parameter identification by finite element model updating."* Archives of Computational Methods in Engineering, 12 (2), 123-164.

[28] Vanik M.W., Beck J.L, Au S.K. (2000), *"Bayesian probabilistic approach to structural health monitoring."* Journal of Engineering Mechanics (ASCE), 126, 738-745.

[29] Yuen K.V., Beck J.L. (2003), *"Reliability-based robust control for uncertain dynamical systems using feedback of incomplete noisy response measurements."* Earthquake Engineering and Structural Dynamics, 32 (5), 751-770.

[30] Zitzler E., Thiele L. (1999), *"Multi-objective evolutionary algorithms: A comparative case study and the strength Pareto approach."* IEEE Transactions on Evolutionary Computation, 3, 257-271.